2008

Horizontal shear capacity of composite concrete beams without interface ties

Jonathon D. Kovach
Lehigh University

Kovach, Jonathan D.

Horizontal Shear Capacity of Composite Concrete Beams without Interface Ties

September 2008

Horizontal Shear Capacity of Composite Concrete Beams without Interface Ties

by

Jonathan D. Kovach

A Thesis

Presented to the Graduate and Research Committee

of Lehigh University

in Candidacy for the Degree of

Master of Science

in

Structural Engineering

Lehigh University

September 2008

This thesis is accepted and approved in partial fulfillment of the requirements for the Master of Science.

6/30/08

Date

Dr. Clay Naito, Thesis Advisor

Dr. Stephen Pessiki, Department Chairperson

Acknowledgements

First, I would like to thank my family for their endless support and encouragement throughout the entire process of my Master's Thesis project.

Next, I would like to thank the ATLSS staff, especially John Hoffner, Roger Moyer, Dan Dulin, Todd Anthony, Carl Bowman, and Russ Longenbach, for their aid during the fabrication and experimental phases of my research.

I would also like to thank Jun Cao for his help with the ARAMIS system tests and data processing.

I would like to thank Newcrete Products and New Enterprise Stone & Lime Co., Inc for fabricating and donating the prestressed concrete webs for the project. I would like to especially thank Allan Derr, Frank Musselman (Bed Supervisor), David Stultz (Quality Control Manager), and Steve Beck (Quality Control Technician) for all their help and for providing me with a more in depth understanding of prestressed concrete fabrication.

I would like to thank the Precast/Prestressed Concrete Institute (PCI) and the Pennsylvania Infrastructure Technology Alliance (PITA) for their financial support of this project.

Finally, I would like to thank Dr. Clay Naito for his guidance throughout the process of this research project.

Table of Contents

List of Tables

List of Figures

Abstract

The research of this thesis investigates the horizontal shear stress of composite concrete beams without horizontal shear ties. Typically, in composite bridge and building construction shear ties are placed across the web-slab interface to help maintain monolithic behavior of the section once the bond or cohesion is lost between the concrete surfaces. The current standards almost always require that these shear ties are present in composite construction and give very little consideration to the horizontal shear resistance provided by the concrete interaction alone. Therefore, the current requirements prescribed by ACI and AASHTO provide a conservative estimate to the shear capacity of composite concrete sections without horizontal shear ties. This research program examines the feasibility of increasing the allowable horizontal shear capacity between a precast, prestressed concrete web and a cast-in-place concrete slab without interface reinforcement.

A series of structural tests were conducted on composite prestressed beams without horizontal shear ties. The beams were designed and fabricated to represent sections which are typical for composite concrete construction. The contribution to the horizontal shear capacity provided by the roughness of the interface surface finish and the compressive strength of the slab concrete were investigated. Several specimen of each combination of the research variables were fabricated and tested in order to achieve repeatable results.

The horizontal shear stresses achieved from the tests ranged from 475 psi to 1000 psi which is considerably greater than the recommended value of 80 psi presented by the code for composite sections without interface reinforcement. It was concluded from these experiments that the interface roughness had a pronounced effect on the horizontal shear capacity of the composite section. The effect of the slab concrete compressive strength was found to be inconclusive. It was also found that when a relatively large time period occurred between the placement of the

concrete slab and the precast web, differential shrinkage will occur which may initiate delamination between the pieces and decrease the composite action. In the end, recommended horizontal shear capacities of 435, 465, and 570 psi were made for composite concrete sections with a broom, as-placed, and rake surface finishes, respectively.

1 Introduction

This thesis presents research conducted on the horizontal shear stress of composite concrete beams without horizontal shear ties. The composite beams are comprised of a precast, prestressed concrete web and a cast-in-place concrete slab. This research study consist of designing, fabricating, and testing composite concrete T-beams with varying concrete slab strengths and interface surface roughness in order to determine the horizontal shear strength of the composite concrete interface. This chapter presents an overview of the concept of horizontal shear stress along with the benefits of reducing or eliminating shear ties across the composite interface of the beams. Also, the research objectives, project overview, and scope of the thesis are presented.

1.1 Overview of Horizontal Shear Stress

The use of precast, prestressed concrete beams is typical in bridge and building construction. The precast beams are fabricated at a prestressing plant and then shipped to the job site and set in place. Once in place, a field cast concrete slab is poured over the precast beams in order to provide integrity and stability to the structural system. As the concrete cures, a bond will form between the prefabricated and cast-in-place concrete thus allowing the composite beam to possess the continuity and efficiency of a monolithic member.

In order for the composite beams to behave as purely monolithic, the composite interface bond must remain intact. If the bond is strong, the composite member will deform as a single beam when loaded (Figure 1-1a). The fully bonded interface will allow for forces to be transferred across the interface as seen in Figure 1-1b. However, when a composite beam with a weaker bond is loaded, there is a greater chance for the interface to fail, resulting in relative slip between the two composite elements (Figure 1-1c). If slip occurs and the interface is lost, then the slab and flange will independently resist a portion of the load as two separate members (Figure 1-1d).

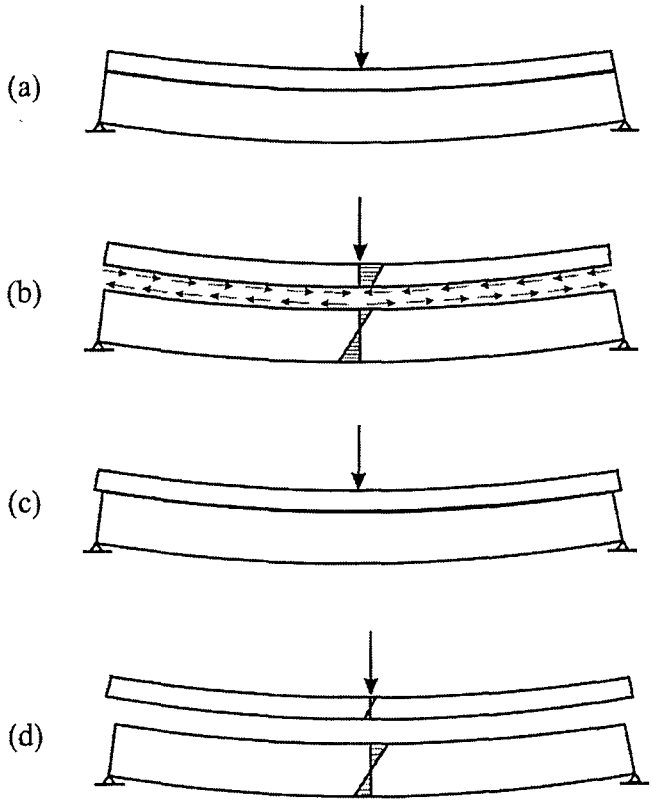

Figure 1-1: (a) Fully Composite Section (b) Shear Transfer of Composite Section, (c) Horizontal Slip, (d) Non-Composite Section

It is imperative for composite bridge and building systems that the beam-slab interface transfers all unbalanced forces, without slipping. The strength of these composite flexural members may be considerably reduced if the components are not acting similar to monolithic construction. The horizontal shear forces are transferred across the joint due to the natural interface bond (or cohesion) and aggregate interlock (if present) (Figure 1-1b). If the system loading exceeds the horizontal shear stress capacity, the bond is compromised and the elements will begin to slide relative to one another. Horizontal shear ties extending across the interface (if present) are then engaged to resist further slip and maintain integrity of the beam-slab system. Horizontal shear ties are typically an extension of the shear reinforcement from the precast beam section and are later cast into the slab (Figure 1-2).

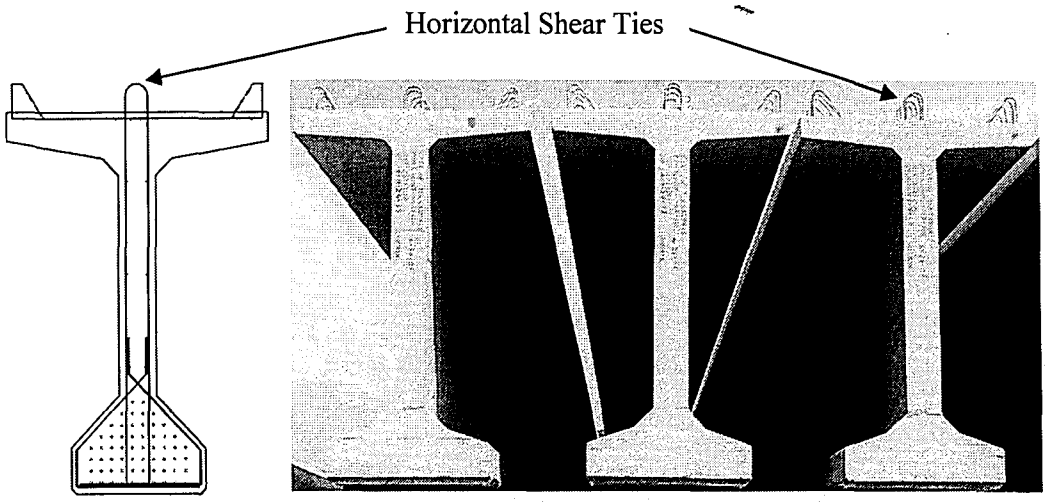

Figure 1-2: Horizontal Shear Ties in Bulb Tee Precast Bridge Beams

In the ACI and AASHTO codes, the use of horizontal shear ties is usually recommended but not necessarily required for composite beams. However, the horizontal shear resistance the code permits for an un-reinforced interface is very limited. ACI 318-08 allows a maximum horizontal shear stress of 80 psi for a section if the "contact surfaces are clean, free of laitance, and intentionally roughened" to ¼ inch. AASHTO LRFD Bridge Design Specification (2007) allows for 240 psi for similar conditions if the requirement for the interface reinforcement is disregarded. It is implied in the code that the interface concrete-to-concrete interaction alone provides little resistance to the horizontal shear stress. Contrary to this, research that has been conducted since the 1950s suggest that the same un-reinforced, roughed interface could achieve an average horizontal shear stress of approximately 450 psi before the breakdown of composite action (Hanson, 1960; Evans & Chung, 1969; Nosseir & Murtha, 1971). Even though the reported horizontal shear stress capacities of the previous research have considerable variation, it can be seen that the code recommendations are clearly conservative.

If research is able to show that a greater reliance can be placed on the cohesion and aggregate interlock of the composite concrete interface then it is possible to reduce or even eliminate the need of shear ties for horizontal shear stresses above 80 or 240 psi. Even though the use of

horizontal shear ties is manageable in current construction, significant advantages can be achieved by reducing the requirements. Specifically, the reduction of horizontal shear ties can produce the following benefits:

1. *Reduction of Fabrication Cost*

    - Additional reinforcement would not need to be bent and tied before the pour thus reducing the prefabrication time.

    - The reduction or absence of extended shear ties from the top of the beam will decrease the time needed for finishing the surface after placement of the precast concrete.

    - The chance of damaging the ties while the beams are being stored or transported prior to erection is reduced or eliminated.

2. *Improved Construction Safety*

    - During field construction, the presence of shear ties on top of the precast beams creates a tripping hazard for the workers. Since the beams are typically placed at high elevations, severe injury could occur.

3. *Reduction of Life-Cycle Cost*

    - The presence of horizontal shear ties provides a direct path for corrosion to transfer into the precast element. Elimination of the ties would provide a barrier against the propagation of corrosion and the associated durability problems.

    - Over time, the field-cast slab requires replacement due to wear or durability problems. Removal of the slab is typically achieved using a jackhammer around the shear ties, making rehabilitation cost substantial. Reduction or elimination of shear ties would ease replacement.

1.2 Research Objectives

Even though successful past practices are difficult to argue with, the conservative nature of the codes and the benefits that go along with reducing or even eliminating the need of horizontal shear ties justify a reassessment of horizontal shear stress capacity requirements. This research study hopes to present a new insight into the resistance provided to the horizontal shear stress by the concrete alone.

The objectives of this research are to:

- Perform an extensive literature survey of past research consisting of composite concrete beams without horizontal shear ties.
- Design test specimens which, when loaded, will achieve high levels of horizontal shear stress before the section begins to crack.
- Experimentally evaluate the behavior and performance of the composite beams under loading in order to determine the horizontal shear capacity which can be achieved.
- Recommend methods to improve the current code based on experimental results in order to better represent the horizontal shear capacity of composite concrete beams without horizontal shear ties.

1.3 Project Overview

The research project covered in this thesis is a continuation of a two phase experimental program investigating the horizontal shear stress of composite concrete beams without horizontal shear ties. The first phase (which will be summarized in Chapter 5 of this thesis) consisted of preliminary tests to determine the specifics of the test procedures and ascertain the horizontal shear capacity that can be achieved for various concrete slab compressive strengths and surface finishes. The second phase utilizes the conclusions and recommendations from the first phase in

order to design a new composite concrete test specimen without horizontal shear ties and select research variables in the hope of achieving repeatable test results.

1.4 Scope of Thesis

The remainder of this thesis consists of nine chapters. Chapter 2 presents the current methods of calculating the horizontal shear stress demand. In Chapter 3, an extensive literature review is conducted of composite beams that were tested without interface reinforcement. Chapter 4 presents the code approach of calculating the horizontal shear stress capacity. Chapter 5 summarizes the work and results of the first phase of the experimental program. In Chapter 6, the discussion of the second phase of the experimental program begins by providing an overview of this phase including the research variables considered. This chapter also describes the design of the composite concrete beams and the verification of the design using a finite element model. Chapter 7 presents an account of the fabrication process of the prestressed precast web and cast-in-place slab along with the problems experienced during fabrication and the resulting solutions. In Chapter 8, the test setup and testing procedure of the composite specimens are described. Chapter 9 presents an analysis of the experimental data along with a discussion and summary of the results. In Chapter 10, the results from the second phase of the experimental program are compared to those of the first phase and previous research. The research is then summarized and conclusions and recommendations are derived.

1.5 Notation

a = the distance from the support to the load point [in.]

A_{cv} = area of concrete considered to be engaged in interface shear transfer [in.^{2}]

A_{thr} = area of the threaded rod [in.^{2}]

b_v = width of the interface between the web and slab [in.]

c = cohesion factor [ksi]

C_1 = compression force in the topping slab at point 1 [lb.]

C_2 = compression force in the topping slab at point 2 [lb.]

d = the distance from the extreme compression fiber for the entire composite section to the centroid of the prestressed and non-prestressed longitudinal tension reinforcement, if any, but need not be taken less than 0.80h for prestressed concrete members, where h is the height of the composite section [in.]

d_p = distance from the extreme compression fiber to the centroid of the prestressing steel [in.]

d_v = the distance between the centroid of the tension steel to the mid-thickness of the slab [in.]

E = modulus of elasticity of the section [ksi]

E_{thr} = modulus of elasticity of the threaded rod [ksi]

f'_c = compressive strength of concrete [ksi]

I = the moment of inertia of the entire composite cross-sectional area [in.^{4}]

I_{tr} = transformed moment of inertia of the entire composite cross-sectional area [in.^{4}]

I_{trnc} = the transformed moment of inertia of the non-composite beam found by the sum of the individual I_{tr}'s for the web and the slab sections [in.^{4}]

k = variable relating the compressive strength to the modulus of elasticity

K_1 = fraction of concrete strength available to resist interface shear

K_2 = limiting interface shear resistance [ksi]

ℓ = length of the interface between two points [in.]

L = the total length of the beam [in.]

L_{thr} = original length of the threaded rod [in.]

L_{vi} = interface length considered to be engaged in shear transfer [in.]

M = bending moment [lbs-in.]

$M(x)$ = the equation of the internal moment along the beam [kip-in]

P = the point load applied to the beam [kip]

P_c = permanent net compressive force normal to the shear plane [kip]

P_{thr} = load applied to one threaded rod [kip]

Q = first moment of inertia with respect to the neutral axis of the slab, calculated as $Q = A \cdot \bar{y}$; where A is the area of the slab and $\bar{y}$ is the distance from the centroid of the slab to the neutral axis of the composite section [$in.^3$]

Q_{tr} = transformed first moment of inertia [$in.^3$]

t = time after the end of the initial wet curing [days]

v_h = horizontal shear stress of the interface [psi]

V_h = horizontal shear force [lb.]

V_{nh} = the nominal horizontal shear strength [lb.]

V_{ni} = nominal interface shear resistance [kip]

V_u = factored vertical shear force [lb.]

V_{ul} = maximum factored vertical shear force of a section [kip]

x	=	the distance from the support to a location along the beam [in.]
X	=	ratio of shear span to effective depth
y	=	distance from the neural axis of a section [in.]
Y	=	ultimate shear strength
γ_{sh}	=	correction factor for ultimate shrinkage strain
δ_{thr}	=	change in length of the threaded rod [in.]
$\Delta(x)$	=	deflection along the beam [in.]
$(\varepsilon_{sh})_t$	=	shrinkage strain at time t for moist cured concrete [in./in.]
$(\varepsilon_{sh})_u$	=	ultimate shrinkage strain [in./in.]
$\theta(x)$	=	the slope of the elastic curve along the beam [rad.]
μ	=	friction factor
σ_x	=	nominal axial stress [psi]
ϕ	=	0.75 for shear

2 Horizontal Shear Stress Demand

2.1 General

There are three general methods used to calculate the horizontal shear demand of a composite concrete beam. These methods are global force equilibrium, simplified elastic beam behavior, and the classical elastic method. These methods will be explained using the simply supported, uniformly loaded, composite beam shown in Figure 2-1 and Figure 2-2 as a reference.

2.2 Global Force Equilibrium

The global force equilibrium method determines the horizontal shear demand from the change in the compression forces occurring on the topping slab at two points along the beam. As seen in Figure 2-1, a small section of the beam has been removed and the compression forces that are applied are shown.

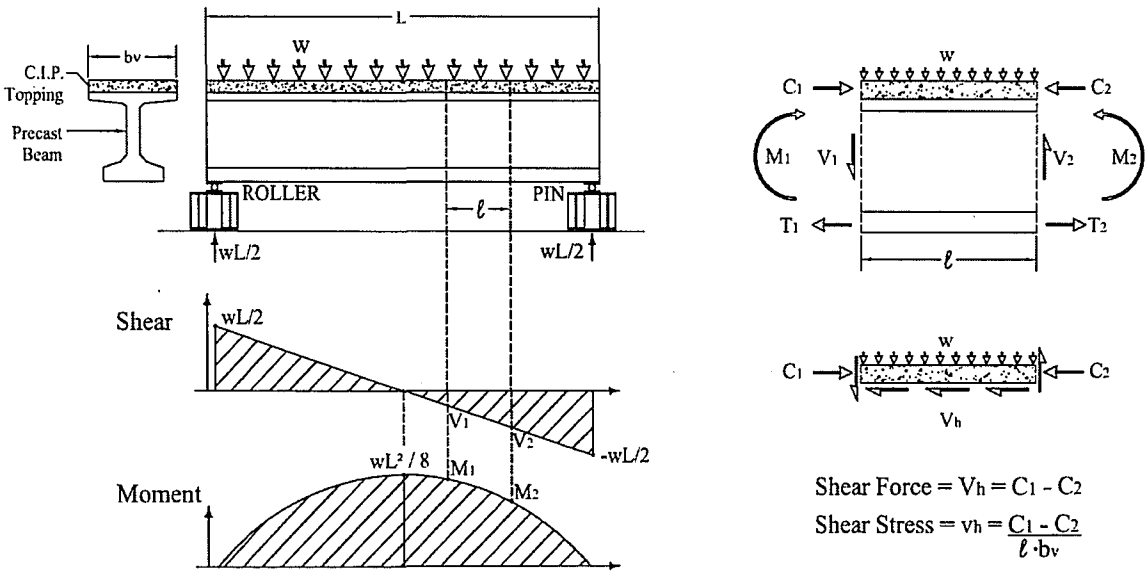

Figure 2-1: Horizontal Shear Demand - Global Force Equilibrium Method

The difference of the compression forces results in the horizontal shear force (Eq. 1).

$$V_h = (C_1 - C_2) \quad \text{(Eq. 1)}$$

where,

V_h = horizontal shear force between points 1 and 2 [lb.]

C_1 = compression force in the topping slab at point 1 [lb.]

C_2 = compression force in the topping slab at point 2 [lb.]

To obtain the horizontal shear stress, the change in compression force is divided by the contact area which the difference in the compression force is transferred (Eq. 2).

$$v_h = (C_1 - C_2) / (\ell \cdot b_v) \quad \text{(Eq. 2)}$$

where,

v_h = horizontal shear stress of interface between points 1 and 2 [psi]

ℓ = length of the interface between points 1 and 2 [in.]

b_v = width of the interface between the web and slab [in.]

This method of calculating the horizontal shear demand is permitted in the AASHTO LRFD Bridge Design Specifications (2007) Section §5.8.4 and ACI 318-08 Section §17.5.4.

2.3 Simplified Elastic Beam Behavior

The second method uses flexural beam theory to equate the horizontal shear demand to the vertical shear acting on the section. Using force equilibrium, a relationship between the vertical shear on the section and the horizontal shear stress can be determined over a small segment (Δx). The derivation of this method is summarized in Figure 2-2.

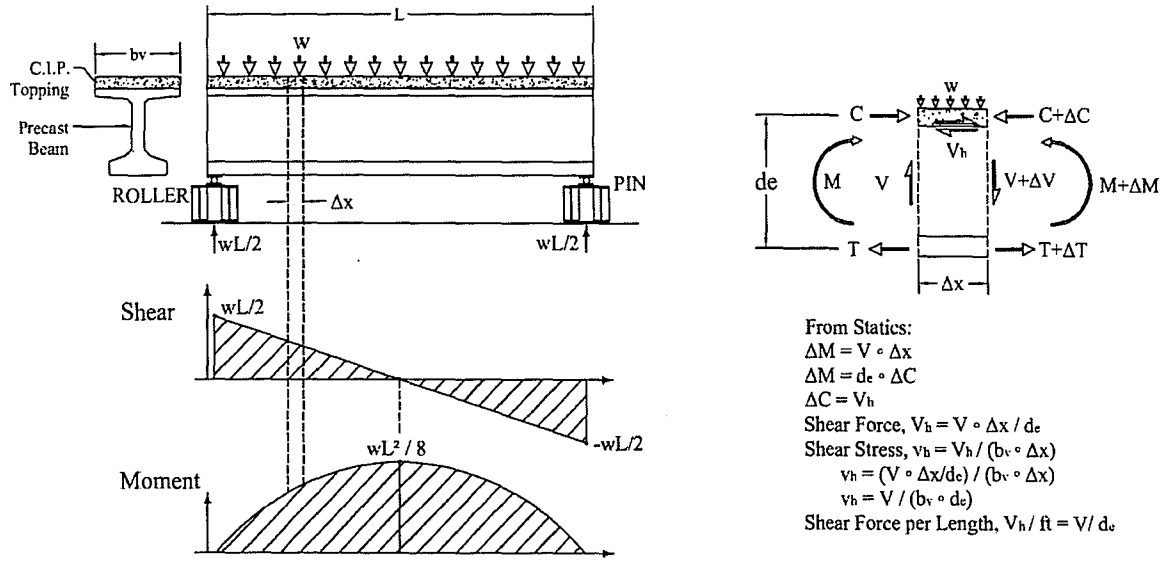

Figure 2-2: Horizontal Shear Demand – Simplified Elastic Beam Behavior Method

The final result is given in Equation 3. This approach is permitted by ACI 318-08 Section §17.5.4.

$$v_h = {V_u}/{b_v d} \qquad \text{(Eq. 3)}$$

where,

v_h = horizontal shear stress [psi]

V_u = factored vertical shear force [lb.]

b_v = width of the interface between the web and slab [in.]

d = the distance from the extreme compression force for the entire composite section to centroid of the prestressed and non-prestressed longitudinal tension reinforcement, if any, but need not be taken less than 0.80h for prestressed concrete members, where h is the height of the composite section [in.]

AASHTO (2007) Section §5.8.4.2 has a slight variation of this equation for girder/slab bridges. The only difference between the equations is that AASHTO takes "d" as the distance from the

prestressed steel to the mid-thickness of the slab rather than to the extreme compression fiber. The following equation calculates the factored interface shear stress for a concrete girder/slab bridge:

$$v_{ui} = {}^{V_{ul}}\!/_{b_{vi} d_v} \qquad \text{(Eq. 4)}$$

where,

v_{ui} = factored interface shear stress [ksi]

V_{ul} = maximum factored vertical shear force of a section [kip]

b_{vi} = interface width considered to be engaged in shear transfer [in.]

d_v = the distance between the centroid of the tension steel to the mid-thickness of the slab [in.]

The factored interface shear force for a concrete girder/slab bridge may be determined as:

$$V_{ui} = v_{ui} A_{cv} = v_{ui} 12 b_v \qquad \text{(Eq. 5)}$$

where,

V_{ui} = factored interface shear force [kip/ft]

v_{ui} = factored interface shear stress [ksi]

A_{cv} = area of concrete considered to be engaged in interface shear transfer [in.^{2}]

b_v = interface width considered to be engaged in shear transfer [in.]

2.4 Classical Elastic Method

Another method allowed by AASHTO (2007) is the classical elastic method. A majority of the previous research conducted on horizontal shear stress utilized the classical elastic method as a

means to determine the horizontal shear stress at service and failure loads. The elastic method for determining the horizontal shear stress is given in Equation 6.

$$v_h = {}^{VQ}\!/_{Ib_v} \qquad \text{(Eq. 6)}$$

where,

v_h = horizontal shear stress [psi]

Q = first moment of inertia with respect to the neutral axis of the slab, calculated as $Q = A \cdot \bar{y}$; where A is the area of the slab and $\bar{y}$ is the distance from the centroid of the slab to the neutral axis of the composite section [in.^{3}]

I = the moment of inertia of the entire composite cross-sectional area [in.^{4}]

b_v = width of the interface between the web and slab [in.]

It should be noted that this equation is based on the elastic response of a composite beam, and therefore is not valid if the section is cracked. Additionally, the uncracked transformed section properties for I and Q should be used in this equation if the two concretes that make up the composite section have different compressive strengths.

2.5 Comparison of Horizontal Shear Demand Calculation Methods

Using a standard PCI Double Tee section (Figure 2-3) taken from the PCI Design Handbook (2004), three of the methods for determining the horizontal shear demand are compared. The beam was simply supported over 32 feet with an applied uniform load of 3.184 kip/ft (this value is the factored load calculated from the dead load of the section and the safe superimposed service load given by the PCI Handbook (2004)). A graph of the horizontal shear stresses at service loads of the left span of the beam is show in Figure 2-4.

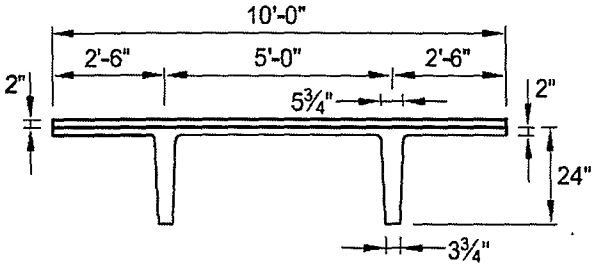

Figure 2-3: Standard PCI Double Tee Section

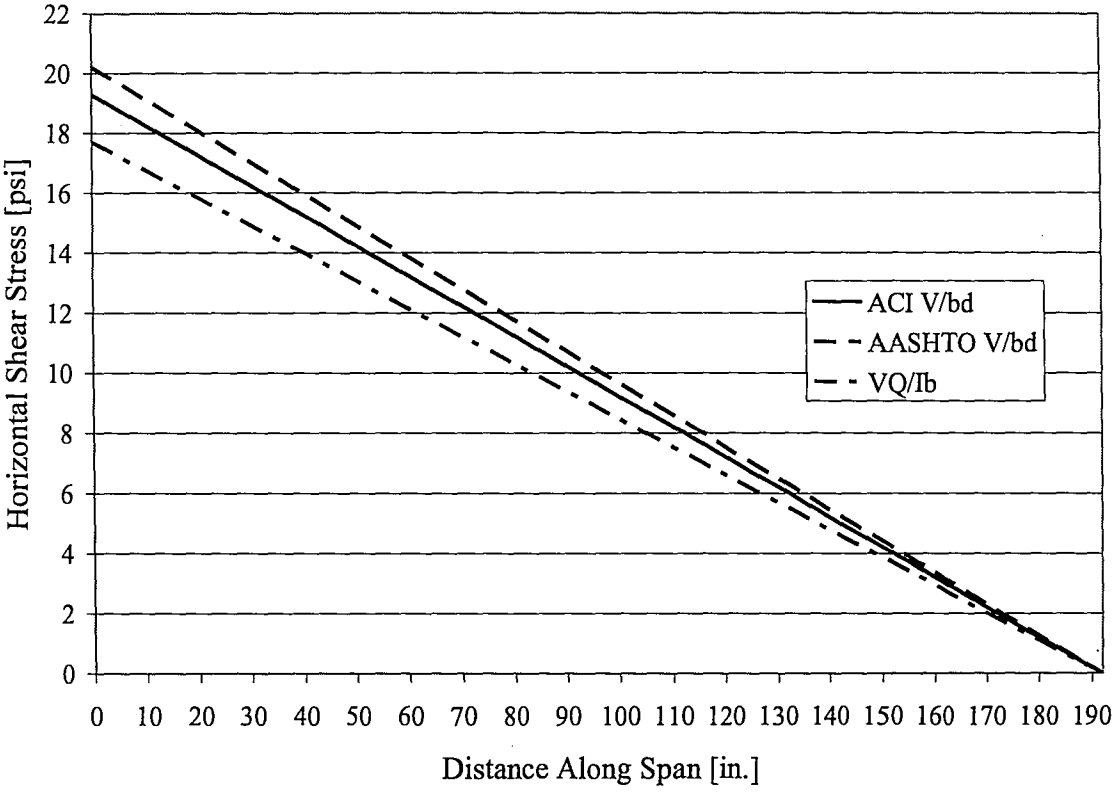

Figure 2-4: Comparison of Horizontal Shear Demand Equations

This graph compares the horizontal shear stress demand at service loads estimated by the simplified elastic beam behavior method for ACI (Eq. 3) and AASHTO (Eq. 4) along with the classical elastic method (Eq. 6). It can be seen that Equations 3 and 4 predict relatively similar values for the horizontal shear stress. This is because the only difference between the two methods is the value of the depth. For Equation 3 (ACI, 2008) the depth, d, is the distance from the top of the slab to the centroid of tension steel, while for Equation 4 (AASHTO, 2007) the depth, d_v, is the distance from the mid-thickness of the slab to the centroid of the tension steel.

This results in the AASHTO method providing a more conservative prediction of the horizontal shear stress for the sample beam.

For this section, the elastic method (VQ/Ib_v) predicts horizontal shear stresses lower than the simplified elastic beam behavior method. However, this prediction will vary based on the section dimensions and the resulting ratio of Q/I. Depending of the section properties, the classical elastic method will calculate horizontal shear stresses which are greater than, less than, or fall between those found by the ACI and AASHTO equations. Since the classical elastic equation is dependant on the section properties of a beam, it will result in a more accurate representation of the horizontal shear stresses of a composite member. For this reason, the classical elastic method was the primary equation used for this research program.

2.6 Summary

There are three general methods permitted by the ACI 318-08 and AASHTO LRFD Bridge Design Specifications (2007) codes for calculation of horizontal shear demands of a composite concrete beam. ACI (2008) permits the use of two of these methods while AASHTO (2007) allows the use of all three. A summary of the different methods for determining the horizontal shear stress demand is presented in Table 2-1.

Table 2-1: Horizontal Shear Stress Demand Methods

Horizontal Shear Stress Demand Method	**Equation**	**Code in Which This Method Is Allowed**
Global Force Equilibrium	$v_h = (C_1 - C_2)/(\ell \cdot b_v)$	ACI AASHTO
Simplified Elastic Beam Behavior	$v_h = V_u / b_v d$	ACI
	$v_{ui} = V_{u1} / b_{vi} d_v$	AASHTO
Classical Elastic Method	$v_h = VQ / Ib_v$	AASHTO

3 Previous Research

3.1 General

Previous research and observations of the horizontal shear capacity of composite concrete beams have been conducted since the 1950s. There were several experimental programs performed to determine the horizontal shear stress of a composite beam's interface. However, only a small portion (if any) of the specimens tested in these experiments did not have horizontal shear ties across the composite interface. In order to determine the potential horizontal shear stresses that can be achieved by the concrete cohesion and interlock alone, an extensive literature survey of past research was conducted.

3.2 Push-Off Tests and Beam Tests

There are two types of tests that have typically been performed to study the horizontal shear stress; specifically, push-off tests and beam tests. The push-off tests, in which a cast-in-place concrete element is pushed-off a precast concrete element, have been conducted by Hanson (1960), Seible (1990), Gohnert (2003), and others. Figure 3-1 shows a side view of a typical push-off specimen tested by Hanson (1960).

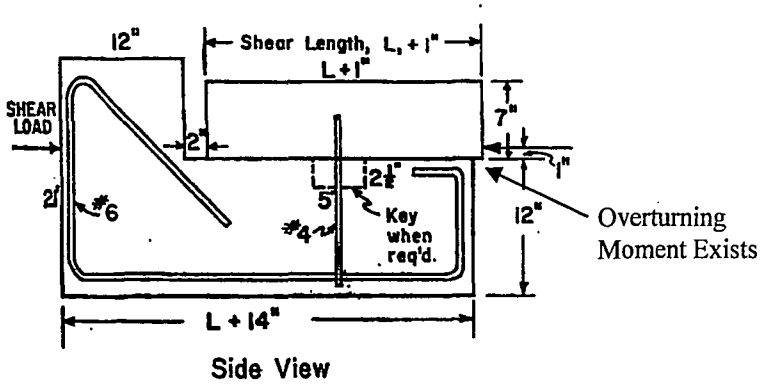

Figure 3-1: Side View of Hanson's Push-Off Test Specimen

Even though the push-off tests simplify the specimen fabrication and testing method, there are a few issues with this type of test that could affect its representation of actual beam behavior. The

shear loads which are applied to the specimen concentrically still produce some eccentricity between the location where the point load is applied to the cast-in-place element and where the forces are transferred to the precast element (Figure 3-1). This eccentricity will result in an overturning moment at the interface which would cause the cast-in-place element to pull away from the precast element near the edge where it is being loaded.

The push-off specimen can also experience areas of high stress concentration. A standard push-off specimen is shown in Figure 3-2a. Depending on the accuracy of the setup and boundary conditions, stress concentrations can occur resulting in a non-conservative estimate of the horizontal shear capacity. The stress concentrations are demonstrated by the finite element model shown in Figure 3-2b.

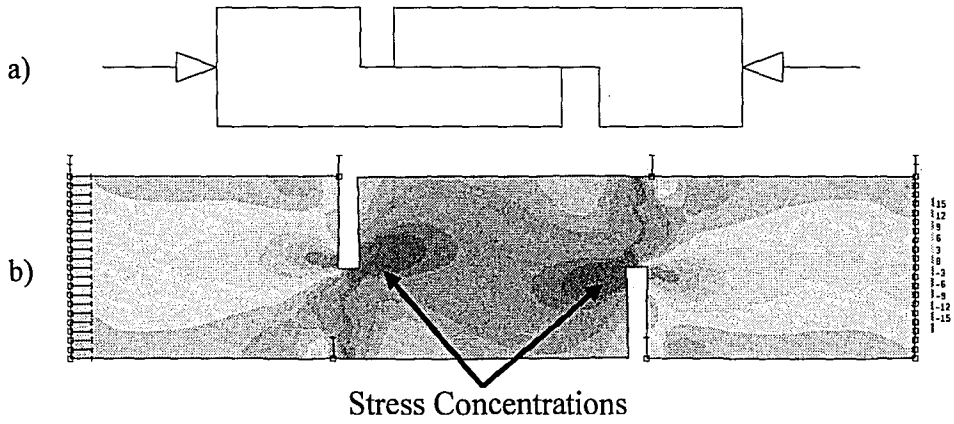

Figure 3-2: Push-off Test Specimen: a) Concentric loading; b) Non-uniform shear stress

Since the accuracy of the push-off tests cannot be certain, the proper way to assess the horizontal shear capacity is to evaluate the composite interface as part of a beam section. Therefore, only the results of the previous research of beam tests will be considered. The next several sections provide a detailed summary of previous research and the resulting test data for the horizontal shear stress of composite concrete beams without horizontal shear ties.

3.3 Revesz (1953)

Revesz tested five composite T-beams as shown in Figure 3-3. Four of the beams were prestressed with high tensile strength wire (specimen L, J, G, and F) and one was reinforced with mild steel (specimen N). For all the beams, the roughness of the web surface was smooth, and there were no shear ties across the interface. The load was applied at the third-points of the 14 foot beam. The estimated ultimate loads were exceeded in every case. Out of the five beams, four failed in flexure and one in horizontal shear (specimen J). At the time of the test, the concrete cylinder strength of specimen J was approximately 2480 psi for the cast-in-place flange and 5225 psi for the precast web. The age of the concrete at the time of the test was 4 days for the cast-in-place flange and 85 days for the precast web.

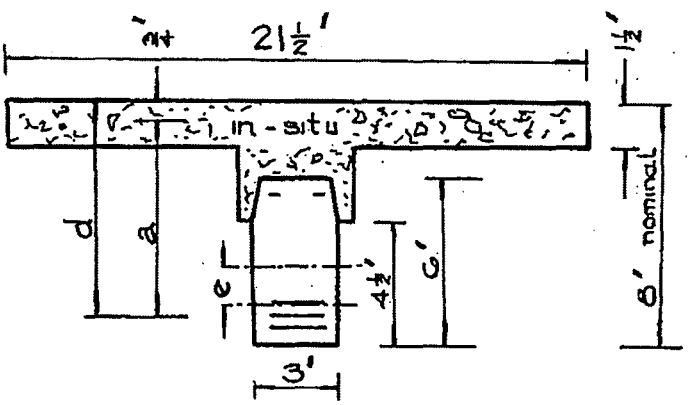

Figure 3-3: Cross-Section of Beam Tested by Revesz

There have been some discrepancies on the value of horizontal shear stress at which specimen J failed. Revesz reported that at failure "the calculated shear intensity was 134 psi." The ACI-ASCE Committee 333 (1960) listed the horizontal shear stress to be 122 psi while CTA-74-B6 (1974) and CTA-76-B4 (1976) reported the calculated horizontal shear stress (using VQ/Ib_v) to be 143 psi and 157 psi, respectively. Using the information provided and the equation $v_h = VQ/Ib_v$, the horizontal shear stress was calculated to be approximately 137 psi.

Overall, Revesz suggested that "it is desirable to roughen contact surfaces of the precast web and cast-in-place concrete of composite beams, or even introduce shallow serrations, to prevent failure by horizontal shear."

3.4 Hanson (1960)

Hanson tested ten T-shape composite girders of which two did not have shear ties crossing the interface. One of the beams had a rough interface (specimen BR-I) and the other was cast monolithically (specimen M-I). The purpose of this experimental program was to study the process of horizontal shear transfer. The test variables included surface bond, roughness, the effect of keys, and the effect of stirrups. The girders were "designed in such a way that the horizontal shear at the girder/slab contact surface reached high values at loads well below flexural failure." The section was designed so that the neutral axis of bending strains was near the contact surface. The cross-section of the girder can be seen in Figure 3-4. There were two series of tests. It can be seen in Figure 3-4 that for the second series Hanson reduced the area of the interface in order to increase the value of the horizontal shear stress. Hanson reported that "the calculation of the horizontal shear stress was based on the equation $v = VQ/Ib_v$, in which Q is the first moment about the neutral axis of all areas from the horizontal section considered to the extreme compression edge. This equation was applied to the contact surface section, considering the cracked transformed cross section of the T-shaped composite girder, and the resulting relationship between shearing force and shearing stress was used in relating stress to slip."

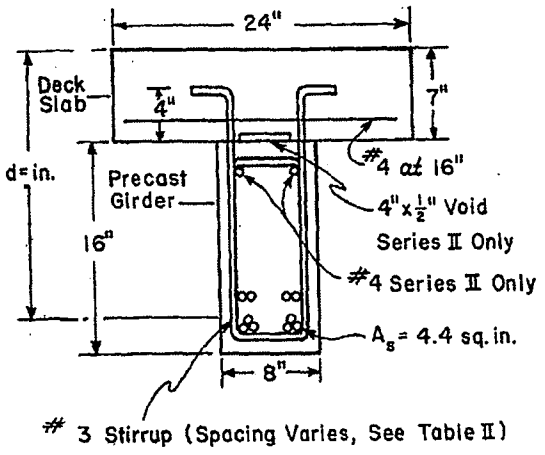

Figure 3-4: Cross-Section of Beam Tested by Hanson

The beams were cast as follows. The web was poured, consolidated and the contact surface was prepared. The beams were then wet cured for seven days followed by seven days of drying. At this point, the top deck was cast. Another cycle of seven days wet curing and seven days drying preceded the testing of the composite girder. At the time of the test, the concrete cylinder strength of specimen BR-I was 3170 psi for the cast-in-place slab and 4200 psi for the precast web. The surface finish of BR-I was recorded as being rough.

The series of tests including BR-I were tested over a 145 inch simple span with two loads 25 inches apart as seen in Figure 3-5. The girders failed in a manner described as "a shear-compression failure preceded by loss of composite action." It was reported that flexural cracks progressed upward from the bottom of the girder until they reached the interface. At this point, the cracks traveled along the joint for a short distance. Hanson did not give a calculated value for the horizontal shear stress at ultimate load, but Figure 15 of the original paper shows that at a slip of 0.005 inches the horizontal shear stress was approximately 310 psi. Hanson concluded from his beam and push-off tests that the maximum shearing stress for a rough bonded surface is 500 psi and that for a smooth bonded surface is 300 psi. He also stated that "a slip of 0.005 in. seems to be a critical value beyond which composite action is rapidly destroyed."

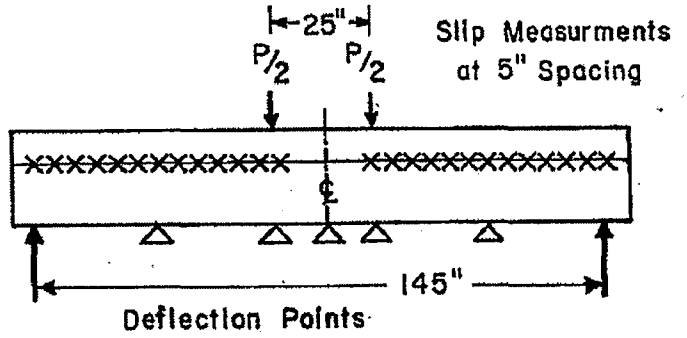

Figure 3-5: Elevation View of Test Setup for Hanson's Tests

3.5 Saemann and Washa (1964)

Saemann and Washa tested 42 composite T-beams of which two did not have any horizontal shear ties crossing the interface (specimen 15C and 16C). The beams were designed so that "high horizontal shear values at the contact surface were reached at loads well below those required for flexural failure." The cross-section of the girder can be seen in Figure 3-6. The span for beams 15C and 16C were 11 feet and 8 feet, respectively. The horizontal shear stress was calculated by the equation $v = VQ/Ib_v$ and based on cracked section properties.

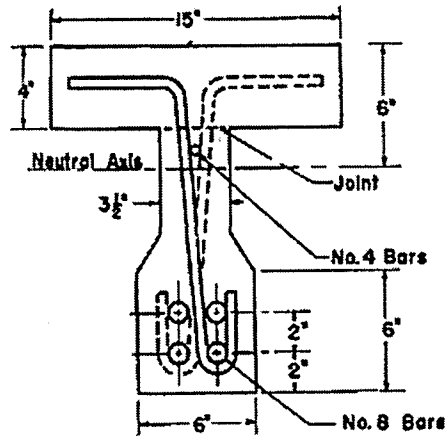

Figure 3-6: Cross-Section of Beam Tested by Saemann and Washa

After the webs were poured, the surface finish was applied. Beams 15C and 16C had what was described as an intermediate roughness. This surface finish was obtained by using a retarding agent "to enable brushing out the mortar between the pieces of course aggregate." This process

resulted in surface depressions that were 1/8 in. deep. Seven days after the webs were made the slabs were cast. The concrete strength of specimen 15C was 3220 psi for the cast-in-place slab and 3030 psi for the precast web. For specimen 16C, the concrete strength was 3060 psi for the cast-in-place slab and 3030 psi for the precast web.

The beams were loaded with two points load; each at one foot to the left and the right of the center of the beam. Beams 15C and 16C were reported at ultimate load to have reached horizontal shear values of 420 psi and 606 psi, respectively. However, at this point, significant slip of the interface had already taken place. Saemann and Washa also reported the horizontal shear stress at an interface slip of 0.005 in. was 329 psi and 443 psi for beams 15C and 16C, respectively. It was not stated exactly when the composite interface failed or at what value of horizontal shear stress. The authors did mention that non-composite action was observed before ultimate load. Therefore, the horizontal shear values at an interface slip of 0.005 in. will be considered as a conservative estimate of when the beam lost their composite behavior.

Saemann and Washa presented the following equation for the ultimate shear strength (Y) without shear ties:

$$Y = \frac{2700}{X+5} \qquad \text{(Eq. 7)}$$

where,

X = the ratio of shear span to effective depth

This equation is the same as the one previously recommended by Mattock and Kaar (1961) for their series of tests of composite beams with horizontal shear ties.

3.6 Bryson, Skoda, and Watstein (1965)

This series of tests was focused on the flexural behavior of prestressed split beams. The specimens consisted of 6 post-tensioned, prestressed composite beams constructed by the split-beam method. The split-beam method consists of only prestressing the cross-sectional area that is usually subjected to tension in bending. Therefore, the tension portion of the web is precast and prestressed, and then the compression section is cast-in-place on top. This type of fabrication results in the neutral axis being located at the interface. The test specimens included three types of prestressed split beams designated A, B, and C as shown in Figure 3-7. Shear connects were not provided across the interface of the two concrete elements. The surface roughness was applied with a stiff wire hand brush to the extent that the largest size aggregate was exposed.

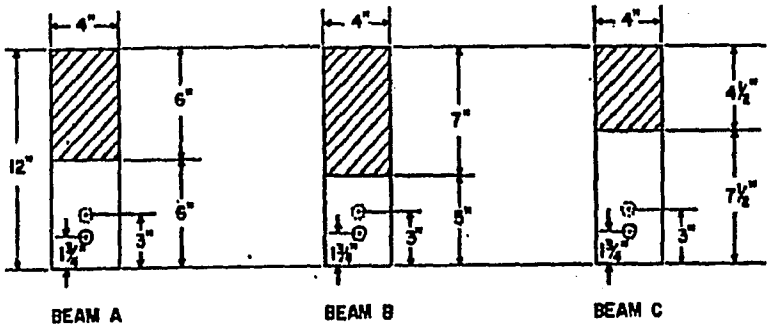

Figure 3-7: Cross-Section of Beam Tested by Bryson and Carpenter

The specimens were tested simply supported over a length of 9 feet with loads applied at the third points. Strain gauges were used to measure longitudinal concrete strains in the beam during loading. All the specimens failed in flexural compression which was described as "crushing of the concrete in the region of constant moment above a flexural crack which has reduced the area available for resisting compressive stresses." The strain gauges showed a linear distribution of strains over the cross-section which indicated composite action of the interface throughout the test. At the ultimate load, the horizontal shear stress ranged from 304 – 328 psi. These values

were calculated using VQ/Ib_v; however, the authors did not state if these calculations considered cracked, uncracked, or transformed sections properties.

The authors concluded by stating that the "procedure that was used for combining the two elements of the split beams proved to be adequate for the development of sufficient bond for monolithic beam action throughout the test."

3.7 Evens and Chung (1969)

The purpose of this series of test was to determine the affect of lightweight aggregate to horizontal shear failure. Since lightweight aggregates are softer than normal weight aggregates, the interlocking action will not produce as much resistance to horizontal shear, posing a larger danger of horizontal shear failure.

Five prestressed, composite T-beams were tested. The beams consisted of a prestressed granite concrete web and a lightweight concrete flange. The cross-section of the beam is shown in Figure 3-8. One of the five beams did not have horizontal shear ties across the interface (Beam 1). The interface condition of the web was "an exposed-aggregate surface prepared by wet-brushing the top surface of the granite concrete before it hardened." The concrete strength of Beam 1 was 3826 psi for the cast-in-place lightweight flange and 6900 psi for the precast web.

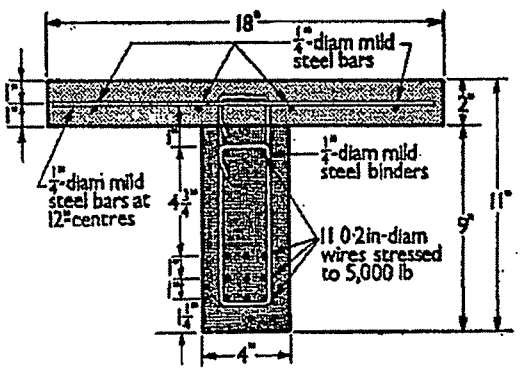

Figure 3-8: Cross-Section of Beam Tested by Evans and Chung

were calculated using VQ/Ib_v; however, the authors did not state if these calculations considered cracked, uncracked, or transformed sections properties.

The authors concluded by stating that the "procedure that was used for combining the two elements of the split beams proved to be adequate for the development of sufficient bond for monolithic beam action throughout the test."

3.7 Evens and Chung (1969)

The purpose of this series of test was to determine the affect of lightweight aggregate to horizontal shear failure. Since lightweight aggregates are softer than normal weight aggregates, the interlocking action will not produce as much resistance to horizontal shear, posing a larger danger of horizontal shear failure.

Five prestressed, composite T-beams were tested. The beams consisted of a prestressed granite concrete web and a lightweight concrete flange. The cross-section of the beam is shown in Figure 3-8. One of the five beams did not have horizontal shear ties across the interface (Beam 1). The interface condition of the web was "an exposed-aggregate surface prepared by wet-brushing the top surface of the granite concrete before it hardened." The concrete strength of Beam 1 was 3826 psi for the cast-in-place lightweight flange and 6900 psi for the precast web.

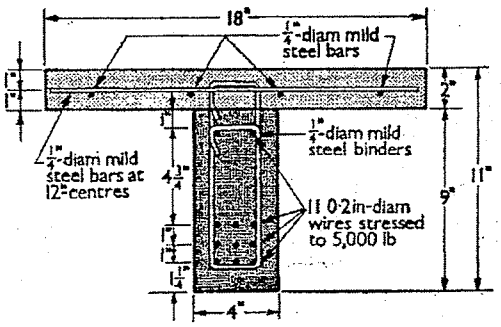

Figure 3-8: Cross-Section of Beam Tested by Evans and Chung

The test setup consisted of the beam being simply supported over a span of 7ft 6 in. The beam was loaded at two points 2 feet apart and symmetric about the midspan. Beam 1 failed suddenly in horizontal shear at a stress of 460 psi. The authors concluded that the horizontal shear strength of a rough surface finish without shear ties for a precast granite concrete web and a cast-in-place lightweight concrete flange is 400 psi. Above this value, the interface begins to deteriorate. Evens and Chung stated that horizontal shear failures "occur suddenly and should be avoided."

3.8 Bryson and Carpenter (1970)

This series of tests consisted of 22 prestressed composite T-beams constructed by the split-beam method. The cross-section of the split-beam is shown in Figure 3-9.

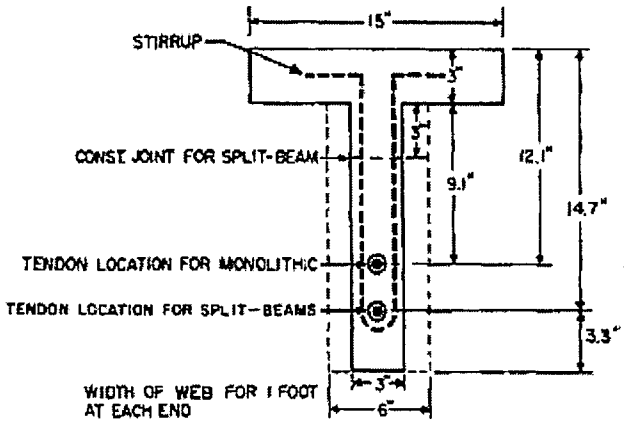

Figure 3-9: Cross-Section of Beam Tested by Bryson and Carpenter

Studying the interface of composite sections was not the main objective of this series of tests. However, 11 of the 22 composite beams did not have reinforcement across the interface. The surface roughness of the interface was not mentioned in the report. The beams were tested over a simply supported span of 18 feet and loaded at two points as seen in Figure 3-10. Of the 11 beams without interface reinforcement, only one failed by "complete separation of the interface of the tension and compression elements in the shear zone under load" (beam SG-2). The

strength of the concrete at the time of testing for SG-2 was 2400 psi for the top compression section and 4800 psi for the bottom tension section.

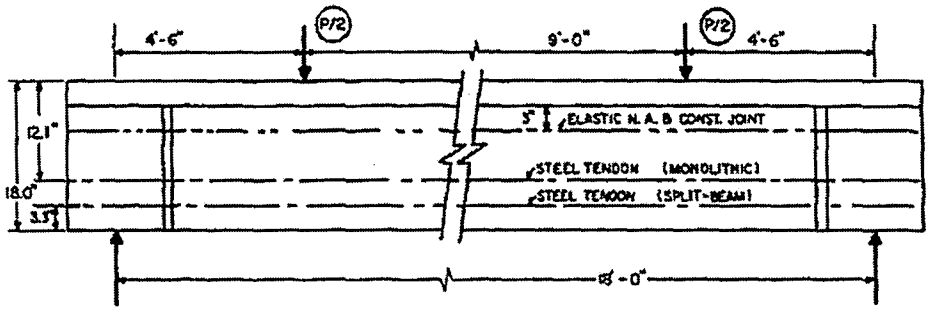

Figure 3-10: Elevation View of Loading Setup for the Split-Beam Tests

The horizontal shear stresses were not calculated in this report. However, a later study by CTA (1976) in their Technical Bulletin 76-B4 stated that "specimen SG-2 failed in horizontal shear at a calculated stress of 324 psi, while all other [specimen without interface reinforcement] failed in different modes at maximum shearing stresses ranging from 295 to 482 psi."

3.9 Nosseir and Murtha (1971)

The purpose of this series of tests was to study the horizontal shear resistance and behavior of prestressed, composite concrete beams where the interface is located at the neutral axis of the section. The eight simply supported composite members in this study were split-beams. Two of the eight beams did not have horizontal shear ties across the interface (specimen R0.0 and S0.0). Specimens R0.0 (rough interface) and S0.0 (smooth interface) failed in horizontal shear at calculated stresses of 565 psi and 469 psi, respectively. Nosseir and Murtha stated that the horizontal shear resistance of the test beams failing in horizontal shear was much higher than the recommended values based on the ACI code.

3.10 Concrete Technology Associates Technical Bulletin 74-B6 (1974)

The purpose of this CTA report was to "examine the concept of composite systems without roughness, particular attention being directed toward the performance of such systems under

service and cracking loads and the ability of composite beams to achieve the ultimate flexural capacity of a monolithic beam of identical properties." The report begins by presenting a comprehensive survey of all the previous research in this area.

The report then lays out the plan for a series of tests to study the performance of 16 prestressed composite beams without ties. The following parameters were taken into account: degree of contact surface roughness, surface condition before casting the slab, and the strength and density of the topping concrete. The specimens were designed to simulate the behavior of composite single and double tees or other members that have a thin topping and a wide contact surface. The design of the precast beam and the cast-in-place slab are shown if Figure 3-11. The spans of the beam were either 4 feet (S series) or 9 feet (L series) in length. The surface roughness varied from smooth to rough.

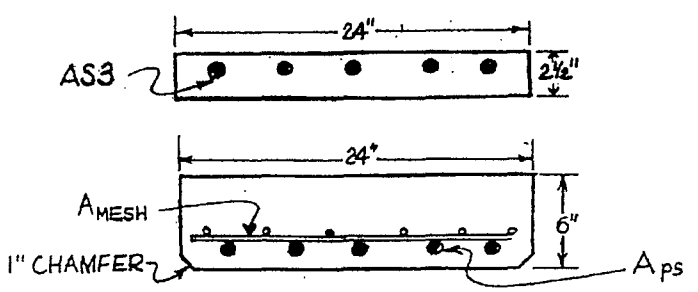

Figure 3-11: Cross-Section of Beam Tested by CTA-74-B6

The beams were loaded by a single concentrated load at midspan. Of the 16 beams, two failed in horizontal shear. Using the equation VQ/Ib_v, specimen S-7-S and S-8-S failed at a horizontal shear stress of 429 psi and 398 psi, respectively. Specimen S-7-S had an interface condition that was clean with a smooth and sandblasted finish. Specimen S-8-S had a surface finish described as "smooth-cement slurry-clean." The strength of the topping concrete was 5500 psi and 4060 psi for specimen S-7-S and S-8-S, respectively. The remaining fourteen specimens failed in shear,

flexure, or shear-flexure and at the time of failure had horizontal shear stresses of 139 psi to 477 psi.

For this series of tests, it was found that all of the beams failed at loads above those allowed by the code for monolithic members of the same dimension. Also, no apparent correlation exists between the degree of roughness at the interface and the observed ultimate moment. All of the beams exhibited full composite action with the range of working loads, regardless of the degree of surface roughness for the interface.

3.11 Concrete Technology Associates Technical Bulletin 76-B4 (1976)

Similar to the previous CTA report, a survey was conducted on the available past data of the horizontal shear strength of composite concrete beams without interface reinforcement. An additional series of tests were also carried out at the CTA laboratories. Using this data, recommendations for the design of composite concrete flexural members without ties were presented.

The test report was titled, "Strength of Bonded and Partially Bonded Composite Beams without Ties." The primary objective of the series of tests carried out by CTA was to "determine the ultimate strength of composite beams without ties, as measured by the maximum horizontal shear stress across the interface between the two [composite concrete] elements." Secondary objectives of the test series included the following:

1. Determine how construction procedures influence the degree of bond.
2. Determine how the bond effects the development of horizontal shear strength.
3. Determine how the roughness of the interface influences the horizontal shear strength of the composite joint.

4. Determine the effect that the shear span-effective depth ratio, the topping thickness-effective depth ratio, and the concrete strength and density have on the horizontal shear strength in composite flexural members without ties across the interface.

5. Develop a practical method for computing the horizontal shear stress of prestressed concrete members under conditions corresponding to ultimate loading.

In order to achieve the objectives, twenty-one prestressed composite beams without shear ties were fabricated and tested. Several different variables were taken into account when designing the specimen. The following were the variables included in the test program:

1. *Specimen Length:* 12-ft or 20-ft.

2. *Contact Surface Finish:* Wood float ($^1/_{16}$" roughness) or rough raked (¼" roughness).

3. *Topping Thickness:* 2 in., $3^5/_8$ in., 4 in., or $5^5/_8$ in.

4. *Topping Strength and Density:* 2500 to 5000 psi strength concrete, 115 or 150 pcf density.

5. *Contact Surface at Time of Topping Placement:* Dry or saturated, clean or oiled (to simulate poor, unsupervised construction practices).

6. *Compaction of Topping Concrete:* No compaction or full compaction.

The cross sections of the test specimens are shown in Figure 3-12. P-1 was the only specimen that was designed to the dimensions of the second cross-section shown in Figure 3-12. This beam was also the only one of the test specimens not constructed to achieve partial bond across the interface. All the rest of the specimens were fabricated to simulate poor construction practices. This task was accomplished by fabricating the topping under the following conditions:

1. *Dry Mix – No Consolidation*: A low slump concrete was cast without vibration.

2. *Wet Mix – Surface Saturated*: The top surface of the bottom beam was saturated with the maximum amount of free standing water that was possible. On top of this, a high slump mix was cast and vibrated.

3. *Dry Mix – Surface Oiled*: Oil was applied lightly or heavily to the top surface of the bottom beam. On top of this, a low slump mix was cast and vibrated.

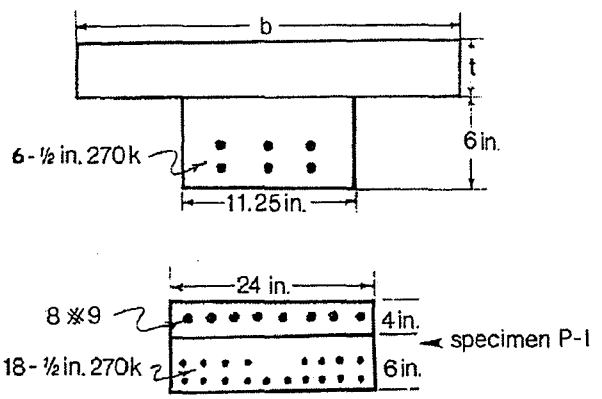

Figure 3-12: Cross-Section of Beams Tested by CTA-76-B4

The beams were tested over a simply supported span and loaded at their third point, except for specimen P-1 which was loaded with a single point load at midspan. Eleven of the twenty-one beams failed due to loss of composite action. The horizontal shear stress was calculated using the equation VQ/Ib_v and uncracked transformed section properties. Table 3-1 presents a summary of the test variable and horizontal shear stress values for all of the beams tested.

SPECIMEN	LENGTH (ft)	X[1]	TOPPING					SURFACE FINISH[2]	CONSTRUCTION METHOD[3]	FAILURE MODE[4]	MAXIMUM LOAD P_u (kips)	MAXIMUM SHEAR STRESS	
			THICKNESS t (in.)	WIDTH b (in.)	DENSITY (pcf)	STRENGTH f'_{ct} (psi)	SLUMP AT PLACEMENT (in.)					$\frac{V_u Q}{Ib}$ (psi)	$\frac{V_u}{bd}$ (psi)
P-1	10	8	4.00	24.00	154	4340	4	I	1	H S	104.4	339	295
SCF-2	12	9	2.00	11.25	150	4300	2	I	2	H S	16.5	100	147
SRC-2	12	9	2.00	11.25	150	4800	2	R	2	COMPR	30.0	169	257
SFC-4	12	6	4.00	11.25	150	4900	2	I	2	H S	36.9	233	231
SRC-4	12	6	4.00	11.25	150	4900	2	R	2	H S	45.0	283	280
SFD-2	12	9	2.00	11.25	113	2430	7	I	3	COMPR	26.8	103	231
SRD-2	12	9	2.00	11.25	113	2700	7	R	3	COMPR	26.8	107	231
SFD-4	12	6	4.00	11.25	113	3440	7	I	3	COMPR	42.5	234	264
SRD-4	12	6	4.00	11.25	113	3440	7	R	3	COMPR	42.5	234	264
LFC-3	20	11	3.63	20.88	155	3820	4	I	2	H S	10.1	88	84
LRC-3	20	11	3.63	20.88	155	3820	4	R	2	H S	20.4	156	149
LFC-5	20	9	5.63	20.88	155	4090	4	I	2	H S	23.6	158	136
LRC-5	20	9	5.63	20.88	155	4090	4	R	2	H S	36.3	231	199
LFD-3	20	11	3.63	20.88	153	2790	6	I	4	COMPR	30.0	217	210
LRD-3	20	11	3.63	20.88	153	3440	6	R	4	COMPR	31.2	226	218
LFD-5	20	9	5.63	20.88	153	2790	6	I	4	COMPR	41.0	258	222
LRD-5	20	9	5.63	20.88	153	2850	6	R	4	COMPR	45.7	285	245
LFE-3	20	11	3.63	20.88	156	3970	4	I	5	H S	14.0	114	109
LRE-3	20	11	3.63	20.88	156	3970	4	R	5	COMPR	35.0	253	242
LFE-5	20	9	5.63	20.88	156	3420	4	I	5	H S	14.0	103	89
LRE-5	20	9	5.63	20.88	156	3970	4	R	5	H S	42.5	267	230

[1]Shear span to effective depth ratio

[2]I: Intermediate (wood float) finish
R: Rough (raked) finish

[3]1: Surface clean and dry, topping vibrated
2: Surface clean and dry, topping not vibrated
3: Surface saturated (ponded), topping vibrated
4: Surface wiped and sprayed lightly with oil, topping vibrated
5: Surface brushed with heavy coat of oil, topping vibrated

[4]H S: Horizontal shear failure
COMPR: Flexural compression failure

Table 3-1: Summary of the CTA-76-B4 Test Series

The conclusions the authors made on the test series are as follows:

- The two factors that seemed to prevent a bond from forming were "a heavy coating of oil and the combination of a stiff, dry mix and the lack of consolidation." The bond was not affected by the presence of a light film of oil or the use of a high slump mix with a saturated surface.
- Full bond appears to contribute approximately 230 psi to the horizontal shear strength.
- The contribution of the interface roughness to the horizontal shear strength corresponding to a wood float (intermediate) finish is approximately 100 psi and a rough rake finish is approximately 200 psi.
- The ratio of shear span to effective depth did not seem to have an effect on the horizontal shear strength.
- Specimens with a thicker topping achieved a higher value of horizontal shear than the similar specimens with a thin topping.

Based on the data gathered from this test series along with past research data, the following recommendations for the design of composite concrete flexural members without ties is presented by CTA.

Design Value of Horizontal Shear Stress due to Factored Loads: The horizontal shear stress may be calculated as either

$$v_{dh} = {V_u Q}/{\phi I b_v} \qquad \text{(Eq. 8)}$$

or

$$v_{dh} = {V_u}/{\phi b_v d} \qquad \text{(Eq. 9)}$$

For these equations, ϕ is 0.75 for shear. Equations 8 and 9 are similar to equations 6 and 3, respectively.

For simply supported composite construction, the calculated horizontal shear stress shall not be less than the smaller of:

$$v_{dh} = \frac{T_u}{\frac{\ell}{4} b_v} \qquad \text{(Eq. 10)}$$

and

$$v_{dh} = \frac{C_u^*}{\frac{\ell}{4} b_v} \qquad \text{(Eq. 11)}$$

For these equations: T_u is the full breaking strength of the longitudinal reinforcement below the interface, C_u* is the full crushing strength of the concrete and reinforcement above the interface, and ℓ is the span length. The author states that a reasonable distance to develop these forces is one-quarter of the span. This method is permitted in the ACI code (2008) Section §17.5.4.

Horizontal Shear Strength and Roughness: "When no ties across the interface are provided, but the contact surface is clean and the topping concrete is properly consolidated, the following values of horizontal shear strength may be assumed in design:"

- **Smooth Contact Surface– 90 psi**
- **Intermediate Contact Surface– 160 psi:** For this surface roughness, the contact surface is either "finished by a wood float or vibrating screed; or retarded and brushed, leaving irregularities of not less that 1/16 in. from peak to trough."

- **Rough Contact Surface – 300 psi:** For this surface roughness, "the contact surface has been raked, scarified, or retarded and brushed leaving irregularities of not less than ¼ in. from peak to trough."

The values of horizontal shear strength are acquired by taking the specimen of each surface roughness from previous research that failed in the lowest horizontal shear stress and applying a factor of safety of approximately 2.

Unsupervised Construction: The values of horizontal shear strength given before shall be reduced by a factor of 0.5 for unsupervised construction. This reduction is based on the tests and results of the test series conducted by CTA (1976).

Slab on Narrow Rectangular Beams: Due to large twisting moments that could occur for composite beams consisting of wide slabs cast on narrow rectangular sections, the interface of the two elements could crack. Therefore, shear ties should be considered for these beams.

3.12 Patnaik (1999)

Patnaik tested nine composite beams with an as-placed surface finish and no shear ties across the interface. The concrete strengths for the flange and web along with the interface width were varied for the beams. The specimens were designed to be strong in diagonal shear and flexure so that they would fail in horizontal shear. The typical cross-section and reinforcement detail are shown in Figure 3-13.

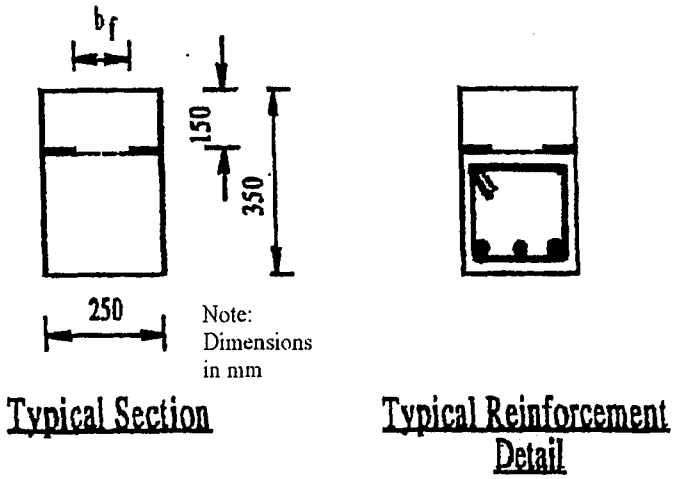

Figure 3-13: Cross-Section of Beams Tested by Patnaik

The specimens were fabricated to simulate a composite beam with a precast girder and cast-in-place flange. The web concrete was placed and allowed to set for three days before the flange concrete was cast. There were some problems achieving the desired as-placed surface finish which would leave coarse aggregate protruding from the interface. The slump of the concrete mix was reported to be too high to develop the proper surface finish. Therefore, in order to try and obtain the adequate roughness "concrete was sprinkled firmly over the top surface (interface) of the web of test beams from a height of approximately 300 mm, and made rough by running fingers through the wet concrete." The author stated that the sprinkled concrete was able to become firmly fixed in the matrix of the web concrete.

For the test setup, the beams were simply supported over a span of about 8.2 ft and loaded with a single point load at midspan (Figure 3-14). Of the nine beams tested, eight failed in horizontal shear. The other beam failed by a triangular wedge of the concrete flange breaking off while the interface was still intact. The horizontal shear stresses were found using the global force equilibrium method ($v = C/b_v\ell$) and resulted in horizontal shear stresses ranging from 228 psi to 474 psi.

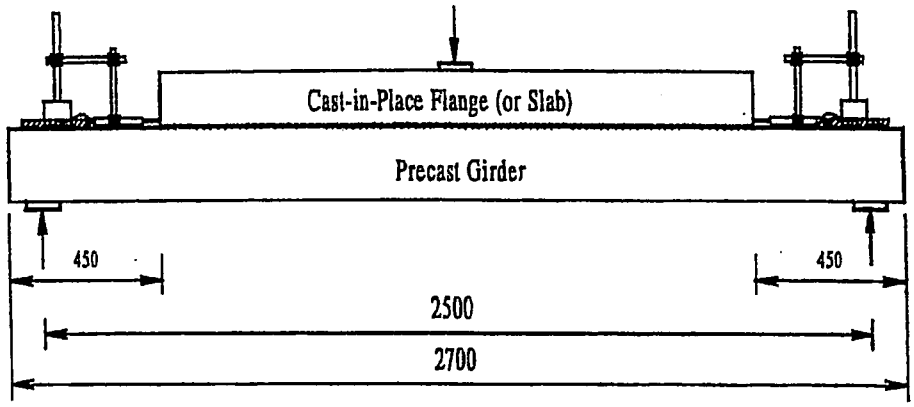

Figure 3-14: Elevation View of Loading Setup for the Beam Tests by Patnaik

Patnaik presented the following equation as a lower bound for finding the horizontal shear stress of composite beams without shear ties:

$$v_{uf0} = 0.35\sqrt{f'_c} \qquad \text{(Eq. 12)}$$

The value of f'_c is the concrete strength of the web or slab (whichever has the lower strength). The author states that the "use of this equation will result in a strength prediction which is well over two times of that of most design standards and codes, and will better utilize the strength of rough interfaces without ties."

3.13 Summary

As seen from the previous sections, a large number of tests have been completed on the horizontal shear stress of composite concrete sections without horizontal shear ties; some research being more substantial then others. Table 3-2 presents a summary of the results. It can be concluded from this table that most of the tests resulted in horizontal shear stresses that are well above those permitted in the current codes. The only exception is a few of the tests performed by CTA in 1976. However, these composite beams did not reach high horizontal shear levels because they were deliberately fabricated in a way that prevented a bond from occurring (i.e., not

consolidating the slab concrete, applying oil to the interface surface, etc.). Therefore, these stresses should be taken as an extreme lower bound of the horizontal shear capacity.

Table 3-2: Summary of Previous Research Results

ID	Surface Finish	f'_c [ksi]	Horizontal Shear Stress [psi]	Equation Used[5]	Section Properties Used	Event When Values Reported	Source
J	Smooth	2.48	134	a	Uncracked	Ultimate Failure	Revesz (1953)
BR-I	Rough	3.17	310	a	Cracked	Slip = 0.005"	Hanson (1960)
15C	Intermediate	3.03	329	a	-	Slip = 0.005"	Saemann and Washa (1964)
16C	Intermediate	3.03	443	a	-	Slip = 0.005"	Saemann and Washa (1964)
1	Rough	3.83[1]	460	-	-	Interface Failure	Evans and Chung (1969)
SG-2	-	2.4	324[2]	-	-	-	Bryson and Carpenter (1970)
R0.0	Rough	-	565[2]	-	-	-	Nosseir and Murtha (1971)
S0.0	Smooth	-	469[2]	-	-	-	Nosseir and Murtha (1971)
S-7-S	Smooth	5.5	429	a	Uncracked	-	CTA-74-B6 (1974)
S-8-S	Smooth	4.06	398	a	Uncracked	-	CTA-74-B6 (1974)
P-1	Intermediate	4.34	339	a	Cracked	-	CTA-76-B4 (1976)
SFC-2	Intermediate[3]	4.3	100	a	Cracked	-	CTA-76-B4 (1976)
SFC-4	Intermediate[3]	4.9	233	a	Cracked	-	CTA-76-B4 (1976)
SRC-4	Rough[3]	4.9	283	a	Cracked	-	CTA-76-B4 (1976)
LFC-3	Intermediate[3]	3.82	88	a	Cracked	-	CTA-76-B4 (1976)
LRC-3	Rough[3]	3.82	156	a	Cracked	-	CTA-76-B4 (1976)
LFC-5	Intermediate[3]	4.09	158	a	Cracked	-	CTA-76-B4 (1976)
LRC-5	Rough[3]	4.09	231	a	Cracked	-	CTA-76-B4 (1976)
LFE-3	Intermediate[4]	3.42	103	a	Cracked	-	CTA-76-B4 (1976)

ID	Surface Finish	f'_c [ksi]	Horizontal Shear Stress [psi]	Equation Used[5]	Section Properties Used	Event When Values Reported	Source
LFE-5	Intermediate[4]	3.97	114	a	Cracked	-	CTA-76-B4 (1976)
LRE-5	Rough[4]	3.97	297	a	Cracked	-	CTA-76-B4 (1976)
RR1.1	As-Placed	2.87	228	b	-	-	Patnaik (1999)
RR2.1	As-Placed	3.41	273	b	-	-	Patnaik (1999)
RR2.2	As-Placed	3.41	270	b	-	-	Patnaik (1999)
RR3.1	As-Placed	2.47	252	b	-	-	Patnaik (1999)
RR3.2	As-Placed	2.47	258	b	-	-	Patnaik (1999)
RHR1	As-Placed	9.05	463	b	-	-	Patnaik (1999)
RHR2	As-Placed	9.05	428	b	-	-	Patnaik (1999)
RHR3	As-Placed	9.05	474	b	-	-	Patnaik (1999)

Notes:

1. Lightweight concrete was used for the flange of the T-beam.
2. Horizontal shear values obtained from CTA-76-B4 because they were not stated in the authors paper.
3. Low slump mix used; no attempt to vibrate or consolidate the topping; only 50% of slab and bottom beam made contact at the interface.
4. Interface surface brushed with a heavy coat of oil before slab was cast.
5. Horizontal shear stress equation used: a. $v = VQ/Ib$; b. $v = C/lb$

There were several instances in the previous research where the composite beams, which in most cases were designed to fail in horizontal shear, ultimately failed in another mode. These specimens were able to act compositely above the ultimate capacity of the section. Table 3-3 summarizes the results of the specimen tests which did not fail in horizontal shear. The results illustrate that relatively high values of horizontal shear stress can be achieved while the section remains composite.

Table 3-3: Summary of Previous Research Specimen Not Failing in Horizontal Shear

ID	Failure Mode	Surface Finish	f'_c [ksi]	Horizontal Shear Stress at Failure [psi]	Source
A-1	Flexural Compression	Rough	4.77	328[1]	Bryson et al. (1965)
A-2	Flexural Compression	Rough	4.97	308[1]	Bryson et al. (1965)
B-1	Flexural Compression	Rough	5.34	311[1]	Bryson et al. (1965)
B-2	Flexural Compression	Rough	5.00	315[1]	Bryson et al. (1965)
C-1	Flexural Compression	Rough	5.29	306[1]	Bryson et al. (1965)
C-2	Flexural Compression	Rough	4.53	304[1]	Bryson et al. (1965)
S-1-I	Shear	Intermediate	3.64	302[1]	CTA-74-B6 (1974)
L-1-I	Shear	Intermediate	2.40	139[1]	CTA-74-B6 (1974)
S-2-I	Shear	Intermediate	3.96	356[1]	CTA-74-B6 (1974)
L-2-I	Flexure	Intermediate	4.76	169[1]	CTA-74-B6 (1974)
S-3-R	Shear Flexure	Rough - Dirty	4.76	477[1]	CTA-74-B6 (1974)
L-3-R	Shear Flexure	Rough - Dirty	5.08	168[1]	CTA-74-B6 (1974)
S-4-I	Shear Flexure	Intermediate	3.22	392[1]	CTA-74-B6 (1974)
L-4-I	Flexure	Intermediate	4.34	150[1]	CTA-74-B6 (1974)
S-5-I	Flexure	Intermediate - Dirty	4.76	421[1]	CTA-74-B6 (1974)
L-5-I	Flexure	Intermediate - Dirty	4.62	155[1]	CTA-74-B6 (1974)
S-6-R	Shear Flexure	Rough - Dirty	4.12	411[1]	CTA-74-B6 (1974)
L-6-R	Flexure	Rough - Dirty	5.45	158[1]	CTA-74-B6 (1974)
L-7-S	Flexure	Smooth	5.45	164[1]	CTA-74-B6 (1974)
L-8-S	Shear Flexure	Smooth - Cement Slurry	4.32	139[1]	CTA-74-B6 (1974)
SRC-2	Flexural Compression	Rough[2]	4.80	169	CTA-76-B4 (1976)
SFD-2	Flexural Compression	Intermediate[3]	2.43	103	CTA-76-B4 (1976)
SRD-2	Flexural Compression	Rough[3]	2.70	107	CTA-76-B4 (1976)
SFD-4	Flexural Compression	Intermediate[3]	3.44	234	CTA-76-B4 (1976)
SRD-4	Flexural Compression	Rough[3]	3.44	234	CTA-76-B4 (1976)
LFD-3	Flexural Compression	Intermediate[4]	2.79	217	CTA-76-B4 (1976)
LRD-3	Flexural Compression	Rough[4]	3.44	266	CTA-76-B4 (1976)
LFD-5	Flexural Compression	Intermediate[4]	2.79	258	CTA-76-B4 (1976)

ID	Failure Mode	Surface Finish	f'_c [ksi]	Horizontal Shear Stress at Failure [psi]	Source
LRD-5	Flexural Compression	Rough[4]	2.85	285	CTA-76-B4 (1976)
LRE-3	Flexural Compression	Rough[5]	3.97	253	CTA-76-B4 (1976)
RR1.2	Cracking of Flange	As-Placed	2.87	263[1]	Patnaik (1999)

Notes:

1. Not stated if the calculation of the shear stress considered cracked, uncracked, or transformed sections properties.
2. Low slump mix used; no attempt to vibrate or consolidate the topping
3. Surface saturated (ponding), topping was vibrated
4. Interface surface was wiped and sprayed lightly with oil before slab was cast
5. Interface surface brushed with a heavy coat of oil before slab was cast

Due to the fact that the previous research results come from tests with different beam designs, fabrication methods, testing conditions, and loading rates and locations, there is considerable difficulty in trying to quantify and formulate observations from the data. Also, for most of the experimental programs (if not all) the composite sections experienced some flexural cracking before the interface failed. Therefore, the classical elastic equation for calculating the horizontal shear stress ($v = VQ/Ib_v$), which was used for a majority of the experimental programs, cannot be considered an exact representation of the actual horizontal shear stress since this equation is based upon the uncracked, linear elastic properties of the composite section. It has been suggested by Hanson (1960) that this equation be implemented with the cracked section properties of Q and I and used as a common basis for comparison. Some of the following researchers took Hanson's advice while others either used uncracked section properties or did not mention their method of calculation. Since the method in which the classical elastic equation is utilized varies between the experimental programs, it is difficult to make an accurate comparison the previous research results.

When analyzing the previous research, another problem arises due to the fact that the horizontal shear stress at the instance the composite interface fails is sometimes not clearly stated. This

indistinct reporting of data can result in inaccurate interpretation of the horizontal shear stress. An example of this is seen in the test performed by Hanson (1960). Hanson never explicitly stated the horizontal shear stress at which the composite interface failed. He did provide graphs of shear stress versus deflection and shear stress versus slip (Figure 3-15) from which a few authors from following research projects pulled the horizontal shear failure value. The value the authors selected from the graph for specimen BR-I was 350 psi which occurred at the ultimate load and a slip value of 0.02 inches. However, Hanson stated in this paper that the contact surface stops acting compositely at a slip of 0.005 inches which corresponds in the graph to a shear stress of 310 psi (Figure 3-15). Another instance is in the report by Saemann and Washa (1964) in which the authors tabulate the calculated values of the horizontal shear at an interface slip of 0.005 in. and at ultimate load but never state exactly when the interface failed. The value at ultimate load can be chosen, but again this value occurs at a substantial value for interface slip. Therefore, one must be cautious when analyzing the results of the previous research.

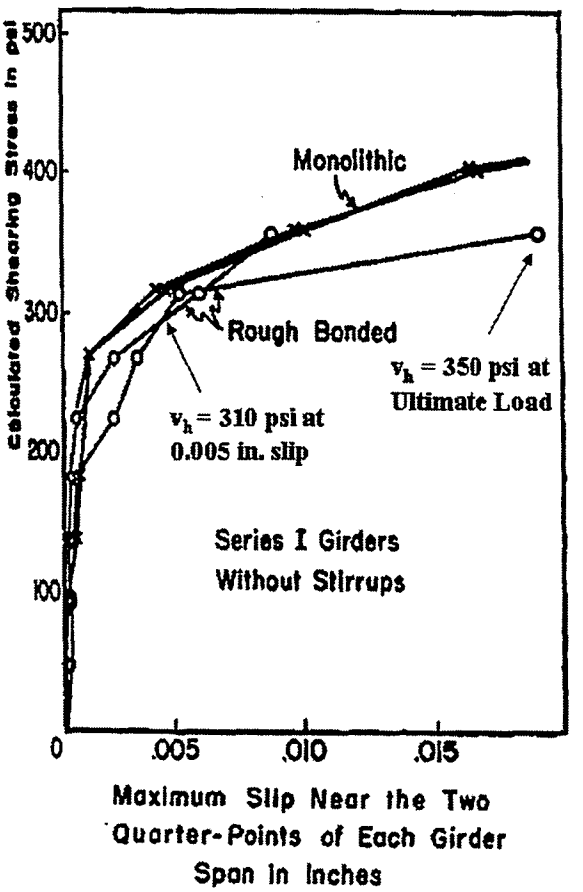

Figure 3-15: Shear Stress versus Slip from Hanson's (1960) Test Series

Conclusions on the behavior of the non-reinforced interface of composite concrete beams can be formulated from the test series which incorporated several specimens of the same design and method of calculating the horizontal shear stress; such as those of CTA (1976) and Patnaik (1999). From the observations made by the authors of the previous research a few conclusions can be drawn about the influence of roughness, surface conditions, and concrete strength on the horizontal shear strength capacity.

Surface Roughness of Interface – Research indicates that the surface roughness of the interface is one of the main factors that influence the horizontal shear strength of composite concrete beams. In general, it was found that with an increase of surface roughness from smooth up to a roughness of ¼ inch there is an increase in the horizontal shear capacity for the section (Hanson, 1960; Saemann & Washa, 1964; CTA, 1976).

Surface Conditions – Poor construction practices such as leaving dirt, oil, or other materials on the interface before the topping is cast, the use of a low slump mix, and neglecting to consolidate the topping can decrease the bond of the composite interface (CTA, 1976). However, it should be noted that the beams that failed in horizontal shear due to these poor construction practices consisted of a heavy coat of oil across the interface allowing for only about 50% of the interface to bond. Another series of beams in the CTA 1976 test series that had only a light coating of oil did not fail in horizontal shear. Similarly, the CTA 1974 test series had six specimens with dirty interfaces that consisted of dust, oil, and paper being scattered before the topping was cast. None of these beams failed in horizontal shear thus proving that even though there is a possibility of affecting the bonding capability by poor construction practices, the composite interface is still able to produce sufficient bonds a majority of the time.

Concrete Strength – Tests have shown that with an increase in compressive strength, there is an increase in horizontal shear capacity (Saemann & Washa, 1964; Patnaik, 1999). This trend can be observed by looking at the data for Patnaik's tests in Table 3-2. The interface shear capacity of a composite member is usually limited by the concrete with the lower compressive strength (usually the slab concrete).

Even though these observations help in understanding the effects that different variables have on the horizontal shear stress, there is still a limited amount of repeatable data on the subject. Therefore, further research must to be conducted in order to validate the horizontal shear capacity of composite concrete members.

4 Horizontal Shear Stress Capacity

4.1 General

The first recommendations for the design of composite beams were made by ACI-ASCE Committee 333 in 1960. This committee used the test results of nine composite beams which were reported to have failed in horizontal shear to make their recommendations. The tests were conducted by Revesz (1953), Ozell and Cochran (1956), Kaar, Kriz, and Hognestad (1960), and Hanson (1960). Table 4-1 presents a summary of the horizontal shear failure results reported by ACI-ASCE Committee 333. From these test results, the committee recommended allowable bond stresses at working loads of 40 psi for smooth surfaces and 160 psi for rough surfaces. The allowable bond stresses at ultimate load were taken to be twice the stresses at working loads. These recommendations required that a minimum amount of shear ties be present across the interface of the beam to prevent separation of the elements in the direction normal to the contact surface. The recommendations of the committee were eventually integrated into the 1963 edition of ACI 318. Table 4-2, which was originally presented in a report by CTA (1974), provides a summary of the horizontal shear stresses recommended by ACI-ASCE Committee 333 and the resulting standards incorporated into the following two editions of ACI 318. It can be seen from this table that the standard for composite beams without interface reinforcement appeared in the 1963 edition of ACI 318 and that in the following edition the allowance of 80 psi was introduced. From this, it has to be assumed that the present-day requirement of 80 psi for an intentionally roughened contact surface without interface reinforcement derived from the recommendations made by ACI-ASCE Committee 333.

Table 4-1: Horizontal Shear Failure Results Reported by ACI-ASCE Committee 333

Specimen	Reference	Type of Joint Surface	Ties	Horizontal Shear Strength [psi]
BS-I	Hanson (1960)	Smooth	#3 - 6" O.C.	350
BS-II	Hanson (1960)	Smooth	#3 - 16" O.C.	340
A2	Ozell and Cochran (1956)	Smooth	None	78
C2	Ozell and Cochran (1956)	Smooth	#4 - 6" O.C.	100
A3	Ozell and Cochran (1956)	Smooth	None	119
J	Revesz (1953)	Smooth	None	122
BRS-I	Hanson (1960)	Rough	#3 - 6" O.C.	450
BRS-II	Hanson (1960)	Rough	#3 - 16" O.C.	580
III-0.6-1.66	Kaar, Kriz, and Hognestad (1960)	Rough	#3 - 6" O.C.	418

Table 4-2: Evolution of the Horizontal Shear Capacity Allowed by ACI [psi] (CTA, 1974)

Surface	Ties		ACI-ASCE 333 (1960)	ACI 318-63 (1963)	ACI 318-71 (1971)
Rough	None	Working	--	40	--
		Ultimate	--	76	80
Smooth	Min.	Working	40	40	--
		Ultimate	80	76	80
Rough	Min.	Working	160	160	--
		Ultimate	320	304	350

The validity of these recommendations made by ACI-ASCE Committee 333 is questionable. First, the value of the horizontal shear stress for the test conducted by Revesz (1953) was reported by the committee to be 122 psi even though it has been calculated using VQ/Ib to be approximately 137 psi. Additionally, for Ozell and Cochran's (1956) test series, the specimen's referenced by the committee never appeared in the original paper, and none of the test specimens were reported by Ozell and Cochran to have failed in horizontal shear or to have shear ties. For the data reported from Hanson's (1960) tests, it is unclear how the committee arrived at some of these values. As mentioned in the previous chapter, it is difficult to accurately determine the

value of the horizontal shear stress that represents the failure of the composite interface since it is not clearly stated by Hanson. The values reported by the committee for specimens BS-I and BRS-I appear to be the horizontal shear stress when the interface slip begins to increase. These values seem appropriate since an increase in slip would signify the failure of the interface. However, it is difficult to infer the reasoning behind the values chosen for specimens BS-II and BRS-II since they do no correlate with any specific event from the given data. Also, specimen BR-I, which did not have any interface reinforcement and failed at a horizontal shear stress of 310 psi, was not considered by the committee. With all of these discrepancies, it is difficult to draw any reliable conclusions from the data considered by ACI-ASCE Committee 333. Therefore, the current code requirements which are based on the committee's recommendations are also questionable and could be limiting the horizontal shear capacity of composite sections without ties to low levels.

Two standards are typically used when calculating the horizontal shear stress capacity for buildings and bridges; specifically, American Concrete Institute's ACI 318 standard and the American Association of State Highway and Transportation Officials LRFD Bridge Design Specification. Current recommendations used for estimating the interface shear capacity for these two standards are presented in the following sections.

4.2 American Concrete Institute (ACI) (2008)

The design approach for the horizontal shear capacity of a composite concrete beam is outlined in Section §17.5 of the ACI 318-08 standard. Addressing interface design in terms of forces, the code specifies that the factored horizontal shear force capacity, φV_{nh}, must exceed the factored vertical shear force demand, V_u. Although the horizontal shear capacity is defined for four different interface conditions, only one applies to an un-reinforced interface. As stated in ACI

Section §17.5.3.1, an interface that is "clean, free of laitance, and intentionally roughened" to a ¼ inch amplitude shall not have a capacity greater than:

$$V_{nh} = 80 b_v d \quad \text{(Eq. 13)}$$

where,

V_{nh} = the nominal horizontal shear strength [lb.]

b_v = width of the cross section at the contact surface being investigated for horizontal shear [in.]

d = the distance from the extreme compression force for the entire composite section to centroid of the prestressed and non-prestressed longitudinal tension reinforcement, if any, but need not be taken less than 0.80h for prestressed concrete members, where h is the height of the composite section [in.]

The horizontal shear stress is found by dividing the shear force by $b_v d$ thus resulting in:

$$v_{nh} = 80 \text{ psi} \quad \text{(Eq. 14)}$$

The value of the horizontal shear stress is constant for any contact surface width or depth from the extreme compression fiber to the centroid of the tension reinforcement.

4.3 American Association of State Highway and Transportation Officials (AASHTO) (2007)

Like the ACI standard, AASHTO LRFD Bridge Design Specification (2007) Section §5.8.4 addresses horizontal shear design in terms of forces at the interface. The factored interface shear capacity, φV_{ni}, must exceed the factored interface shear demand, V_{ui}. The AASHTO code does require that the minimum area of interface shear reinforcement be satisfied for all interfaces. However, for the purpose of comparison, the shear reinforcement contribution from AASTHO

Equation 5.8.4.1-3 is removed to see how much resistance is allowed for the concrete interface alone. This results in the following equation for the nominal shear resistance of the interface:

$$V_{ni} = cA_{cv} + \mu P_c \quad \text{(Eq. 15)}$$

Additionally, the nominal shear resistance, V_{ni}, used in design shall not be greater than the lesser of:

$$V_{ni} \leq K_1 f'_c A_{cv}, \text{ or} \quad \text{(Eq. 16)}$$

$$V_{ni} \leq K_2 A_{cv} \quad \text{(Eq. 17)}$$

in which:

$$A_{cv} = b_{vi} L_{vi} \quad \text{(Eq. 18)}$$

where,

V_{ni} = nominal interface shear resistance [kip]

c = cohesion factor (the effects of cohesion and/or aggregate interlock), as specified below [ksi]

A_{cv} = area of concrete considered to be engaged in interface shear transfer [in.^{2}]

μ = friction factor, as specified below [dim.]

P_c = permanent net compressive force normal to the shear plane; if force is tensile, P_c = 0.0 [kip]

f'_c = specified 28-day compressive strength of the weaker concrete on either side of the interface [ksi]

K_1 = fraction of concrete strength available to resist interface shear, as specified below

K_2 = limiting interface shear resistance, as specified below [ksi]

L_{vi} = interface length considered to be engaged in shear transfer [in.]

The following values shall be taken for c, μ, K_1, and K_2:

- For a cast-in-place concrete slab on clean concrete girder surfaces, free of laitance with surface roughened to an amplitude of 0.25 in.:

  $c = 0.28$ ksi

  $\mu = 1.0$

  $K_1 = 0.3$

  $K_2 = 1.8$ ksi for normal-weight concrete

  1.3 ksi for lightweight concrete

- For normal-weight concrete place monolithically:

  $c = 0.40$ ksi

  $\mu = 1.4$

  $K_1 = 0.25$

  $K_2 = 1.5$ ksi

- For lightweight concrete placed monolithically, or nonmonolithically, against a clean surface, free of laitance, with surface intentionally roughened to an amplitude of 0.25 in.:

  $c = 0.24$ ksi

  $\mu = 1.0$

  $K_1 = 0.25$

  $K_2 = 1.0$ ksi

- For normal-weight concrete placed against a clean surface, free of laitance, with surface intentionally roughened to an amplitude of 0.25 in.:

  $c = 0.24$ ksi

  $\mu = 1.0$

  $K_1 = 0.25$

  $K_2 = 1.5$ ksi

- For concrete placed against a clean concrete surface, free of laitance, but not intentionally roughened:

  $c = 0.075$ ksi

  $\mu = 0.6$

  $K_1 = 0.2$

  $K_2 = 0.8$ ksi

If P_c was taken to be zero, then the horizontal shear stress could be determined from Equation 15 by dividing by the area of concrete considered to be engaged in interface shear transfer, A_{cv}. This would result in the following horizontal shear stress values for the different surface conditions if the requirement for the interface reinforcement is disregarded:

- For a cast-in-place concrete slab on clean concrete girder surfaces, free of laitance with surface roughened to an amplitude of 0.25 in.:

$$v_{ni} = 280 \text{ psi} \qquad \text{(Eq. 19)}$$

- For normal-weight concrete place monolithically:

$$v_{ni} = 400 \text{ psi} \qquad \text{(Eq. 20)}$$

- For lightweight concrete placed monolithically, or non-monolithically, against a clean surface, free of laitance, with surface intentionally roughened to an amplitude of 0.25 in.:

$$v_{ni} = 240 \text{ psi} \quad \text{(Eq. 21)}$$

- For normal-weight concrete placed against a clean surface, free of laitance, with surface intentionally roughened to an amplitude of 0.25 in.:

$$v_{ni} = 240 \text{ psi} \quad \text{(Eq. 22)}$$

- For concrete placed against a clean concrete surface, free of laitance, but not intentionally roughened:

$$v_{ni} = 75 \text{ psi} \quad \text{(Eq. 23)}$$

The 2007 AASHTO code represents a significant change in the horizontal shear recommendations. This was undertaken to more accurately address the lower bound of experimental data from previous research. One of the test series considered was that of Patnaik (1999) in which his test specimens did not have shear ties across the interface. The current code now allows for a greater horizontal shear capacity compared to the previous standards in 2005. The equation in the code now results in a horizontal shear stress of 240 psi for a reinforced, clean, roughened surface compared to 100 psi in the previous 2005 AASHTO standards. However, the recommended quantity of horizontal shear ties is still required across the interface of all composite beams.

This update shows a promising step forward. However, standard and code methods do not exist for interfaces without horizontal shear ties. The absence of such standards results in composite concrete members being equipped with horizontal shear ties even though composite action could be achieved without them. For example, the horizontal shear stresses for the standard PCI double tee section (shown in Figure 2-3) subjected to service or ultimate loads is well under the

AASHTO capacity requirements. As seen if Figure 2-4, the calculated horizontal shear stress demand using the classical elastic method is approximately 18 psi at service loads. However, the section is required to have the minimum level of shear ties under the AASHTO 2007 code. This conservative requirement results in horizontal shear ties being fabricated in sections that would otherwise not need them. The research conducted as part of this thesis provides valuable data that justifies additional relaxation of the code recommendations.

4.4 Summary

The ACI 318-08 code allows a maximum horizontal shear stress of 80 psi for sections in which the "contact surfaces are clean, free of laitance, and intentionally roughened" to a ¼ inch amplitude. The AASHTO LRFD Bridge Design Specifications (2007) would allow a horizontal shear stress of 240 psi for the same conditions if the requirement for the interface reinforcement is disregarded. Even though the ACI allowance of horizontal shear stress is very conservative, it still permits a horizontal shear capacity for sections that do not have horizontal shear ties, unlike the AASHTO code. However, AASHTO has recently made steps toward increasing the allowed capacity of composite concrete interfaces. If positive experimental tests are conducted for composite interfaces without horizontal shear ties, perhaps the ACI and AASHTO codes could be updated to incorporate a realistic capacity for these interface conditions.

5 Experimental Program – Phase 1 Summary

5.1 General

The first phase of this two phase research study was completed by Dean Deschenes and Dr. Clay Naito in the first half of 2006. The objective was to conduct preliminary tests to determine the maximum interface horizontal shear capacity that can be obtained from composite concrete beams without interface ties. Nineteen test specimens consisting of different research variables were designed, fabricated, and tested. A detailed summary of the first phase of the experimental program will be presented in this chapter.

5.2 Research Variables

For this phase of the experimental program, two different variables that were documented in previous research to influence the horizontal shear stress of composite concrete beams were investigated; specifically, the interface roughness and the compressive strength of the slab concrete. The interface surface roughness was varied using five surface finishing techniques typically conducted in precast operations (Figure 5-1):

1. As-placed roughness – After the concrete is poured and vibrated, no attempt was made to smooth or roughen the surface.
2. Rough broom finish – A stiff broom is run across the surface transverse to the beam length.
3. ¼" rake finish – A rake is run across the surface transverse to the beam length leaving a very rough textured finish.
4. Smooth – Once the concrete is poured and vibrated, a hard trowel is run across the interface to smooth the surface.

5. Sheepsfoot voids – This represents a mechanical surface finish consisting of 1-in. diameter, ½-in. deep impressions made at a spacing of 3½-in.

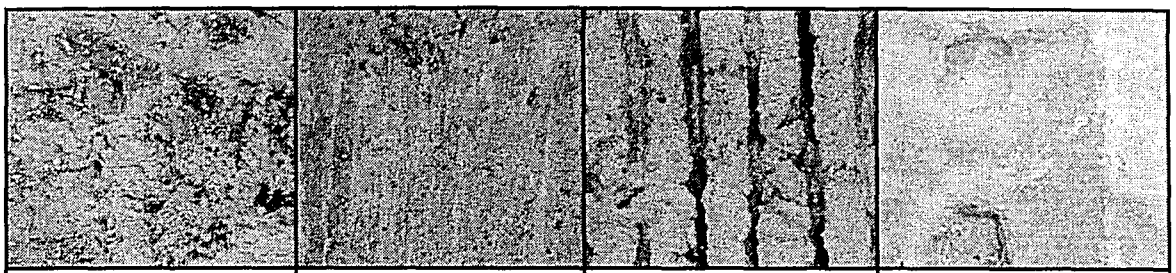

a) As-Placed	b) Broom	c) ¼" Rake	d) Sheepsfoot

Figure 5-1: Interface Finishes for Phase 1

The flange concrete compressive strength was varied to represent typical strengths used in precast construction. The measured concrete strengths used for the cast-in-place slab were 3.11, 5.67, 8.75 and 9.71 ksi. The precast, prestressed web fabricated with a measured compressive strength of 9.71 ksi. Along with the composite beams of varying interface finishes and compressive strengths, three monolithic specimens were included in this experimental program to provide an upper bound to the horizontal shear stress capacity.

5.3 Test Specimen Design and Fabrication

The test specimen's section size was designed on the order of previous horizontal shear studies (Hanson, 1960; Saemann & Washa, 1964; Evans & Chung, 1969; Patnaik, 1999). Also taken into account was an issue recognized by Loov and Patnaik (1994) in which the slab length within an effective depth of the beam restrains the horizontal shear failure mode. Thus, the cast-in-place flange was shortened on either end to prevent any undesirable effects on the horizontal shear behavior of the interface. Transverse shear ties were used in the web in order to avoid web-shear failure. The design of the slab reinforcement was governed by the PennDOT bridge design code. In order to ensure the horizontal shear failure of Beams 8-19, the interface width was reduced by cutting an inch and a half of concrete from each side with a concrete saw. The final designed sections would allow Beams 1-7 and Beams 8-19 to achieve horizontal shear stress levels in

5. Sheepsfoot voids – This represents a mechanical surface finish consisting of 1-in. diameter, ½-in. deep impressions made at a spacing of 3½-in.

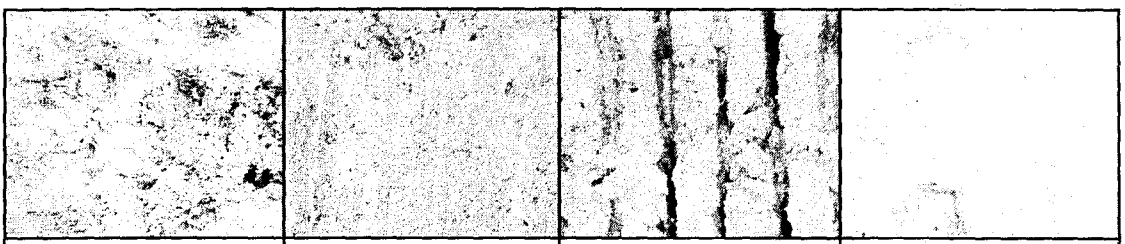

a) As-Placed	b) Broom	c) ¼" Rake	d) Sheepsfoot

Figure 5-1: Interface Finishes for Phase 1

The flange concrete compressive strength was varied to represent typical strengths used in precast construction. The measured concrete strengths used for the cast-in-place slab were 3.11, 5.67, 8.75 and 9.71 ksi. The precast, prestressed web fabricated with a measured compressive strength of 9.71 ksi. Along with the composite beams of varying interface finishes and compressive strengths, three monolithic specimens were included in this experimental program to provide an upper bound to the horizontal shear stress capacity.

5.3 Test Specimen Design and Fabrication

The test specimen's section size was designed on the order of previous horizontal shear studies (Hanson, 1960; Saemann & Washa, 1964; Evans & Chung, 1969; Patnaik, 1999). Also taken into account was an issue recognized by Loov and Patnaik (1994) in which the slab length within an effective depth of the beam restrains the horizontal shear failure mode. Thus, the cast-in-place flange was shortened on either end to prevent any undesirable effects on the horizontal shear behavior of the interface. Transverse shear ties were used in the web in order to avoid web-shear failure. The design of the slab reinforcement was governed by the PennDOT bridge design code. In order to ensure the horizontal shear failure of Beams 8-19, the interface width was reduced by cutting an inch and a half of concrete from each side with a concrete saw. The final designed sections would allow Beams 1-7 and Beams 8-19 to achieve horizontal shear stress levels in

excess of 300 and 750 psi, respectively. The resulting composite beam dimensions can be seen in Figure 5-2.

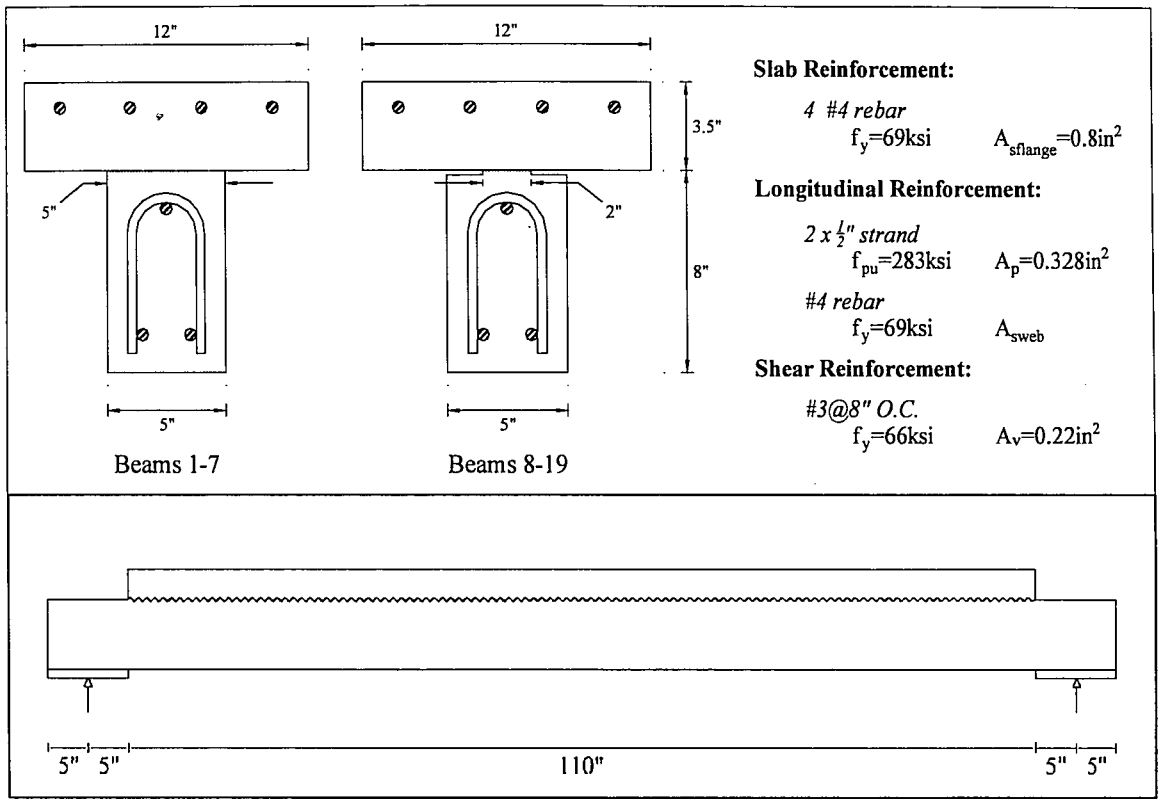

Figure 5-2: Cross-Section and Elevation View of Beams Tested By Deschenes and Naito

The specimens were fabricated at a local prestressed, precast concrete manufacturer named Schuylkill Products, Inc located in Cressona, Pennsylvania. The nineteen webs (and the three slabs of the monolithic members) were cast from the same high early strength concrete mix. Special care was then taken in finishing the beam interface before casting the slabs. Transfer of the prestress occurred within twenty-four hours of the concrete web pour. The slabs were cast of three different high early strength mixes approximately a day after the web was poured. The interface was clean and free of laitance prior to the placement of the flange concrete. The concrete mix designs and the measured stress-strain response of each concrete is presented in Table 5-1 and Figure 5-3, respectively.

Table 5-1: Concrete Mix Design and Properties

Property	Units	Properties per Cubic Yard			
		9.7 ksi Web	3.1 ksi Flange	5.7 ksi Flange	8.8 ksi Flange
Cement Type III	lbs.	556	377	589	558
Coarse Aggregate SSD – Dyer 67	lbs.	1290	1819	1918	1290
MB Glenium 3030 NS HRWR	oz.	84.9	-	-	84.7
Pozzolith 100 XR Retarder	oz.	25.2	-	-	9.6
VR Standard Air Entrainment	oz.	6.9	6.1	5.8	7.0
Design Water / Cement Ratio	-	0.3	0.7	0.5	0.3
Air Content	%	6.1	7.5	5.1	5.3
Slump	in.	5.9	5.0	4.8	5.9

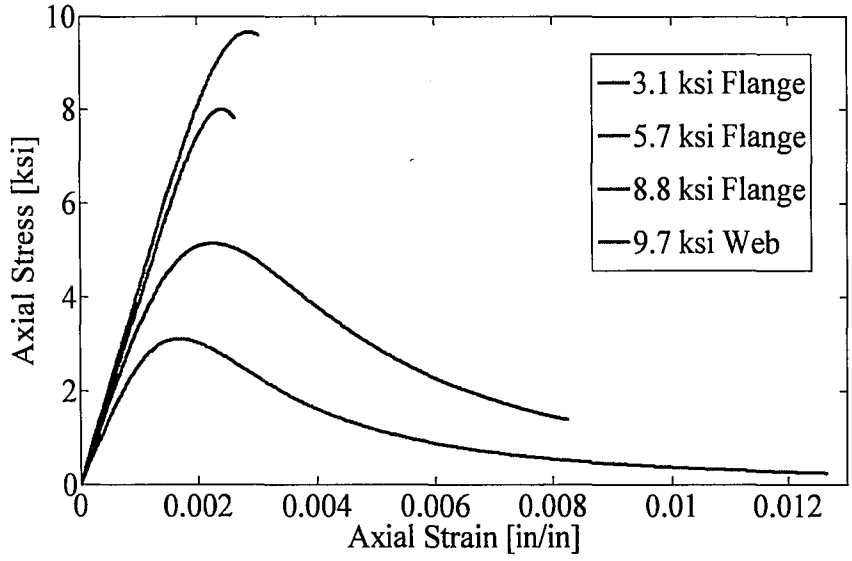

Figure 5-3: Concrete Stress Strain Curves

5.4 Test Setup

The composite beams were tested over a simple span of ten feet. The beams were inverted in a self-reacting test setup for loading convenience. The normal force acting on the interface is altered by inverting the sections; however the change was considered to be insignificant in comparison to the applied load. There were two loading configurations used to investigate the behavior of the non-reinforced interface: five-point and two-point loading (Figure 5-4).

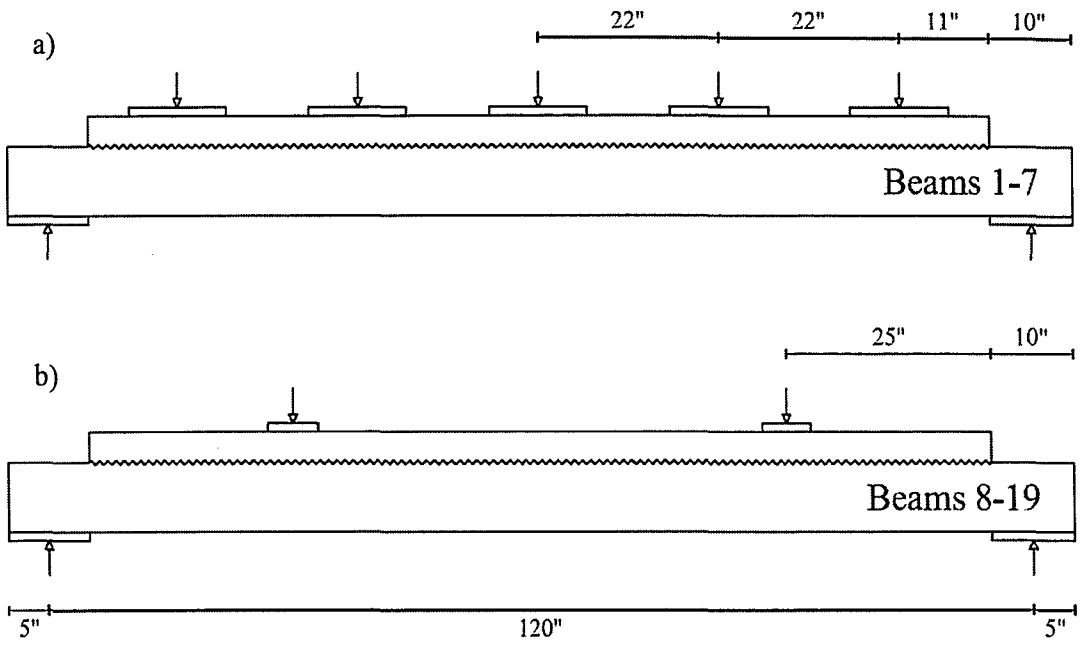

Figure 5-4: Test Specimen Loading Configuration

The five-point load configuration (Figure 5-4a) was used to examine the service state of horizontal shear stresses. The point loads were distributed through twelve-inch neoprene bearing pads to simulate a uniform load. The distribution of the load also reduced the normal stress on the interface thus minimizing the shear friction mechanism of the interface and obtaining a lower bound for service state horizontal shear stresses.

The two-point load configuration (Figure 5-4b) was used to examine the failure state of the horizontal shear stresses. The use two point loads placed equidistant from the midspan, along with reducing the interface width (as mentioned before), created regions of high horizontal shear at both ends of the beam. This ensures that the specimens would fail in a horizontal shear mode before flexural or flexural-shear cracking occurred. Again, neoprene bearing pads (at a reduced length of six-inches) were used to distribute the point loads and reduce the local normal stress on the section.

5.5 Instrumentation

The values of the point loads and midspan deflection were collected by load cells and an LVDT, respectively. The interface slip was monitored by three or four slip gauges placed at equal intervals along the predicted failure plane (Figure 5-5a). The horizontal shear stresses at the interface were measured using two surface mounted strain gauges along the flange depth (Figure 5-5b). The strain values obtained from the gauges, along with the stress-strain data from concrete cylinder tests, produced a stress profile of the slab. Integrating the stress profile over the flange depth and width resulted in the compression force in the flange. The horizontal shear force was then calculated using the global force equilibrium equation. This process is summarized in Figure 5-6.

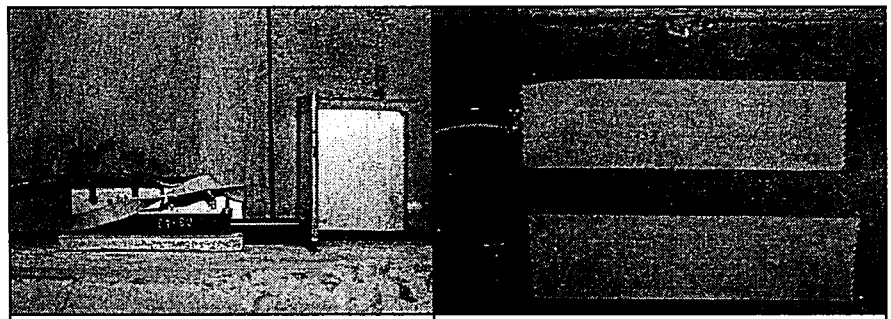

a) Slip Gauge | b) Surface Mounted Strain Gauges

Figure 5-5: Instrumentation to Monitor Interface

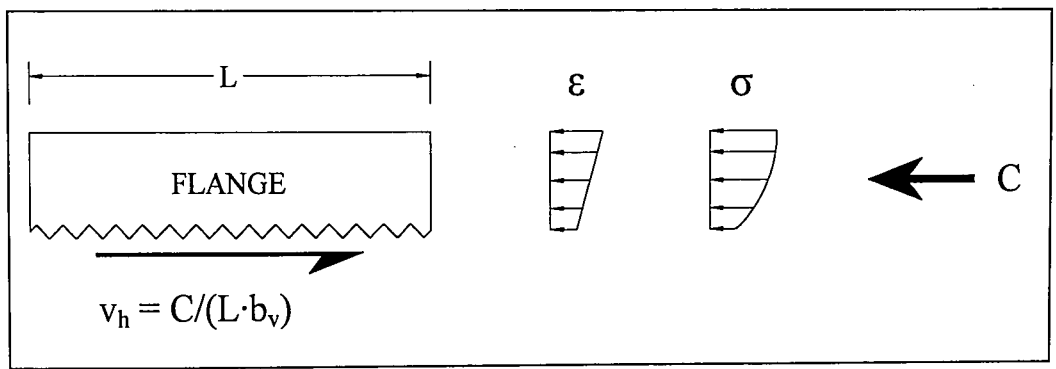

Figure 5-6: Determining Horizontal Shear Stress from Strain Data

5.5 Instrumentation

The values of the point loads and midspan deflection were collected by load cells and an LVDT, respectively. The interface slip was monitored by three or four slip gauges placed at equal intervals along the predicted failure plane (Figure 5-5a). The horizontal shear stresses at the interface were measured using two surface mounted strain gauges along the flange depth (Figure 5-5b). The strain values obtained from the gauges, along with the stress-strain data from concrete cylinder tests, produced a stress profile of the slab. Integrating the stress profile over the flange depth and width resulted in the compression force in the flange. The horizontal shear force was then calculated using the global force equilibrium equation. This process is summarized in Figure 5-6.

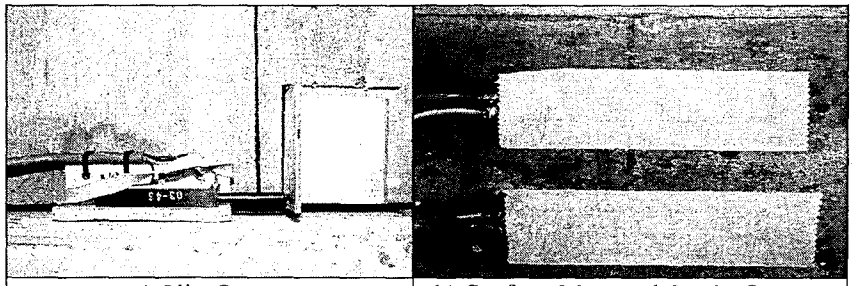

a) Slip Gauge | b) Surface Mounted Strain Gauges

Figure 5-5: Instrumentation to Monitor Interface

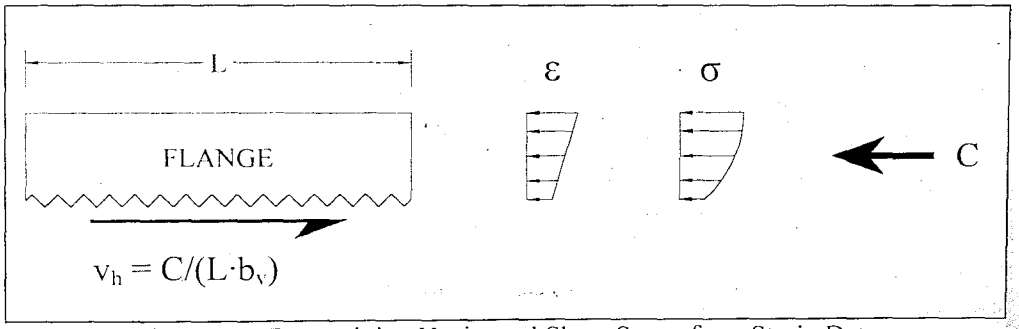

Figure 5-6: Determining Horizontal Shear Stress from Strain Data

5.6 Testing Procedure

Nineteen composite beams without horizontal shear ties were tested for this phase of the experimental program. Table 5-2 summarizes the variables of each test specimen.

Table 5-2: Test Matrix for Phase 1

Beam	Specimen ID	Interface Finish	Loading Method	Interface Width [in.]	Web Steel Area, A_{sweb} [sq.in.]	Flange Strength [ksi]	Effective Prestress [ksi]
1	A4.4	As-Placed	Five Point	5	0.2	5.67	141.3
2	B4.1	Broom	Five Point	5	0.2	5.67	142.1
3	M10.1	Monolithic	Five Point	5	0.0	9.71	139.9
4	R2.1	Rake	Five Point	5	0.2	3.11	141.5
5	R4.4	Rake	Five Point	5	0.2	5.67	143.1
6	R10.1	Rake	Five Point	5	0.0	8.75	140.3
7	S4.1	Sheepsfoot	Five Point	5	0.2	5.67	140.3
8	A4.1	As-Placed	Two Point	2	0.2	5.67	140.2
9	A4.3	As-Placed	Two Point	2	0.2	5.67	140.1
10	B4.3	Broom	Two Point	2	0.2	5.67	140.2
11	M10.2	Monolithic	Two Point	2	0.0	9.71	140.2
12	M10.3	Monolithic	Two Point	2	0.0	9.71	140.2
13	R2.2	Rake	Two Point	2	0.2	3.11	140.2
14	R2.3	Rake	Two Point	2	0.2	3.11	140.2
15	R4.2	Rake	Two Point	2	0.2	5.67	140.2
16	R4.3	Rake	Two Point	2	0.2	5.67	140.2
17	R10.2	Rake	Two Point	2	0.0	8.75	140.2
18	R10.3	Rake	Two Point	2	0.0	8.75	140.2
19	S4.2	Smooth	Two Point	2	0.2	5.67	140.2

The beams were inverted and placed in a simply supported self-reacting test setup. Two or five equal loads were then applied at a quasi-static rate to the specimens through the use of thirty ton jacks serviced by a single hydraulic pump (Figure 5-7 and Figure 5-8). The applied load was paused every five kips in order to inspect the beam and the composite interface. The test was stopped once the specimen failed.

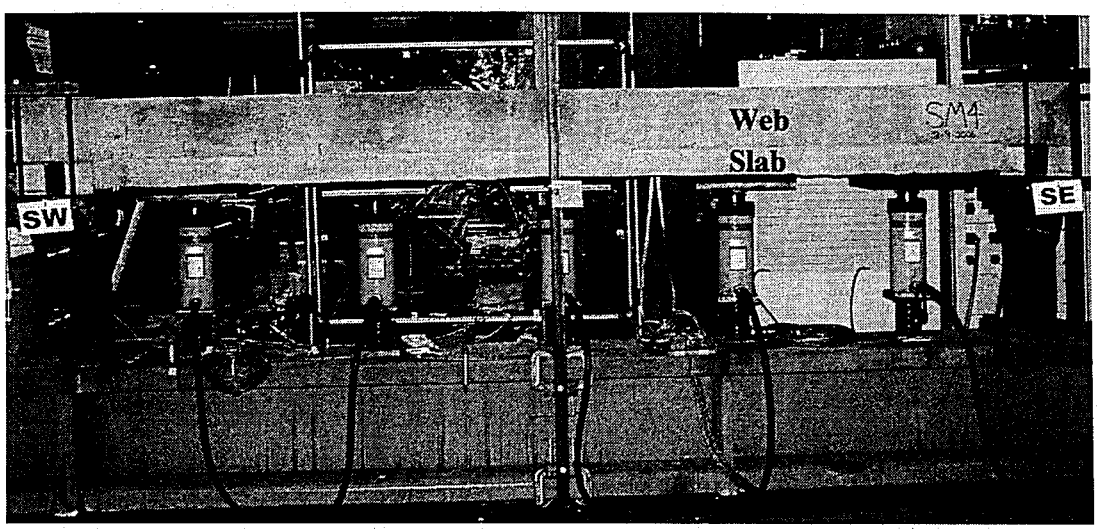

Figure 5-7: Five Point Load Configuration

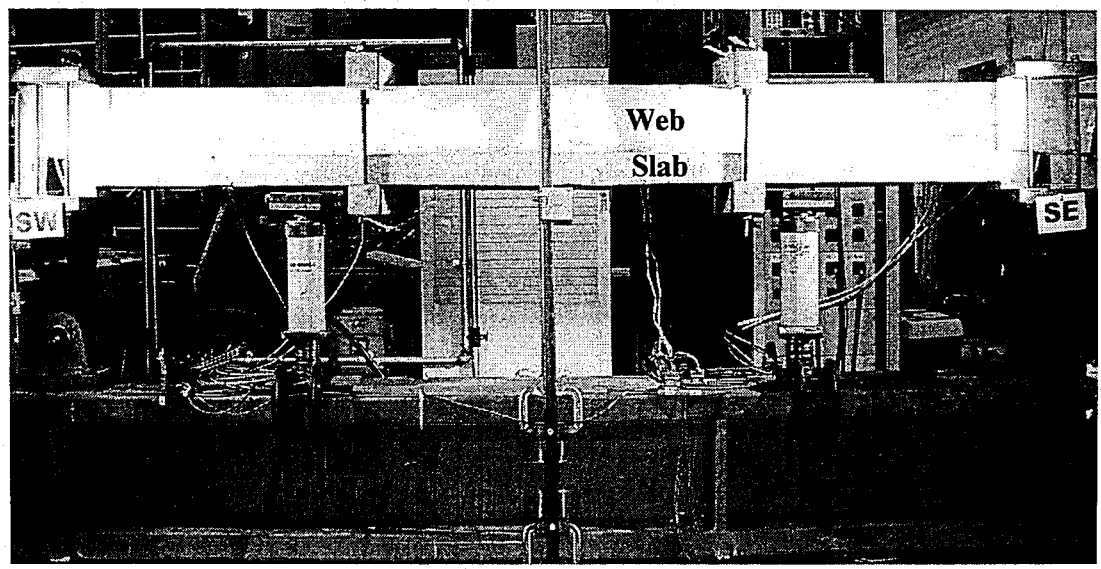

Figure 5-8: Two Point Load Configuration

5.7 General Behavior of Test Beams

5.7.1 Five-Point Load Specimens

After a few increments of load (at about twenty-eight kips), flexural cracks began forming on the tensile face of the beam. As the load increased, flexural-shear cracks started forming near the support of the beam and extending to the beam-flange interface. Failure of the section occurred between thirty-five and sixty kips when a flexural-shear crack opened up. One of the specimen

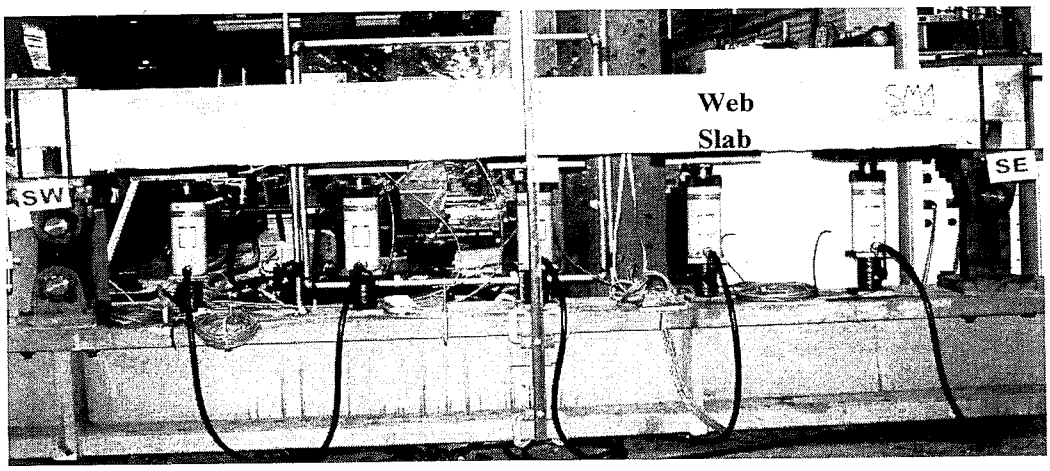

Figure 5-7: Five Point Load Configuration

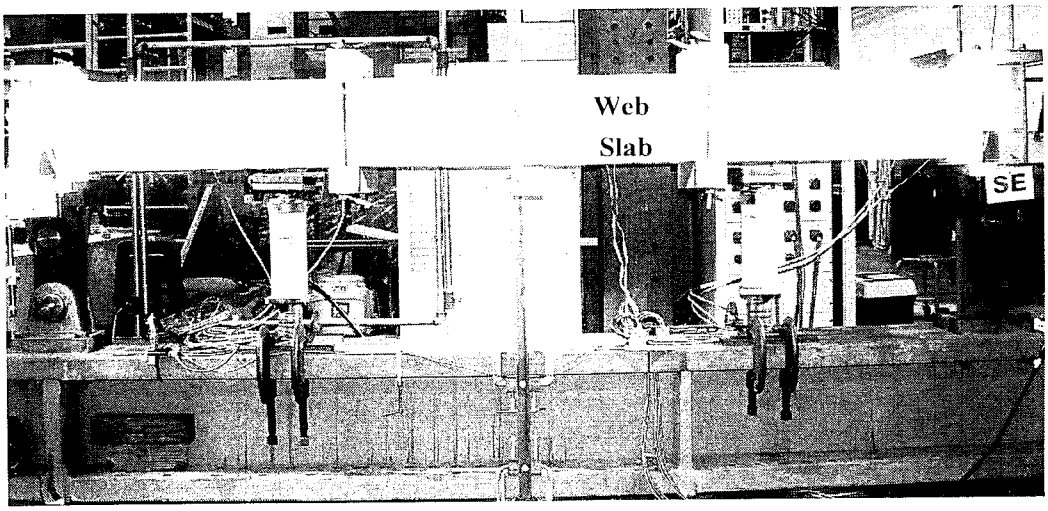

Figure 5-8: Two Point Load Configuration

5.7 General Behavior of Test Beams

5.7.1 Five-Point Load Specimens

After a few increments of load (at about twenty-eight kips), flexural cracks began forming on the tensile face of the beam. As the load increased, flexural-shear cracks started forming near the support of the beam and extending to the beam-flange interface. Failure of the section occurred between thirty-five and sixty kips when a flexural-shear crack opened up. One of the specimen

(Beam 5: R4.4) experienced pure flexural failure due to the fracture of the tensile strands. Figure 5-9 illustrates the typical failure modes for the five-point loaded specimen.

a) Flexural [Beam 5: R4.4] | b) Flexure-Shear [Beam 4: R2.1]

Figure 5-9: Typical Five-Point Loaded Specimen Failures

During testing, the interface was visually examined and the load-slip relationship measured by the instrumentation was monitored. No physical distress of the interface was visually observed for any of the five-point load test specimen. The load-slip measurement displayed a minute increase in slip with rising load; however the slip rarely exceeded one-hundredth of an inch at cracking and returned to zero once the specimen was unloaded. The increase in the measured slip was reported to be a result of compatibility with the interface. Due to the elastic nature of the results, the interface was believed to have remained composite throughout each of the five-point load tests. Because the classical elastic horizontal shear equation (Eq. 6) is not valid once flexural cracking occurs, the cracking loads were determined in order to calculate the corresponding horizontal shear stresses. A summary of the specimen, failure mode, cracking load, and the measured interface slip at the initiation of flexural cracking is presented in Table 5-3. The corresponding calculated horizontal shear stresses at the initiation of flexural cracking are presented in Table 5-4.

(Beam 5: R4.4) experienced pure flexural failure due to the fracture of the tensile strands. Figure 5-9 illustrates the typical failure modes for the five-point loaded specimen.

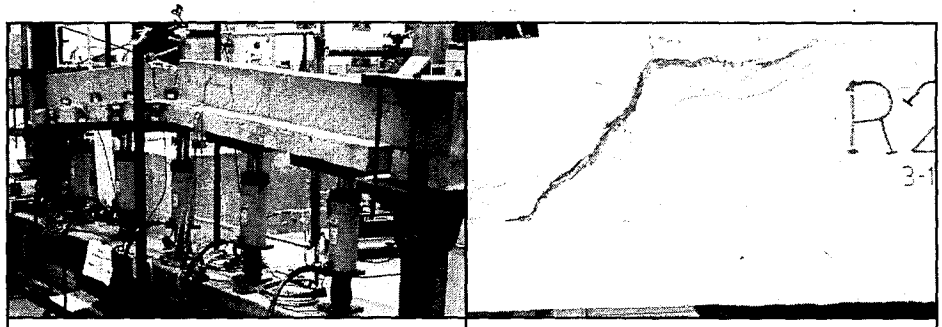

a) Flexural [Beam 5: R4.4] b) Flexure-Shear [Beam 4: R2.1]

Figure 5-9: Typical Five-Point Loaded Specimen Failures

During testing, the interface was visually examined and the load-slip relationship measured by the instrumentation was monitored. No physical distress of the interface was visually observed for any of the five-point load test specimen. The load-slip measurement displayed a minute increase in slip with rising load; however the slip rarely exceeded one-hundredth of an inch at cracking and returned to zero once the specimen was unloaded. The increase in the measured slip was reported to be a result of compatibility with the interface. Due to the elastic nature of the results, the interface was believed to have remained composite throughout each of the five-point load tests. Because the classical elastic horizontal shear equation (Eq. 6) is not valid once flexural cracking occurs, the cracking loads were determined in order to calculate the corresponding horizontal shear stresses. A summary of the specimen, failure mode, cracking load, and the measured interface slip at the initiation of flexural cracking is presented in Table 5-3. The corresponding calculated horizontal shear stresses at the initiation of flexural cracking are presented in Table 5-4.

Table 5-3: Five-Point Load Results

Beam	Specimen ID	Failure Mode	Calculated Cracking Load [kip]	Interface Slip at Cracking [in]
1	A4.4	Flexure-Shear	27.6	0.0046
2	B4.1	Flexure-Shear	27.6	0.0021
3	M10.1	Flexure-Shear	28.0	0.0035
4	R2.1	Flexure-Shear	26.6	0.0018
5	R4.4	Flexure	27.6	0.0028
6	R10.1	Flexure-Shear	27.8	0.0020
7	S4.1	Flexure-Shear	27.6	0.0365
			Average	0.0076

Table 5-4: Horizontal Shear Stress at Cracking for Five-Point Load [psi]

Beam	Specimen ID	Elastic VQ/Ib_v	ACI V/b_vd_p	AASHTO V/b_vd_v
1	A4.4	341.1	276.0	334.5
2	B4.1	341.1	276.0	334.5
3	M10.1	350.1	280.0	339.4
4	R2.1	321.6	266.0	322.4
5	R4.4	341.1	276.0	334.5
6	R10.1	345.6	278.0	337.0
7	S4.1	341.1	276.0	334.5
	Average	340.2	275.4	333.9

5.7.2 Two-Point Load Specimens

After a few increments of loading, fine diagonal cracks were observed at the interface. As the load was increased, the interface cracks grew and connected with one another until a continuous separation was formed from the load point to the end of the slab. Immediately after the interface failed, a flexural shear failure occurred due to the reduced section capacity. Figure 5-10 and Figure 5-11 illustrate the progression of the horizontal shear failure observed in the two-point loaded specimens. The failure of the specimen typically occurred between twenty-five and forty kips. In comparison to the monolithic section, it was reported that the composite sections achieved 60-90% of full composite action. A summary of the specimen, failure mode, failure

load, and the measured interface slip is presented in Table 5-5. The corresponding calculated horizontal shear stresses at failure are presented in Table 5-6. For these horizontal shear stresses, the contribution of friction which is seen in the AASHTO capacity equation (Eq. 9) as μP_c was not subtracted off because there is essentially no clamping force near the end of the slab-beam interface where the slip failure occurs. Also, when comparing the results in the next few sections, the calculated horizontal shear results found from the classical elastic equation (Eq. 6) were used.

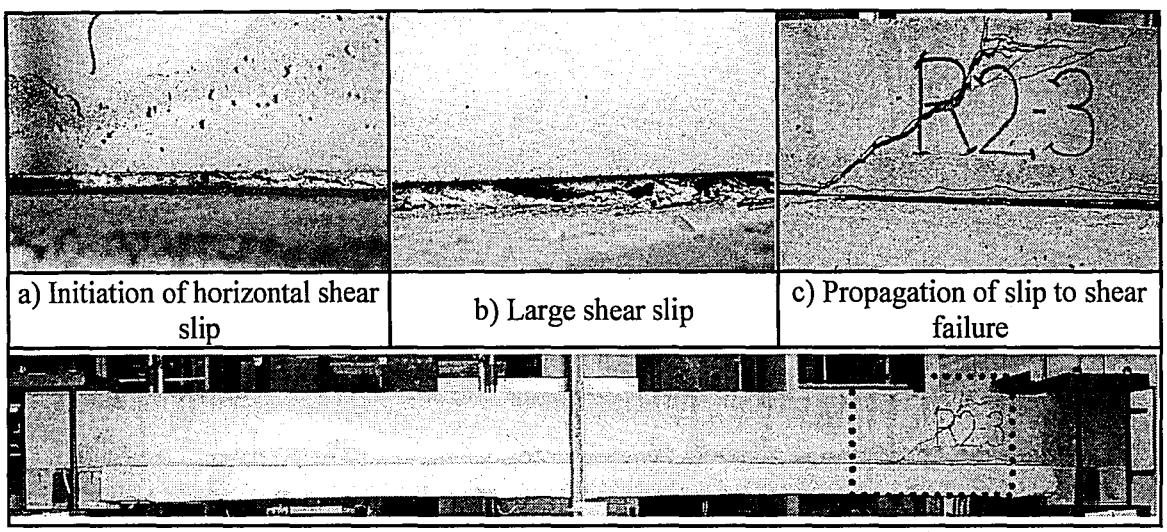

Figure 5-10: Typical Failure Progression [Beam 14: R2.3]

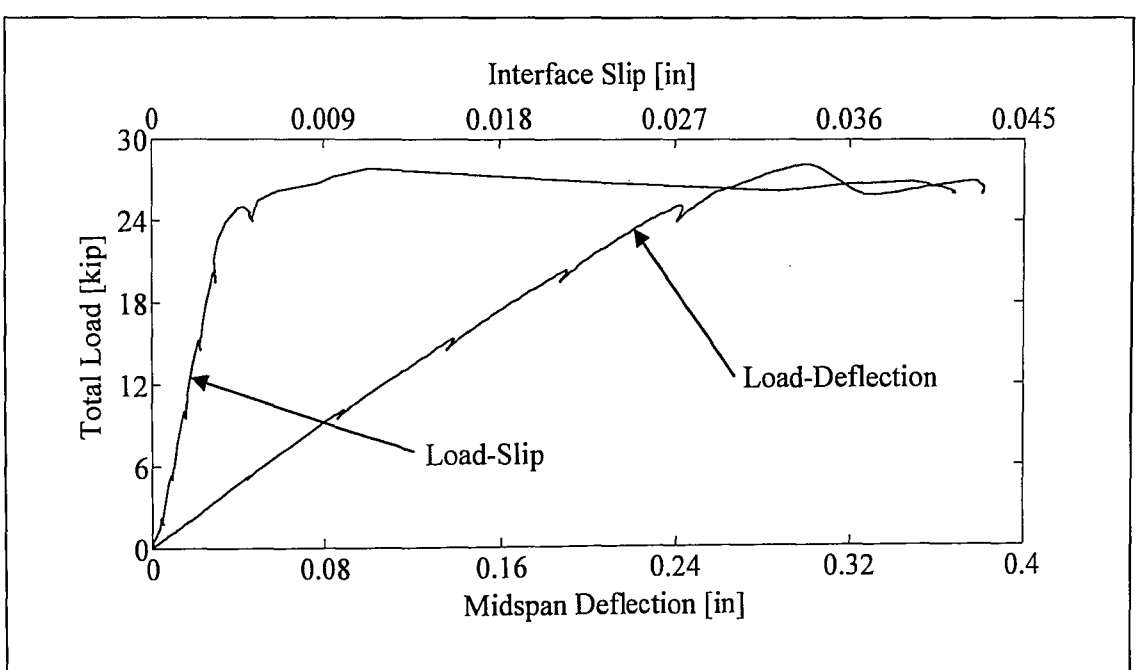

Figure 5-11: Typical Load-Slip and Load-Deflection Curves [Beam 13: R2.2]

load, and the measured interface slip is presented in Table 5-5. The corresponding calculated horizontal shear stresses at failure are presented in Table 5-6. For these horizontal shear stresses, the contribution of friction which is seen in the AASHTO capacity equation (Eq. 9) as μP_c was not subtracted off because there is essentially no clamping force near the end of the slab-beam interface where the slip failure occurs. Also, when comparing the results in the next few sections, the calculated horizontal shear results found from the classical elastic equation (Eq. 6) were used.

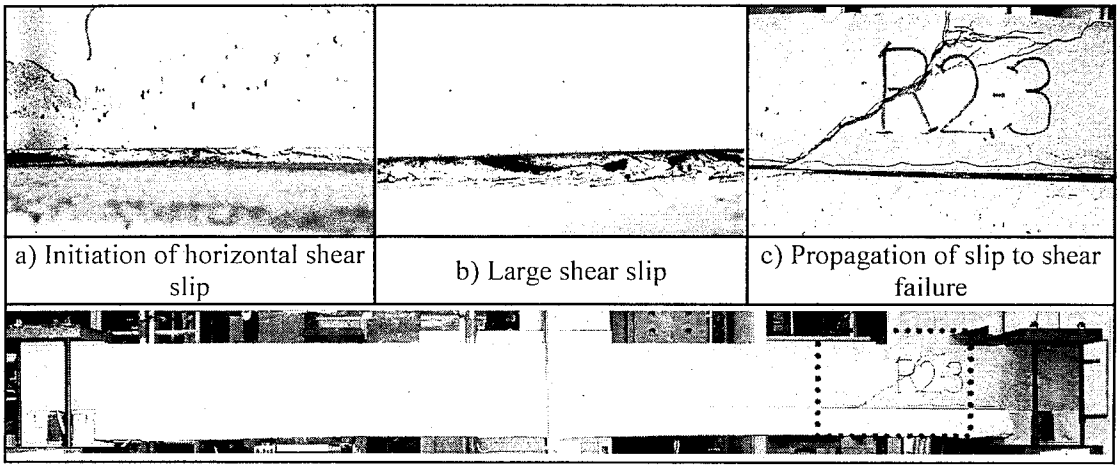

Figure 5-10: Typical Failure Progression [Beam 14: R2.3]

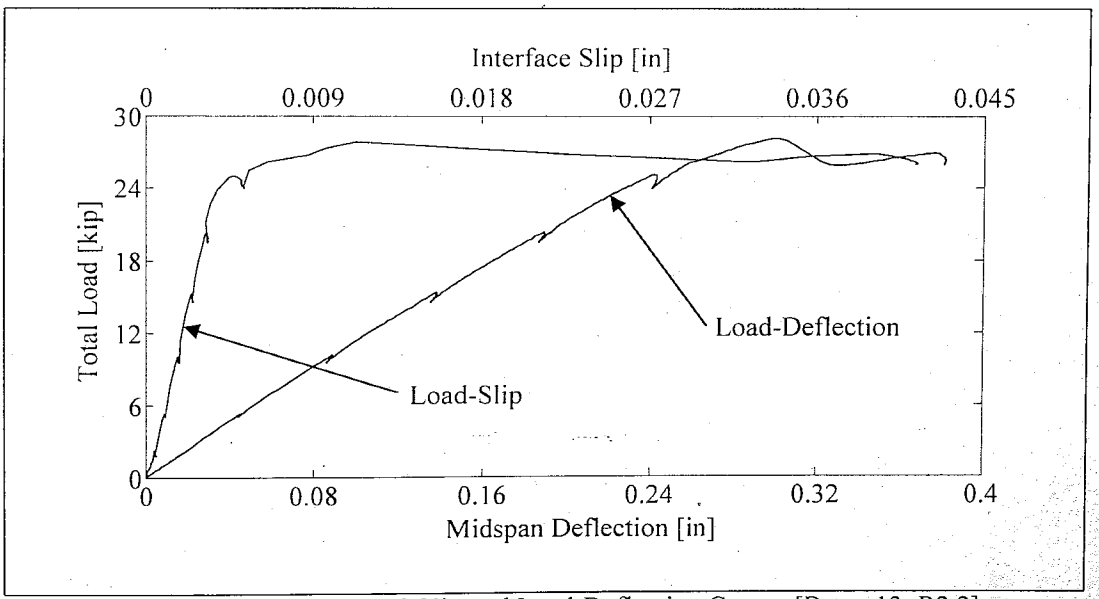

Figure 5-11: Typical Load-Slip and Load-Deflection Curves [Beam 13: R2.2]

Table 5-5: Two-Point Load Results

Beam	Specimen ID	Failure Mode	Failure Load [kip]	Interface Slip at Failure [in]
8	A4.1	Horiz. Shear	27.9	0.0281
9	A4.3	Horiz. Shear	34.4	0.0064
10	B4.3	Horiz. Shear	32.2	0.0105
11	M10.2	Horiz. Shear	33.9	0.0124
12	M10.3	Flexure-Shear	39.2	0.0084
13	R2.2	Horiz. Shear	28.1	0.0133
14	R2.3	Horiz. Shear	33.6	0.0114
15	R4.2	Horiz. Shear	32.4	0.0107
16	R4.3	Horiz. Shear	37.9	0.0090
17	R10.2	Horiz. Shear	37.4	0.0121
18	R10.3	Horiz. Shear	34.9	0.0119
19	S4.2	Horiz. Shear	25.5	0.0176
			Average	0.0127

Table 5-6: Horizontal Shear Stress at Failure for Two-Point Load [psi]

Beam	Specimen ID	From Strain C/Lb_v	Elastic VQ/Ib_v	ACI V/b_vd_p	AASHTO V/b_vd_v
8	A4-1	482.2	863.2	698.4	846.6
9	A4-3	814.0	1060.8	860.7	1043.2
10	B4-3	915.6	993.2	804.6	975.3
11	M10-2	1075.0	1067.0	848.4	1028.4
12	M10-3	1288.0	1248.1	981.1	1189.2
13	R2-2	639.0	850.6	703.7	852.9
14	R2-3	1182.0	1015.1	840.2	1018.4
15	R4-2	1348.0	1001.0	811.1	983.2
16	R4-3	1245.0	1165.9	948.1	1149.2
17	R10-2	1054.0	1141.3	934.3	1132.5
18	R10-3	1194.0	1073.6	873.1	1058.3
19	S4-2	787.4	787.9	637.5	772.7
	Average	1002.0	1022.3	828.4	1004.1

5.7.3 Horizontal Shear Capacity versus Interface Roughness

The effects of the interface roughness on the horizontal shear stress were observed by tabulating a series of beams that were fabricated from the same slab concrete. Thus, the only difference

between the beams was the interface finish. The specimens and their corresponding horizontal shear stresses are presented in Table 5-7.

Table 5-7: Horizontal Shear Capacity versus Interface Roughness

Specimen ID	Interface Finish	Flange Strength [ksi]	Horizontal Shear Stress at Failure [psi]
S4	Smooth	5.67	787.72
A4	As-Placed	5.67	962.01
B4	Broom	5.67	993.17
R4	Rake	5.67	1083.5

The roughness of the interface was not assigned numerical values; however, it was reported that the interface roughness increased as the surface finish went from smooth, to as-placed, to broom, and finally to rake. Thus, it can be observed from Table 5-7 that the horizontal shear stresses increase with an increased interface roughness.

The failed interfaces of the two-point load specimens were inspected after the completion of the tests (Figure 5-12). It was observed that for the weaker finishes (as-placed and broom), the slab and web sections moved relative to one another without shearing significant amount of aggregate (Figure 5-12b & c). The original interface finish was clearly distinguishable for some of the beams. In contrast, the rake surface finish caused the interface to fail in a monolithic mode (Figure 5-12d & e). The interface bond of the rake finish remained intact and the surrounding aggregate in the reduced interface width sheared off.

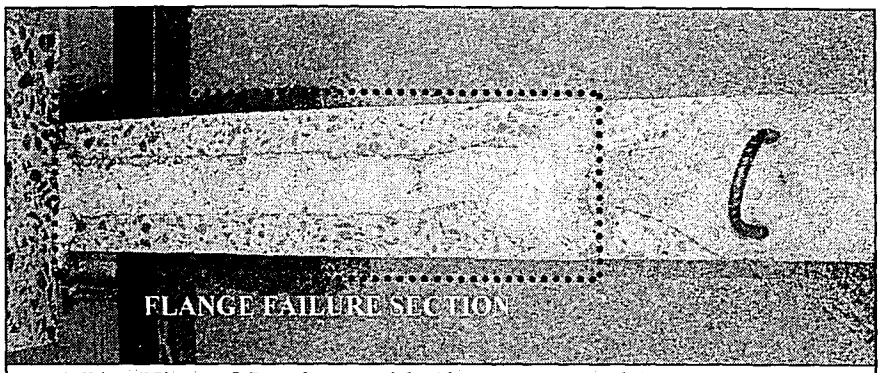

a) Plan View of Specimen with Flange Removed [Beam 10, B4.3]

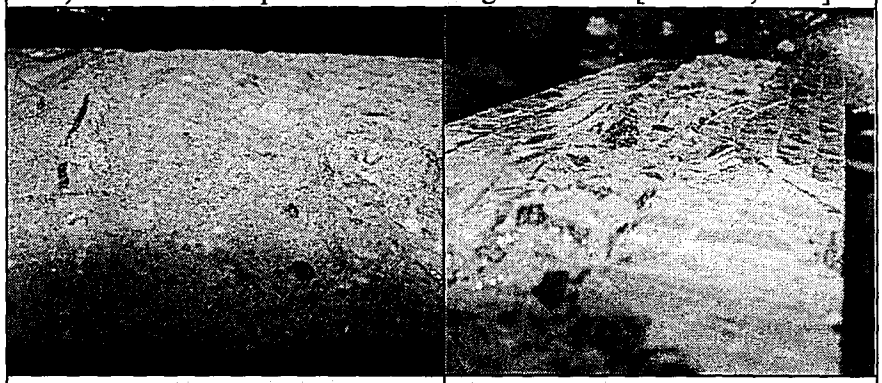

b) As-Placed [Beam 9, A4.3] | d) Monolithic [Beam 12, M10.3]

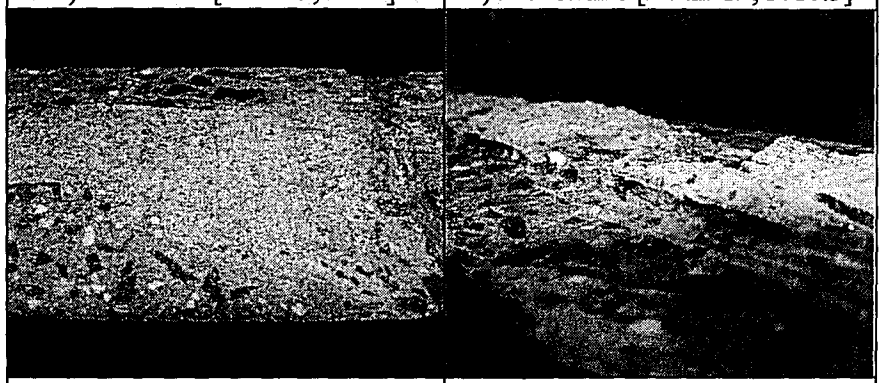

c) Broom [Beam 10, B4.3] | e) Rake [Beam 16, R4.3]

Gradual Slip | Brittle Fracture

Figure 5-12: Failed Interfaces Due to Varying Surface Finishes

5.7.4 Horizontal Shear Capacity versus Concrete Strength

Similarly, the effects of the concrete strength on the horizontal shear stress were observed by comparing data for beams that possessed the same surface finish. Thus, the only difference between the beams was the concrete strength of the topping slab. The specimens and their corresponding horizontal shear stresses are presented in Table 5-8. Even though the horizontal

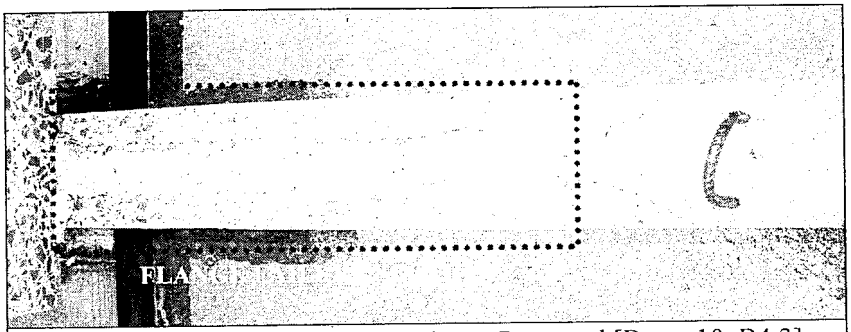

a) Plan View of Specimen with Flange Removed [Beam 10, B4.3]

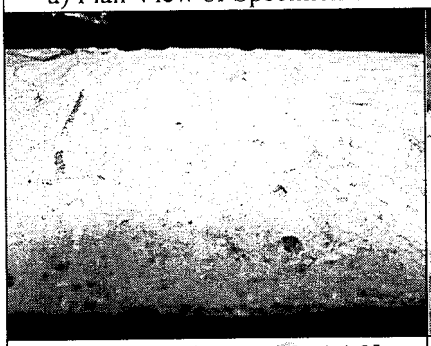

b) As-Placed [Beam 9, A4.3]

d) Monolithic [Beam 12, M10.3]

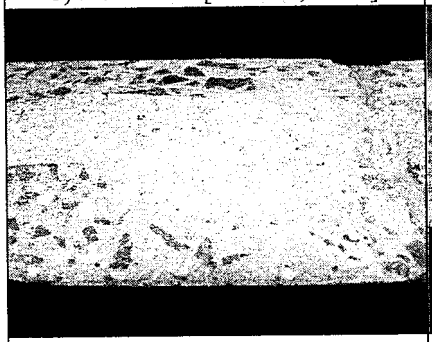

c) Broom [Beam 10, B4.3]

e) Rake [Beam 16, R4.3]

Gradual Slip	Brittle Fracture

Figure 5-12: Failed Interfaces Due to Varying Surface Finishes

5.7.4 Horizontal Shear Capacity versus Concrete Strength

Similarly, the effects of the concrete strength on the horizontal shear stress were observed by comparing data for beams that possessed the same surface finish. Thus, the only difference between the beams was the concrete strength of the topping slab. The specimens and their corresponding horizontal shear stresses are presented in Table 5-8. Even though the horizontal

shear stresses for the three specimens are relatively close to one another, there is a general trend that higher flange concrete strength will result in a higher horizontal shear capacity.

Table 5-8: Horizontal Shear Capacity versus Concrete Strength

Specimen ID	Interface Finish	Flange Strength [ksi]	Horizontal Shear Stress at Failure [psi]
R2	Rake	3.11	932.62
R4	Rake	5.67	1083.5
R10	Rake	8.75	1107.5

5.8 Conclusions

The following are the conclusions made by Deschenes and Naito (2006) based on the data obtained for the first phase of the experimental program:

1. "An average horizontal shear stress of 340 psi was achieved for the service state. This result is more than three times the least conservative code estimate for horizontal shear capacity at failure."

2. "An average horizontal shear stress of 1022 psi was achieved for the failure condition. Again, this result is more than ten times the least conservative code estimate for horizontal shear capacity at failure."

3. "A positive trend is revealed when specimen capacities of the same topping strength, but different interface roughness are compared. That is, horizontal shear strength increases with increasing interface roughness."

4. "A similar trend is revealed when specimen capacities of the same interface roughness, but different flange strength are compared. That is, horizontal shear strength increases with increasing flange strength."

5. "The service state and failure load behavior of the ¼" rake finish was very similar to that of the monolithic section. Although a time consuming finish, the rake application is recommended for the best composite performance."

6 Experimental Program – Phase 2 – Program Overview, Research Variables, and Specimen Design

6.1 General

The second phase of the experimental program utilizes the conclusions and recommendations from the first phase in order to design a new composite concrete test specimen without horizontal shear ties and select research variables in the hope of achieving repeatable test results. If repeatable horizontal shear stress values for composite members without interface reinforcement are obtained, then recommendations and equations to properly approximate the horizontal shear capacity can be made. These recommendations will result in the design and fabrication of more economical composite concrete beams.

This phase of the experimental program is focused on examining the failure state horizontal shear stresses. Therefore, the two-point load configuration that was utilized in the first phase will be applied to the test specimen for this phase. The section that is designed will consist of a precast web, which is fabricated using high strength concrete and prestressed tensile reinforcement, and a cast-in-place slab, which will be fabricated several months later to simulate the fabrication process typical for construction practices. The final composite specimen will not have ties across the interface and will be able to reach high levels of horizontal shear stress before cracking of the section occurs.

6.2 Research Variables

In order to evaluate the repeatability of horizontal shear results, an adequate amount of composite beams possessing the same section properties would need to be tested. Therefore, the quantity of research variables was reduced from those of the first phase to focus on the parameters which most strongly influence horizontal shear strength. As with previous research, the variables that appear to have the most significant effect on the horizontal shear capacity were considered;

namely, the roughness of the composite interface surface finish and the compressive strength of the slab concrete. Due to the fact that the correlation with the horizontal shear capacity in the first phase was not as distinguishable for the concrete compressive strength as it was for the interface surface roughness, it was decided to focus more attention on varying the roughness of the composite interface.

Four surface finishes were chosen to be utilized in this research program. The selection of the surface finishes were based on the typical finishes used in bridge and building construction, the finishes that would provide varying levels of interface roughness (this would aid in observing the correlation between the degree of surface roughness and horizontal shear capacity), and the surfaces finishes tested in previous research (this would help in correlating results from the current experimental program to those in the past). With this in mind, the surface finishes chosen for this research program were smooth, broom, as-placed, and rake. The actual method used to apply these surface finishes will be described in detail in the web fabrication section of this thesis.

Two compressive strengths were chosen for the cast-in-place concrete slab based on those typically used in bridge and building construction. It was desired that the concrete strengths were fairly different so that their effect on the horizontal shear capacity would be noticeable. Also, since the compressive strength of the weaker concrete would be the limiting factor on the composite interface capacity, the slab concrete strength was selected to be less than the strength of the web as is typical in composite concrete construction. On the basis of this reasoning, a low and high strength concrete with compressive strengths of 3 ksi and 6 ksi, respectively, was chosen for this research program. Additionally, a compressive strength of 8 ksi was chosen for the prestressed concrete web.

In order to ensure a sufficient amount of data will be generated to determine if repeatable test results on the horizontal shear capacity are possible, four test specimens would be fabricated for

each possible combination of surface finish and compressive strength. This results in thirty-two total test specimens for this project. The test matrix is summarized in Table 6-1.

Table 6-1: Original Test Matrix for Phase 2

Specimen ID	Surface Finish				Slab Strength		Number of Specimens
	Smooth	Broom	As-Placed	Rake	3 ksi	6 ksi	
3S	■				■		4
3B		■			■		4
3A			■		■		4
3R				■	■		4
6S	■					■	4
6B		■				■	4
6A			■			■	4
6R				■		■	4
						Total =	32

6.3 Specimen Design

6.3.1 Overview

For this phase of the experimental program, a composite concrete beam consisting of a precast, prestressed web and cast-in-place slab without horizontal shear ties across the interface was designed. The main objective for the design of the test specimen was to enable the composite interface to reach the levels of horizontal shear stress achieved in the first phase (approximately 1000 psi) before flexural or flexural-shear cracking of the section occurred. This is an important criterion to meet for two reasons. First, even though the elastic equation for calculating the horizontal shear stress ($v = VQ/Ib_v$) has been used in past experimental programs with cracked section properties, the horizontal shear stress calculated cannot be considered accurate since the equation is based upon the uncracked, linear elastic properties of the composite section. Therefore, in order to find the proper values of horizontal shear stress based on the elastic equation, the section must fail in horizontal shear before cracking occurs. Second, as observed in the specimens tested by Hanson (1960) and Saemann and Washa (1965), the flexural cracks

tended to propagate through the beams to the composite interface. Once there, the cracks traveled along the interface thus initiating a horizontal shear failure. The two issues described above can be avoided if the specimen is designed to fail in horizontal shear before cracking of the section occurs.

6.3.2 Selection of the Specimen Dimensions

The composite specimen dimensions were chosen to be on the order of those used in previous research (Hanson, 1960; Evans & Chung, 1969; Patnaik, 1999; Deschenes & Naito, 2006). The previous research cross-sections were used as a reference point in which to begin the design of the specimen. The composite beam's dimensions were progressively refined in order to create the most efficient section possible that would satisfy the desired objectives.

An issue recognized by Loov and Patnaik (1994) was also taken into consideration when determining the specimen dimensions. These authors determined that cracks formed between the support of the beam and the composite interface at a distance approximately equal to the effective depth of the web section (Figure 6-1a). The slab at the end of the beam would provide restraint against interface slip and thus inhibit the failure of the interface. To correct this, the authors suggested reducing the slab length thus allowing the horizontal shear failure to properly occur (Figure 6-1b). This issue is most likely the reason that other authors of previous research reported that the maximum slip of the composite interface occurred near the quarter points of the span instead of at the end of the slab-web interface where it would be expected (Hanson, 1960; Saemann & Washa, 1964). Thus, for the design of this test specimen, the cast-in-place slab was terminated prior to the supports to prevent any undesired effects on the horizontal shear behavior of the interface. It was decided to terminate the slabs a length of only 2/3 the effective depth from the support location to preclude a premature shear failure of the precast web.

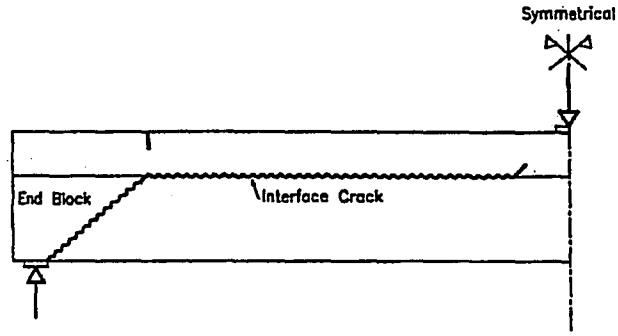

(a) Beam with Full Length Flanges

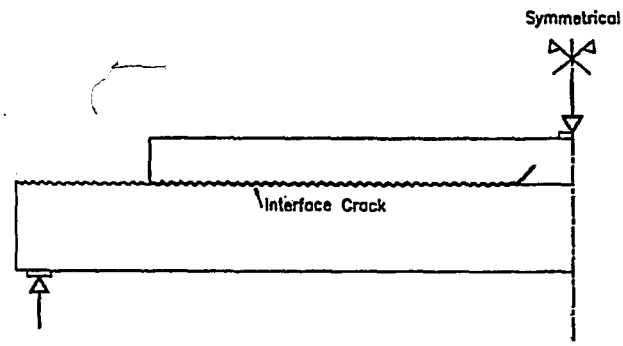

(b) Beam with Short Flanges

Figure 6-1: Length Reduction of the Cast-In-Place Slab (Loov & Patnaik, 1994)

In order to reach the high levels of horizontal shear as achieved in the first phase, the decision was made to reduce the width of the composite interface between the beam and the slab. One must be careful when doing this since it will result in a relatively high level of stress concentration at the composite interface. However, the practice of reducing the interface width was performed in previous research with no apparent problems reported (Hanson, 1960; Patnaik, 1994; Deschenes & Naito, 2006). Taking these observations into account, the interface width was decided to be reduced only enough to enable the desired horizontal shear stress levels to be reached.

6.3.3 Precast Web and Cast-In-Place Slab Design

The ACI 318-05 Building Code (2005) was followed when designing the test specimen. All of the requirements in the code pertaining to the design of composite prestressed beams were met

except for those concerning the horizontal shear strength and provisions for shear ties (ACI Section §17.5-17.6). The following paragraphs provide some detail into the specifics of the design of the composite concrete section.

The decision was made to design a prestressed web section since the use of prestressed beams is the standard for bridge and building construction. An 8 ksi mix was selected for the prestressed web based upon the high strength mixes which are now typically used in practice. The resulting dimensions of the web from the design were as follows: width of 6 in; height of 12 in; and length of 130 in. Four ½" ϕ special prestressed strands (A_p = 0.668 in^2) were used as the tension reinforcement of the web. The initial prestress was designed to be 175.5 ksi. Assuming a loss of twenty percent, the effective prestressing stress was 140.4 ksi. The required concrete and steel checks at transfer and service states for prestressed members were satisfied in accordance to Chapter 18 of the ACI code (2005).

Shear reinforcement was included in the web of the composite section in order to reduce the occurrence of web-shear and flexural-shear cracking and to aid in the prevention of shear failure. The reinforcement was designed according to the provisions given in Chapter 11 of the ACI code (2005). The design resulted in the use of #3 stirrups bent at a diameter of 3.25 inches and spaced every 4.5 inches along the length of the beam. Also included in the web were two smooth rods located approximately 2.5 inches from the top of the web and running the length of the beam. The rods would not provide any type of reinforcement but were used to hold the ties in place during fabrication. Chapter 11 was also used to calculate the web-shear and flexural-shear cracking loads in order to ascertain the horizontal shear stress of the composite interface at these levels.

The composite specimen was designed twice; once with a slab compressive strength of 3ksi, and again with a slab compressive strength of 6 ksi (for reasons discussed previously). For the design

of the composite section, the slab concrete was converted to the concrete web properties by using transformed section analysis. Also, calculations were performed to ensure that the slab width would comply with the requirements given for T-beam construction (ACI Section §8.10). The resulting dimensions of the slab, which turned out to be the same for both concrete compressive strengths, were as follows: width of 22 in; height of 3.5 in; and length of 110 in. The length of the slab was reduced by ten inches on both ends of the beam for reasons discussed in the previous section.

The slab reinforcement was designed to meet the spacing requirements provided in Chapter 7 of the ACI code (2005). #4 reinforcing bars were used for the design of all the slab reinforcement. The spacing of the flexural reinforcing steel was based upon the area of steel needed to resist the moment acting on the slab due to the applied load. The slab was divided into sections of where the applied load would be more and less prominent. The required spacing was then designed for each section in order to provide the proper reinforcement along the beam. Based on these calculations and the maximum spacing requirement provided in the ACI code Section §7.6, the #4 rebar was spaced at five inches under the loading area and nine inches elsewhere. Using ACI Section §7.12, the spacing of the temperature and shrinkage reinforcement was calculated to be 17.5 inches. This spacing would require only two #4 bars to run the length of the slab. However, in order to provide stability to the rebar cage, and additional #4 bar was included. The final spacing of the temperature and shrinkage reinforcement would be nine inches.

The composite test specimen resulting from the design is shown in the following figures. Figure 6-2 and Figure 6-3 show the cross-section and elevation view of the test specimen, respectably. Figure 6-4 details the layout of the slab reinforcement.

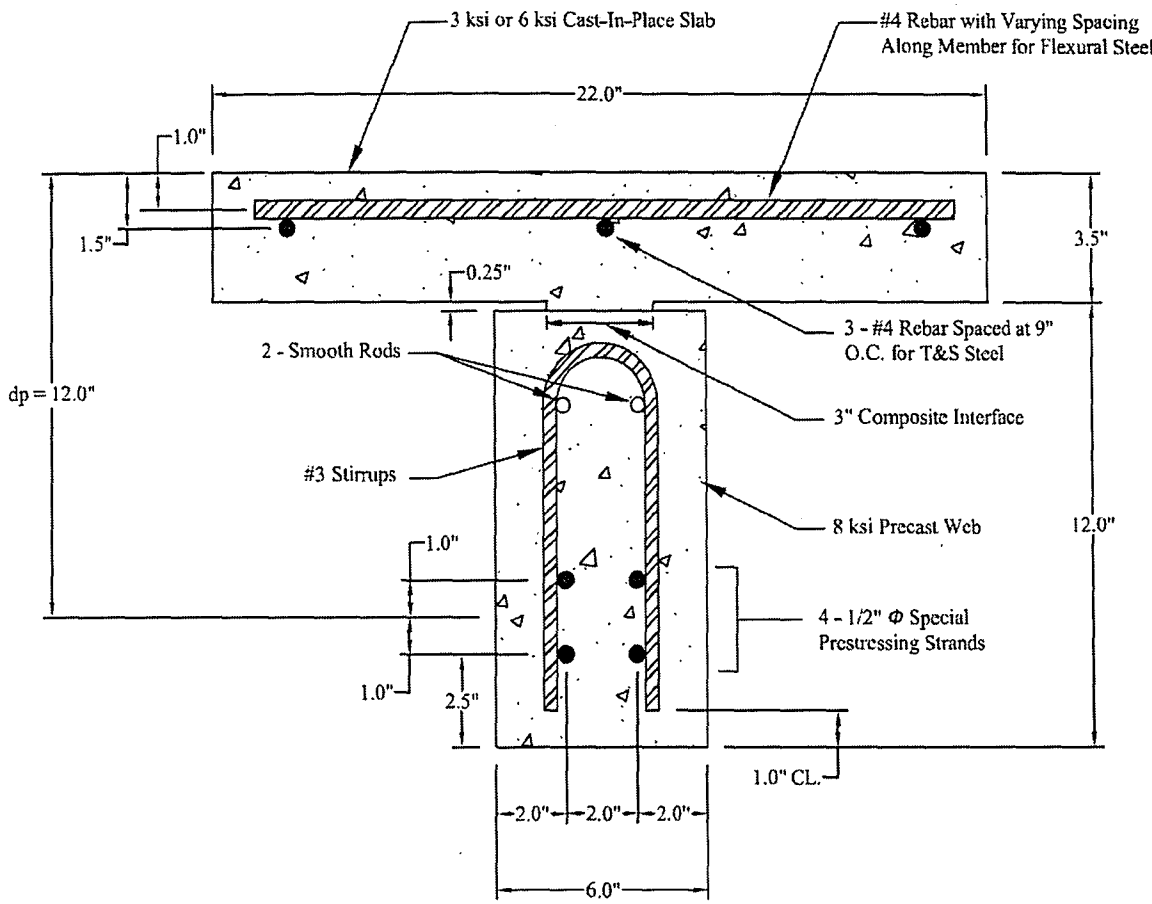

Figure 6-2: Cross-Section View of Phase 2 Test Specimen

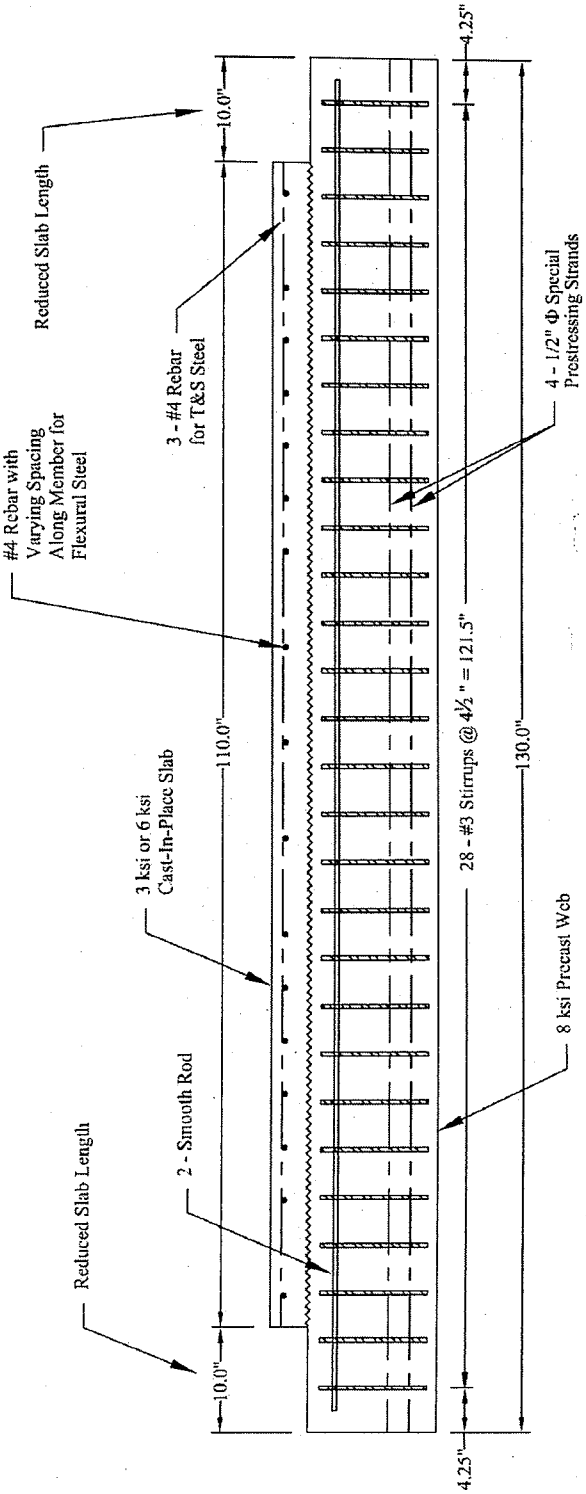

Figure 6-3: Elevation View of Phase 2 Test Specimen

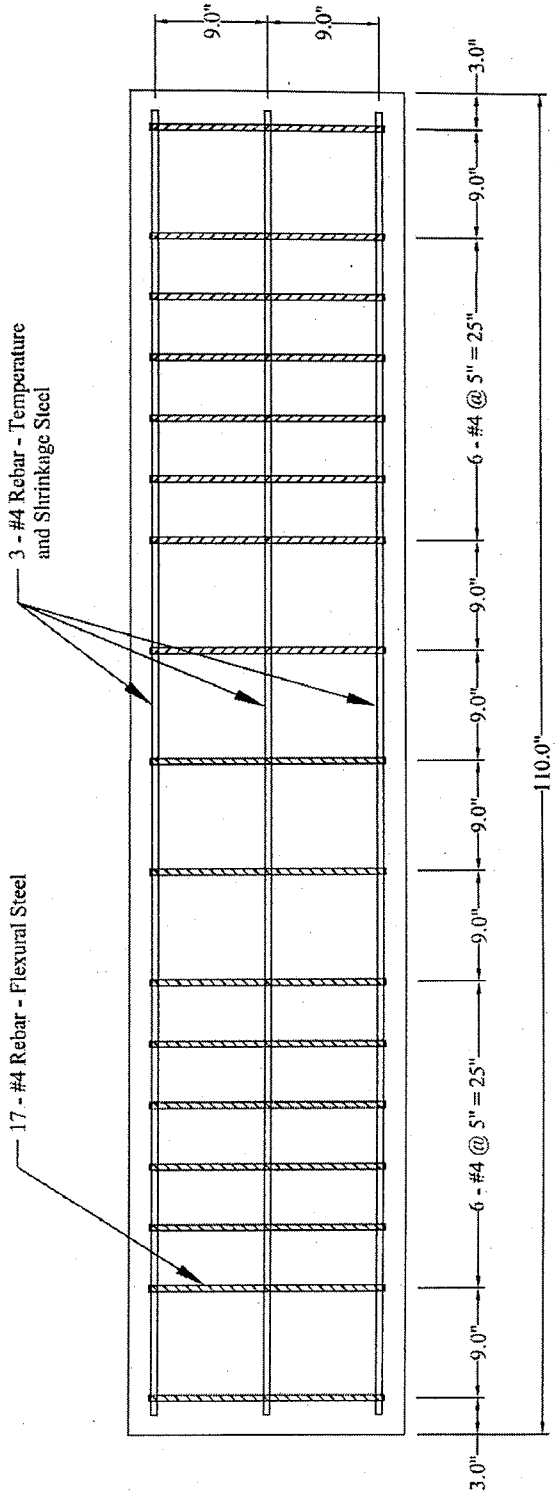

Figure 6-4: Plan View of Slab Reinforcement of Phase 2 Test Specimen

For both of the composite beam designs, the horizontal shear stress demand was calculated at flexural cracking and flexural-shear cracking using the classical elastic method and the simplified elastic beam method for ACI and AASHTO (Chapter 2). In order to achieve the designed horizontal shear stress before cracking of the section occurred, the width of the composite interface was reduced by fifty percent resulting in a three inch interface width (Figure 6-2). The depth of the interface was a quarter of an inch. I and Q were calculated using transformed section properties and considering the contribution of the prestressed strands and slab reinforcement. The shear force at flexural cracking was determined based on the cracking moment calculated using Equation 11-11 in ACI 318-05 Section §11.4.3.1 (ACI 318-08 Section §11.3.3.1). Equation 11-10 in the same section was used to determine the shear force required to initiate flexural-shear cracking of the beam. Table 6-2 tabulates the calculated horizontal shear stresses of the composite sections at the estimated flexural cracking load.

Table 6-2: Calculated Horizontal Shear Stress

Slab Compressive Strength	**Crack Type**	**Shear Force [kip]**	**Horizontal Shear Stress [psi]**		
			$\frac{V}{b_v d}$	$\frac{V}{b_v d_v}$	$\frac{VQ}{Ib_v}$
$f'_c = 3$ ksi	Flexural	35.2	978	1145	993
	Flexural-Shear	38.0	1056	1236	1072
$f'_c = 6$ ksi	Flexural	37.2	1034	1211	1107
	Flexural-Shear	40.0	1111	1301	1189

6.4 Validation of Specimen Design Using Finite Element Analysis

6.4.1 General

A finite element (FE) model was created in order to verify the designed behavior of the composite specimen. The FE model was also implemented to validate the horizontal shear stresses of the composite interface tabulated in Table 6-2. The FE program DIANA was chosen to analyze the

model due to the programs simplicity in incorporating prestressed strands. However, due to the difficulty drawing the section and designing the element mesh in DIANA, FEMAP was chosen to perform the preprocessing work. The following sections will provide a summary of the design and results of the finite element analysis.

6.4.2 FE Model Design

The FE model consisted of a two-dimensional elevation view of a simply supported beam subjected to a two-point load configuration similar to the actual test setup for the beam tests. Four different materials were used when creating the model: concrete for the prestressed web, concrete for the cast-in-place slab (which included the reduced interface), steel plates at the supports and point loads in order to distribute the loads, and prestressed steel in the concrete web. The slab steel and shear reinforcement were not added for simplicity in modeling. Figure 6-5 presents the basic design of the FE model.

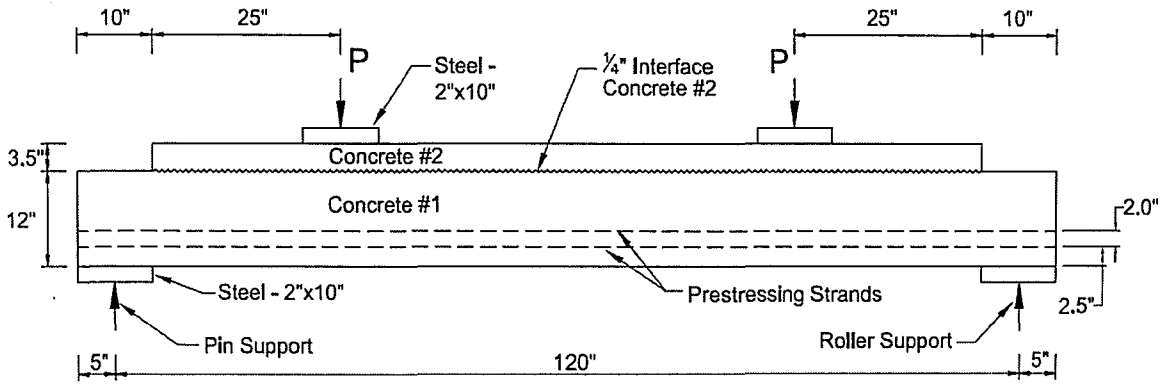

Figure 6-5: Elevation View of the Finite Element Model

The steel plates and concrete are modeled with the CQ16M element (Figure 6-6) which is an eight-node quadrilateral isoparametric plane stress element. It is based on quadratic interpolation and Gauss integration. The polynomial for the displacements in the in the x and y direction presented in Equation 24 is complete through the quadratic terms. Interface elements (N4IF) were applied between the concrete and steel plates in order to allow some movement of the plates

instead of being fixed to the concrete. The concrete-to-concrete interfaces were connected directly to one another assuming a perfect bond was achieved. The properties assigned to the two concretes and the steel plates are tabulated in Table 6-3.

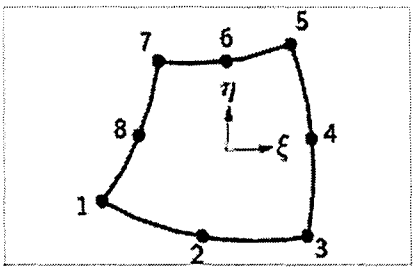

Figure 6-6: CQ16M Element

$$u_i(\xi,\eta) = a_0 + a_1\xi + a_2\eta + a_3\xi\eta + a_4\xi^2 + a_5\eta^2 + a_6\xi^2\eta + a_7\xi\eta^2 \quad \text{(Eq. 24)}$$

Table 6-3: FE Model Properties for Steel and Concrete

Material	Thickness [in]	f'c [ksi]	E [ksi]	ν
Web Concrete	6	8.0	5422	0.2
Slab Concrete	22	6.0	4696	0.2
Interface Concrete	3	6.0	4696	0.2
Steel Plate	10	N/A	29000	0.3

The ½" ϕ special prestressed strands were modeled using a BAR in plane stress element. The prestressing works by strengthening the properties of the stress elements that the BAR element passes through. Two rows of stands were used in the model. The BAR element for each row was assigned the area of two strand (A_p = 0.334 in^2 per row) along with a Young's modulus of 29,000 ksi, a Poisson's ratio of 0.3, and an initial prestressing stress (f_{pi}) of 175.5 ksi. A transfer length of 23.4 in was also incorporated meaning the strand stress will be equal to zero at the end of the beam and f_{pi} at the transfer length.

The element mesh was refined several times until the stress and deflection at midspan and the support reactions converged. Compared to the values found using beam theory, the resulting

values for the stress and deflection obtained from the FE model were approximately 8.4% and 2.8% different, respectively. The final mesh layout is shown in Figure 6-7 and Figure 6-8. It should be noted that the mesh is symmetric about the midspan of the model.

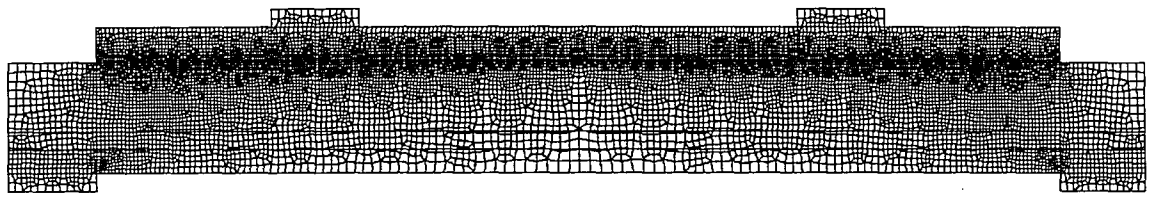

Figure 6-7: Final Mesh Layout

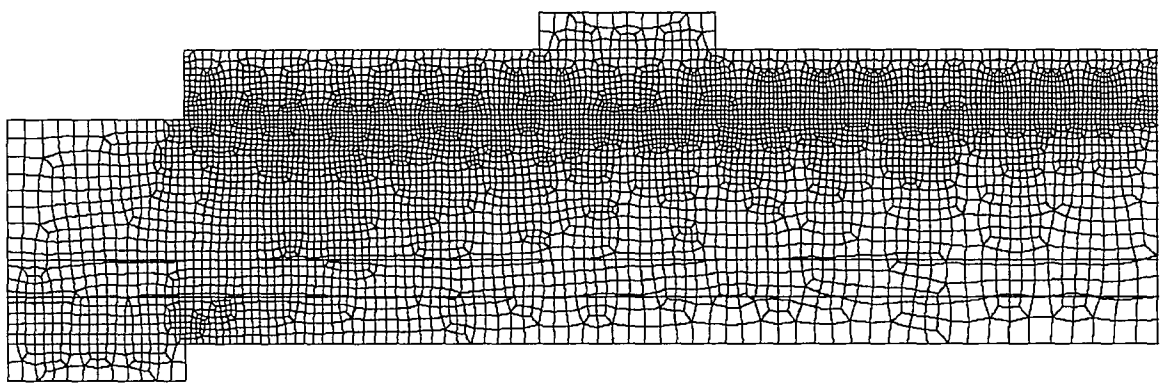

Figure 6-8: Final Mesh Layout – Close-Up of Left Side

The boundary conditions were applied assuming the beam was simply supported resulting in a pinned connection on one end and a roller connection on the other. The supports were assumed to act through the centerline of the supported area (Figure 6-9). Therefore, a pin and roller fixity was applied to the bottom midpoint node of the left and right steel support plate, respectably. The mesh was refined in the steel plates so that the forces would be dispersed and more uniform by the time they reached the concrete.

values for the stress and deflection obtained from the FE model were approximately 8.4% and 2.8% different, respectively. The final mesh layout is shown in Figure 6-7 and Figure 6-8. It should be noted that the mesh is symmetric about the midspan of the model.

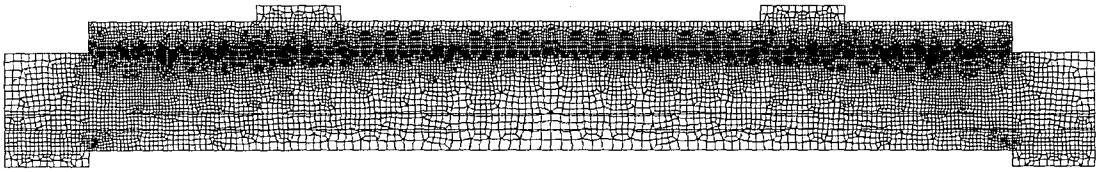

Figure 6-7: Final Mesh Layout

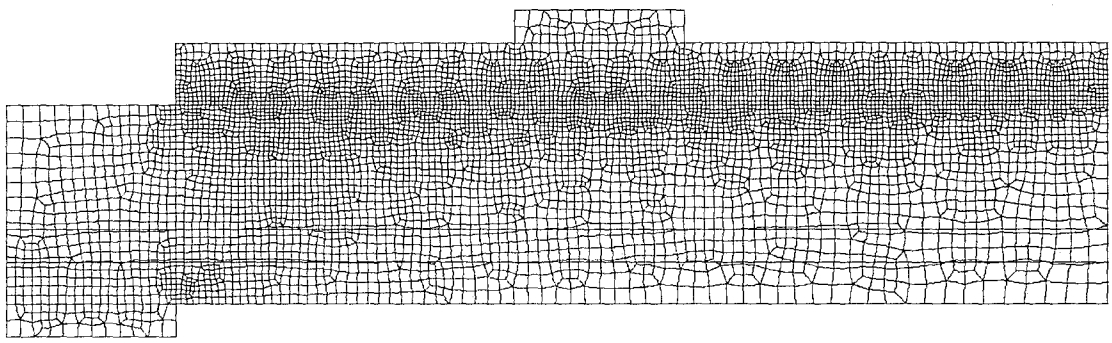

Figure 6-8: Final Mesh Layout – Close-Up of Left Side

The boundary conditions were applied assuming the beam was simply supported resulting in a pinned connection on one end and a roller connection on the other. The supports were assumed to act through the centerline of the supported area (Figure 6-9). Therefore, a pin and roller fixity was applied to the bottom midpoint node of the left and right steel support plate, respectably. The mesh was refined in the steel plates so that the forces would be dispersed and more uniform by the time they reached the concrete.

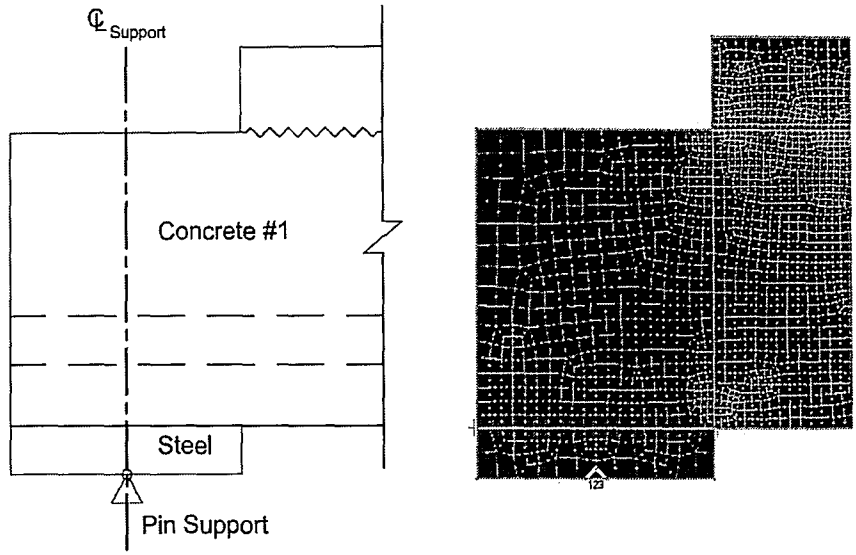

Figure 6-9: Boundary Conditions of FE Model

Two point loads were symmetrically applied to the beam at a distance of thirty inches from the support. The loads were assumed to act through the centerline of the loaded area and the mesh was refined in the steel plates so the forces would be more uniform when the reached the concrete (Figure 6-10). A unit load of -1 kip was applied to the top midpoint node of each loading plate in order to provide a start value and direction for the load steps that would be executed when analyzed in DIANA.

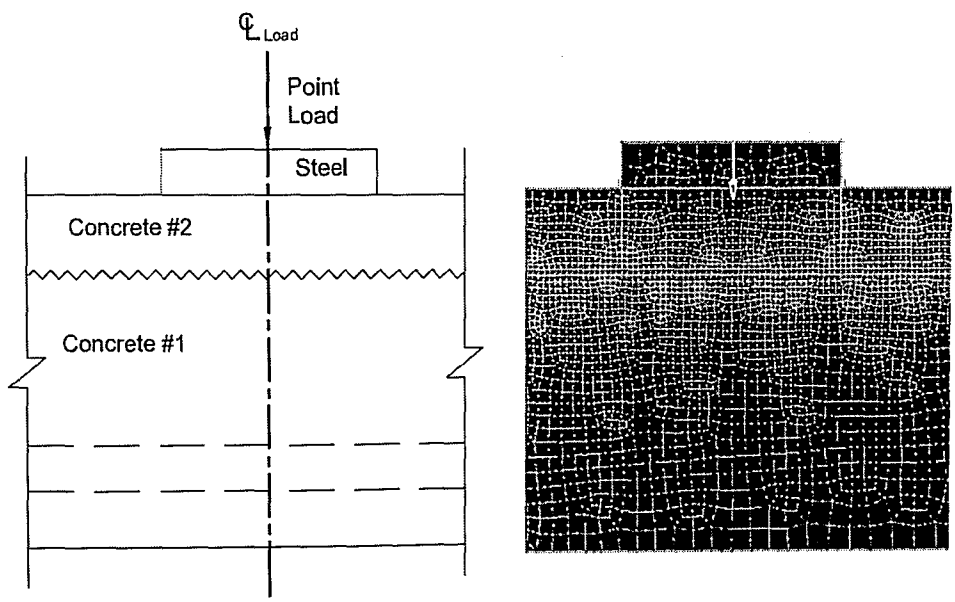

Figure 6-10: Loading Conditions for FE Model

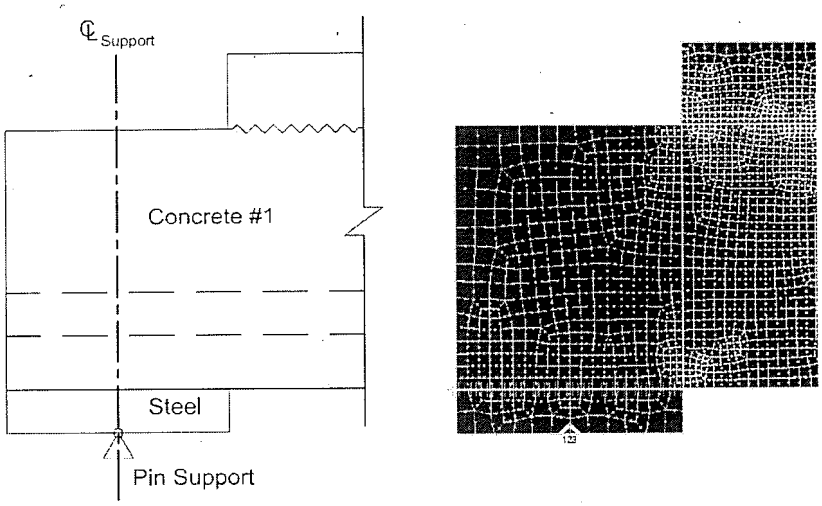

Figure 6-9: Boundary Conditions of FE Model

Two point loads were symmetrically applied to the beam at a distance of thirty inches from the support. The loads were assumed to act through the centerline of the loaded area and the mesh was refined in the steel plates so the forces would be more uniform when the reached the concrete (Figure 6-10). A unit load of -1 kip was applied to the top midpoint node of each loading plate in order to provide a start value and direction for the load steps that would be executed when analyzed in DIANA.

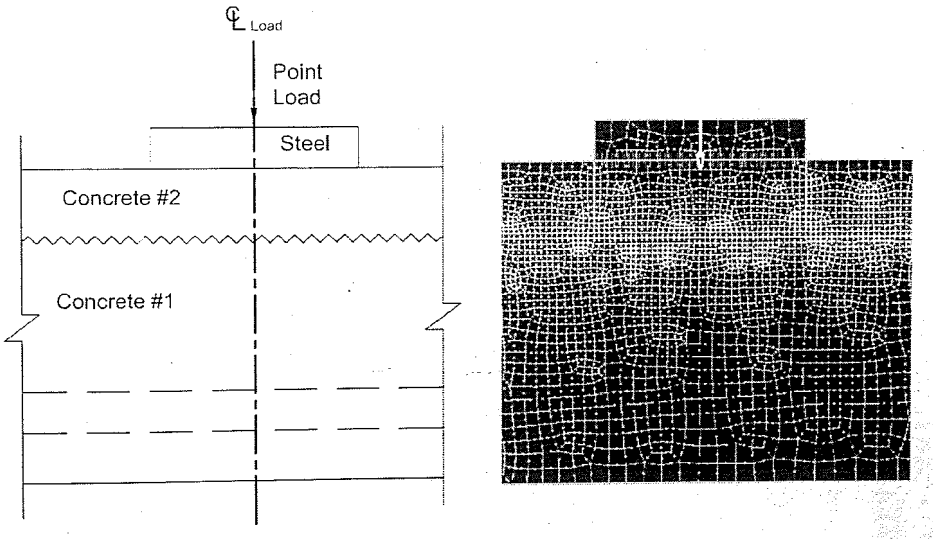

Figure 6-10: Loading Conditions for FE Model

6.4.3 FE Analysis Results

The FE analysis began by applying the stresses due to the prestressed strands. Then, the point loads were linearly and statically applied from 0 to 40 kips in the negative y-direction. The analysis outputted the following results for each load case: displacement, forces, stresses, and strains.

The shear stresses of the FE model were studies at a point load of 37 kips which is the load in which flexural cracking was calculated to initiate in the section. Figure 6-11 presents the shear stresses of the left half of the FE model. The stresses are scaled from 0 to 1.3 ksi in 15 equal levels. The shear stresses of the composite interface are the largest between the load and the end of the slab and virtually zero from the load to the midspan, which is to be expected.

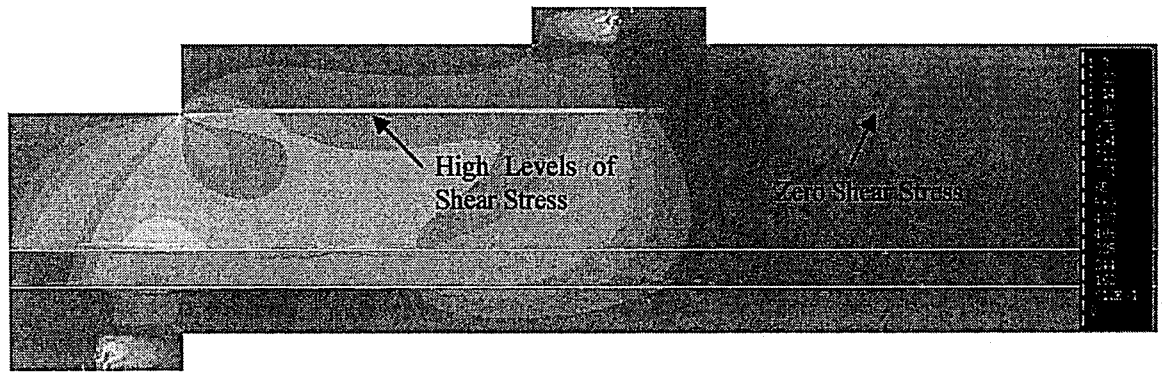

Figure 6-11: Shear Stresses at a Point Load of 37 kips

Figure 6-12 shows a close-up view of the composite interface shear stress between the load point and the end of the slab. The shear stresses are scaled from 0.8 to 1.5 ksi in 12 equal levels. From left to right, the shear stress starts at a very high level of 1500 psi then gradually decrease to 1020 psi. At this point, the shear stresses stay constant for a distance before increasing a little and finally decreasing to zero. The initial high shear stress is most likely the result of a stress concentration since the cross-section of the member changes at that instance. The jump in shear stress near the loading point may be due to a strut and tie scenario as the point load travels

6.4.3 FE Analysis Results

The FE analysis began by applying the stresses due to the prestressed strands. Then, the point loads were linearly and statically applied from 0 to 40 kips in the negative y-direction. The analysis outputted the following results for each load case: displacement, forces, stresses, and strains.

The shear stresses of the FE model were studies at a point load of 37 kips which is the load in which flexural cracking was calculated to initiate in the section. Figure 6-11 presents the shear stresses of the left half of the FE model. The stresses are scaled from 0 to 1.3 ksi in 15 equal levels. The shear stresses of the composite interface are the largest between the load and the end of the slab and virtually zero from the load to the midspan, which is to be expected.

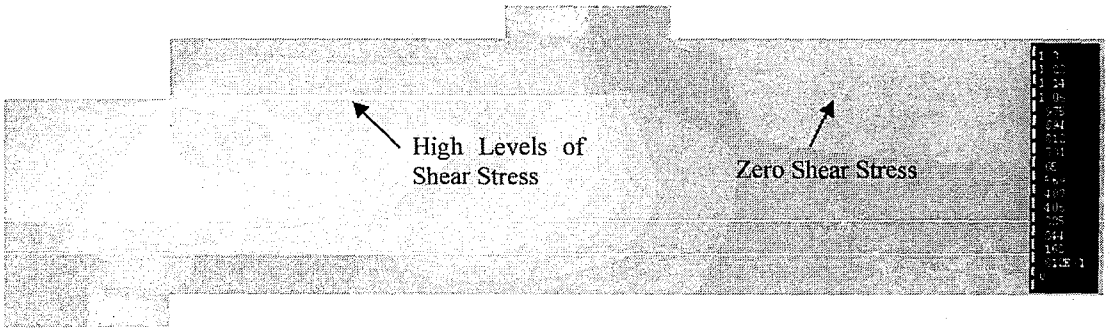

Figure 6-11: Shear Stresses at a Point Load of 37 kips

Figure 6-12 shows a close-up view of the composite interface shear stress between the load point and the end of the slab. The shear stresses are scaled from 0.8 to 1.5 ksi in 12 equal levels. From left to right, the shear stress starts at a very high level of 1500 psi then gradually decrease to 1020 psi. At this point, the shear stresses stay constant for a distance before increasing a little and finally decreasing to zero. The initial high shear stress is most likely the result of a stress concentration since the cross-section of the member changes at that instance. The jump in shear stress near the loading point may be due to a strut and tie scenario as the point load travels

diagonally to the support. In general, the shear stress of the composite interface ranges from approximately 1020 psi to 1500 psi. The average shear stress across the interface is calculated to be about 1108 psi which is on the level of the horizontal shear stress calculated for the design of a composite beam subjected to a load of 37 kips (Table 6-2).

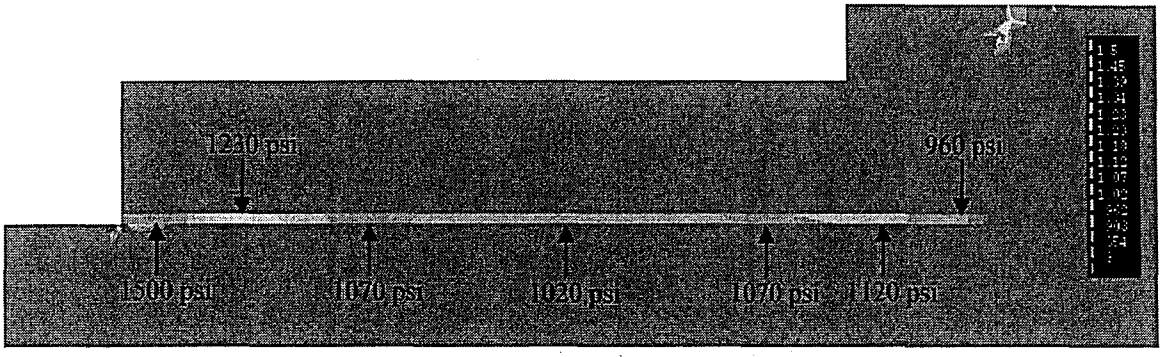

Figure 6-12: Close-Up View of Interface Shear Stress

6.4.4 Summary

The finite element model results indicate the beam designed for the experimental study should produce horizontal shear stress demands in excess of 1000 psi prior to cracking. In addition, the FE analysis indicates that the shear stresses generated are relatively uniform across the interface and do not generate significant stress concentrations. Based on the results, the experimental specimen design was deemed adequate. The resulting demands however indicate that the stresses will be the greatest near the ends of the interface and thus slip should propagate from the ends of the beam to the center. The FE model is used several other times during the course of the specimen testing to validate the levels of stress and deflection.

diagonally to the support. In general, the shear stress of the composite interface ranges from approximately 1020 psi to 1500 psi. The average shear stress across the interface is calculated to be about 1108 psi which is on the level of the horizontal shear stress calculated for the design of a composite beam subjected to a load of 37 kips (Table 6-2).

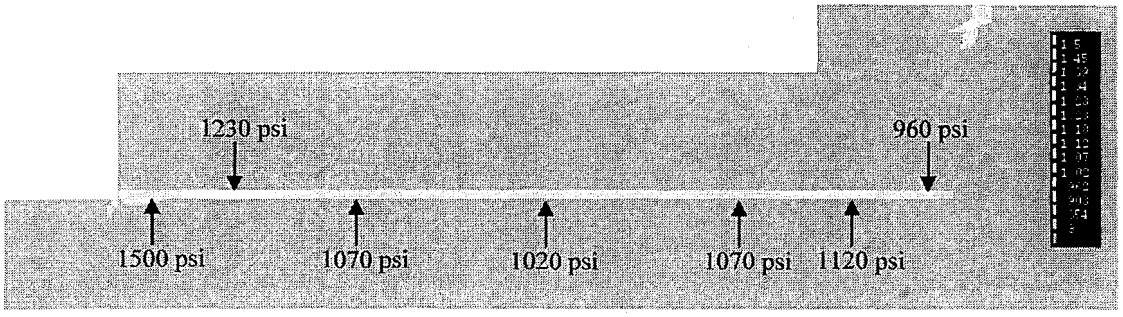

Figure 6-12: Close-Up View of Interface Shear Stress

6.4.4 Summary

The finite element model results indicate the beam designed for the experimental study should produce horizontal shear stress demands in excess of 1000 psi prior to cracking. In addition, the FE analysis indicates that the shear stresses generated are relatively uniform across the interface and do not generate significant stress concentrations. Based on the results, the experimental specimen design was deemed adequate. The resulting demands however indicate that the stresses will be the greatest near the ends of the interface and thus slip should propagate from the ends of the beam to the center. The FE model is used several other times during the course of the specimen testing to validate the levels of stress and deflection.

7 Experimental Program – Phase 2 – Fabrication of Test Specimens

7.1 General

In order to more effectively simulate the typical fabrication methods for composite concrete construction, the test specimens were fabricated in a different manner than those of the first phase. In the first phase, the specimen web and slab were fabricated with a short time period between placement and in the same controlled environment. For the second phase, the cast-in-place slab was poured several months after the precast, prestressed web and in a different location. This process simulates the typical fabrication method used for topped precast sections (i.e., the shipping of the web to the job site, followed by casting of the slab). The extended time between the pouring of the two concrete components will result in greater differential shrinkage between the two members.

The next several sections in this chapter will discuss the fabrication methods for the composite test specimens. The process of fabricating the prestressed, precast web is described first, followed by the design and construction of the slab formwork, and finally the fabrication of the cast-in-place slab.

7.2 Precast Concrete Web Fabrication

7.2.1 General

Since prestressing plants' fabrication practices may vary, a different manufacturer than the one from the first phase was chosen for the fabrication of the prestressed webs thus allowing for a broader range of surface finishes to be considered. The prestressed, precast concrete manufacturer chosen was Newcrete Products located in Roaring Spring, Pennsylvania. Newcrete Products is a division of New Enterprise Stone & Lime Co., Inc.

7.2.2 Concrete Webs Material Properties

The webs were cast from two pours. The first pour consisted of the eight smooth finish webs and eight as-placed finish webs. The second pour consisted of the eight broom finish webs and eight rake finish webs. Both pours consisted of a high early strength, self consolidating concrete mix. Self consolidating concrete (SCC) is a highly workable concrete that has the ability to flow through reinforcement under its own weight and adequately fill all voids. SCC is the type of concrete typically used by Newcrete Products. The design compressive strength of both mixes was 8 ksi. The properties of each mix are presented in Table 7-1.

Table 7-1: Properties of Web Concrete Mix per Cubic Yard

Property	Units	Properties per Cubic Yard	
		Pour 1 Smooth and As-Placed	Pour 2 Broom and Rake
Type III Cement	lbs.	541	541
Coarse Aggregate SSD - #67	lbs.	1689	1689
Fine Aggregate SSD	lbs.	1215	1215
GGBFS	lbs.	291	291
VMA 450	oz.	20	20
Glenium 3000 NS HRWR	oz.	122	122
Pozzolith 200 N WR	oz.	4	4
Pozzolith 100 XR Retarder	oz.	4	4
MB-VR Air Entrainment	oz.	27	27.5
Water/Cement Ratio	-	0.48	0.48
Percent Air	%	6.2	7.0
Spread	in.	22	24

Each web consisted of four ½" ϕ special low relaxation prestressed strands. The seven wire strands had an area of 0.164 in^2 and a modulus of elasticity of 28,990 ksi. The ultimate strength of the prestressed strands was 282.5 ksi.

7.2.3 Web Concrete Pour

The first pour (smooth and as-placed surface finishes) occurred on June 5, 2007 and the second pour (broom and rake surface finishes) occurred on June 8, 2007. Each pour took place on a 108 foot prestressing bed consisting of two rows of forms (Figure 7-1). The ½" ϕ special strands were run the length of the bed and a jacking force of 31.366 kips were applied to each strand by a mechanical jack (Figure 7-2). The two smooth rods and #3 stirrups were then tied into place (Figure 7-3). Finally, the steel forms were fastened together. It should be noted that the steel forms used in fabricating the webs created a ¾" chamfer in the corners of the web (Figure 7-4).

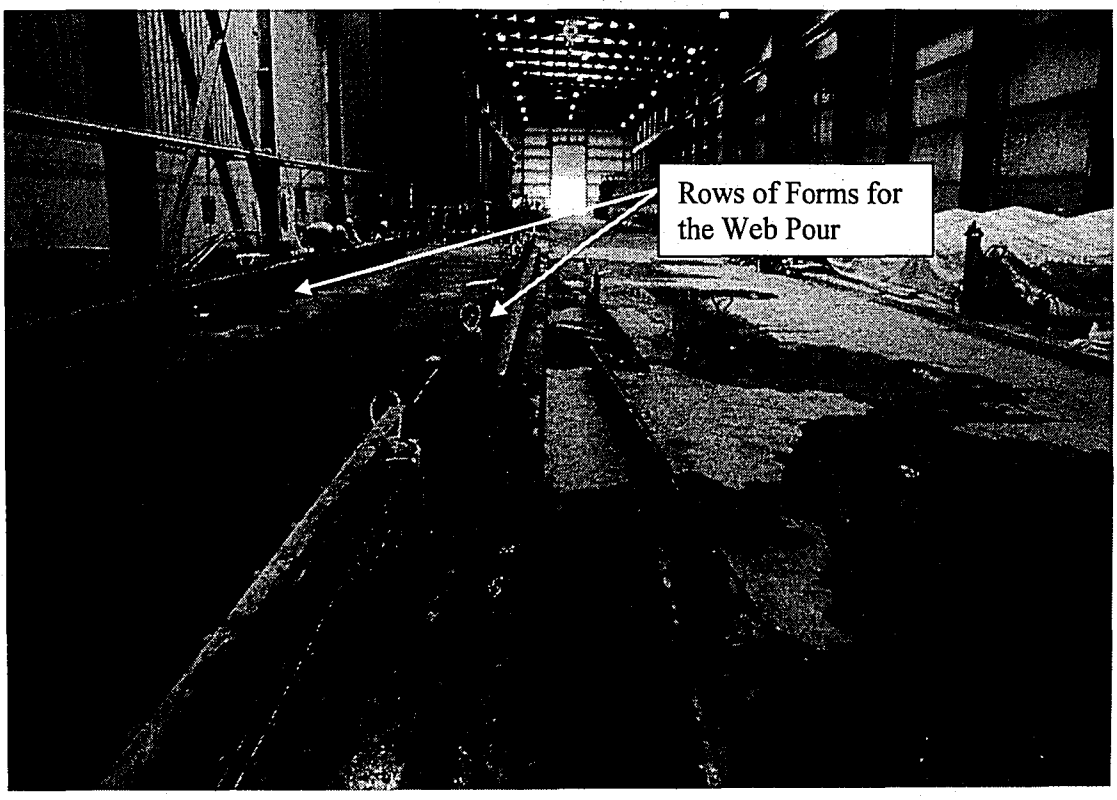

Figure 7-1: Prestressing Bed

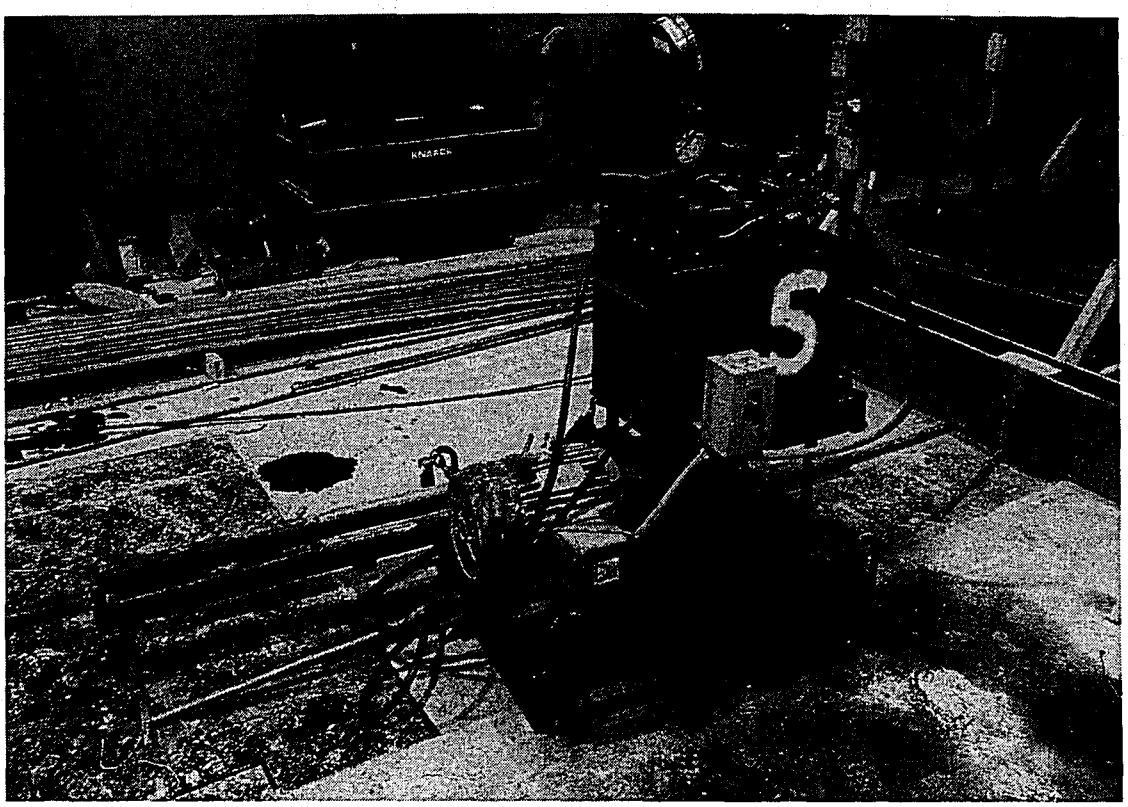

Figure 7-2: Mechanical Jack for Prestressing

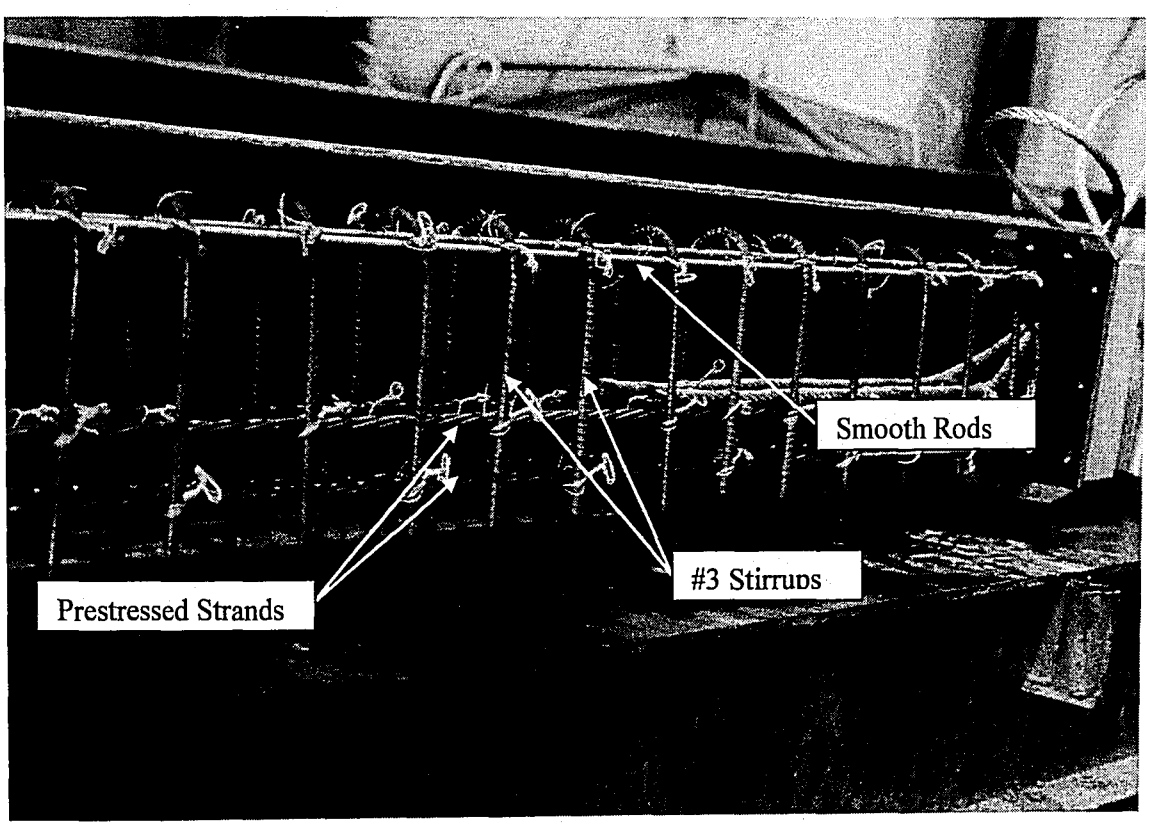

Figure 7-3: Web Reinforcement

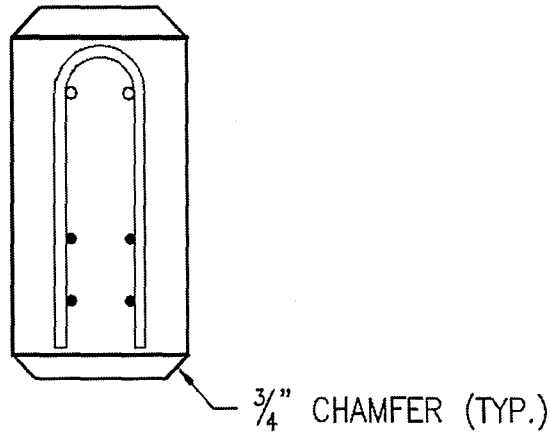

Figure 7-4: Cross-Section of Beam with Chamfer

When the concrete truck arrived, a spread test was performed. The test consisted of filling a standard slump cone, lifting the cone, and then measuring the spread of the concrete (Figure 7-5). Once this test was completed, 4x8 test cylinders were filled and the concrete webs were poured. The concrete was poured either directly from the concrete truck (for the near row of forms) or using a concrete bucket (for the far row of forms) (Figure 7-6). The self consolidating concrete made the pouring processes run much smoother since the concrete flows into the forms easily and only a short amount of vibrating is needed. Once the pour was completed, the concrete was allowed to set for a while until the surface finishes were applied.

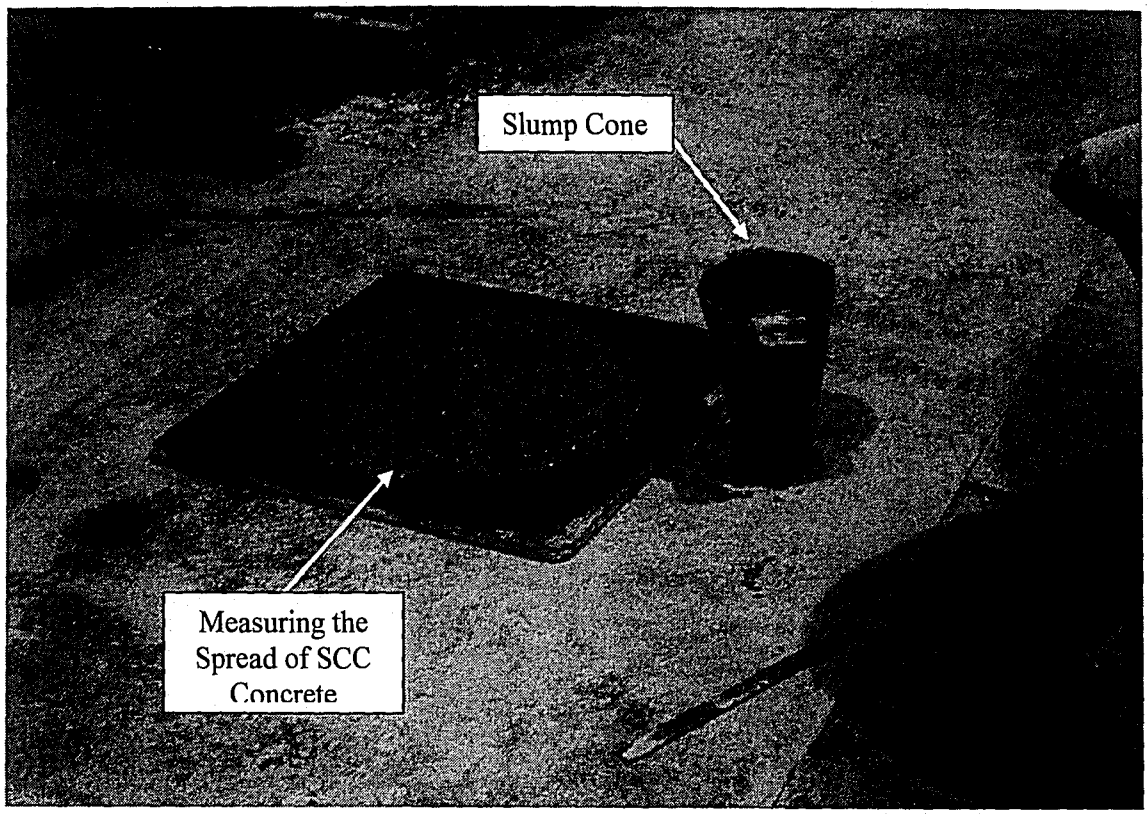

Figure 7-5: Spread Test for SCC

Figure 7-6: Placement of Web Concrete

7.2.4 Surface Finish Application

The finishers were instructed to apply each of the four surface finishes in the way they typically do for other prestressed projects. The procedure of applying the surface finishes varies slightly from the standard method of application due to the use of a self consolidating concrete mixture.

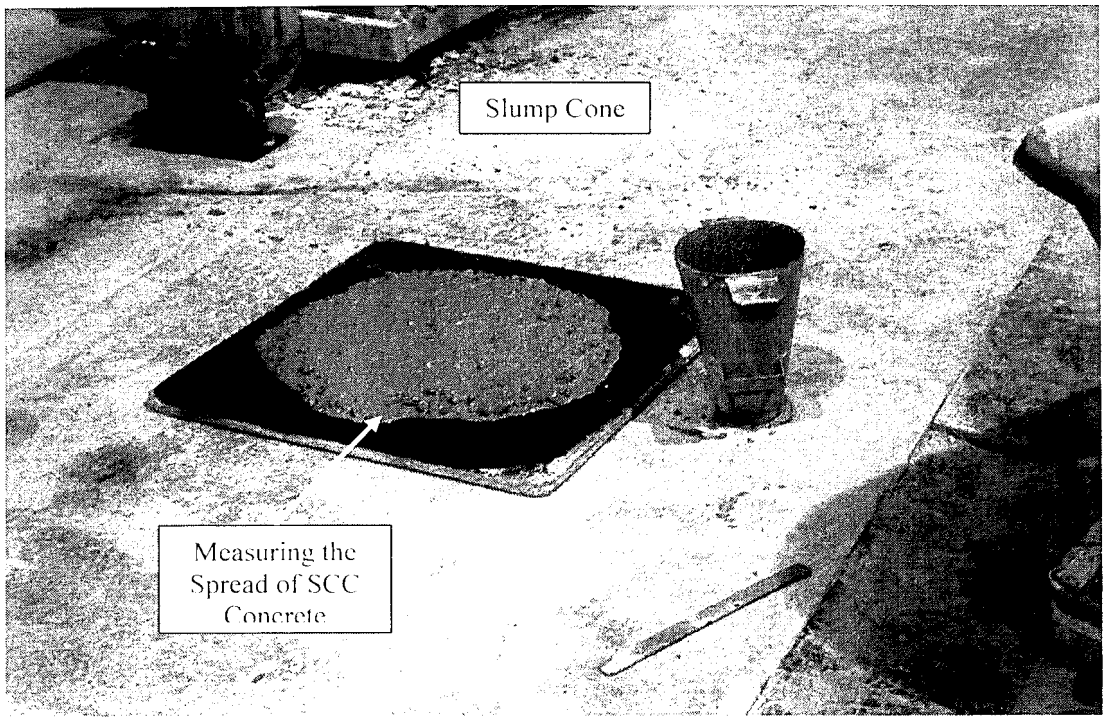

Figure 7-5: Spread Test for SCC

Figure 7-6: Placement of Web Concrete

7.2.4 Surface Finish Application

The finishers were instructed to apply each of the four surface finishes in the way they typically do for other prestressed projects. The procedure of applying the surface finishes varies slightly from the standard method of application due to the use of a self consolidating concrete mixture.

The following sections provide a brief description of the process of applying the four different surface finishes.

7.2.4.1 As-Placed

As implied by the name, the surface finish for the as-placed beams were left as is after the pour. The concrete is leveled out and not disturbed while it cures. The resulting finish allows for aggregate to protrude for the web providing a roughened surface as shown in Figure 7-7.

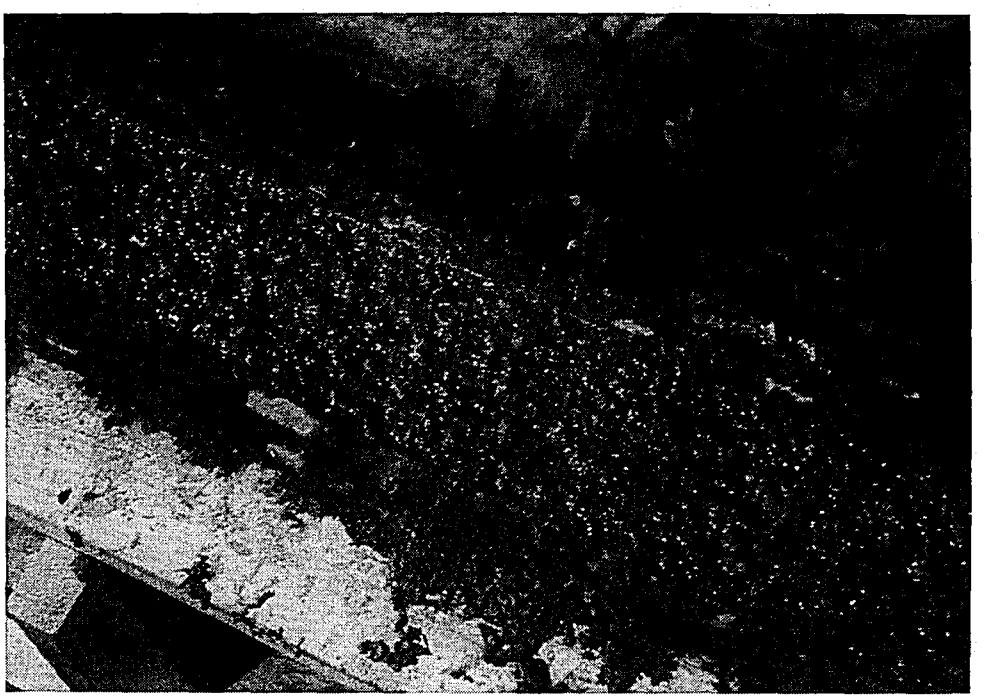

Figure 7-7: As-Placed Surface Finish

7.2.4.2 Smooth

For the application of the smooth surface finish, the concrete was first spread evenly during the pour. A short time later, a hard trowel was run across the surface to smooth it out (Figure 7-8). However, the concrete was sticking to the trowel and tearing the surface. The only way to rectify this problem was to apply a chemical called Confilm to the surface before using the trowel. Confilm is an evaporation reducer which also aids with surface finishes. A smooth surface finish was achieved as seen in Figure 7-9.

The following sections provide a brief description of the process of applying the four different surface finishes.

7.2.4.1 As-Placed

As implied by the name, the surface finish for the as-placed beams were left as is after the pour. The concrete is leveled out and not disturbed while it cures. The resulting finish allows for aggregate to protrude for the web providing a roughened surface as shown in Figure 7-7.

Figure 7-7: As-Placed Surface Finish

7.2.4.2 Smooth

For the application of the smooth surface finish, the concrete was first spread evenly during the pour. A short time later, a hard trowel was run across the surface to smooth it out (Figure 7-8). However, the concrete was sticking to the trowel and tearing the surface. The only way to rectify this problem was to apply a chemical called Confilm to the surface before using the trowel. Confilm is an evaporation reducer which also aids with surface finishes. A smooth surface finish was achieved as seen in Figure 7-9.

Figure 7-8: Applying a Smooth Surface Finish with a Hard Trowel

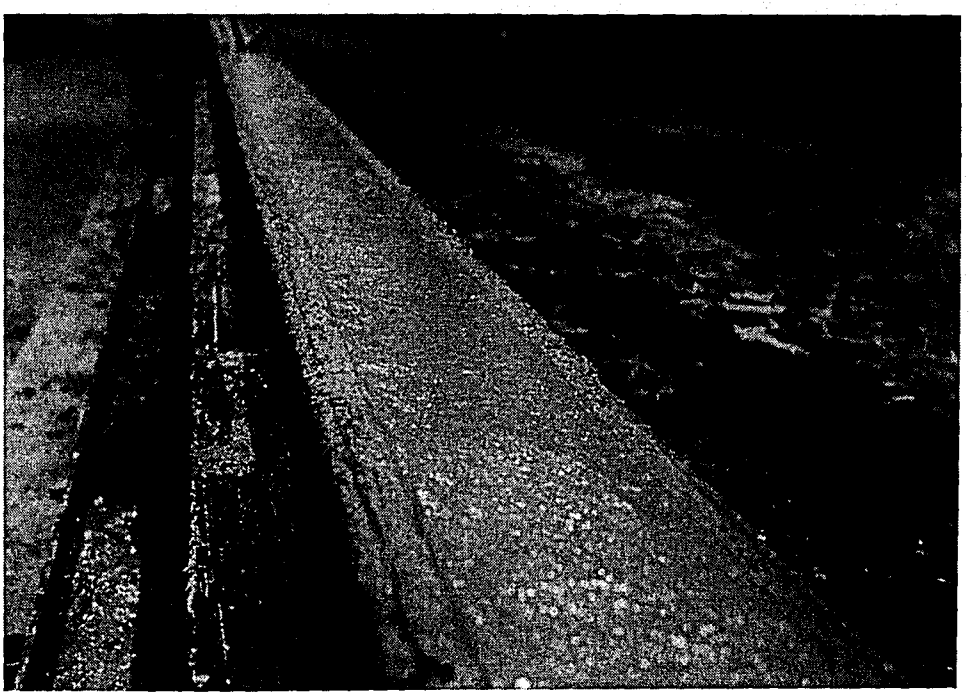

Figure 7-9: Smooth Surface Finish

7.2.4.3 Broom

The broom surface finish was applied to the concrete about an hour after the concrete was poured to allow the concrete to sufficiently harden. Comfilm was used on the surface in order to increase

Figure 7-8: Applying a Smooth Surface Finish with a Hard Trowel

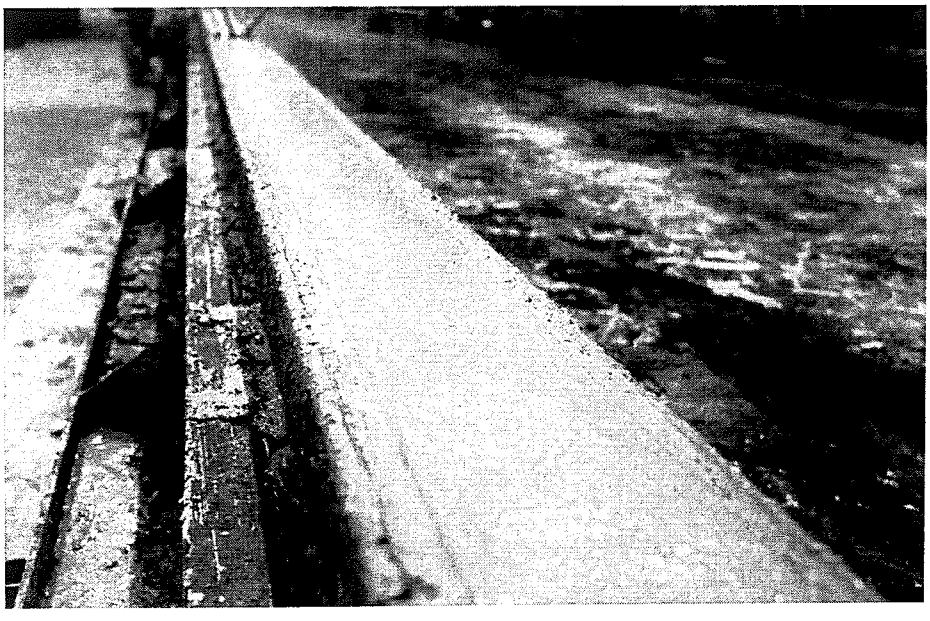

Figure 7-9: Smooth Surface Finish

7.2.4.3 Broom

The broom surface finish was applied to the concrete about an hour after the concrete was poured to allow the concrete to sufficiently harden. Comfilm was used on the surface in order to increase

the workability while smoothing it with a trowel. A broom finish was then applied by running a stiff bristle broom across the surface transverse to the beams length (Figure 7-10 and Figure 7-11).

Figure 7-10: Applying the Broom Surface Finish

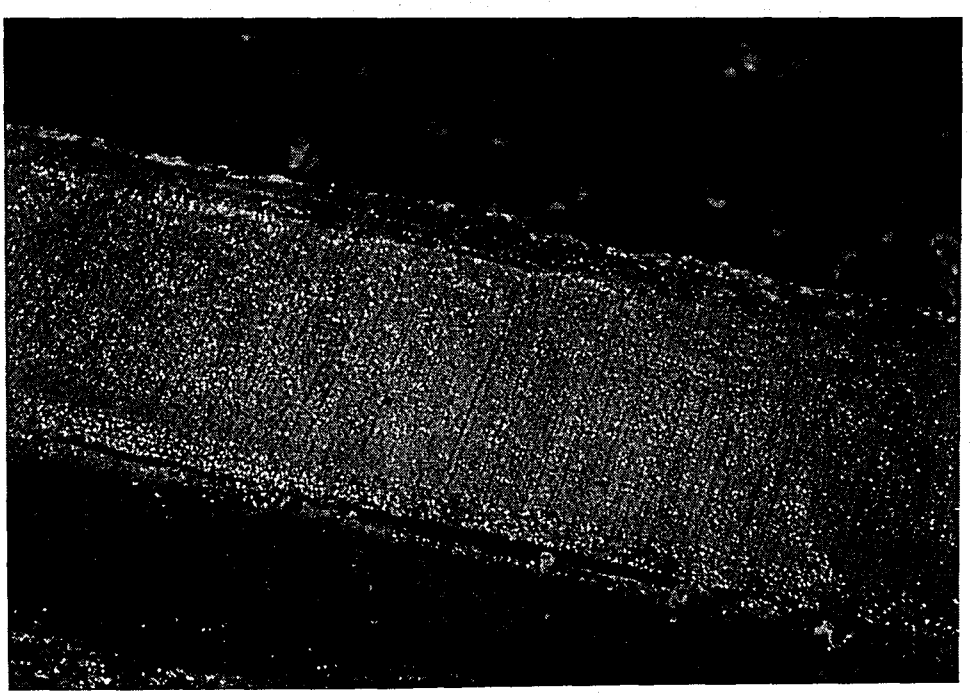

Figure 7-11: Broom Surface Finish

the workability while smoothing it with a trowel. A broom finish was then applied by running a stiff bristle broom across the surface transverse to the beams length (Figure 7-10 and Figure 7-11).

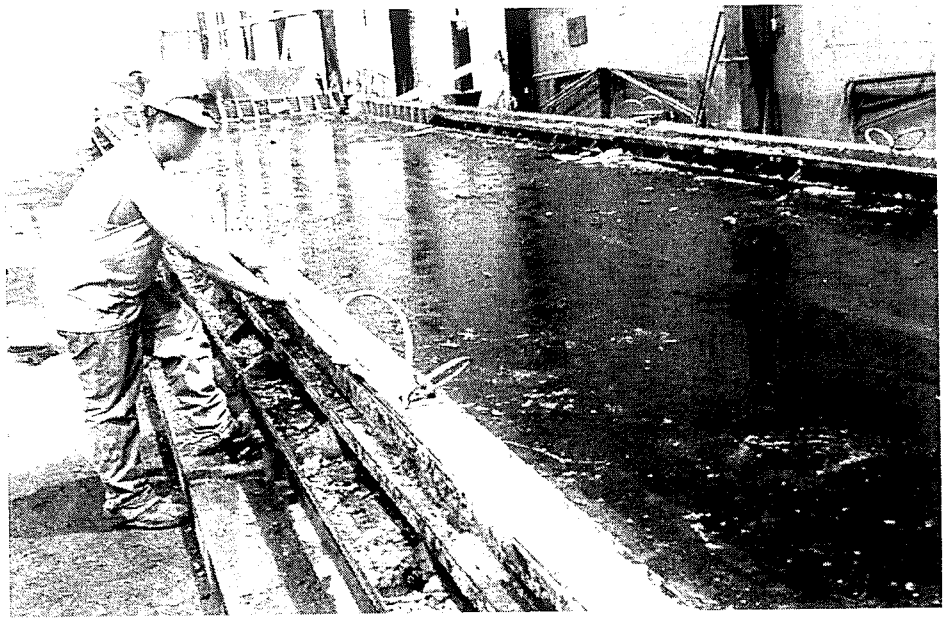

Figure 7-10: Applying the Broom Surface Finish

Figure 7-11: Broom Surface Finish

7.2.4.4 Rake

This surface finish was achieved using a ¼" rake. The surface finish was applied approximately a half hour after the pour. It was important to apply the finish at the proper time. If the finish was applied to early, the concrete would run back together after it was raked; if applied to late, the concrete would be too stiff and cause the concrete to tear. The finish was applied as consistently as possible by running a rake across the surface transverse to the beams length (Figure 7-12). The resulting rake surface finish can be seen in Figure 7-13.

Figure 7-12: Applying the Rake Surface Finish

7.2.4.4 Rake

This surface finish was achieved using a ¼" rake. The surface finish was applied approximately a half hour after the pour. It was important to apply the finish at the proper time. If the finish was applied to early, the concrete would run back together after it was raked; if applied to late, the concrete would be too stiff and cause the concrete to tear. The finish was applied as consistently as possible by running a rake across the surface transverse to the beams length (Figure 7-12). The resulting rake surface finish can be seen in Figure 7-13.

Figure 7-12: Applying the Rake Surface Finish

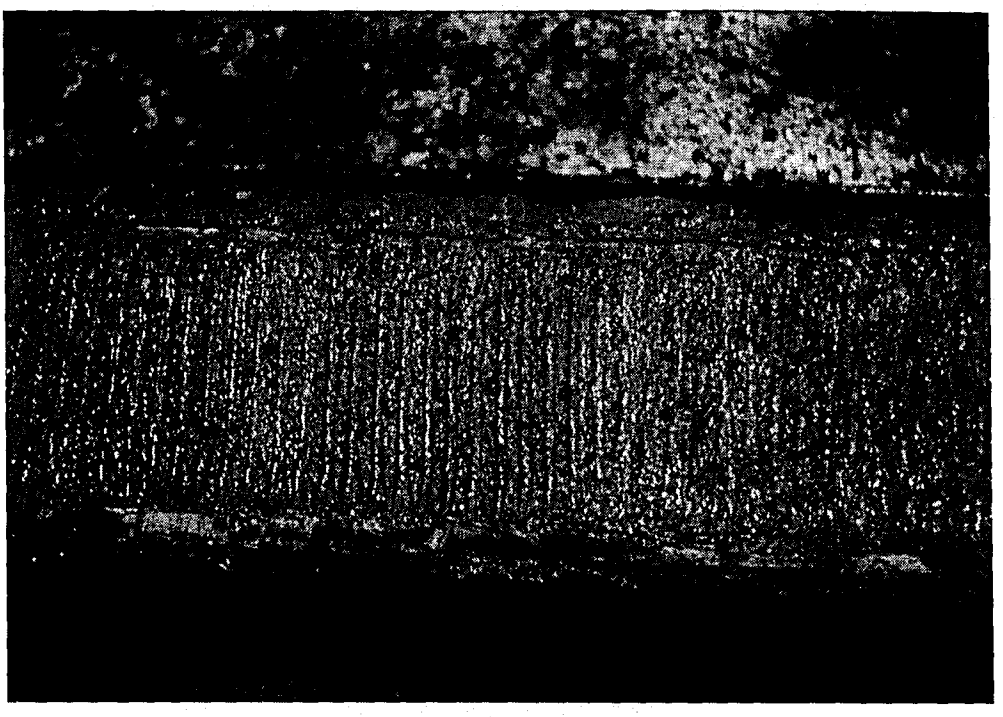

Figure 7-13: Rake Surface Finish

7.2.5 Curing and Release of the Concrete Webs

Once the surface finishes were completed, the bed was covered in plastic and the beams were steam cured for three days. The concrete strengths were then checked by breaking two cylinders to make sure they reached the initial compressive strength before the prestressed strands were released. The release breaks were 7055 and 7537 psi for the first pour (smooth and as-placed), and 7779 and 7773 psi for the second pour (broom and rake). The webs were released on June 8, 2007 for the first pour and June 11, 2007 for the second pour. The webs were then stored at Newcrete Products until they were able to be shipped to Lehigh University.

7.3 Design and Construction of the Slab Formwork

The next stage of the specimen fabrication was to cast the slab on top of the web. In order for this to be done, formwork needed to be designed and constructed to support the slab concrete as it was poured and cured. Due to the limited staging area in the ATLSS Center lab and the large quantity

Figure 7-13: Rake Surface Finish

7.2.5 Curing and Release of the Concrete Webs

Once the surface finishes were completed, the bed was covered in plastic and the beams were steam cured for three days. The concrete strengths were then checked by breaking two cylinders to make sure they reached the initial compressive strength before the prestressed strands were released. The release breaks were 7055 and 7537 psi for the first pour (smooth and as-placed), and 7779 and 7773 psi for the second pour (broom and rake). The webs were released on June 8, 2007 for the first pour and June 11, 2007 for the second pour. The webs were then stored at Newcrete Products until they were able to be shipped to Lehigh University.

7.3 Design and Construction of the Slab Formwork

The next stage of the specimen fabrication was to cast the slab on top of the web. In order for this to be done, formwork needed to be designed and constructed to support the slab concrete as it was poured and cured. Due to the limited staging area in the ATLSS Center lab and the large quantity

of beams to be fabricated, it was decided to cast the slabs in four different groups. Each pour would consist of eight beams; therefore, eight sets of formwork were created.

By considering several factors including cost and reusability, the decision was made to create the forms out of steel. The forms were designed to support the weight and shape of the slab while it was poured and throughout the curing process. The final design resulted in the forms being constructed from 16 gauge steel and L2x2x1/8 angles.

The 16 gauge steel was bent to the shape of the slab and fastened against each side of the web (Figure 7-14). Endplates, which allow the two halves of the forms to be bolted together, would also be fabricated from the 16 gauge steel (Figure 7-15). The L2x2x1/8 angles were welded to the bent steel on the ends and at midspan to support the formwork (Figure 7-16 and Figure 7-17). Bolt holes were also drilled into the angles at the end of the forms to allow the endplates to be fastened to them. One-forth inch threaded rod was used to help hold the two sides of the forms together. Figure 7-14 through Figure 7-18 present the final design drawings of the steel formwork.

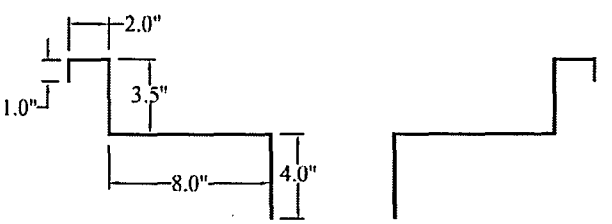

Figure 7-14: Dimensions of Bent 16 Gauge Steel

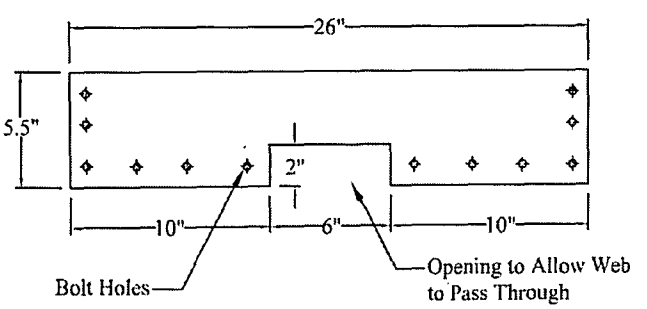

Figure 7-15: Dimensions of End Plate

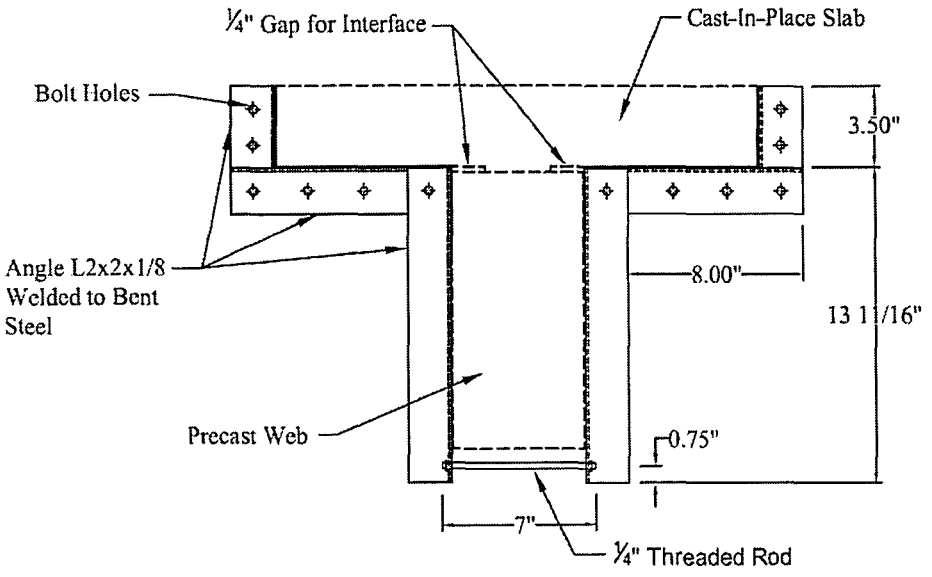

Figure 7-16: Cross-Section View of the Formwork at End of Beam

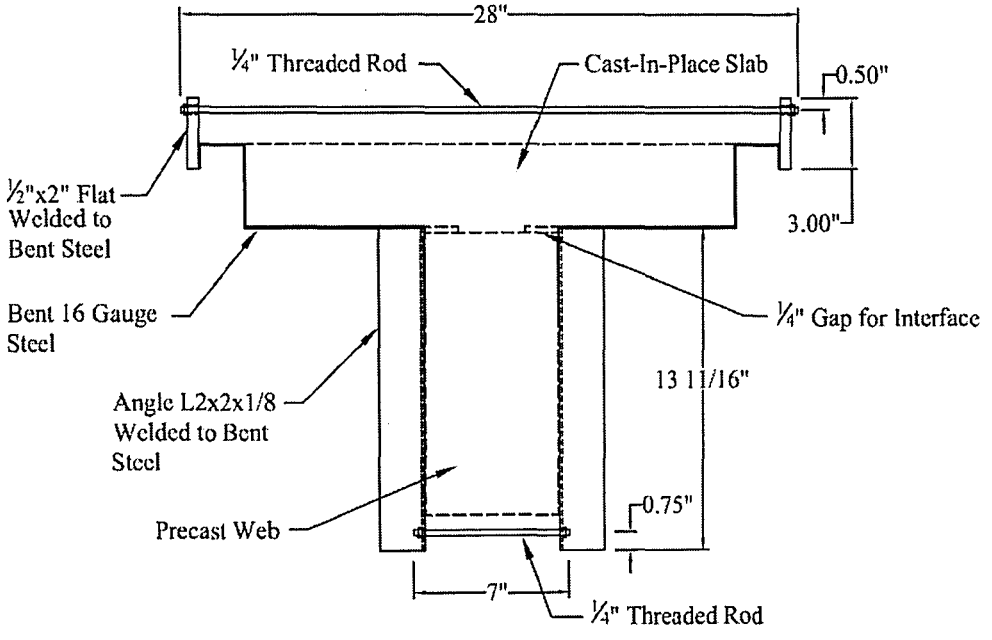

Figure 7-17: Cross-Section View of the Formwork at Midspan

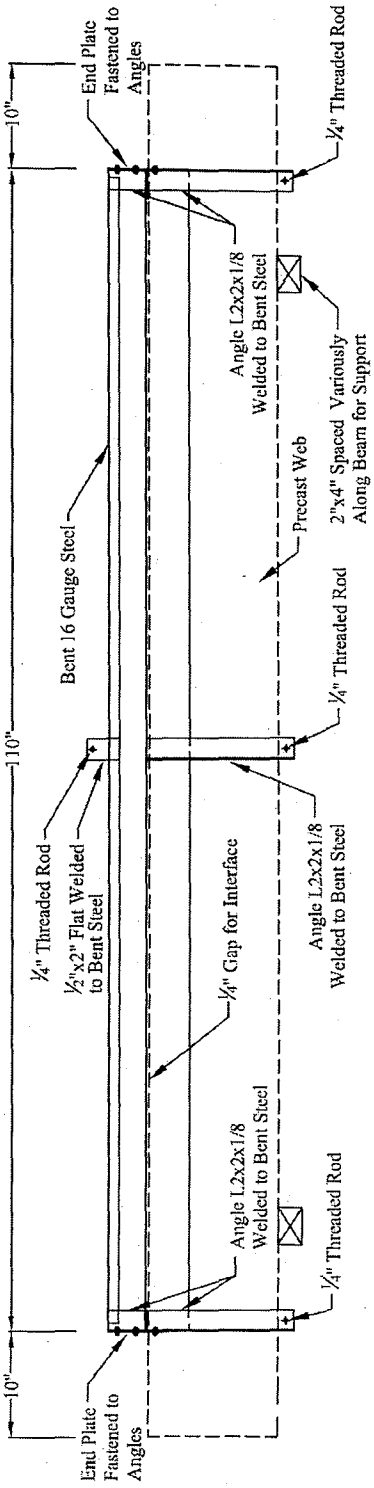

Figure 7-18: Elevation View of the Formwork along the Beam Length

The 16 gauge steel sections were cut and bent to shape at Nazareth Machine Works, Inc. in Mt. Bethel, Pennsylvania. The angle was cut and drilled in-house and then welded onto the bent steel sections. The forms were then assembled and adjusted so that they would fit snug to the web. Three pieces of 2"x4" wood were placed under the form on each side in order to provide extra support and stability. Also, pieces of angle were tightly clamped to the bottom of the form as leg extensions for the L2x2x1/8 sections. Figure 7-19 and Figure 7-20 show the forms set up on the web.

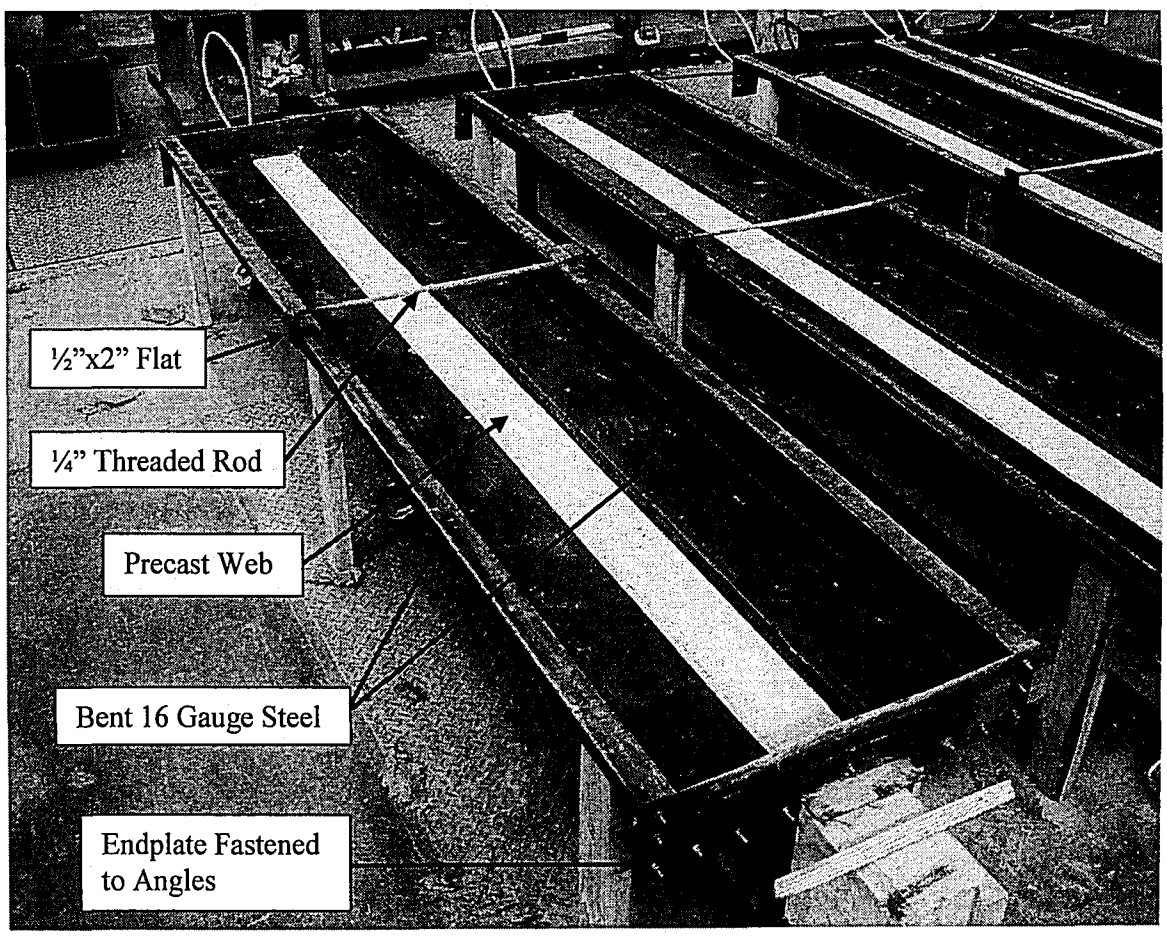

Figure 7-19: Final Form Setup Top View

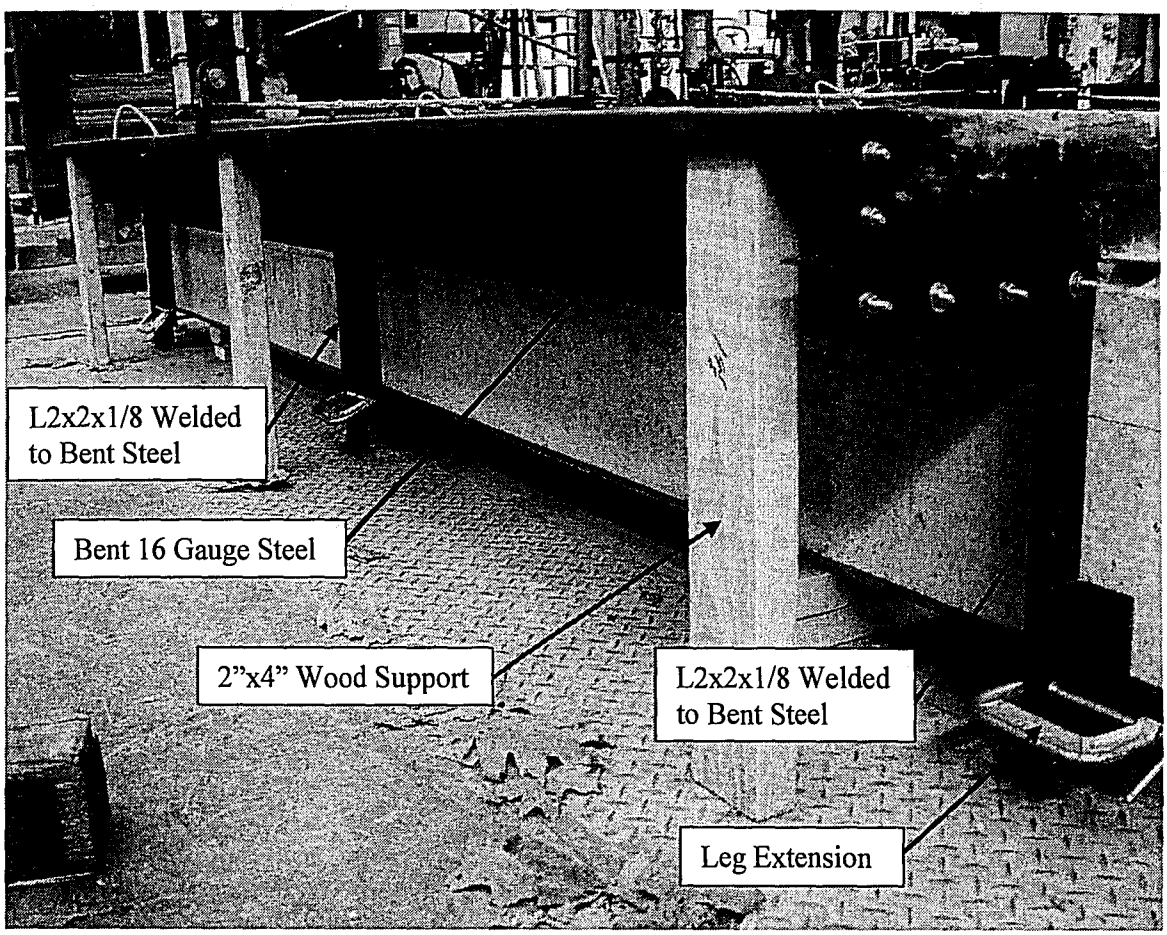

Figure 7-20: Final Form Setup Side View

7.4 Cast-In-Place Concrete Slab Fabrication

7.4.1 General

After the precast webs were shipped to Lehigh University from Newcrete Products, they were stored outside, behind ATLSS lab. The 4x8 concrete cylinders were released and stored in a lime bath until the material tests were performed. As mentioned previously, the slab fabrication would take place in four pours with eight specimens per pour. After each pour, the specimen would be tested in order to free up space in the staging area for the next pour. The following sections will provide an account of the cast-in-place slab concrete pours.

7.4.2 Pour 1

The first pour consisted of two specimens of each surface finish (smooth, broom, as-place, and rake) and a design compressive strength of 3ksi for the slab concrete. The webs were brought into the staging area and set into place. After the forms were set up on the webs and tightened, several tasks had to be completed before pouring the concrete.

The first task was to find a way to create a reduced interface width for the composite beam. This was accomplished by the use of polyethylene foam tape. The polyethylene foam is resistant to chemicals, water, and temperatures up to 160°F while providing adequate firmness to resist the load of the plastic concrete. The foam tape came in three-quarter inch wide by a quarter inch thick strips and therefore was ideal for creating the quarter inch gap between the precast web and cast-in-place slab. In order to create the three inch interface width, two strips of tape were placed side-by-side along the length of the beam on each side of the interface. Before attaching the foam tape, the interface surface of the web was cleaned off with compressed air to remove any particulates. Also, in order to fill in the chamfer on the top of the web (Figure 7-4), wood strips were cut and hot glued into place. The foam tape was then hot glued on top of the wood and the concrete surface. The foam tape and wood strips were later removed before the composite beam was tested. Figure 7-21 shows a picture of the polyethylene foam tape on the web surface.

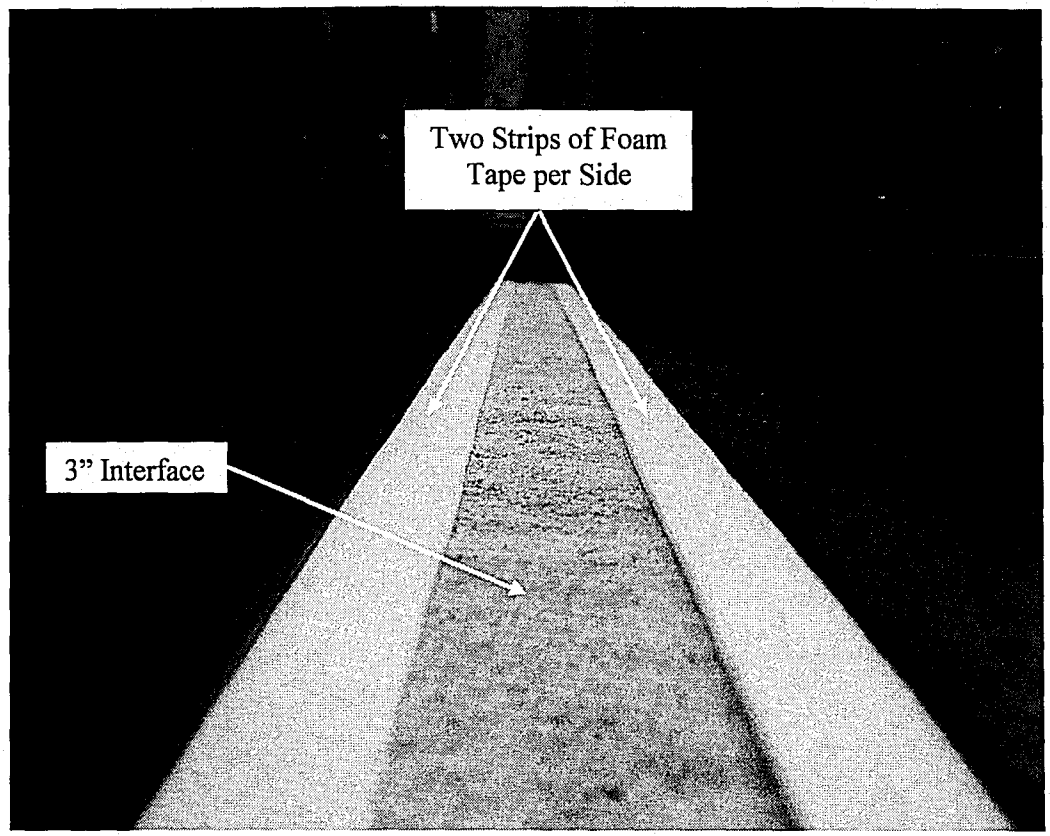

Figure 7-21: Polyethylene Foam Tape on Interface Web Surface

Next, the #4 rebar was cut to the appropriate size and the rebar cages were tied together. Small wire supports to raise the rebar to the correct level in the forms were also cut to size. Before going any farther, notes and observations were taken on the condition and roughness of the interface on each end of the web. Then once again, the interface was cleaned with the use of compressed air. Next, a light coating of form release, named Magic Kote VOC, was carefully brushed onto the steel forms making sure not to drip any on the interface. After that, the rebar and wire supports were positioned and tied in the forms. At this point, the preparation work was completed and the slab concrete was ready to be poured. Figure 7-22 shows a picture of the pour-ready setup.

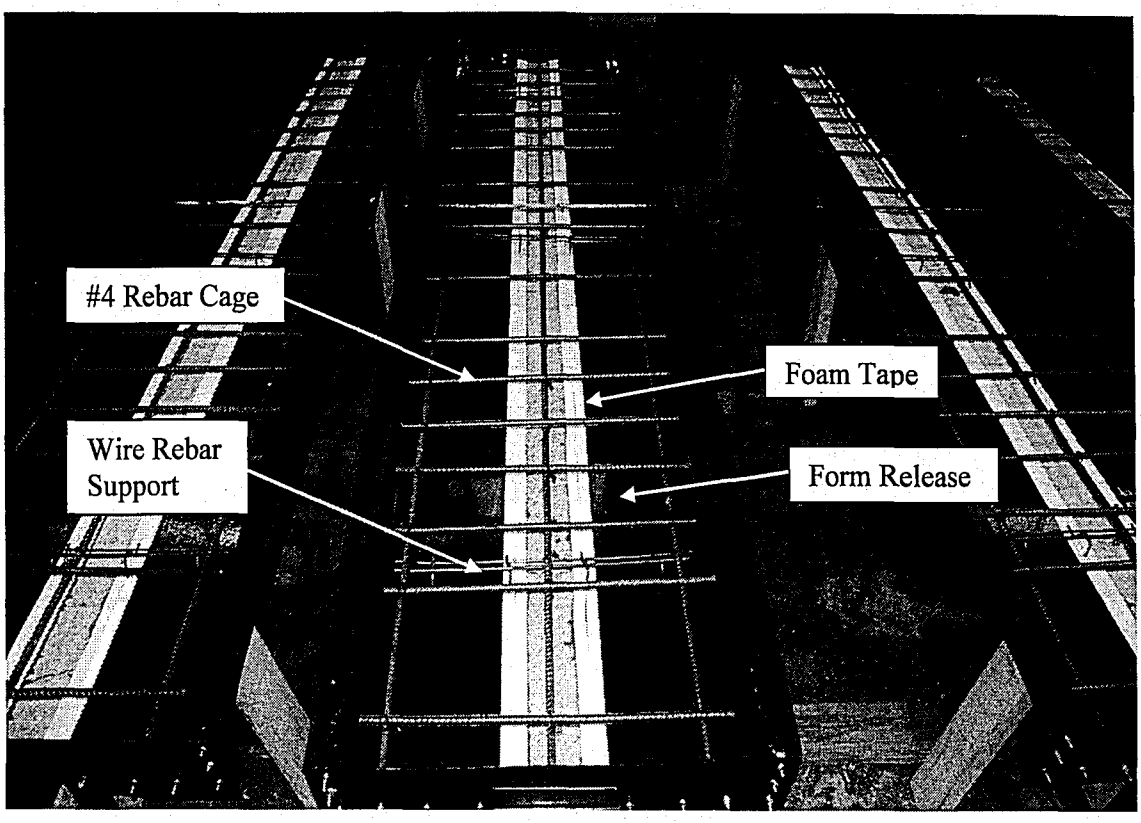

Figure 7-22: Pour-Ready Setup

The design compressive strength of the first pour slab concrete was 3 ksi. The properties of the mix are presented in Table 7-2.

Table 7-2: Properties of the 3ksi Slab Concrete Mix for Pour 1

Property	Units	Quantities for Three Cubic Yards
Type I Cement	lbs.	1201
ProAsh	lbs.	307
Natural Sand	lbs.	4360
2B Stone	lbs.	4760
1B Stone	lbs.	680
Daravair Air Entrainment	oz.	14
Daracem 55 WR	oz.	88
Design Water/Cement Ratio	-	0.5
Slump	in.	4

The first slab concrete pour took place on November 13, 2007. When the concrete truck arrived, the slump of the mix was tested before pouring the concrete. The concrete was poured using a

concrete bucket. The placement of the concrete in the forms began over the interface in order to ensure its integrity. The concrete was then spread to the outer edges of the form and vibrated. While the pour was taking place, 4x8 and 6x12 cylinders were being made in accordance to ASTM C 31. Once the pour was finished, the concrete was allowed to set for a couple hours before applying a smooth finish to the top (Figure 7-23). Subsequently, burlap was soaked in water and draped across the top of the slabs. Plastic was laid over the burlap and taped down so that no moisture would escape (Figure 7-24).

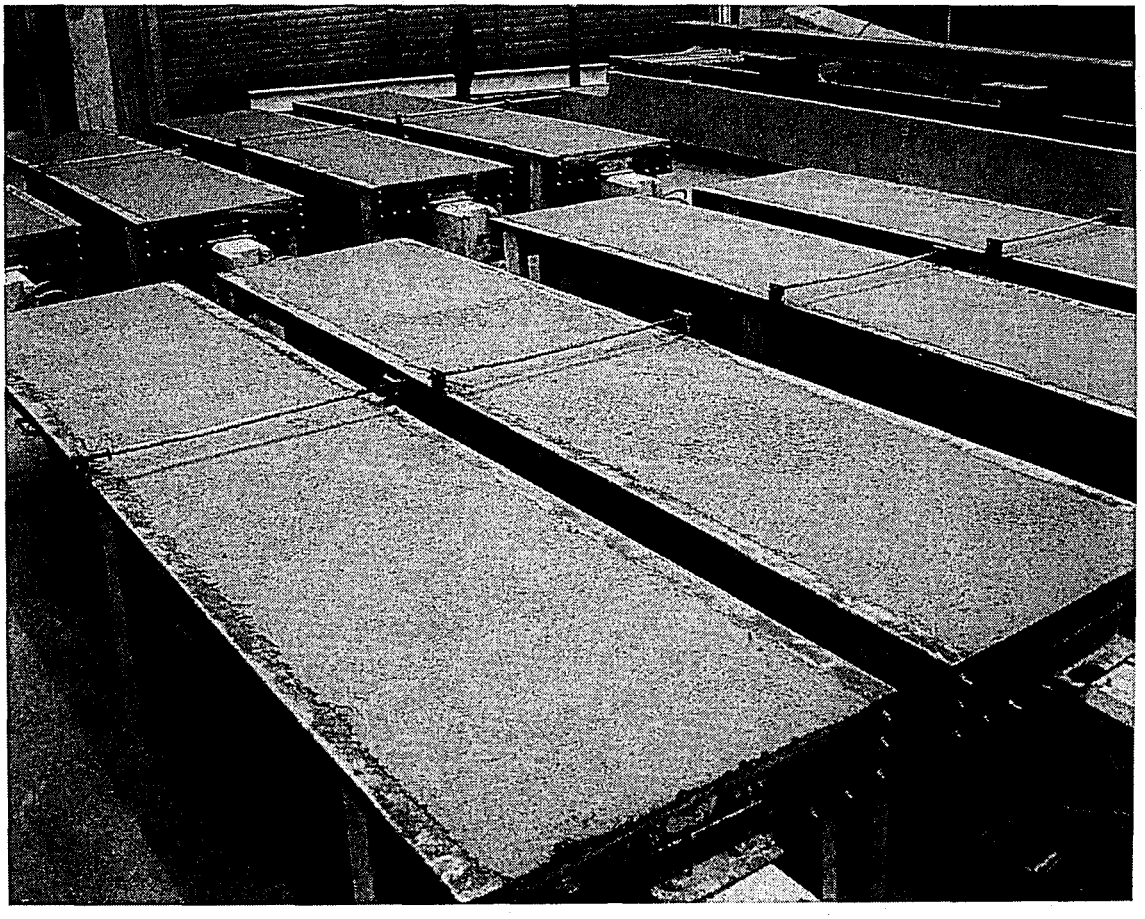

Figure 7-23: Beams After Slab Pour and Surface Finish

Figure 7-24: Slab Concrete Moist Curing

The slabs were moist cured for approximately seventeen days so that the concrete would reach an adequate strength before removing the forms. The beams along with the 4x8 and 6x12 concrete cylinders were then released and allowed to air dry for roughly ten days (Figure 7-25). At this point the specimens would be ready to test.

Figure 7-25: Final Fabricated Test Specimen

7.4.3 Problem with Pour 1 Specimen

A problem occurred with the specimen from the first pour in which most of the slab-web interfaces at the ends of the beams were cracking. The cracks were originally observed after the first test beam (which had a broom finish) was flipped and setup in the testing frame (the test setup and flipping procedure will be described in Chapter 8). The beam was initially set in place approximately twenty-seven days after the concrete pour and remained there as a template for several days as the specifics of the instrumentation and testing procedure was planned out. While being inverted, wood clamps were placed along the length of the beam to hold the slab and web together and secure the interface. A few weeks later, it was noticed that the slab was separating from the web on one end of the beam. The weight of the slab seemed to have caused the wood to slightly creep thus allowing the separation of the interface to occur. When the other specimens

which were still sitting in the staging area were inspected, initial cracks were observed on most of the composite interfaces at the ends of the beams (Figure 7-26). The exact amount of time after the slab concrete was poured that these cracks started to form is unknown. The initial interface cracks could create a potential problem given that they might quickly propagate during the specimen test and cause the interface to slip and fail early. In order to determine the source of the crack formation, further investigation was undertaken.

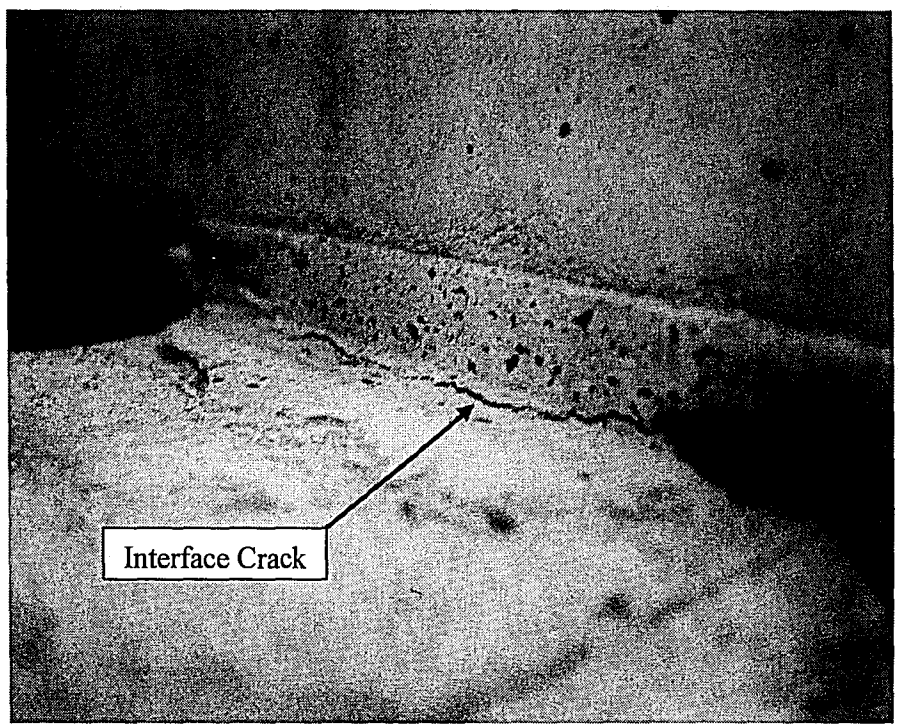

Figure 7-26: Initial Interface Crack

The precise cause of the interface cracks was unknown. However, the observation was made that the initial cracks did not occur on some of the beams with a rougher interface finish (such as the rake and as-placed finishes). Therefore, it was thought that the initial cracks may be affected by the level of bond between the two concretes. In order to assess the level of bond present between the slab and web concrete, the decision was made to try and lift the slab off of the web using the crane in the lab. If the slab concrete did bond to the web, the whole beam should pick up; if the concrete did not bond, the slab would easily lift up off the web. Thus, four clamps were attached

to the four corners of the slab at a distance of about two feet from the centerline of the slab. Slings were subsequently strung from the clamps to the crane. Then, the crane slowly pulled up on the slab to see if the two concrete sections would separate.

The interfaces of two specimens were checked with this process; one had a rake surface finish and the other had a smooth surface finish. The rake specimen had an initial interface crack on one side while the other side was intact. When the specimen was lifted, the web and slab rose up together as one whole member. The beam hung in the air for about a minute or two before it was lowered down to the ground. The result of this process caused the initial interface crack on the one end of the beam to open up more while the interface on the other end remained undamaged. Therefore, the conclusion can be made that the bond successfully developed between the two concretes for the rake beam.

The specimen with the smooth surface finish had substantial initial interface cracks on both ends of the beam that extended about an eighth to a quarter of the slab length. When this beam was lifted, the slab immediately separated from the web establishing that no bond existed between the two concretes. The second smooth specimen was also lifted and resulted in the same instantaneous separation. The deficient bond is most likely due to the formation of a cold joint between the two concretes and a lack of cohesion with the smooth surface finish.

These results indicate that the roughness of the surface finishes and the resulting bond has an effect on whether or not the interfaces will result in initial cracks. However, other theories were created for possible contributions or reasons for the occurrence of the initial cracks. These theories are described next.

Differential Shrinkage between the Slab and Web Concretes

One of the most likely reasons that the initial interface cracks occurred is due to differential shrinkage between the slab and web concrete. If the slab was cast a short time after the web was

fabricated, then the concretes would shrink at the same rate thus negating the formation of interface cracks. These cracks were not observed in the previous research studies most likely due to the short time duration between the pouring of the web and the casting of the slab concrete. Since the web section in this research study was fabricated approximately five months prior to the casting of the slab concrete, the shrinkage rate of the web has already leveled out to a negligible amount leaving the slab concrete to shrink relative to the web.

The ACI 209R-92 document presents an equation to predict the shrinkage of concrete. Equation 25 calculates the shrinkage of concrete after seven days of moist curing:

$$(\varepsilon_{sh})_t = \frac{t}{35+t}(\varepsilon_{sh})_u \qquad \text{(Eq. 25)}$$

where,

t = the time after the end of the initial wet curing [days]

$(\varepsilon_{sh})_u$ = the ultimate shrinkage strain [in./in.]

Using this equation, the shrinkage strain of the concrete was found at the time of the initial interface cracks. The suggested average value for the ultimate shrinkage strain of $(\varepsilon_{sh})_u = 780\gamma_{sh} \times 10^{-6}$ in./in. was used for the equation. Also a correction factor of $\gamma_{sh} = 0.92$ was used to take into account that the concrete was moist cured for more than 7 days. For a time t = 38 days, the shrinkage strain in the slab concrete is 373.5 x 10^{-6} in./in.. This extrapolates to an overall change in length of 0.041 inches for the slab. As mentioned previously, this change in length occurs relative to the web concrete.

The shrinkage strain can be fairly significant when taking into account the reduced interface width. If this strain was large enough and the bond between the slab and the web was not very

strong, the interface could separate as the slab shrinks. This theory or possibly the one described next is most likely the cause of the initial interface cracks.

Concrete Curling

Going along with the first theory, is the one that the concrete could have curled upward when it was drying. If the top of the slab was drying faster than the bottom, the ends of the slab could curl up due to the different shrinkage rates thus causing the cracks to occur at the ends of the composite beam interface.

There is a possibility that this could have occurred during the moist curing of the slab concrete. Typically forms are made out of wood which may absorb the moisture out of the concrete as it is curing. However, for this pour, steel forms were used which kept the water in the concrete. If the burlap and plastic on the top of the slab did not provide as much moisture as the bottom or possibly dried out during the course of the curing process, then the rate of the initial shrinkage could have been greater for the top of the slab compared to the bottom. When the forms were released, the top of the slab would have already been drying for a period of time while the bottom of the slab would just be starting. This would result in the top of the slab shrinking faster than the bottom thus causing the slab to curl upward. This curling effect along with the shrinkage strain could have been the cause of the initial interface cracks.

Web Absorbing Water from the Slab at the Interface

If water was placed on top of a dry concrete, the porous nature of the concrete will have the tendency to soak up the moisture. Therefore, the web could be absorbing the water from the slab concrete when it is cast on top. The extraction of water from the interface concrete would result in a lower water/cement ratio at that surface. Technically a lower water/cement ratio means the concrete will be stronger. However, if there is not enough water for the concrete to cure properly, then the concrete would be weak or brittle thus resulting in a weaker bond between the web and

the slab. If shrinking or curling occurred along with the possible brittle property of the interface concrete, cracks could form more easily.

Stress Concentration at Interface on Ends of Beams

As mentioned before, a stress concentration would occur at the ends of the beams right at the interface due to the change cross section and the reduction of the interface width. Even though there are no external loads applied to the beam when the initial interface cracks occurred, the stress concentration could assist in the formation of the cracks due to strain developed from shrinkage.

Dirt or Particles Attached to the Composite Interface

There is the possibility that dirt or low strength particles could have bonded to the web concrete surface finish as the webs were stored outside for a period of time. The compressed air used to clean the interface surface may not have been strong enough to remove these particles. Subsequently, a portion of the slab could have been cast on top of a layer of particles instead of the web surface. These low strength particles would break from the interface with little force thus easily separating the two concrete sections. This potential problem can be avoided in the future by power-washing the tops of the beams to remove bonded debris.

Using the information and theories just mentioned, the following improvements were made to the slab fabrication process in order to increase the strength of the bond and reduce the chance of initial interface cracking:

- Power-wash the web interface surface before assembling the forms and pouring the slab concrete. This will remove any weak particles that may have bonded to the surface.

- Initially soak the interface and make sure that the surface of the web is saturated before pouring the slab (but ensure there are no puddles of water before pouring). This will prevent the web from absorbing the water from the slab concrete.
- Only keep the forms on the beams and moist cure for a few days (no more than 7). This will reduce the risk of the slab curling.
- Test the specimens soon after the beams reach an acceptable strength so the effect of differential shrinkage will not be as substantial.

It was also decided not to finish fabricating and testing the beams with a smooth surface finish. As mentioned before, the bond between the smooth web and slab cannot be achieved due to the cold joint and the lack of cohesion achieved with the smooth surface. Therefore, only two more pours would take place. These pours would include the remaining six rake and six as-placed specimens (since they had rougher surface finishes and thus could create a stronger bonded) along with four more broom specimens.

7.4.4 Pours 2 and 3

Once all the specimens from the first pour were tested and the details were worked out on how to improve the outcome of the following pours, preparations were made for the next two pours. The process of preparing and conducting these two pour was very similar. Before the webs were brought into the staging area, they were thoroughly cleaned with a power-washer having an effective cleaning pressure of 1750 psi to remove any weak bonded particles. The webs were then brought into the staging area and the forms were set up. The wood strips and polyethylene foam tape were glued into place to provide the proper interface width. Next, notes and observations were taken on the condition and roughness of the interface on each end of the web. Approximately 48 hours before the pour, the interface was cleaned with compressed air and rags which were soaked in water were laid across the interface and covered with plastic allowing the

web surface to absorb the water and become saturated. The #4 rebar cages were cut and tied together along with the wire supports.

On the day of the pour, the damp rags were removed to allow the interface to air dry. This ensured that no free standing water would be present at the interface which could add to the water content of the interface concrete. Next, a light coating of form release was carefully brushed onto the steel forms making sure not to drip any on the interface. Then, the rebar and wire supports were positioned in the forms. At this point, the preparation work was completed and the slab concrete was ready to be poured.

The design compressive strength for slab concrete of Pour 2 and 3 was decided to be 6 ksi. The use of a higher strength concrete would allow the slab to reach an adequate release strength sooner thus shortening the moist curing time along with the time for the slab to air dry before testing. The properties of the 6 ksi mix used for Pour 2 and 3 are presented in Table 7-3.

Table 7-3: Properties of the 6ksi Slab Concrete Mix for Pour 2 and 3

Property	Units	Quantities per Cubic Yards
Type I Cement	lbs.	695
Fly Ash – ProAsh	lbs.	174
Coarse Agg. - #8 Limestone	lbs.	1700
Fine Agg. – Concrete Sand	lbs.	1117
Daracem 55 WR	oz.	52.1
Design Water/Cement Ratio	-	0.39
Percent Air	%	1.5
Slump	in.	4

Slab Pour 2 and 3 took place on February 26, 2008 and March 18, 2008, respectively. When the concrete truck arrived, the slump of the mix was tested. When the slump was correct, the concrete was poured using a concrete bucket. The placement of the concrete in the forms began over the interface in order to ensure its integrity. The concrete was then spread to the outer edges

of the form and vibrated. While the pour was taking place, 4x8 and 6x12 cylinders were being made in accordance to ASTM C 31. Once the pour was finished, the concrete was allowed to set for a couple hours before applying a smooth finish to the top. Then burlap was soaked in water and draped across the top of the slabs. Plastic was laid over the burlap and taped down so that no moisture would escape.

The slabs were moist cured for six to seven days so that the concrete would reach an adequate strength before removing the forms. Three 4x8 cylinders for each pour were tested according to ASTM C 39 to determine the strength of the concrete before it was released. The Pour 2 beams were released on March 3 and 4, 2008 with an average release strength of 3.39 ksi. The Pour 3 beams were released on March 24, 2008 with an average release strength of 4.46 ksi. Once the slabs and the concrete cylinders were released, the specimens were allowed to air dry for roughly three to eight days. All of the composite beams were tested within eight days of being released.

The composite interface on each end of the beam was inspected before they were tested. A few small initial cracks were observed on some of the beams that did not have a rough surface finish. However, the degree of cracking was greatly reduced. From these observations, it can be concluded that the roughness of the composite interface can provide an adequately strong bond to prevent differential shrinkage from occurring between composite concretes.

8 Experimental Program – Phase 2 – Test Program and Procedure

8.1 General

Since the tests were reported to have worked well for the first phase of the experimental program, the test setup and procedure for the second phase were similar to those for the first. Due to the problems experienced during the fabrication of the slab concrete for the second phase specimens, the number of tests was reduced. Table 8-1 presents the revised test matrix for this phase of the experimental program. The following sections will provide a description of the test setup, the process of installing the test specimen, the instrumentation, and the testing procedure.

Table 8-1: Revised Test Matrix for Phase 2

Specimen ID	Surface Finish			Slab Strength		Number of Specimens
	Broom	As-Placed	Rake	3 ksi	6 ksi	
3B	■			■		2
3A		■		■		2
3R			■	■		2
6B	■				■	4
6A		■			■	6
6R			■		■	6
					Total =	22

8.2 Test Setup

The composite beams were inverted and tested in a simply supported self-reacting loading frame. The specimen was simply supported over a span of ten feet. The beams were inverted in order to simplify the setup of the loading frame. By inverting the beams, the normal forces due to the self weight acting on the interface were altered. However, the load due to the self weight was negligible when compared to the static applied load. Also, thorough calculations were performed to determine if the stresses in the system would be acceptable when the specimen was flipped. It was found that the stresses in the beam were increased in tension (at the top of the web) and compression (at the bottom of the web) by 300 psi. However, this increase in stress did not bring

the section close to the point of cracking. Therefore, it was considered acceptable to invert the beams when testing.

The loading frame setup consisted of a W14x398 section used as a reaction beam on which the other components were fastened. Two support links were attached to the reaction beam a distance of sixty inches from the centerline of the beam. One of the support links had only one rotation component and therefore behaved like a pinned support; the other support link had two rotation components and could rotate and translate thus making it behave as a roller support (Figure 8-3). On top of each support was a one and a half inch thick steel plate which was connected by four 5/8" threaded rods to another steel plate set on top of the test specimen (Figure 8-4). These two plates acted as a clamping mechanism to hold the test specimen in place before the test. During the test, the specimen would bear against the top clamping plate and rotate about the centerline of the plate. The threaded rods would translate the forces to the bottom clamping plate which in turn would transfer the forces through the support links to the reaction beam.

Hydraulic cylinders, which were connected to the top of the load cells, were spaced thirty inches from the centerline of the supported area on each end of the beam (Figure 8-5). The cylinders were connected to a single hydraulic hand pump thus insuring that an equal load will be applied to each loading point. A three-fourths inch thick loading plate was connected to the hydraulic cylinder (Figure 8-6). The loading plate was able to pivot by the way of a ball and socket joint allowing the load to be applied completely normal to the slab. In addition, a one inch thick neoprene bearing pad rested on top of the loading plate to distribute the applied load and reduce the local normal stress on the section.

A drawing of the test setup, including the test specimen, is shown in Figure 8-1. A picture of the actual test setup is shown in Figure 8-2 through Figure 8-6.

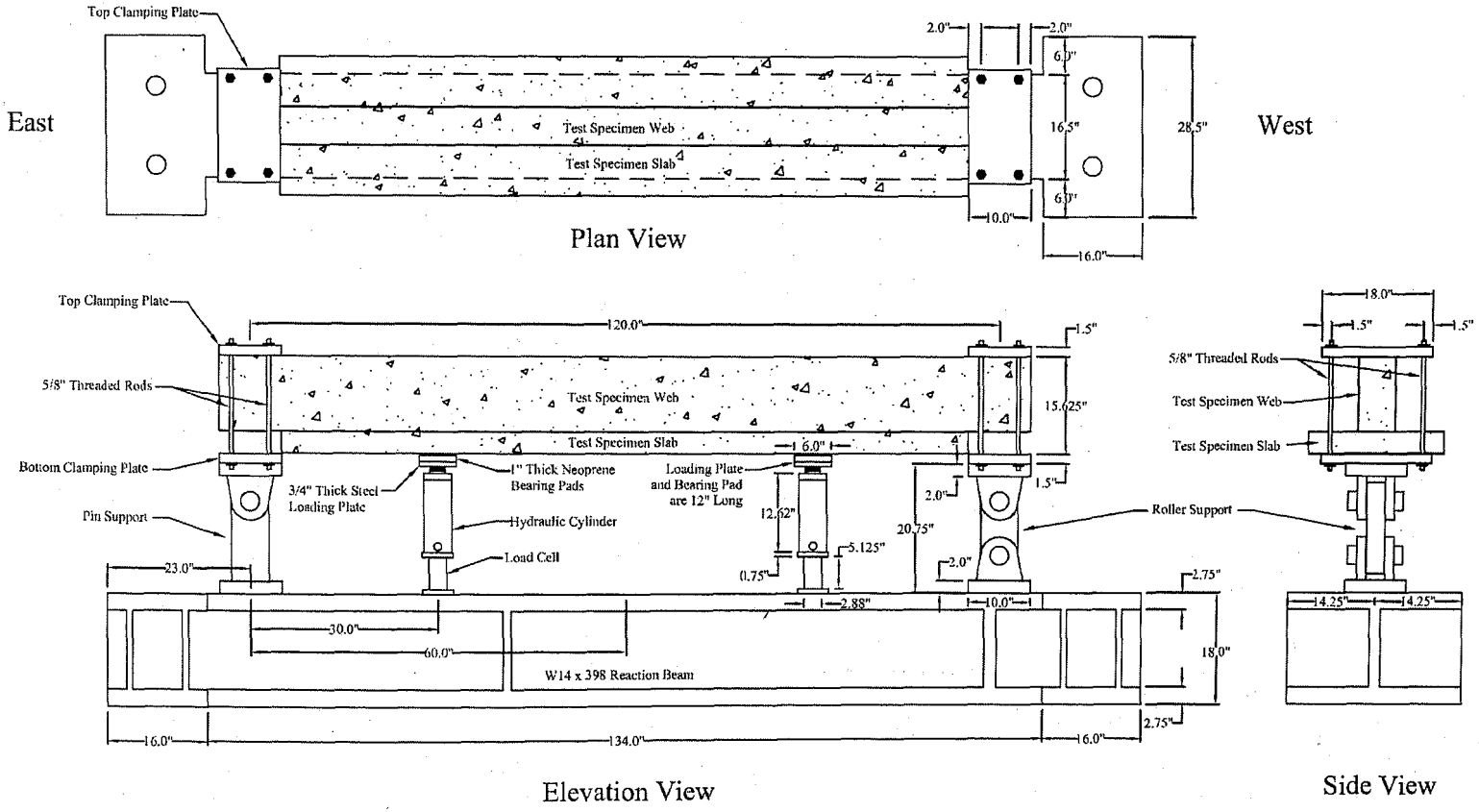

Figure 8-1: Detailed Drawing of the Test Setup

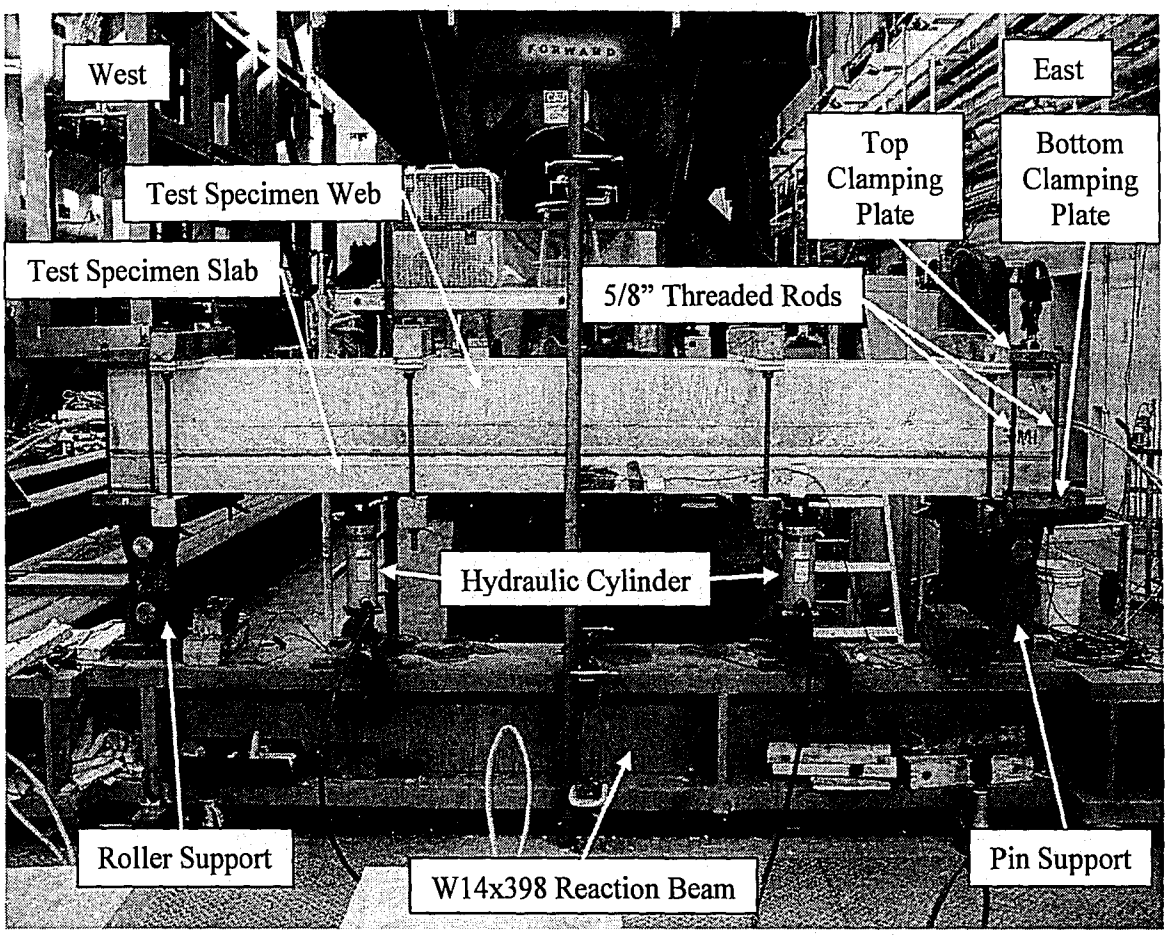

Figure 8-2: Elevation View of the Test Setup

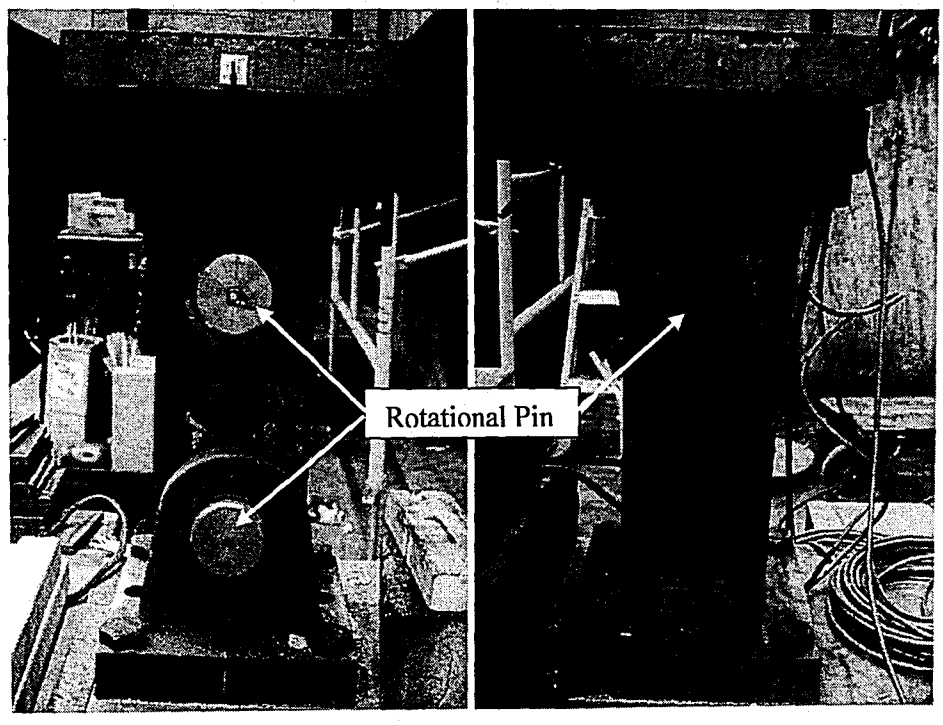

Figure 8-3: Close-Up View of the Roller and Pin Support

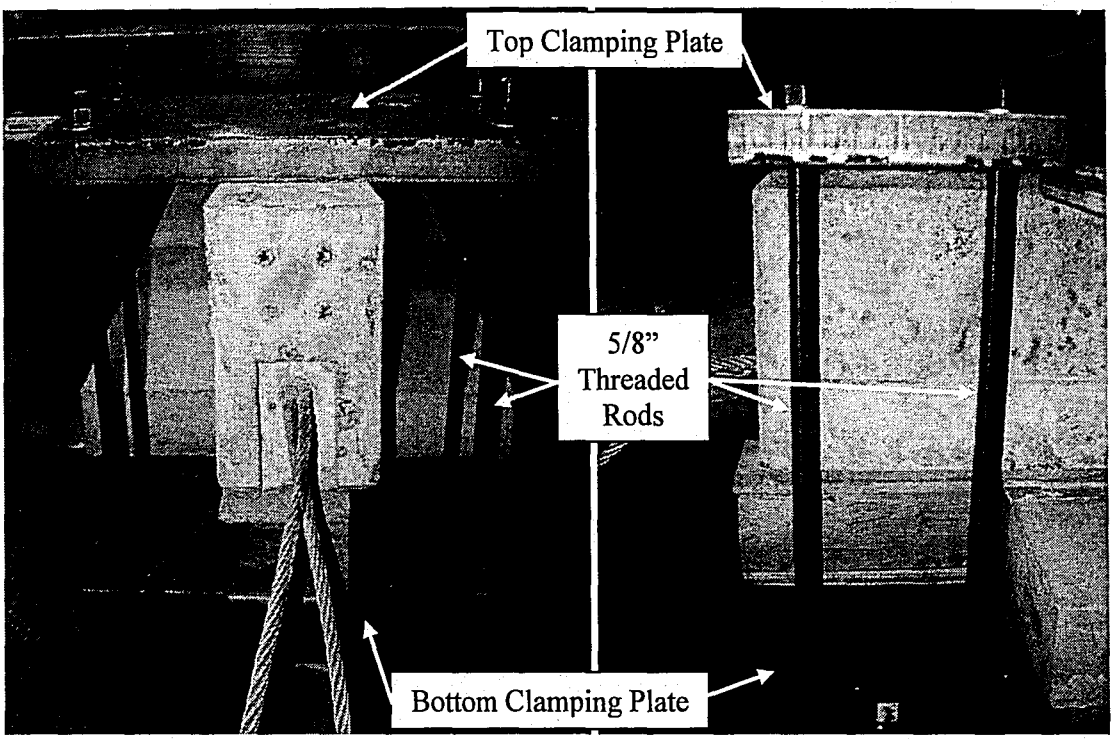

Figure 8-4: Side and Elevation View of the Clamping Plate Setup

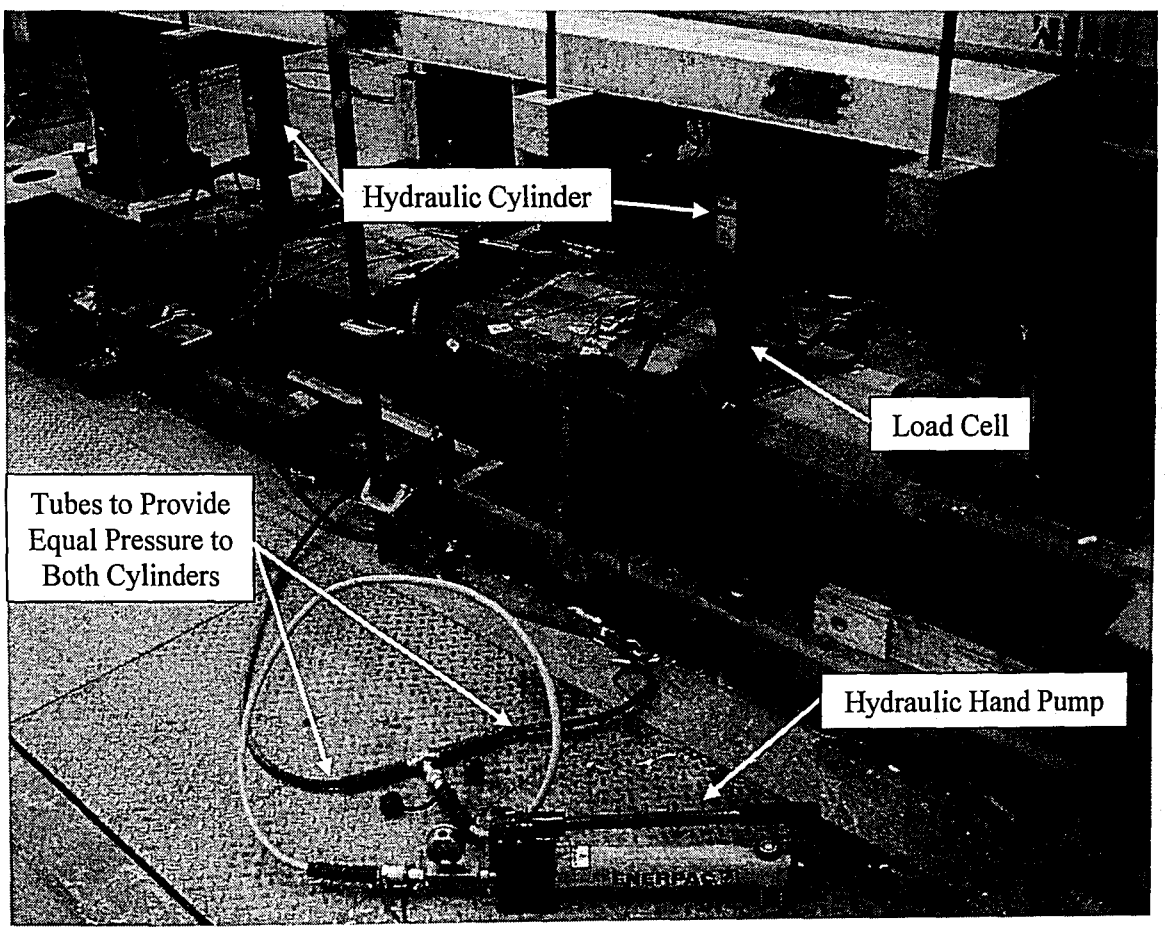

Figure 8-5: View of the Hydraulic Hand Pump and Hydraulic Cylinders

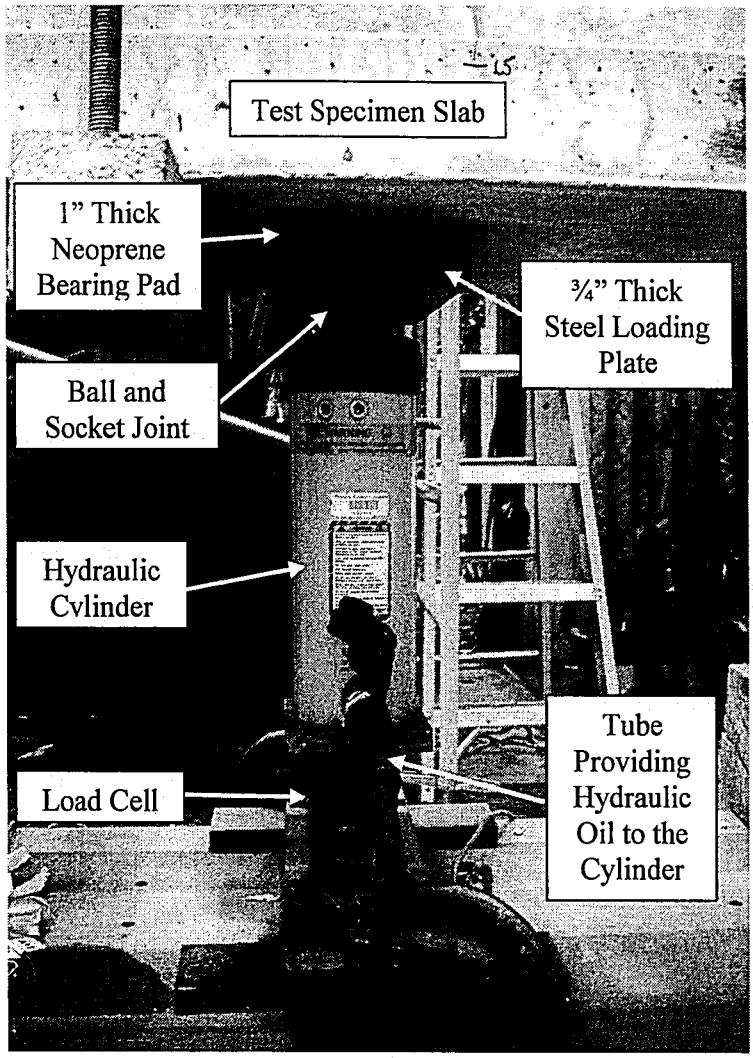

Figure 8-6: Close-Up View of the Hydraulic Cylinder

8.3 Process of Flipping and Installing the Specimen into the Test Setup

The specimens were setup just prior to the actual test to avoid the possibility of the interface separating as a result of the beam hanging upside down for an extended period of time. The interfaces of the beams were inspected before and after they were installed to make sure the processes of flipping the specimens did not compromise the interface. The procedure for properly flipping the beams, which will be described next, was performed on all of the test specimens.

To insure the integrity of the composite interface remained intact, wood clamps consisting of 4x4 lumber and threaded rods were constructed (Figure 8-7). These clamps were fastened at four locations along the beam and tightened snug in order to avoid the possibility of interface separation. Next, slings were rapped around the midsection of the beam and attached to a crane in a way that would cause the beam to flip when lifted (Figure 8-8). On the opposite side of the beam, a hand chain hoist was attached to the crane and the center two wood clamps in order to prevent the beam from rotating when lifted (Figure 8-9). The specimen was then lifted by the overhead crane, and the chain of the hoist was pulled causing the beam to gradually flip over (Figure 8-10). Once flipped, the beam was set down and the slings and chain hoist were taken off. The process of flipping the beam was very smooth and did not appear to cause any distress on the section.

Two pieces of 2x4 were placed on both sides of the pin and roller supports in order to prevent movement while the beam was set into place. Additionally, wood blocks were positioned on the top of the bottom clamping plate in order to raise the beam to the correct level. The section of the web that extended past the slab would sit on top of these blocks for support before the test began. The crane was then attached to the cables embedded in the ends of the web and lifted into the test frame (Figure 8-12). Once in place, the top clamping plate was placed on the bottom of the web and fastened to the bottom clamping plate by threaded rods. Support jacks were placed under both ends of the specimen to aid in supporting the beam until the test began (Figure 8-13). Finally, the interface was cleaned by removing the wood strips and foam tape and inspected before the instrumentation was attached.

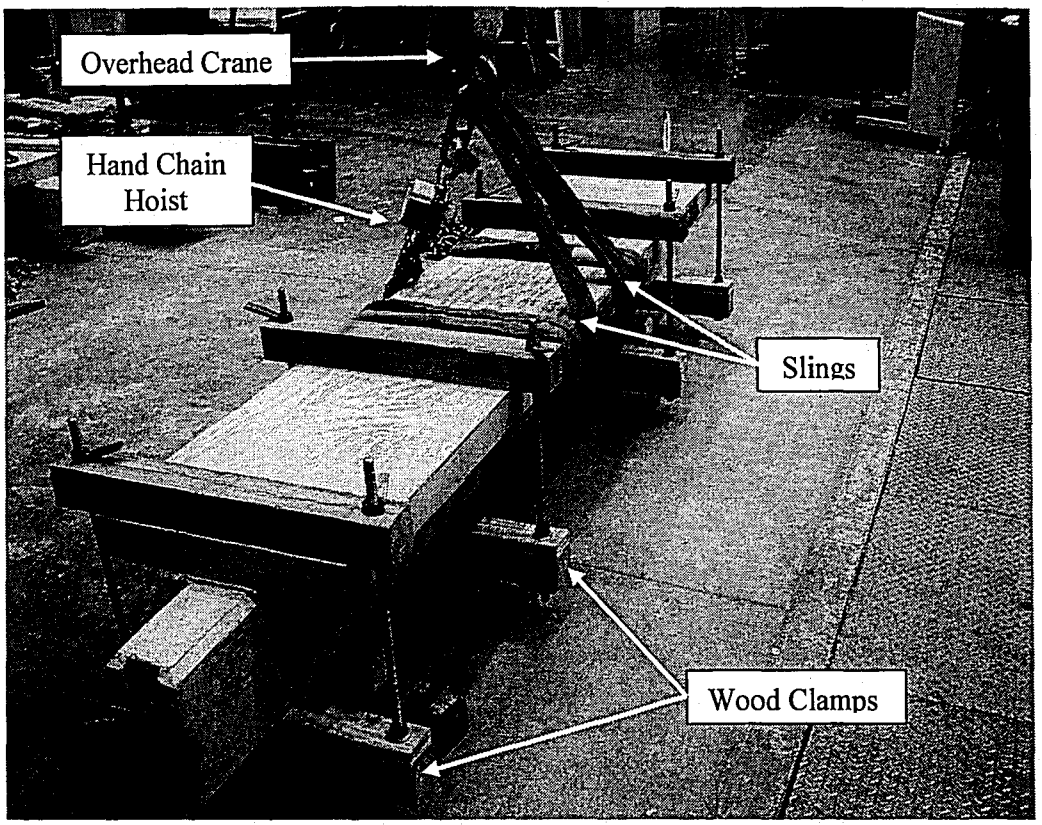

Figure 8-7: Specimen Prior to Flipping

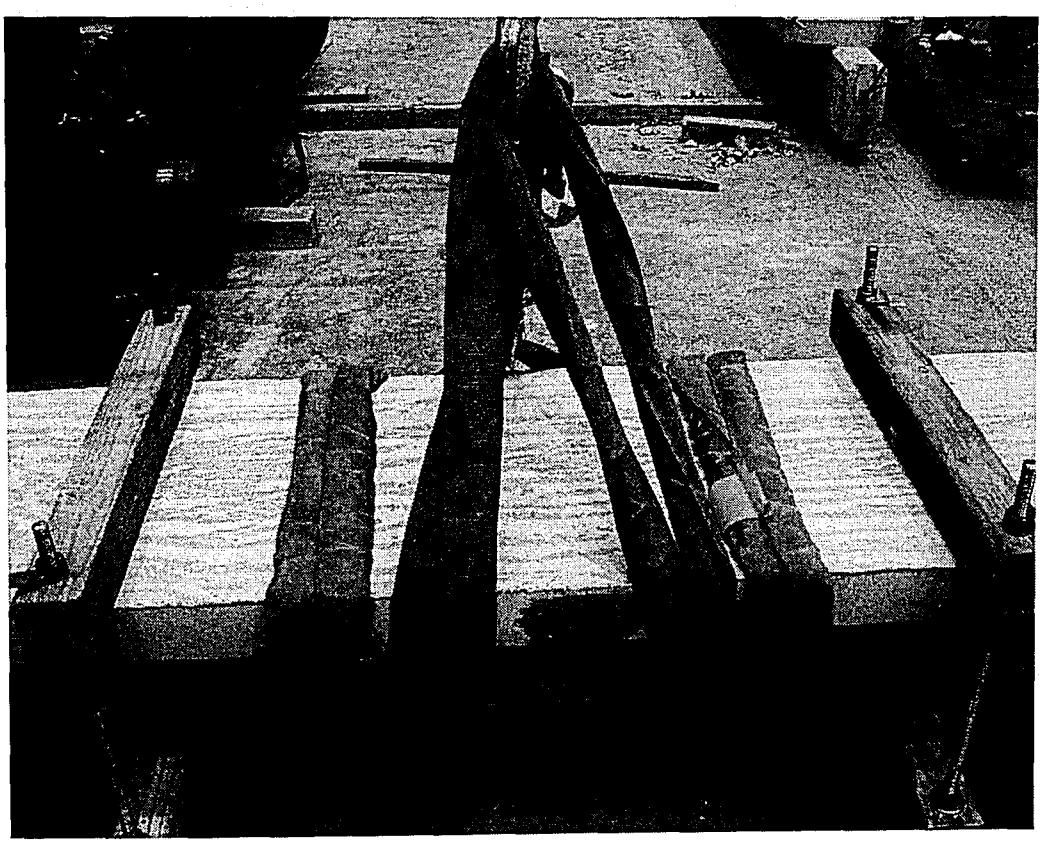

Figure 8-8: Close-Up View of Slings on Test Specimen

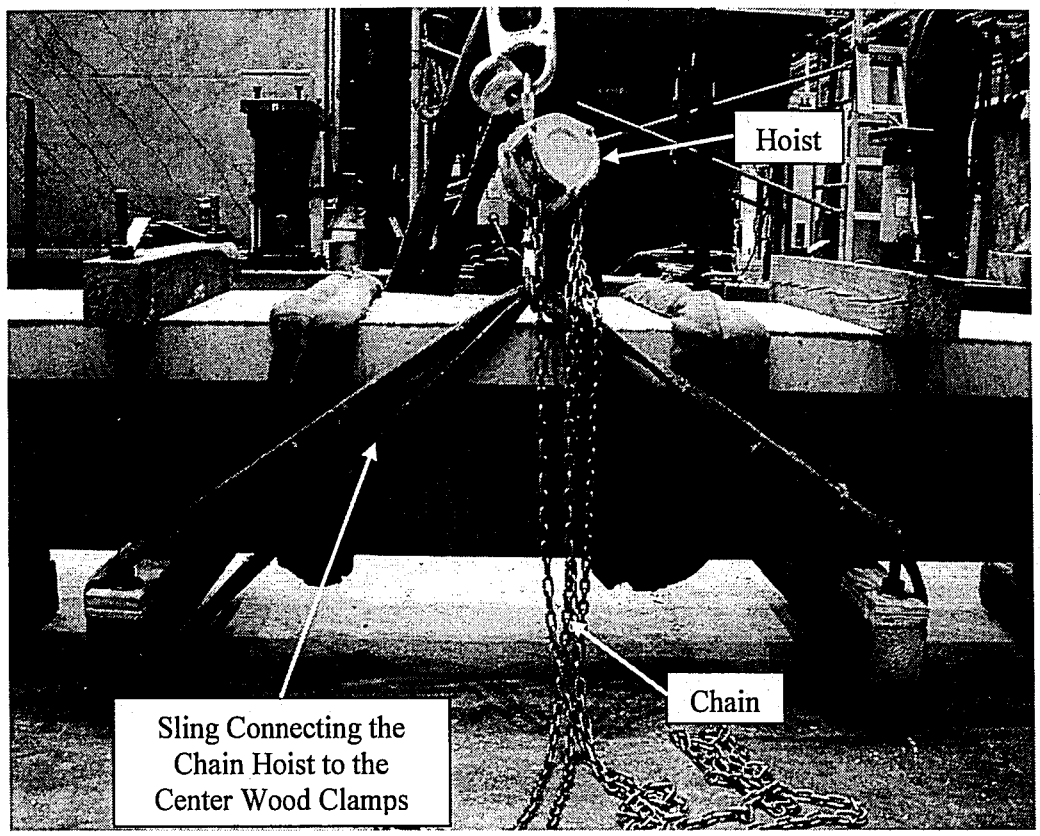

Figure 8-9: Close-Up View of the Hand Chain Hoist Connected to the Test Specimen

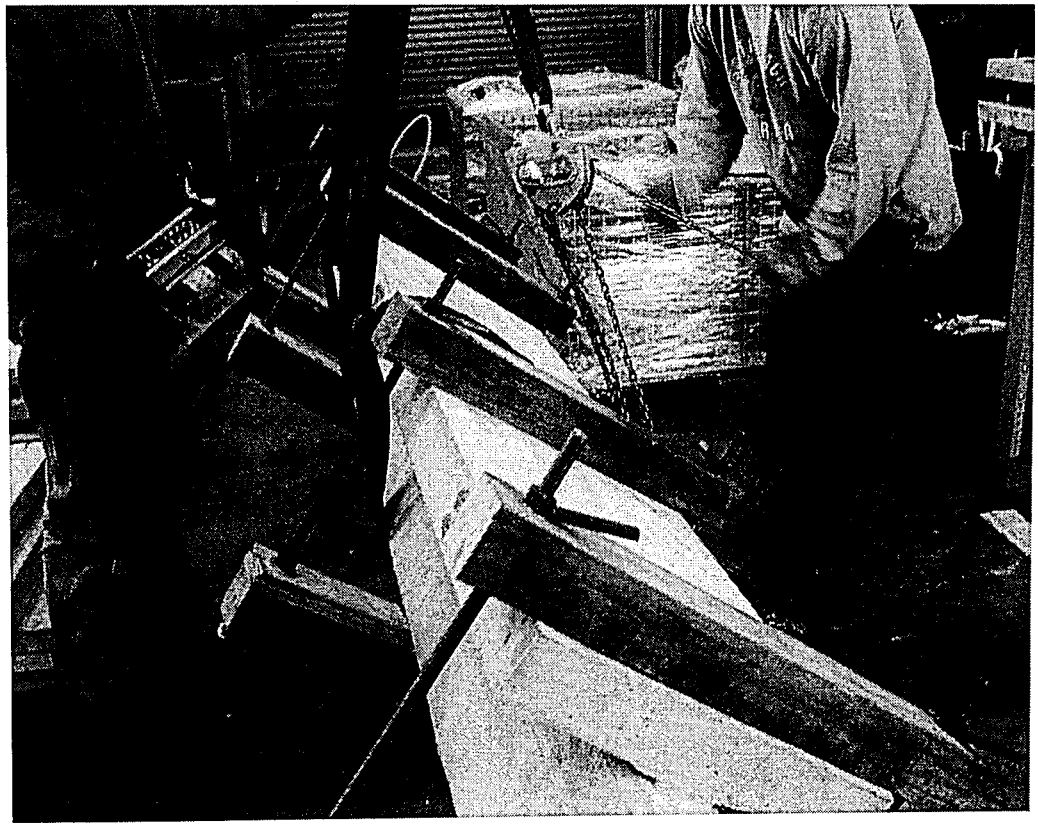

Figure 8-10: Flipping the Test Specimen

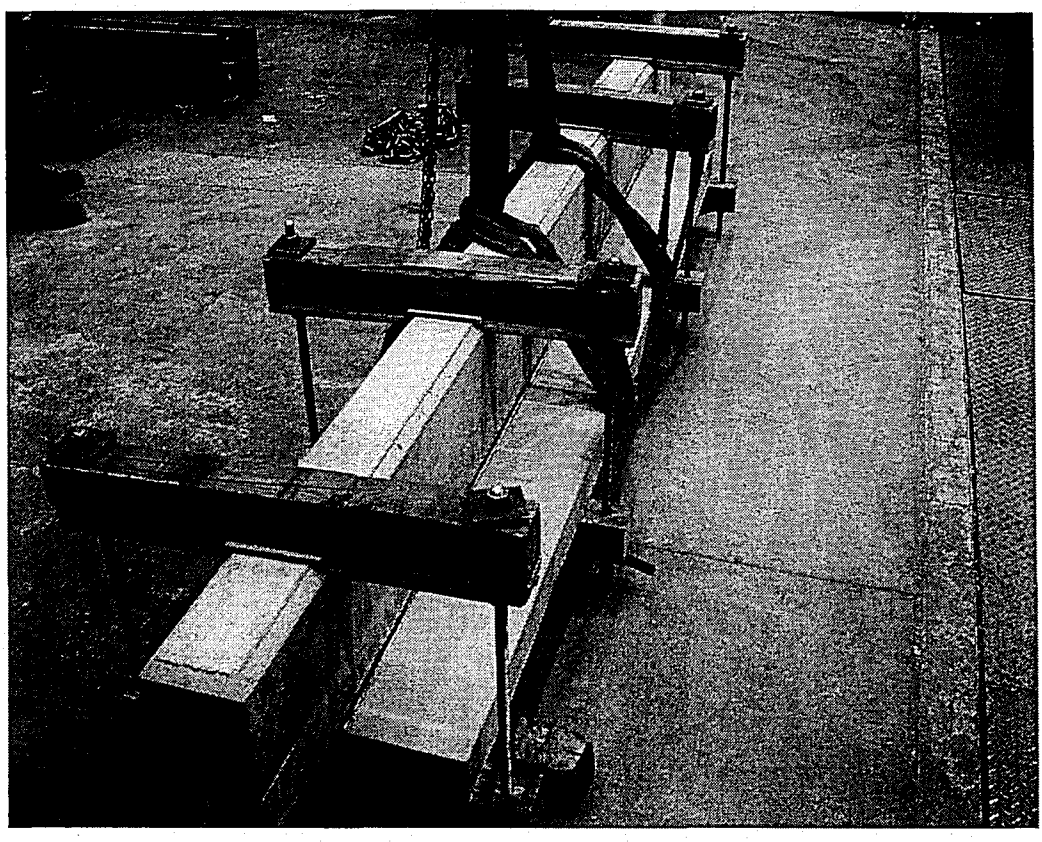

Figure 8-11: Test Specimen after Being Flipped

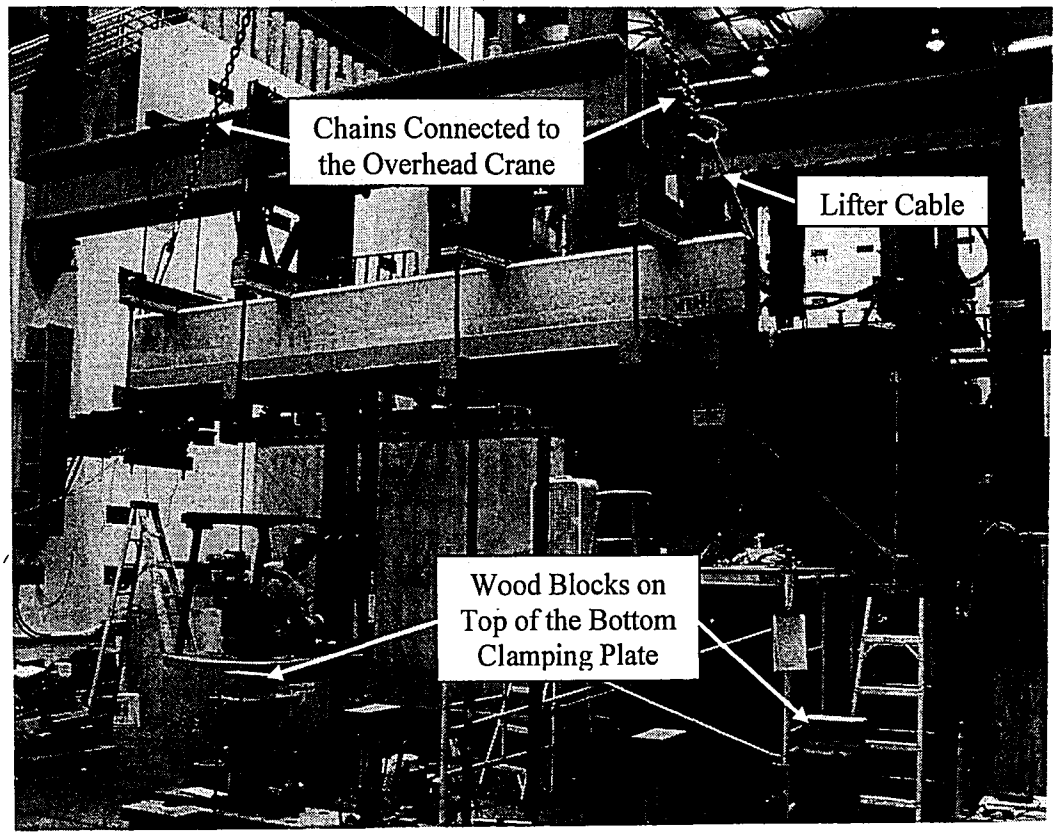

Figure 8-12: Lifting Specimen into the Test Frame

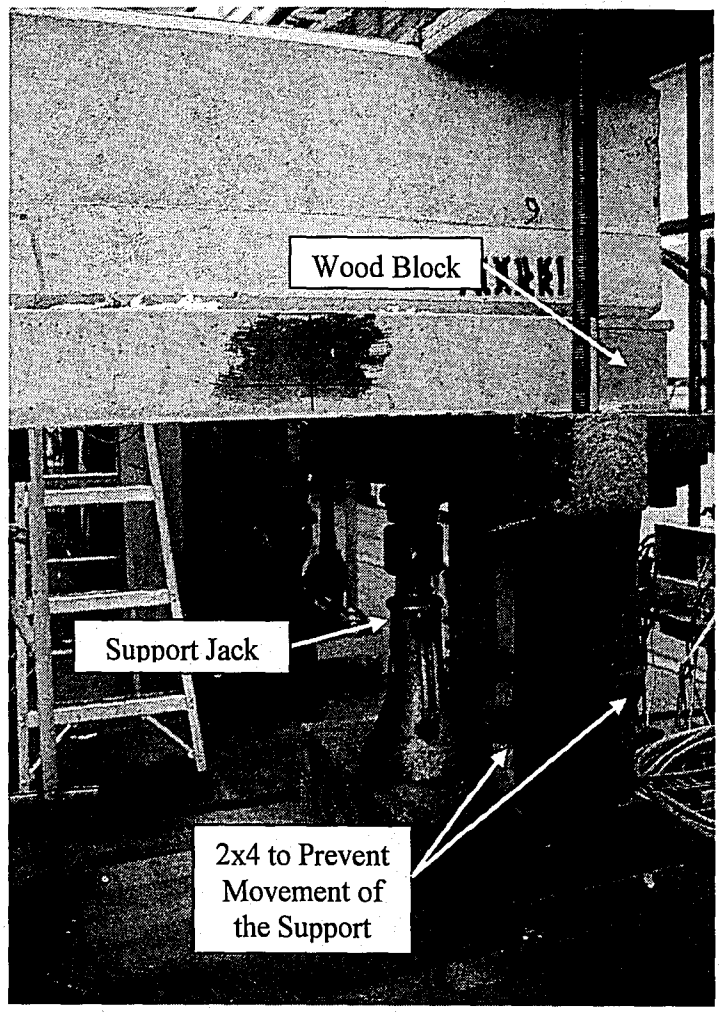

Figure 8-13: Support at End of Specimen in Test Setup

8.4 Instrumentation

Once the beams were installed in the test setup, the instrumentation was attached. The instrumentation consisted of four different components; specifically load cells, a linear variable differential transformer (LVDT), linear motion position sensors (slip gauges), and strain gauges. To properly monitor the behavior of the test specimen as it was loaded, the optimum quantity and location of each instrumentation device was determined. The final instrumentation layout is presented in Figure 8-14. It should be noted that the strain gauges shown in this figure simply provide the possible locations of the gauges. The actual number of strain gauges attached to each

specimen varied from test to test. The remaining instrumentation devices were consistent for all the tests.

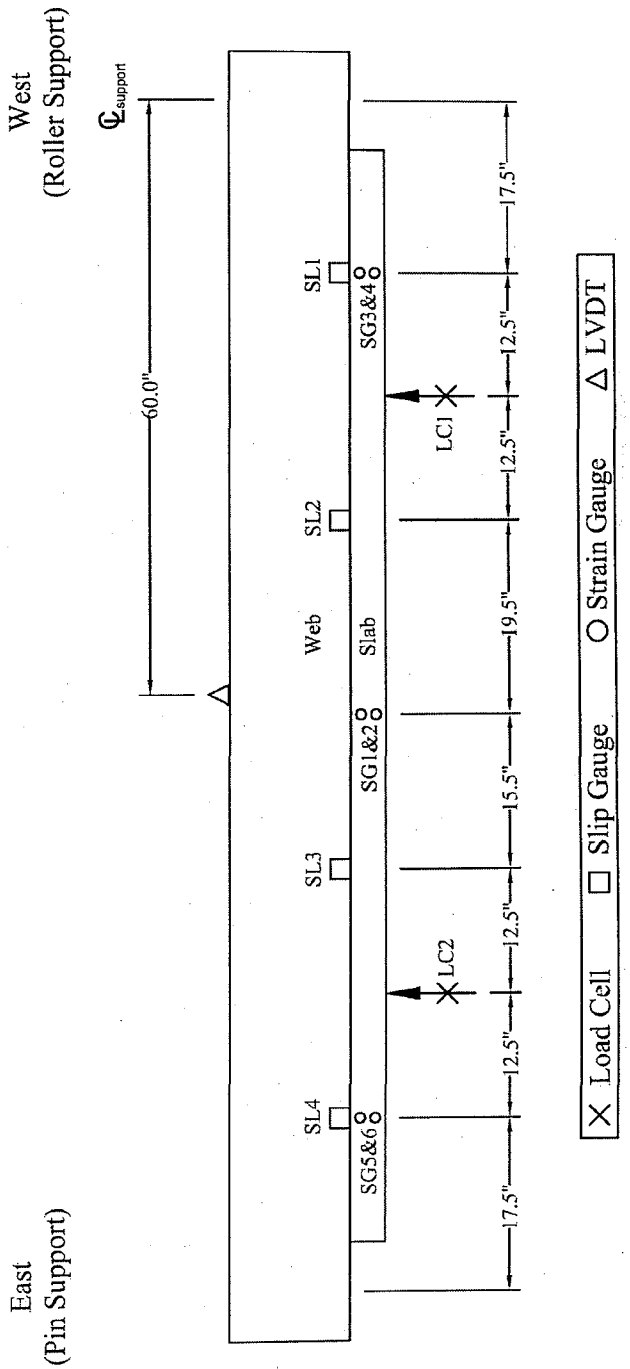

Figure 8-14: Instrumentation Layout

Two load cells were positioned under the hydraulic cylinders to record the applied load. The load cells were fabricated from a seamless extra strong pipe with a 2½ inch nominal diameter. The pipes were instrumented with four longitudinal and four transverse strain gauges which were connected to form a full bridge. This arrangement provides an output of pure axial load. Each load cell was calibrated before being utilized in the tests. Two steel support plates were machined to hold the load cell in position and ensure perpendicular bearing. Holes were also drilled into the plates to bolt the top and bottom plates to the hydraulic cylinder and reaction beam, respectively. Figure 8-15 shows a dimensioned drawing of the load cell and support plates. A picture of the actual load cell in the test setup is presented in Figure 8-16.

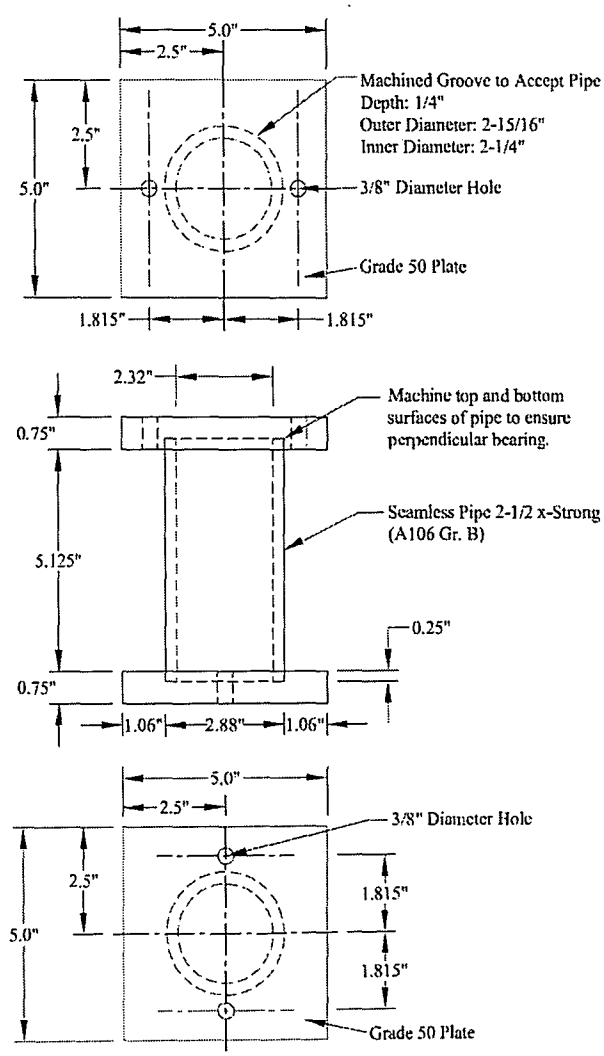

Figure 8-15: Detailed Drawing of Load Cell and Support Plates

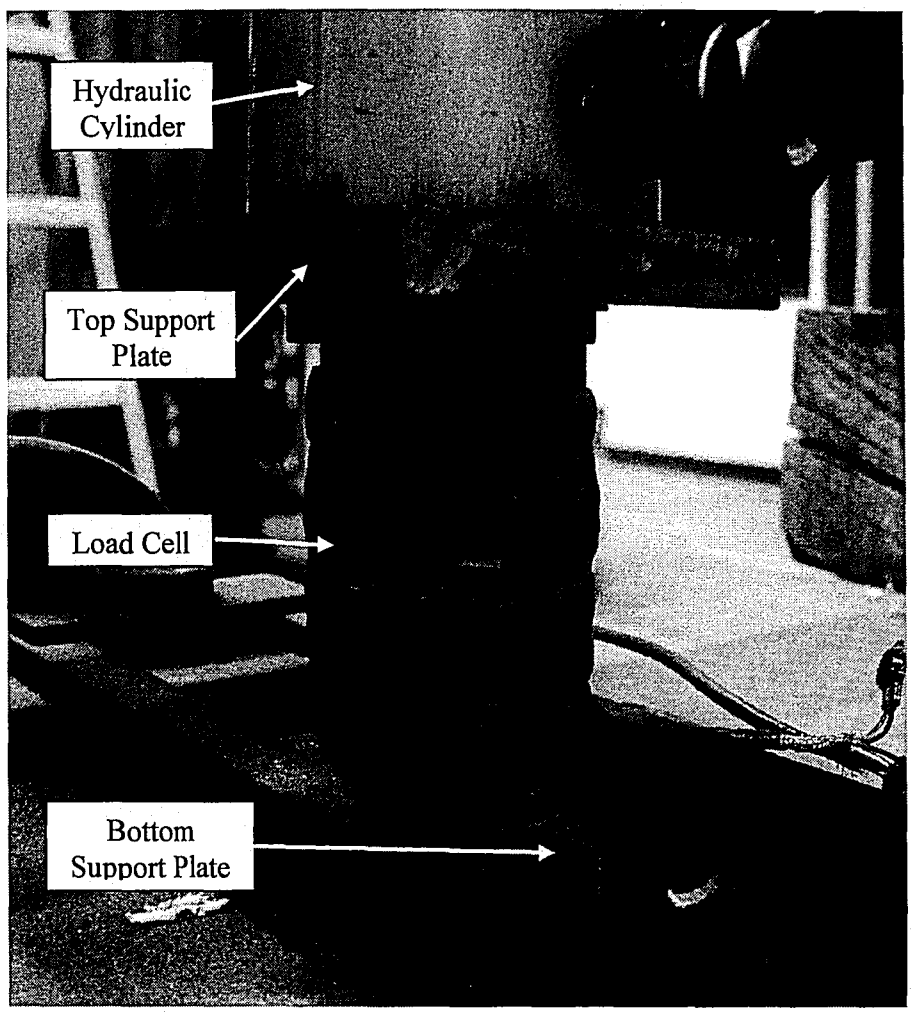

Figure 8-16: Close-Up View of the Load Cell

A linear variable differential transformer (LVDT) was connected to the bottom of the web at the midspan of the test specimen to record the deflection of the beam from the applied load. The LVDT had a total stoke of 4 inches (or a stroke of ±2 inches). A support frame was fabricated from steel angles and attached to the reaction beam to hold the LVDT securely above the test beam. A small piece of aluminum angle was hot glued onto the bottom of the web to which the LVDT was attached by a thin wire. Figure 8-20 shows the setup of the LVDT above the test specimen.

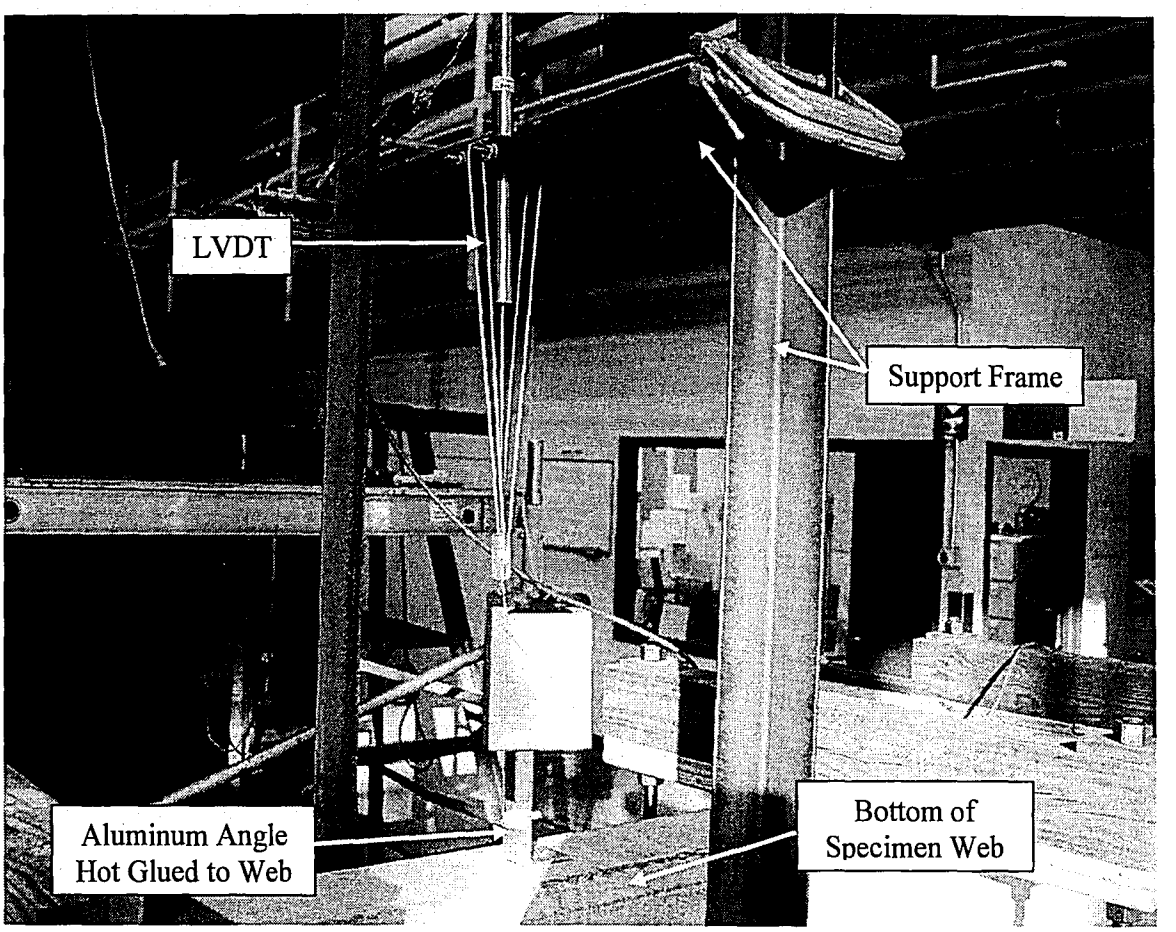

Figure 8-17: LVDT Setup above the Test Specimen

Spring return linear motion position sensors (slip gauges) were attached along the interface to measure the relative movement of the slab and web. These sensors had a total stoke of 1.5 inches (or a stroke of ±0.75 inches) and a resolution of 0.001 inches. A picture of the slip gauge is shown in Figure 8-18. These gauges were fastened to a small piece of aluminum angle which was glued to the slab of the test specimen near the composite interface. Another small section of aluminum angle was glued to the web of the test specimen and acted as a bearing surface for the spring loaded slider piece of the slip gauge. Thus, the slip gauge was able to record any movement occurring between the web and the slab concrete. This setup is shown in Figure 8-19.

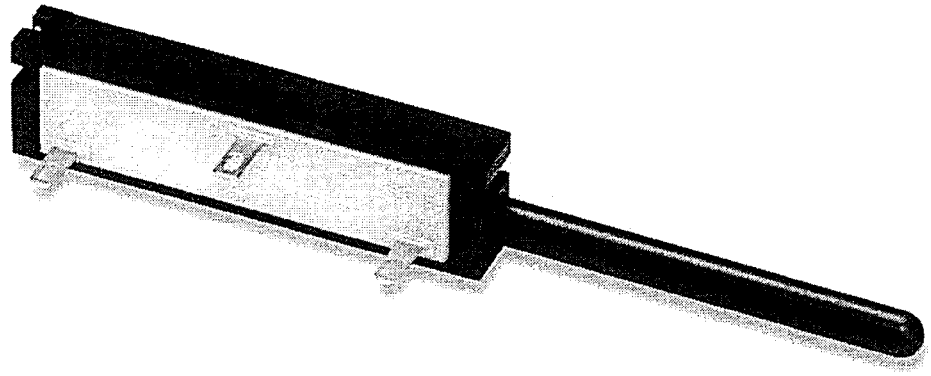

Figure 8-18: Slip Gauge

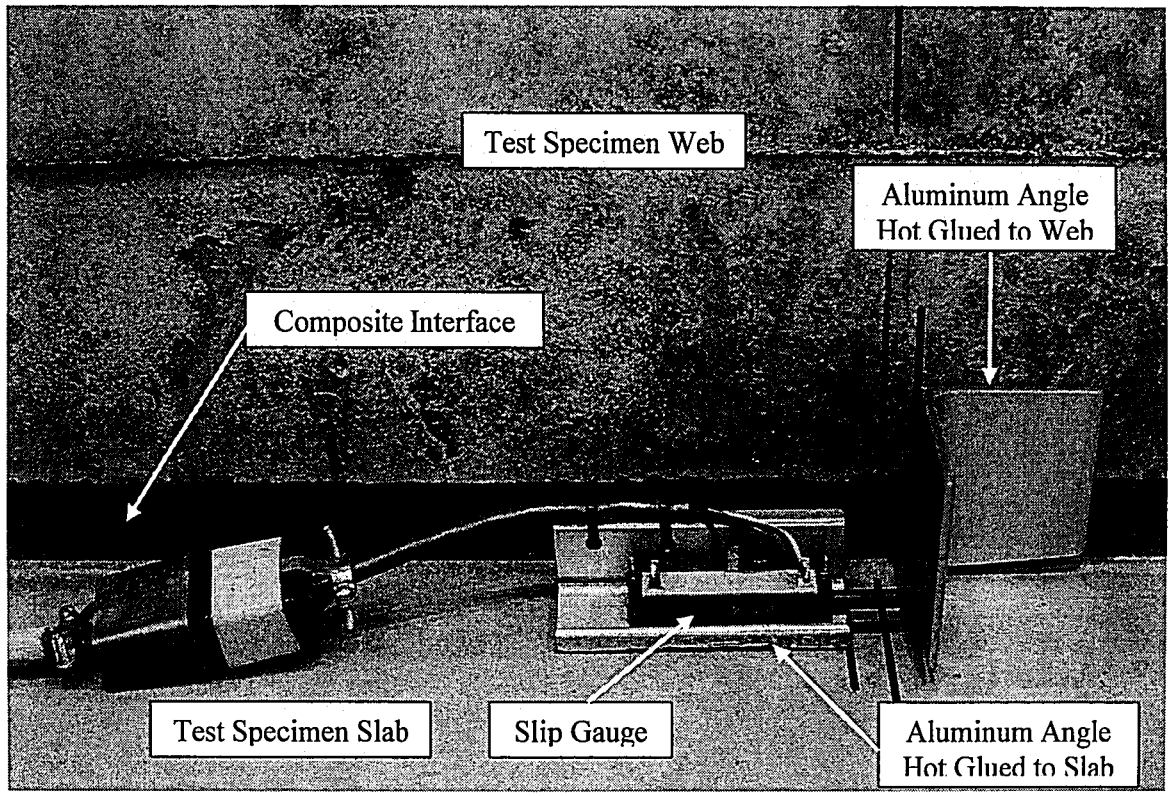

Figure 8-19: Slip Gauge Setup on the Test Specimen

As shown in Figure 8-14, a slip gauge was placed on both ends of the beam at a distance halfway between the loading point and the end of the slab (gauges SL1 and SL4). These two gauges were used to determine the average movement of the end (or outer) interface of the test specimen. The center (or middle) interface was monitored on each end of the beam by another slip gauge (gauges SL2 and SL3). This approximate equal distance placement allows the whole interface to be monitored with a limited quantity of slip gauges. It should be noted that the orientation of the

attached slip gauges will result in the slip recording to be positive on the west end of the beam and negative on the east end of the beam.

Two strain gauges were attached along the slab depth in order to monitor the composite action of the specimen and to calculate the horizontal shear stress of the slab-web interface. The strain gauges had a two inches long gauge length and a resistance of 350 ohms. The larger gauge pattern is ideal for concrete since the average strain is desired. The strain gauge positions along the depth of the slab, as shown in Figure 8-20 and Figure 8-21, remained consistent for every test. However, the location of the gauges along the length of the slab varied from test to test. Figure 8-14 shows the three possible positions along the length of the slab that the strain gauges were attached. The strain gauges located under the outer interface and center interface monitored the composite nature of the interface at their respective locations. The strain recorded by these gauges would linearly increase in compression as the specimen is loaded. When the composite interface finally fails, there will be a decrease in the measured strain. This strain data can then be correlated with the slip data obtained at the corresponding location on the beam to verify the failure of the interface.

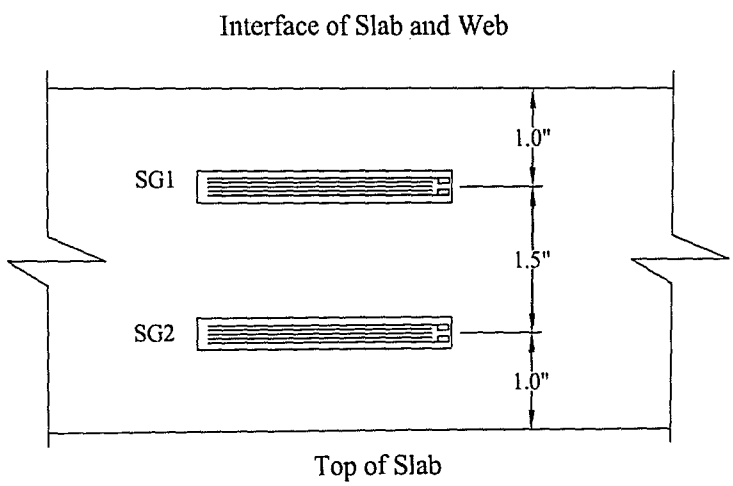

Figure 8-20: Detail of the Strain Gauge Layout along the Depth of the Slab

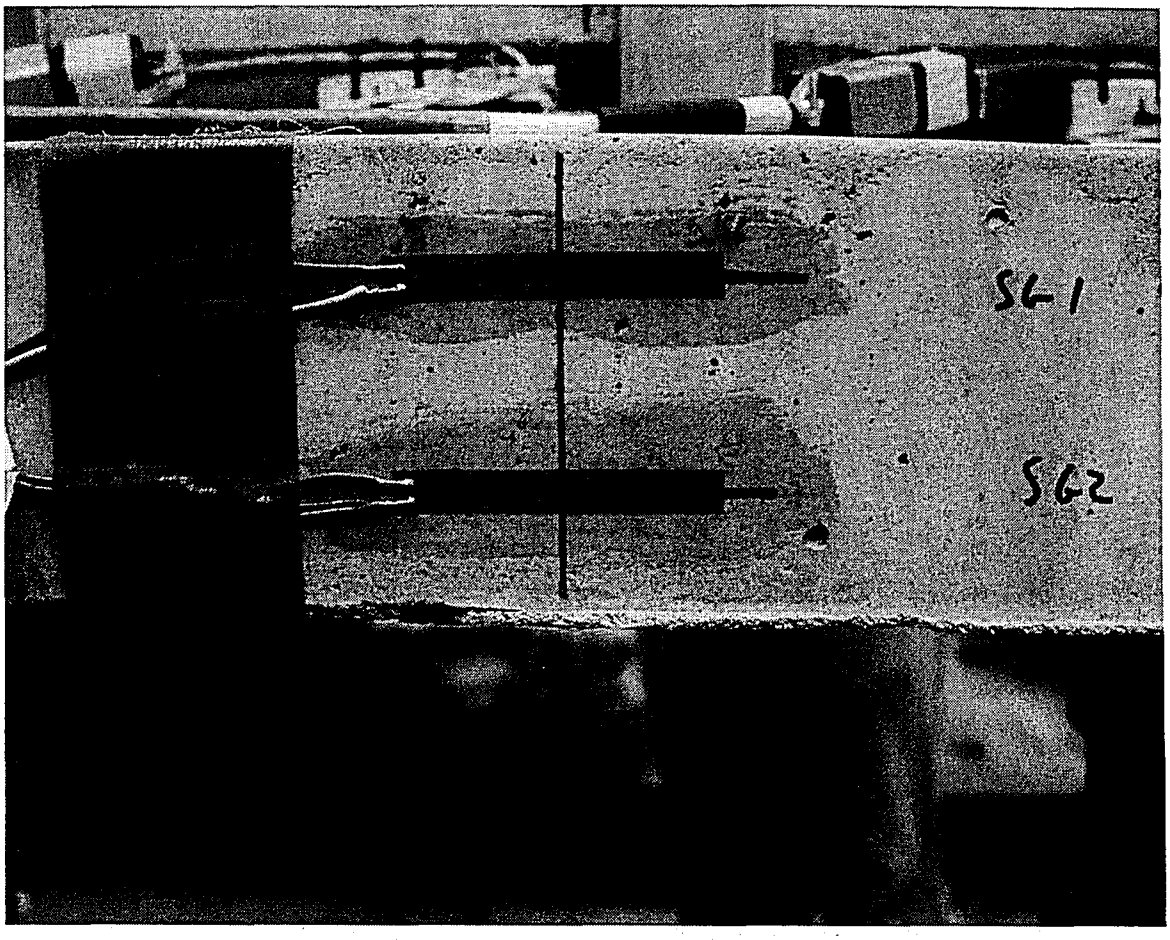

Figure 8-21: Strain Gauges along the Depth of the Specimen Slab

Similar to Deschenes and Naito (2006), the strain gauges were also utilized to determine the horizontal shear stress of the composite interface. The two strain gauges would provide a strain profile along the depth of the slab from which the stress profile can be acquired using the stress-strain data from concrete cylinder tests (Figure 8-22). The resulting compression force acting on the slab can then be calculated as the area under the stress curve multiplied by the width of the slab. It is also know that the compression force at the end of the slab will be equal to zero. Thus using the global force equilibrium method (Eq. 2), the horizontal shear stress can be determined from the change in the compression force from the strain gauge location to the end of the slab (Figure 8-23).

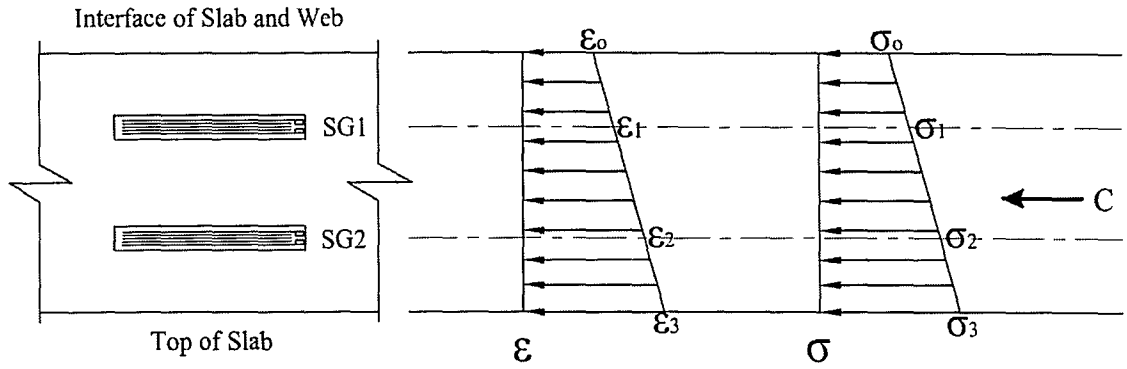

Figure 8-22: Determining Stress and the Resulting Compression Force from Strain

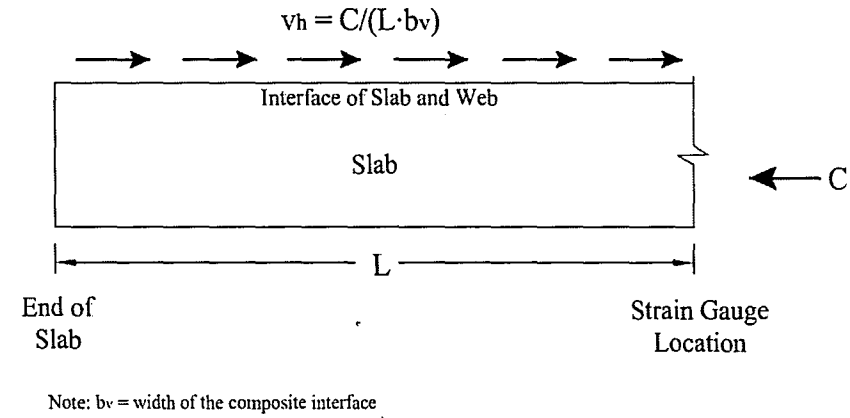

Figure 8-23: Determining the Horizontal Shear Stress from the Compression Force in the Slab

For the strain gauges attached near the midspan of the beam, the compression force acting on the slab and the resulting horizontal shear stress at the interface was assumed to be constant between the loading points. This assumption was based on the following equation:

$$\sigma_x = \frac{M \cdot y}{I} \qquad \text{(Eq. 26)}$$

where,

σ_x = nominal axial stress [psi]

M = bending moment [lbs-in.]

y = distance from the neural axis of a section [in.]

I = moment of inertia of the section [in.^{4}]

Since the values of the moment, moment of inertia, and distance from the neutral axis (for the individual gauges) are all constant between the loading points, the axial stress and thus the compression force will also be constant. The constant levels of axial strain and corresponding levels of axial stress can be seen in the finite element model of the test specimen shown in Figure 8-24 and Figure 8-25, respectively. The compression force will only begin to reduce once you move from the loading point to the end of the slab due to the decrease in the bending moment. Therefore, when calculating the horizontal shear stress from the strain gauges at midspan, the length of the interface in the global force equilibrium equation was taken to be equal to the distance from the load point to the end of the slab.

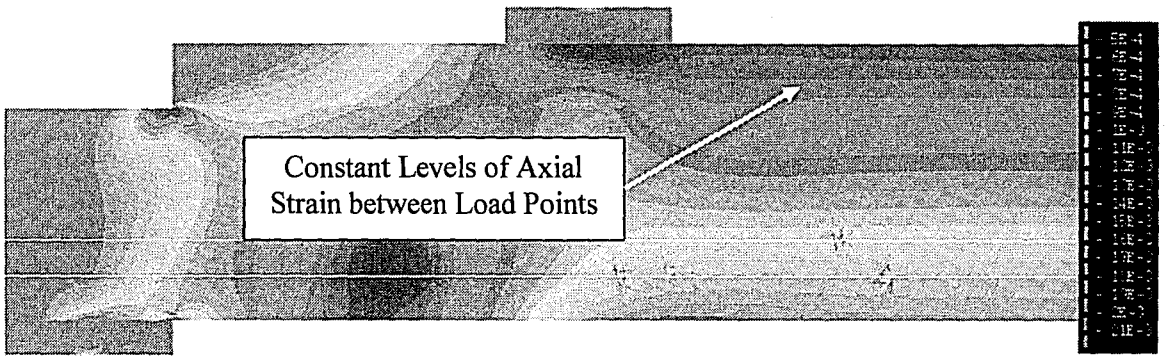

Figure 8-24: FE Model Showing Levels of Axial Strain

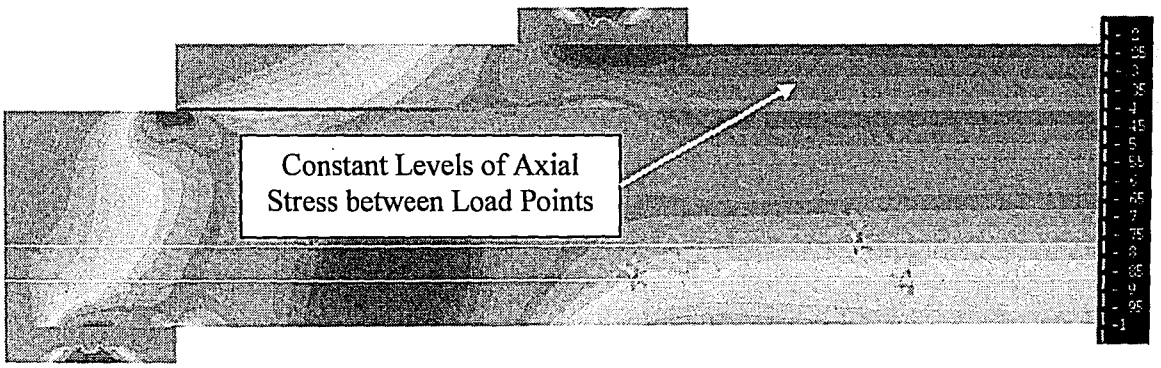

Figure 8-25: FE Model Showing Levels of Axial Stress

All of the instrumentation was attached to the specimen immediately preceding the testing of the beam (Figure 8-26). The devises were wired into a CR5000 datalogger which was controlled by

a laptop computer. The PC9000 software program installed on the computer was used to operate the datalogger, monitor the tests, and export the data once the tests were complete. Additionally, a required external power supply of 15 volts and 10 volts were provided to the LVDT and load cells, respectively, during the test. A picture of the various data collection and monitoring components are presented in Figure 8-27.

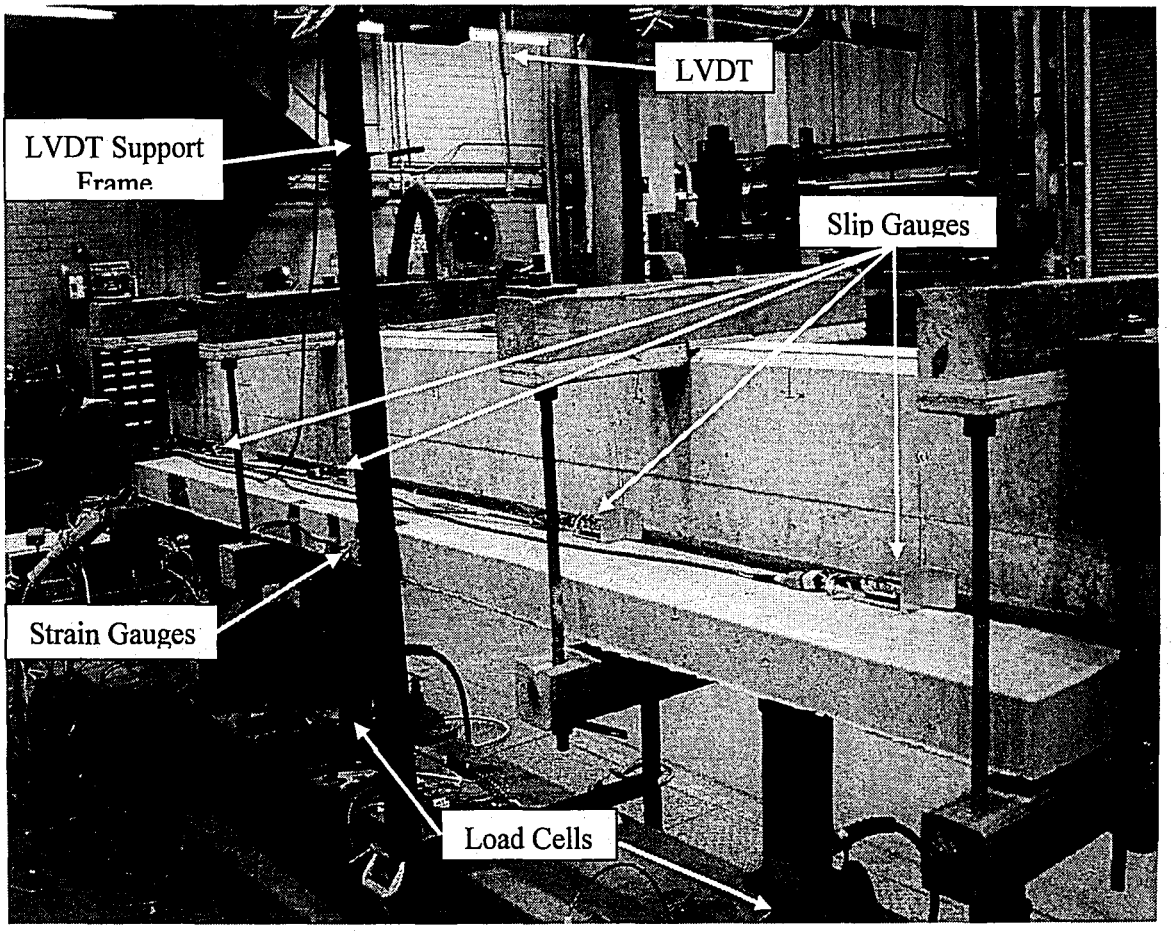

Figure 8-26: Instrumentation along the Test Specimen

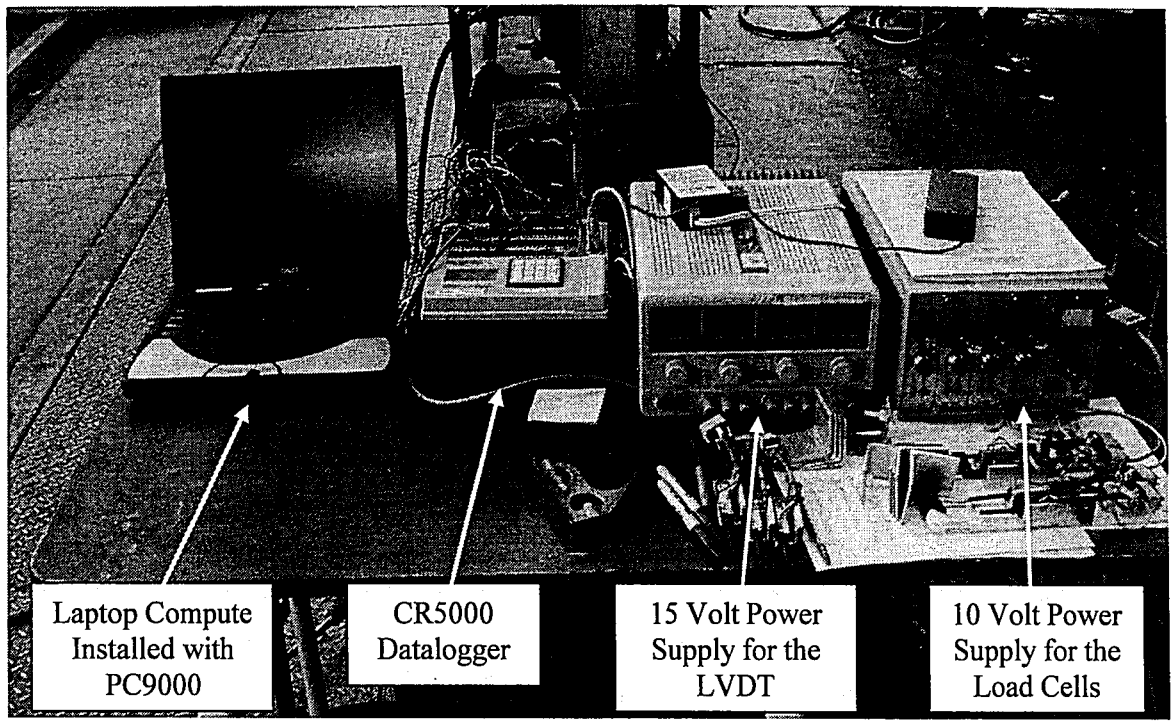

Figure 8-27: Data Collection and Monitoring Equipment

8.5 Test Procedure

The testing procedure began once the beam was in place, the instrumentation was attached and ready to start recording, and the initial observations of the interface conditions were documented. As mentioned previously, a hydraulic hand pump was manually operated to supply an equal amount of hydraulic fluid to both of the cylinders which in turn applied the load to the test specimen. The load was uniformly applied in increments of five kips. Before each increment of load was applied, the test specimen and composite interface are closely inspected for cracks and any observations were documented. The wood supports were removed from the specimen at a total load of fifteen kips which was determined to be a sufficient load to counteract the self weight of the section. During the test, the loading was stopped and the specimen was inspected if there was a significant event that took place such as a drop in load. Once the specimen experienced considerable cracking or failure, the test was stopped and the resulting data was

collected from the datalogger. Final observations were made before removing the failed specimen from the test setup.

8.6 Tests with the ARAMIS 3D Image Correlation System

ARAMIS is a 3D image correlation system, based on photogrammetry, which has the ability to measure three-dimensional deformation and strain distributions of real components under load. This system provides a non-contact and material independent data collection method by the utilization of two high-resolution digital CCD cameras. The ARAMIS system was incorporated into three of the specimen tests in order to validate the finite element model's predicted strain distribution on the slab concrete between the point loads (Figure 8-24) and to correlate with the strain gauge data. The system was also used to measure the deflection of the test specimen to corroborate with the LVDT data. The ARAMIS tests were run with the help of Dr. Jun Cao.

Once the test specimen was set up in the testing frame, a regular pattern of high contrast dots was applied to the designated slab surface with spray paint and permanent markers (Figure 8-28). These dots will deform with the specimen and act as reference or measurement points which will be tracked by the ARAMIS system in each pair of photographs taken. Two cameras attached to a tripod and wired into a computer were positioned in front of the specimen near the applied pattern (Figure 8-29). The ARAMIS system was then calibrated using a calibration panel prior to running the test and recording the images (Figure 8-30). Before load was applied to the specimen, an initial pair of images was taken to record the location of the applied dots in a zero load condition. The 3D coordinates of each dot were then calculated for each successive pair of images using photogrammetric principles. Photographs were taken by the two CCD cameras every five kips to measure the deformation of the structure (Figure 8-31). At higher loads when the specimen was predicted to fail, pictures were taken more frequently to capture the behavior of the strain before the failure of the specimen.

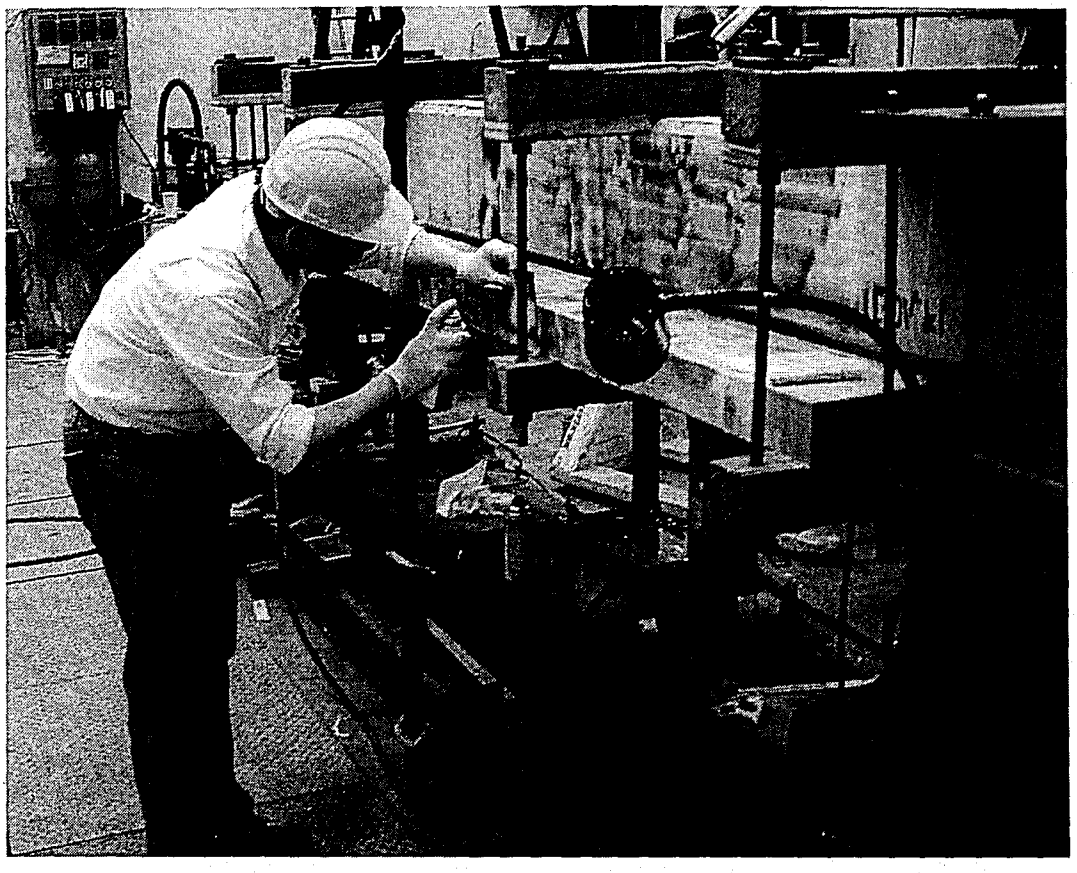

Figure 8-28: Applying Pattern to the Slab Concrete with Spray Paint [Specimen 6A8]

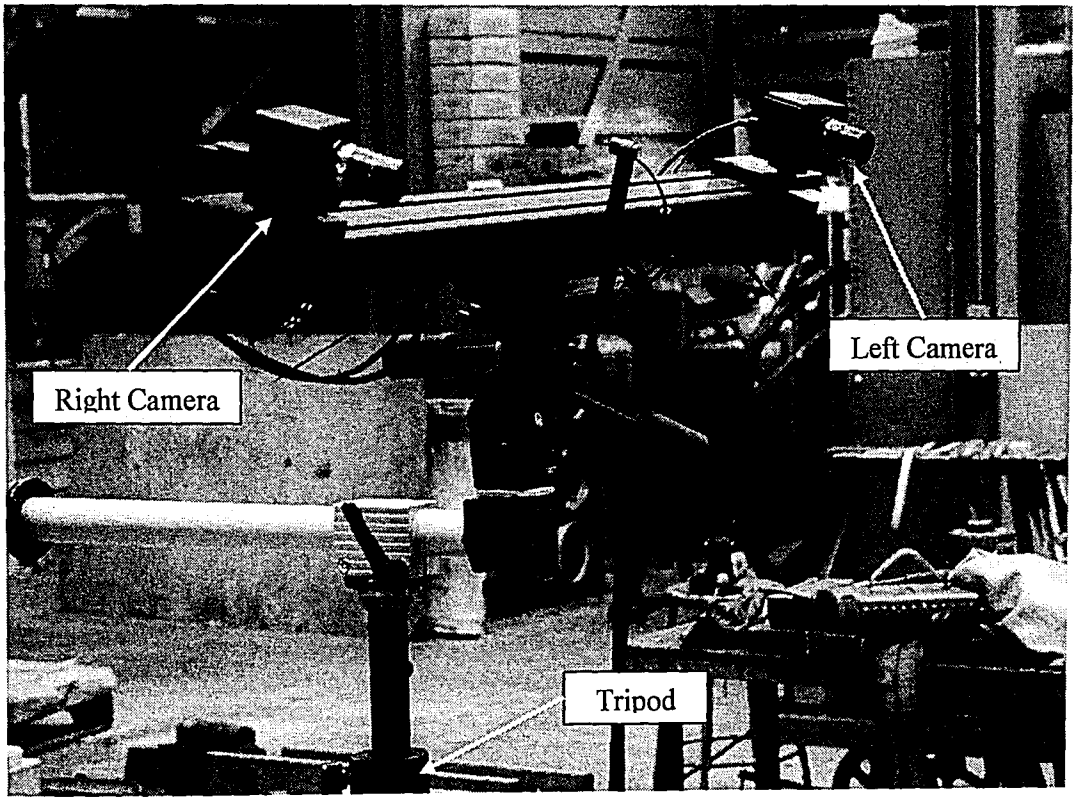

Figure 8-29: High-Resolution Digital CCD Cameras of the ARAMIS System

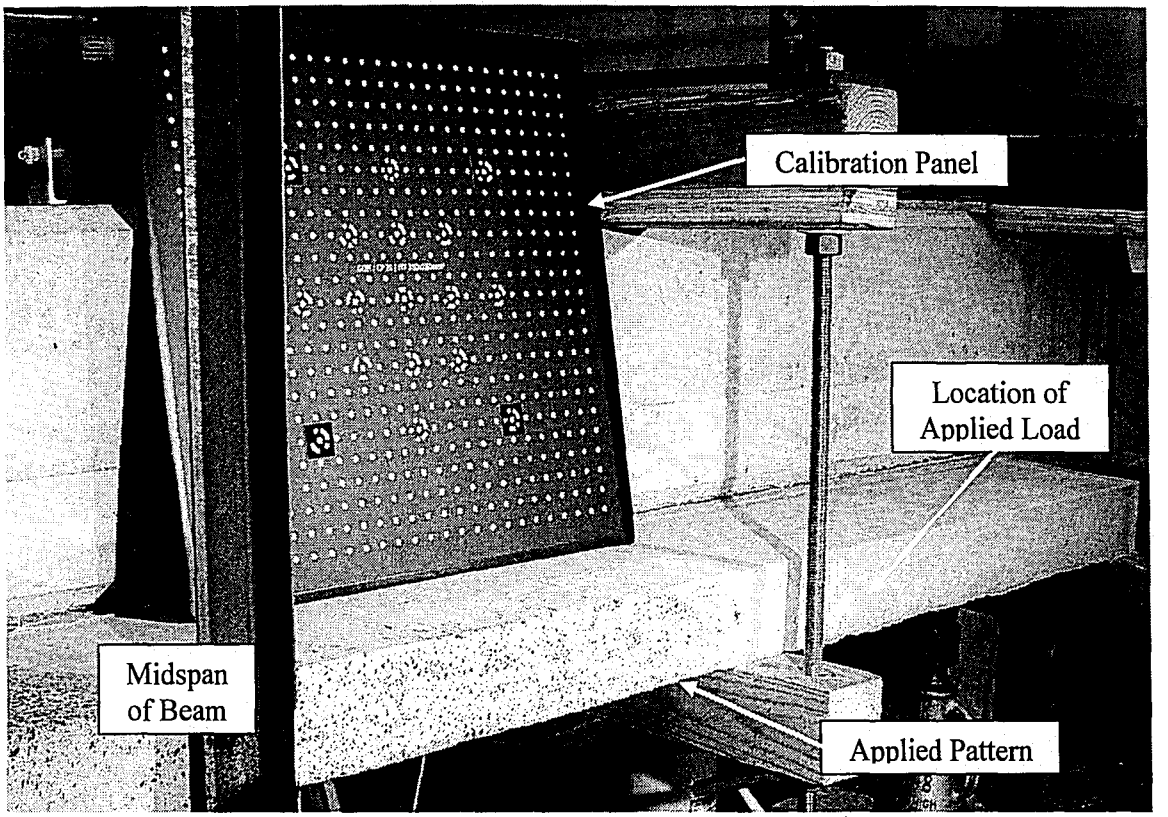

Figure 8-30: Calibration Panel and Pattern on the Slab Concrete [Specimen 6R8]

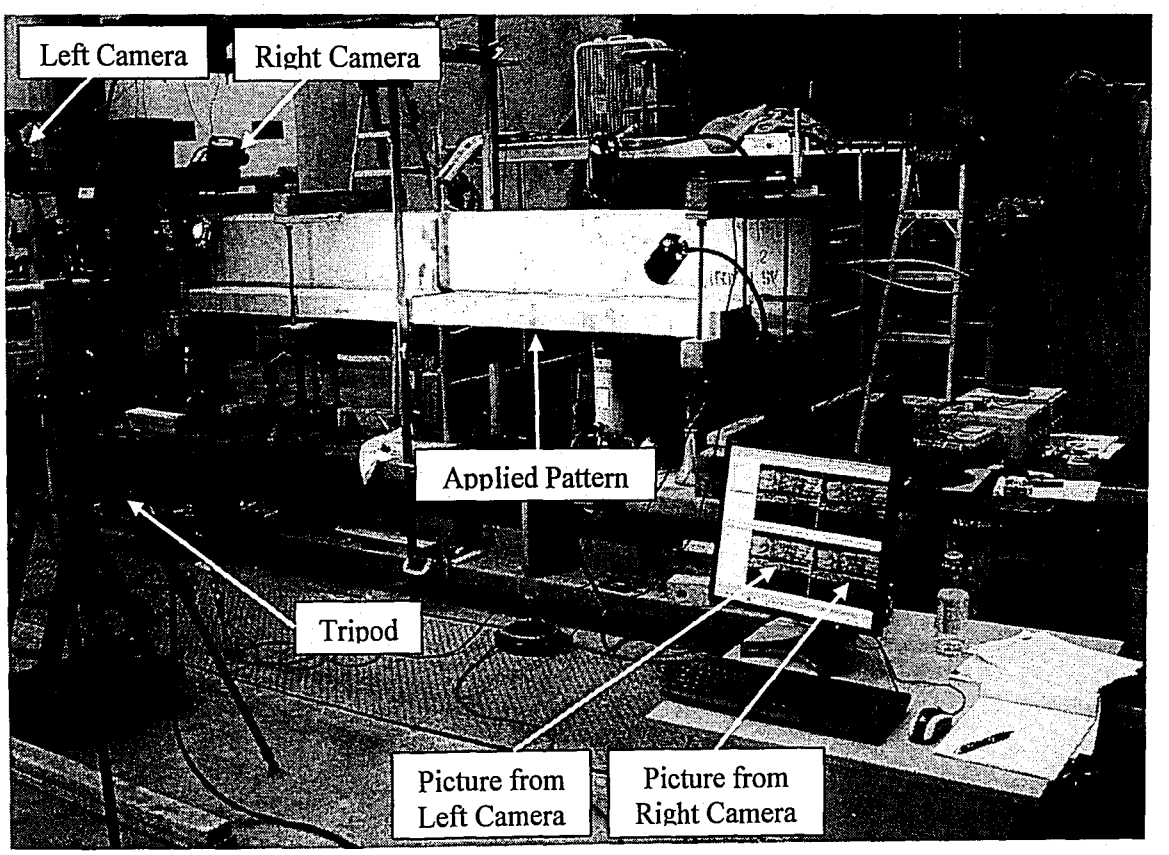

Figure 8-31: ARAMIS Test Setup [Specimen 6A8]

The resulting data recorded by the CCD cameras were evaluated using digital image processing. From this data, three-dimensional displacements and axial strains were calculated and output as text files or overlays on the current visible test specimen. For these tests, the resolution of the ARAMIS system was roughly 50 microstrain which was not high enough to capture some of the smaller strain variations or changes in the distribution. The clarity of the resulting strain distributions improved when smaller sections of the slab were examined compared to larger sections.

8.7 Material Tests

The material tests were performed around the same time as the composite beam tests. Two types of cylinders were tested to determine the material properties for the concrete; specifically, 4x8 cylinders were tested according to ASTM C 39 to find the ultimate compressive strength of the slab and web concretes, and 6x12 cylinders were tested according to ASTM C 469 to obtain the static modulus of elasticity for the slab concrete.

As mentioned previously, all of the slab concrete cylinders were released at the same time the forms were removed from the corresponding concrete slabs. The cylinders were then allowed to air dry and cure in the same conditions as the slab concrete. For the web concrete, the cylinders were released once they arrived at Lehigh University and were cured in a lime bath with water at room temperature until they were tested.

For the first test series which consisted of the specimen from the first slab pour, all the cylinders were tested on January 9 and 11, 2008. The ages of the slab and web concretes were well above 28 days at the time of testing. The tests were performed using the SATEC 600 kip universal testing machine. Four 4x8 cylinders for each of the two web pours were tested to obtain the average ultimate compressive strengths (Figure 8-32). For the slab concrete, the compressive strength and modulus of elasticity were found by testing four 6x12 cylinders. To perform the

ASTM C 469 tests, a test frame equipped with four LVDTs was attached to the cylinders in order to record the deformations (Figure 8-33). Two of the LVDTs measured the longitudinal deformation while the other two measured the lateral deformation. From these measurements, the axial strain was calculated. The modulus of elasticity was then found from the slope of the axial stress versus axial strain curve shown in Figure 8-34. Using the resulting values from the material tests, the properties of the slab concrete and reinforcing steel were converted to the concrete web properties by transformed section analysis. For these calculations, the modulus of elasticity used for the web concrete was found from the equation $E = 57000\sqrt{f'_c}$, the modulus of elasticity found from the material tests was used for the slab concrete (Table 8-2), and the modulus of elasticity of the reinforcing steel was assumed to be 29,000 ksi. With these transformed section properties, the values of I_{tr} and Q_{tr} for each specimen were calculated to be utilized later when determining the horizontal shear stress of the composite interface. The resulting material properties for the specimen of the first test series is presented in Table 8-2. Following should be noted that for the Specimen ID: the first number represents the design compressive strength of the slab concrete in units of ksi; the following letter signifies the surface finish of the composite interface (B = Broom; A = As-Placed; R = Rake); and the final number stands for the order in which the specimen for each surface finish was tested (e.g. 3B1 was tested before 3B2).

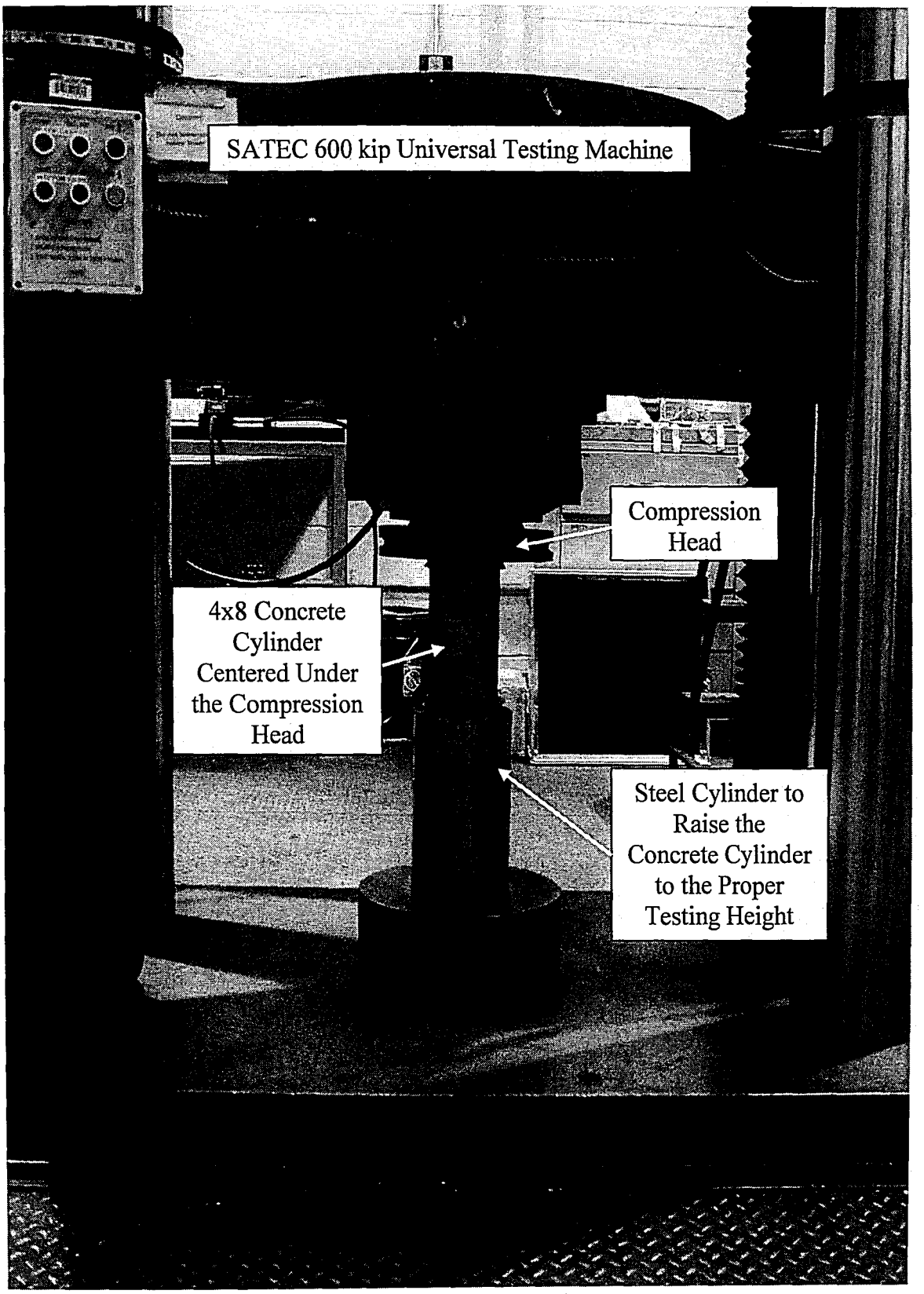

Figure 8-32: Testing a 4x8 Cylinder in the SATEC

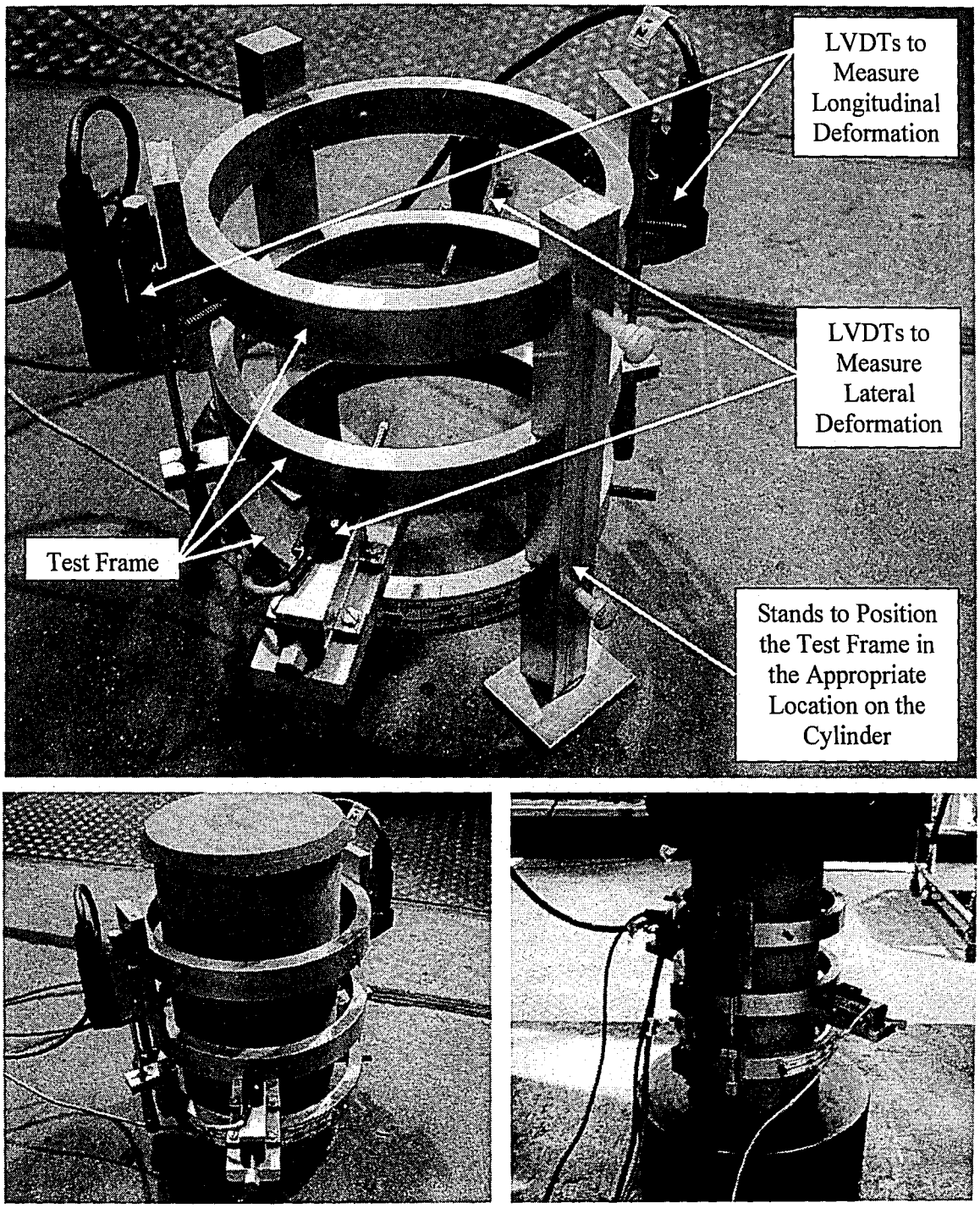

Figure 8-33: Test Frame and Test Setup for a 6x12 Cylinder

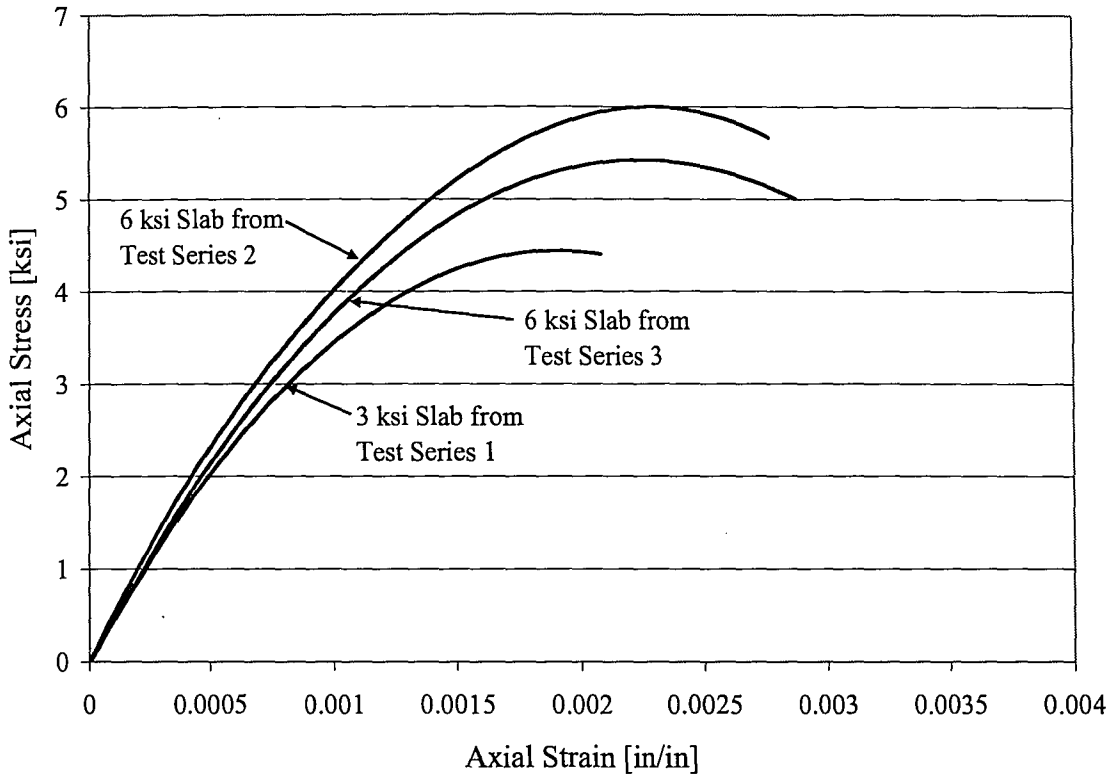

Figure 8-34: Axial Stress versus Axial Strain of the Slab Concrete for the Three Test Series

Table 8-2: Material Properties for the Specimen of the First Test Series

Specimen ID	**Date of the Specimen Test**	**f'_c of Slab [ksi]**	**E of Slab [ksi]**	**f'_c of Web [ksi]**	**I_{tr} [in^4]**	**Q_{tr} [in^3]**
3B1	1/7/08	4.53	3868.7	8.66	2893.2	249.5
3B2	1/11/08	4.53	3868.7	8.66	2893.2	249.5
3A1	1/15/08	4.53	3868.7	8.34	2917.7	252.4
3A2	1/23/08	4.53	3868.7	8.34	2917.7	252.4
3R1	1/29/08	4.53	3868.7	8.66	2893.2	249.5
3R2	2/1/08	4.53	3868.7	8.66	2893.2	249.5

As mentioned previously for the Pour 2 and 3 specimens, the time between casting the slab on the web and testing the composite beams was reduced to avoid differential shrinkage of the concrete. Therefore, the slab concrete did not reach its 28 day strength at the time of the test. In order obtain the compressive strength of the slab concrete for each test specimen, three 4x8 cylinder were tested on the day of the first beam test and another three 4x8 cylinder were tested close to

the last beam test to determine the slab strengths for those specimen. The compressive strength for the remaining test specimens were then found by linear interpolation or extrapolation. This method is illustrated in Figure 8-35 for the beams in test series three. The first set of cylinder tests shown in this figure were performed to find the release strength of the slab concrete.

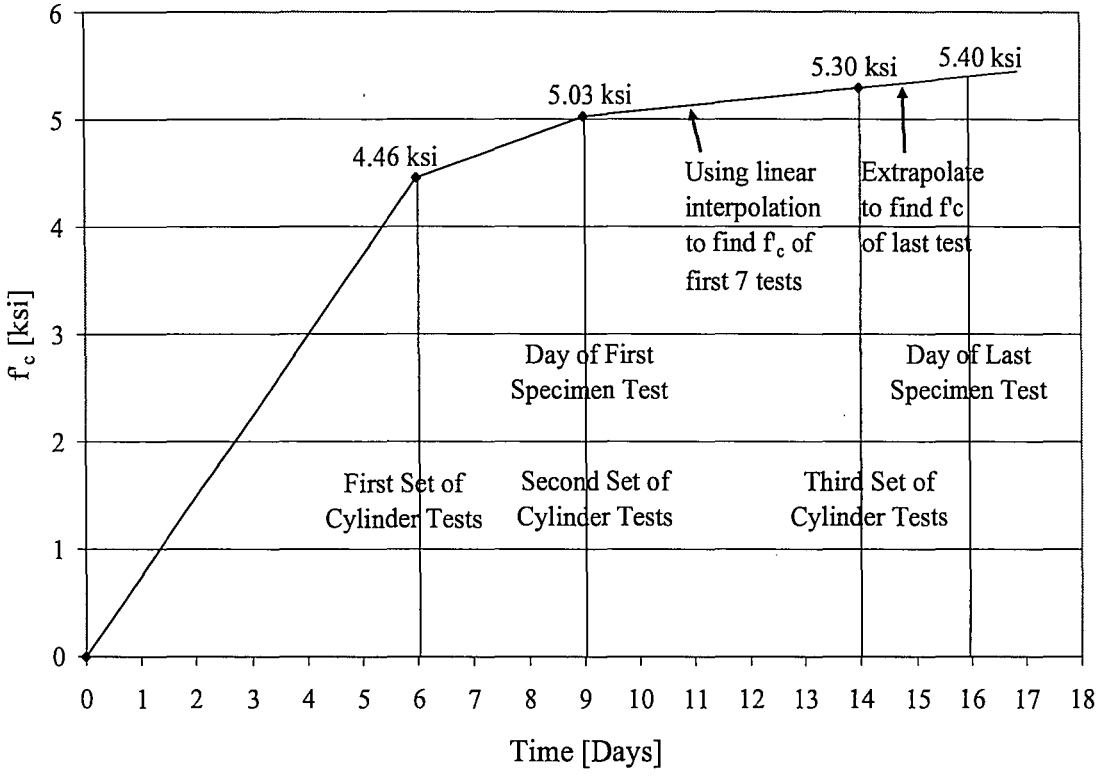

Figure 8-35: Determining the Slab Compressive Strength for the Test Series Three Specimen

The modulus of elasticity of the slab concrete was found for the second and third test series specimens by testing four 6x12 cylinders in the same manner as described for the first test series. These tests resulted in the axial stress versus axial strain curves shown in Figure 8-34. The relationship between the modulus of elasticity and compressive strength found from the 6x12 cylinder tests was determined using Equation 27. The modulus of elasticity was then found for each test specimen by using the slab compressive strength for each beam, the value of k calculated from the 6x12 cylinder test data, and Equation 27.

$$E = k \cdot \sqrt{f'_c} \qquad \text{(Eq. 27)}$$

where,

E = modulus of elasticity of the section [psi]

k = variable relating the compressive strength to the modulus of elasticity

- For the second test series, k = 56405
- For the third test series, k = 58054

f'_c = compressive strength of concrete [psi]

The compressive strengths of the two web concrete pours were found by testing 4x8 cylinders for each test series. Using the transformed material properties of the web concrete, slab concrete, and reinforcing steel found in the same way as mentioned previously, the values of I_{tr} and Q_{tr} for each specimen were calculated to be utilized later when determining the horizontal shear stress of the composite interface. The resulting material properties for the specimen of the second and third test series is presented in Table 8-3 and Table 8-4, respectively.

Table 8-3: Material Properties for the Specimen of the Second Test Series

Specimen ID	**Date of the Specimen Test**	**f'_c of Slab [ksi]**	**E of Slab [ksi]**	**f'_c of Web [ksi]**	**I_{tr} [in^4]**	**Q_{tr} [in^3]**
6R3; 6R4	3/6/08	5.19	4063.7	8.86	2933.6	254.4
6R5; 6R6	3/7/08	5.46	4166.6	8.86	2962.0	257.9
6A3	3/7/08	5.46	4166.6	8.74	2971.0	258.9
6A4; 6A5	3/10/08	6.25	4461.0	8.74	3049.3	268.4
6A6	3/11/08	6.52	4554.9	8.74	3037.4	271.3

Table 8-4: Material Properties for the Specimen of the Third Test Series

Specimen ID	Date of the Specimen Test	f'_c of Slab [ksi]	E of Slab [ksi]	f'_c of Web [ksi]	I_{tr} [in^4]	Q_{tr} [in^3]
6A7; 6A8	3/27/08	5.03	4116.1	8.74	2957.1	257.3
6R7; 6B3	3/28/08	5.08	4138.0	8.86	2954.1	256.9
6B4; 6R8	3/31/08	5.24	4203.0	8.86	2971.9	259.1
6B5	4/1/08	5.30	4224.5	8.86	2977.7	259.8
6B6	4/3/08	5.40	4267.1	8.86	2989.2	261.2

9 Experimental Program – Phase 2 – Data Analysis and Specimen Behavior

9.1 General

The data from all 22 tests were collected and analyzed. The results illustrated significant variation in the slip, strain, and deflection data between the different tests. Some of the data behaved as expected while others diverged from the predicted values. In order to determine the reason for this discrepancy, a thorough and comprehensive study of the test data and specimen behavior was undertaken.

9.2 Calculated Slip and Deflection from Beam Theory

Since the difference in the behavior of the data could be caused by a level of non-composite action at the interface, the principles of beam theory were used to calculate the actual quantity of slip and deflection that would result from these different levels. The calculations were carried out for three possible cases:

- Fully Composite – The beam is fully composite along the entire length
- Non-Composite – The beam is non-composite along the entire length
- Middle Composite – The beam is composite in the middle (between the loads) and non-composite at the ends (between the load and the end of the slab).

The last scenario was considered based on the behavior of some of the specimen during the test. The reasoning for this partial composite condition is that since the point load creates a concentrated amount of normal force on the interface directly under the load, the interface will have to overcome a greater amount of horizontal shear stress due to the slightly increased clamping force and friction in order to fail. However, it should be noted that the clamping force does not create a significant effect on the horizontal shear stresses as seen from the FE model in Figure 6-12. In addition to the clamping force, the shear forces drop to zero between the loading

points which results in the horizontal shear stress being theoretically zero up to high load levels. Therefore, the middle interface can remain composite between the point loads and experience no relative slip even after the outer interface between the point load and the end of the slab fails.

The amount of slip relative to the applied load was calculated for the middle composite and non-composite cases. The fully composite case would result in a theoretical slip value of zero since no differential movement between the slab and web would occur. For the other two cases, the slip was determined by first calculating the slope along the beam as the integral of the moment equation as presented in Equation 28.

$$\theta(x) = \int \frac{M(x)}{E \cdot I(x)} dx \qquad \text{(Eq. 28)}$$

where,

$\theta(x)$ = the slope of the elastic curve along the beam [rad.]

$M(x)$ = the equation of the internal moment along the beam [kip-in]

E = the modulus of elasticity of the section [ksi]

$I(x)$ = the moment of inertia along the beam [in.^{4}]

When this integral was calculated and simplified for the two point loading condition, the following equation resulted for the non-composite scenario:

$$\theta = \frac{P(a^2 - L \cdot a + x^2)}{2E \cdot I_{trnc}} \qquad \text{(Eq. 29)}$$

where,

θ = the slope of the elastic curve along the beam [rad.]

P = the point load applied to the beam [kip]

a = the distance from the support to the load point [in.]

L = the total length of the beam [in.]

x = the distance from the support to a location along the beam [in.]

E = the modulus of elasticity of the section [ksi]

I_{trnc} = the transformed moment of inertia of the non-composite beam found by the sum of the individual I_{tr}'s for the web and the slab sections [in.^{4}]

When Equation 28 was calculated for the middle composite scenario, the following equation resulted:

$$\theta = \frac{P(x^2 - a^2)}{2E \cdot I_{trnc}} + \frac{P \cdot a \cdot (a - L/2)}{E \cdot I_{tr}} \qquad \text{(Eq. 30)}$$

where,

I_{tr} = transformed moment of inertia of the entire composite cross-sectional area [in.^{4}]

E was taken as the modulus of elasticity of the web concrete. The section properties of the slab concrete and reinforcing steel were transformed to those of the web. Based on these properties, the transformed moment of inertia was determined for the web and slab sections individually and also for the full composite section. For the non-composite beam calculations, the moment of inertia was taken as the sum of the individual I_{tr}'s for the web and the slab sections. For the middle composite calculations, the moment of inertia was the sum of the web and slab sections for the location between the load point and end of the slab, and the composite moment of inertia for the location between the two load points. For the calculations, the average value of E and the corresponding I_{tr} found from the material tests described in Chapter 8 was used. It was found that using the largest or smallest values of E and I_{tr} did not change the results that significantly.

Next, the slope was used to find the distance over which the web and slab will slide relative to each other at the location of the slip gauge between the load and the end of the slab. The relative slip of the web and the slab was found by multiplying the slope or rotation by half the depth of the web and slab, respectively. If the two sections are acting non-compositely they will rotate about their own neutral axis. This is why the rotation is multiplied by half the depth of the web or slab. For the non-composite case, the total rotation at the slip gauge was used to find the slip (Figure 9-1b). For the middle composite case, the rotation used was equal to the rotation at the slip gauge minus the rotation at the loading point (Figure 9-1c). This represents the amount the section of the slab between the loading point and the end of the beam would rotate and thus slip when the interface is still composite under the loading point.

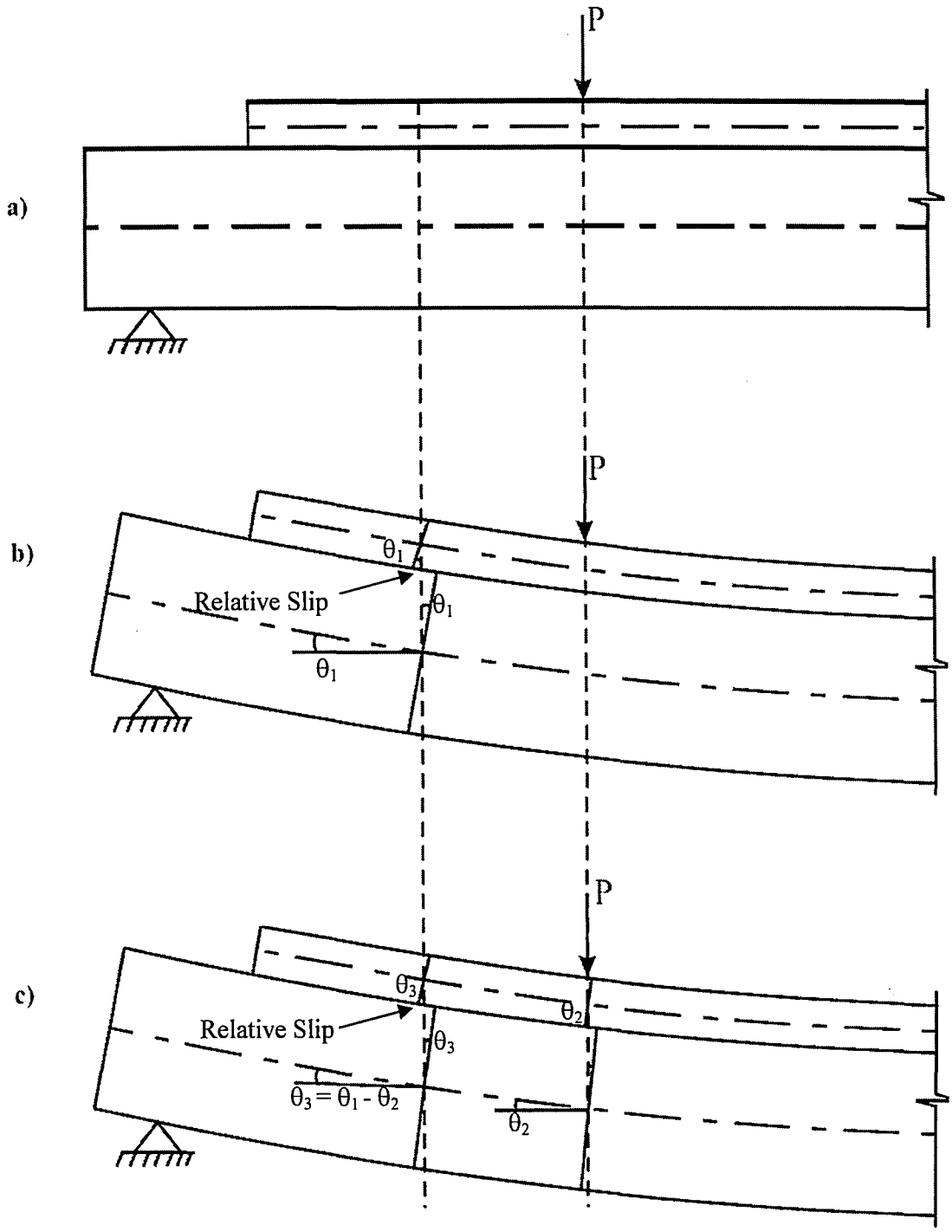

Figure 9-1: Rotation and Slip of Specimen: a) Beam Before Loading; b) Non-Composite; c) Middle Composite

The calculations for non-composite and middle composite slip were performed for applied loads ranging from 0 to 70 kips. The resulting values of slip for the various loads are plotted in Figure 9-2.

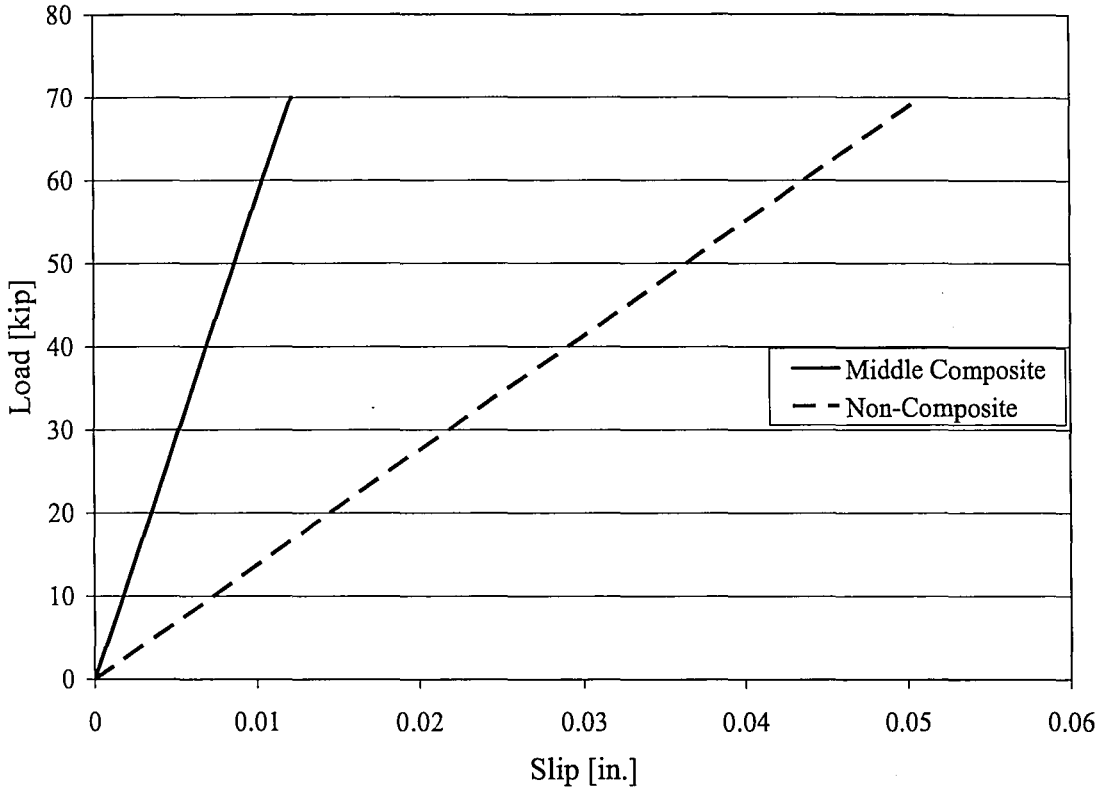

Figure 9-2: Calculated Middle Composite and Non-Composite Slip

The deflection along the beam ($\Delta(x)$) was calculated for the composite, non-composite, and middle composite cases as the integral of the slope equation or the second integral of the moment equation as shown in Equation 29.

$$\Delta(x) = \int \theta(x)\,dx = \iint \frac{M(x)}{E \cdot I(x)}\,dx\,dx \qquad \text{(Eq. 31)}$$

The values of E and I_{tr} were calculated and utilized in the same way as mentioned for determining the slope. Using Equation 31 and the calculated properties of E and I_{tr}, the values of deflection corresponding to applied loads ranging from 0 to 70 kips were found at midspan for the

composite, non-composite, and middle composite cases. The resulting values of deflection for the various loads are plotted in Figure 9-3. A check for the deflection at midspan for the composite beam was preformed using the finite element model described in Section 6.4. Using the properties of E and I_{tr} for the composite section, the FE load-deflection response was very similar to the one calculated from beam theory as seen in Figure 9-3. At a load of 70 kips, there was only a 2.7% difference between the deflections found from beam theory and the FE model.

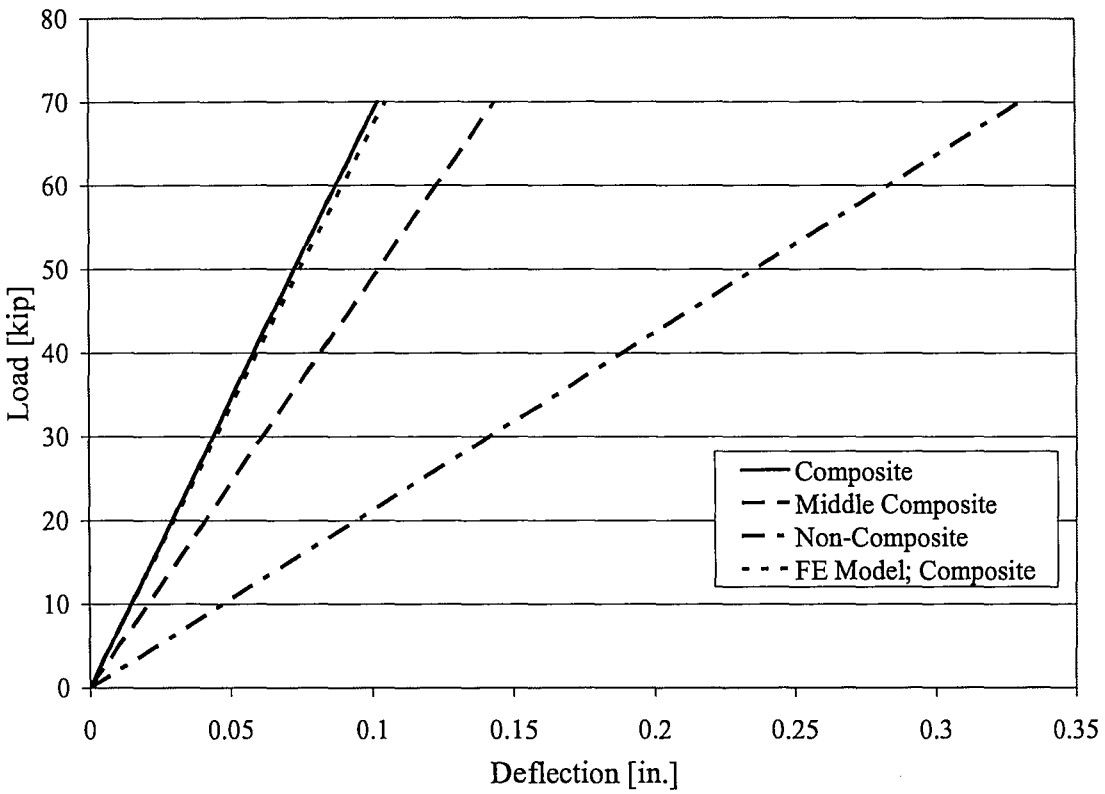

Figure 9-3: Calculated Composite, Middle Composite, and Non-Composite Deflection

These calculations for the slip and deflection were used as reference lines in which to compare the experimental data. The utilization of these reference lines will aid in determining the behavior and level of composite action of the test specimens.

9.3 Variation in the Data from the Specimen Tests

Variation from the predicted response was observed in the measured results for slip of the interface, deflection at midspan of the beam, and strain in the slab concrete. This section provides a brief discussion of the overall correlation and discrepancy between the results and the expected responses.

The most noticeable variation between the results occurred in the slip measured outside of the applied loads. In this region the slips were the greatest; however, they varied from that of a fully composite behavior to one of non-composite. A plot of the load versus slip for a number of tests is presented in Figure 9-4. The response varies from fully composite, as observed in specimen 6R7 up to a load of 63 kips, to non-composite as observed in specimen 3R2 which followed the non-composite slip line. In general, the variation correlated with the level of roughness. Specific details on the correlation are discussed in subsequent sections.

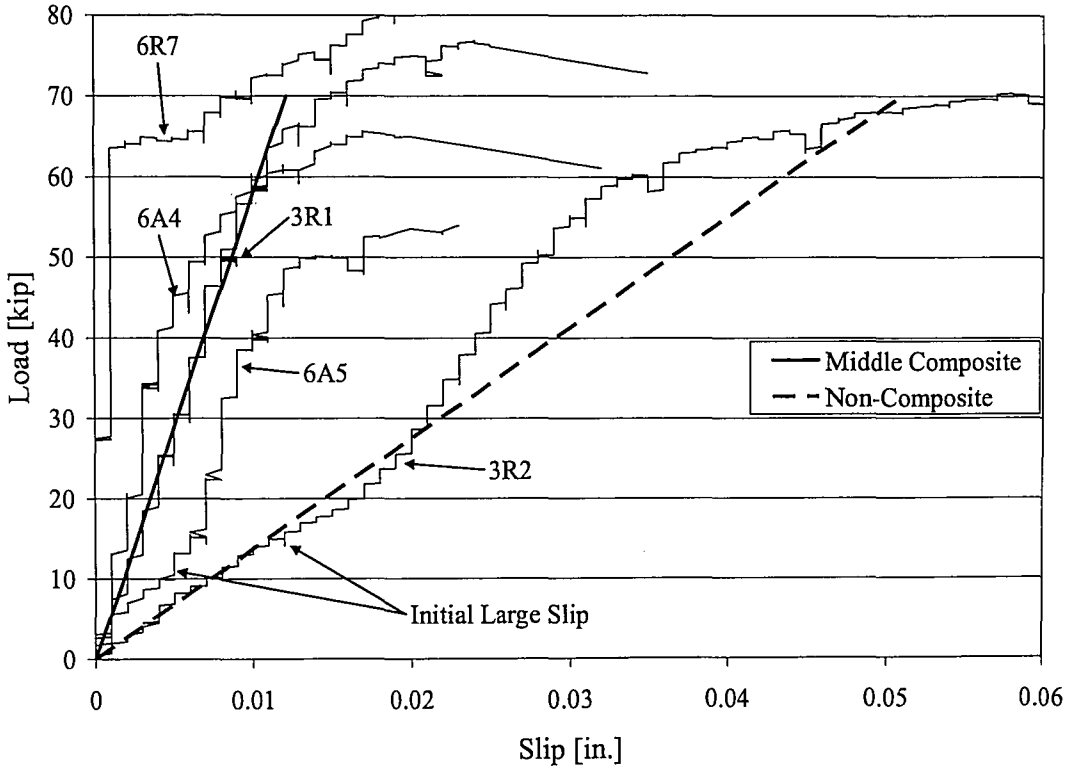

Figure 9-4: Varying Levels of Slip Recorded

A number of specimens exhibited a large initial slip with the applied load as seen with Specimen 6A5 in Figure 9-4. This behavior typically occurred when the load-slip stiffness was less than the scenario where only the middle interface is assumed to be composite. For these specimens, an initial large slip with load occurred followed by a stiffening of the slip response at a load of approximately 10 to 15 kips. This could be indicative of a small movement followed by interlock of the interface.

The differences in slip behavior often times occurred between one end of the beam and the other. This can be observed in the slip measured on the east and west end of beam 6A6 (Figure 9-5). It should be noted that the orientation of the attached slip gauges will result in the slip recording to be positive on the west end of the beam and negative on the east end of the beam as mentioned previously. In most cases, the variation in slip could be correlated with differences in the amount of roughness between each end of the beam. Since the beams could be loaded beyond the first occurrence of slip, data from both ends of the beam were used independently. This was only conducted when the failure on one end did not influence the response on the other end.

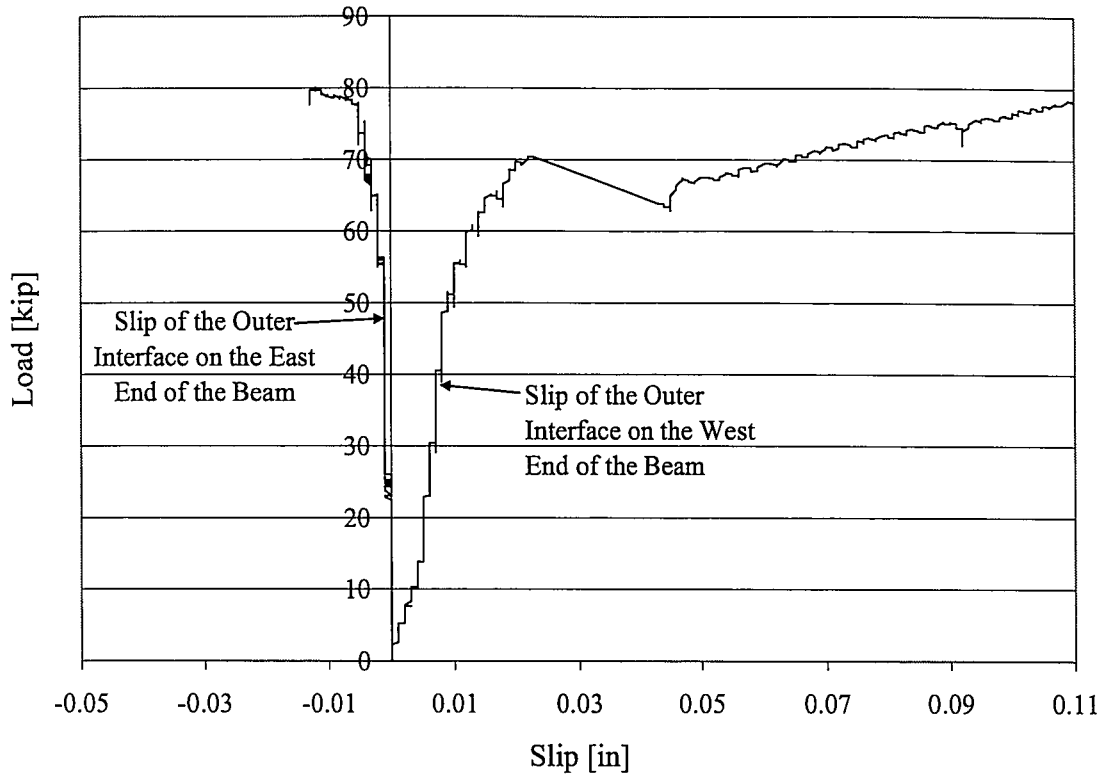

Figure 9-5: Variation in the Slip Behavior on Opposite Ends of a Beam [Specimen 6A6]

Variation also occurred between the predicted deflection and the resulting data from the experimental tests. The experimental results exhibit a considerable lack of stiffness in all of the test specimens. Figure 9-6 shows a typical plot of the load versus deflection recorded for the test specimens. It can be seen from the plot that an initial large deflection takes place between 0 and 8 kips. During this duration, it seems as though the slope is following the calculated non-composite load-deflection line. After the initial large deflection dissipates, the slope of the line between 8 and 30 kips increases. Eventually the slope becomes linear and remains this way until the outside interface between the load and the end of the slab fails. It should be observed that during the time the load-deflection line is linear, the slope or stiffness is closer to the slope of the calculated composite or middle composite line rather then the non-composite line. This behavior is found to be related to the testing fixture and is discussed in further detail in Section 9.6.

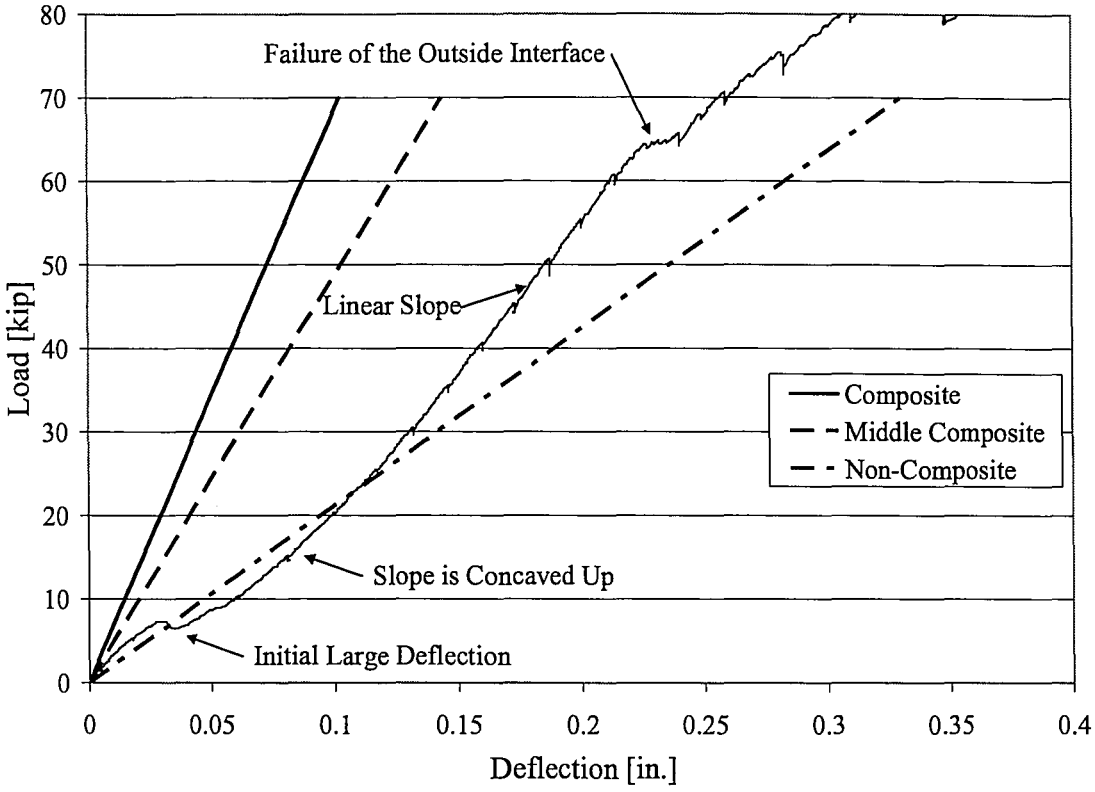

Figure 9-6: Typical Recorded Load versus Deflection Plot [Specimen 6R7]

The strain measurements in the middle of the beam always behaved in a similar manner; the strain would increase in compression (with the strain gauge near the top of the slab experiencing more compression then the one near the bottom) until the interface below the strain gauge was lost. The interface failure was associated with an abrupt jump in strain (Figure 9-7). After this failure, the top strain gauge would increase in compression and the bottom strain gauge would increase in tension. This behavior is inline with a transition to a non-composite response.

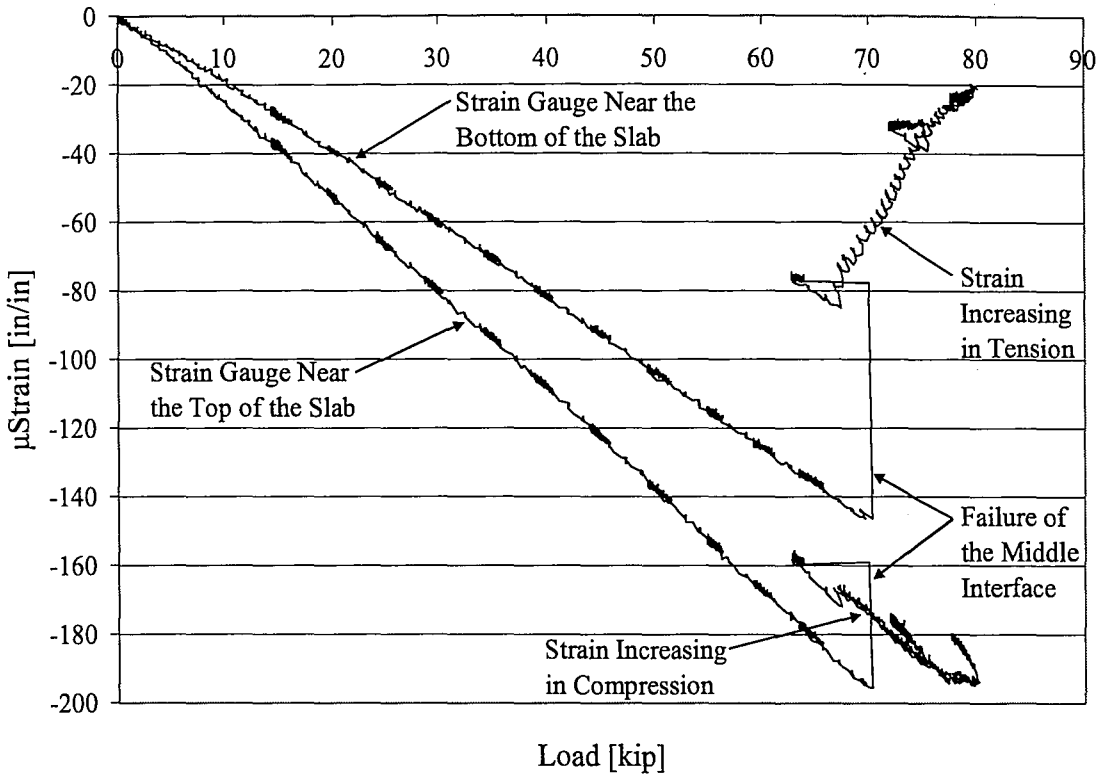

Figure 9-7: Typical Strain Gauge Data in the Middle of the Beam [Specimen 6A6]

The data recorded by some of the strain gauges attached to the slab between the load point and the end of the beam deviated from the expected behavior. The strain gauge at the bottom of the slab initially increased in tension until the specimen was loaded to about 10 to 20 kips, at which point the strain began to gradually transition into compression (Figure 9-8). This behavior was observed for some of the specimens which had strain gauges attached at this location and was not observed for others. Typically, this initial tensile strain occurred for the specimen that had a larger quantity of outer slip such as Specimen 6A5 in Figure 9-4. An initial tension strain is indicative of non-composite behavior; however, if the beams were non-composite, the strain near the interface would continue to increase in tension with applied load. It is theorized that the tension strain excursion observed outside of the applied loads is due to a marginal slip at initial loading.

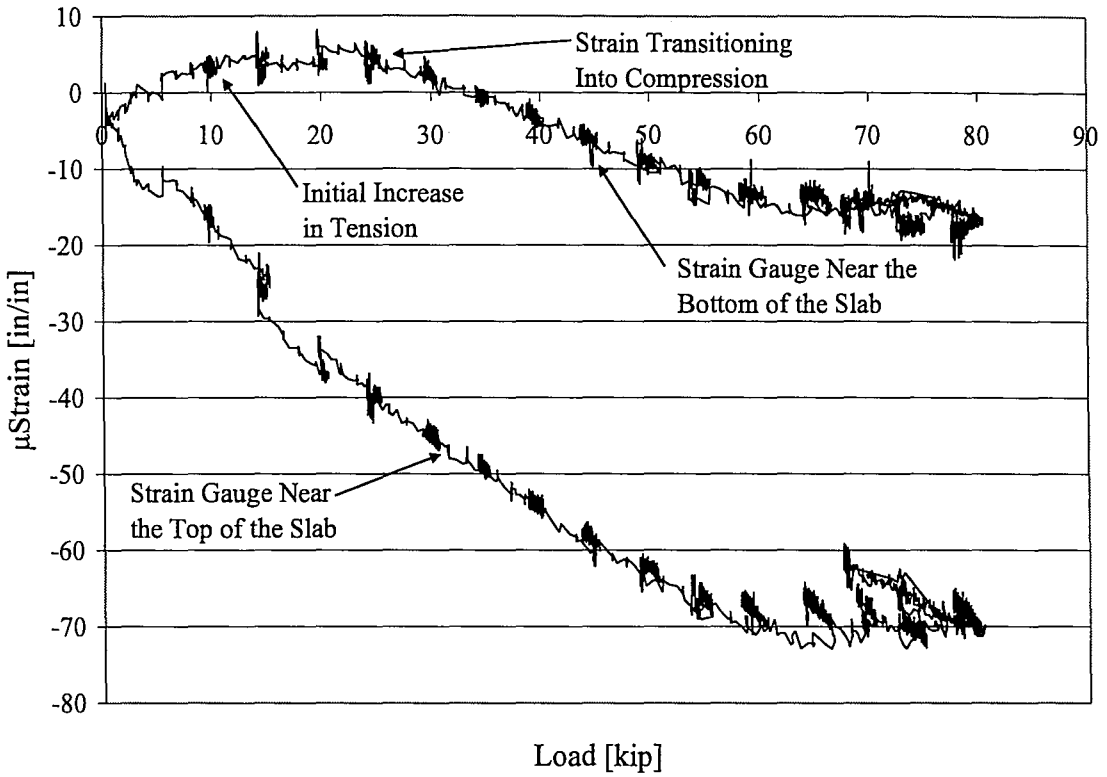

Figure 9-8: Typical Strain Gauge Data near the End of the Beam [Specimen 3R1]

For the specimens that did not experience the initial tensile strain, the strain data near the end of the beam behaved similar to strain data at the center of the beam. The variation in strain between the different specimens is attributed to a decreased level of bond resulting from the different levels of surface roughness at the interface of the beams. The roughness variation is described in the following section.

9.4 Variation in Roughness of the Surface Finishes

Observations of the web interface roughness were made prior to placement of the slab concrete. Each end of the beam was inspected independently to account for variations in roughness along the length. The broom surface finish was fairly consistent across all the beams. This surface preparation provided the lowest level of roughness. Figure 9-9 shows a specimen with a broom surface finish.

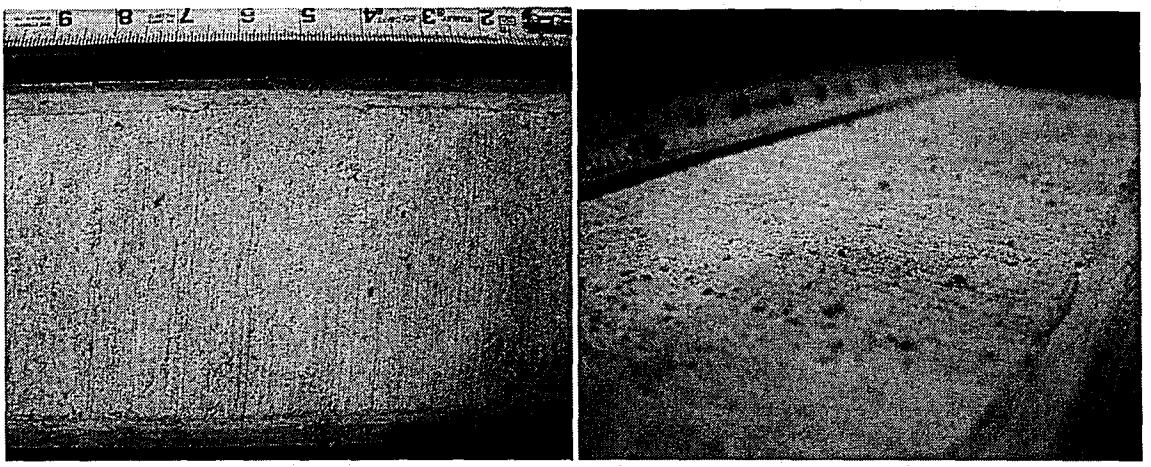

Figure 9-9: Broom Surface Finish [Specimen 6B6]

The as-placed and rake surface finishes exhibited substantial variation in the level of roughness. To appropriately compare the responses, the interface roughnesses for these two conditions were further categorized into three levels: "not so rough", "intermediate", or "rough." Figure 9-10 through Figure 9-15 presents the different levels of roughness for the as-placed and rake surface finishes.

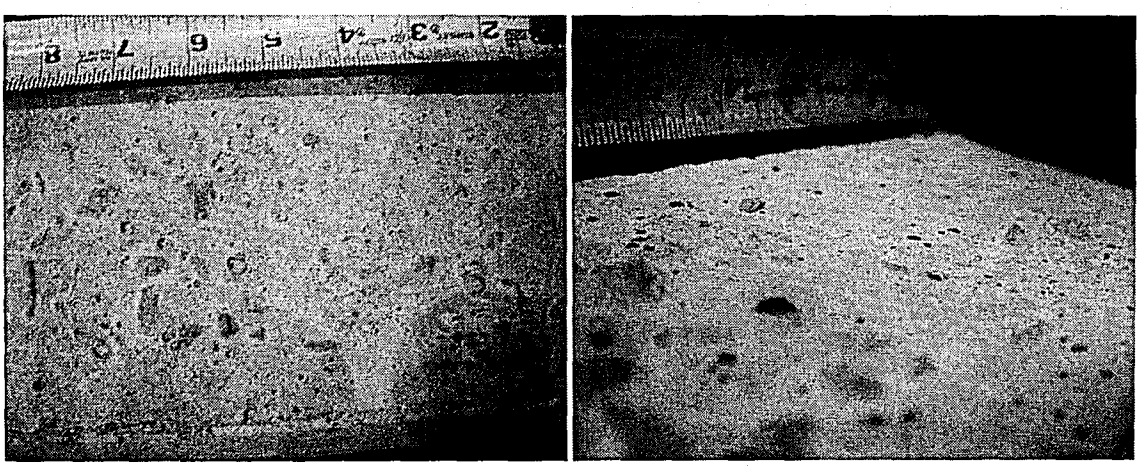

Figure 9-10: As-Placed Surface Finish – "Not So Rough" [Specimen 6A4]

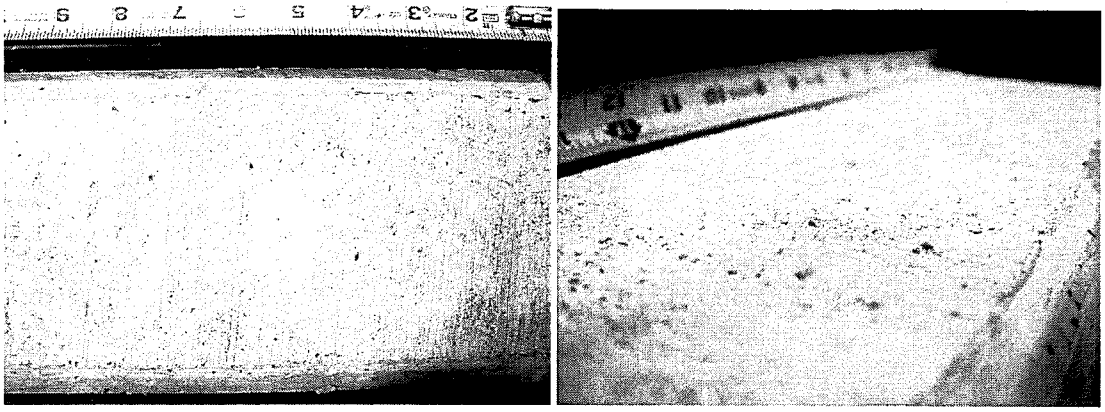

Figure 9-9: Broom Surface Finish [Specimen 6B6]

The as-placed and rake surface finishes exhibited substantial variation in the level of roughness. To appropriately compare the responses, the interface roughnesses for these two conditions were further categorized into three levels: "not so rough", "intermediate", or "rough." Figure 9-10 through Figure 9-15 presents the different levels of roughness for the as-placed and rake surface finishes.

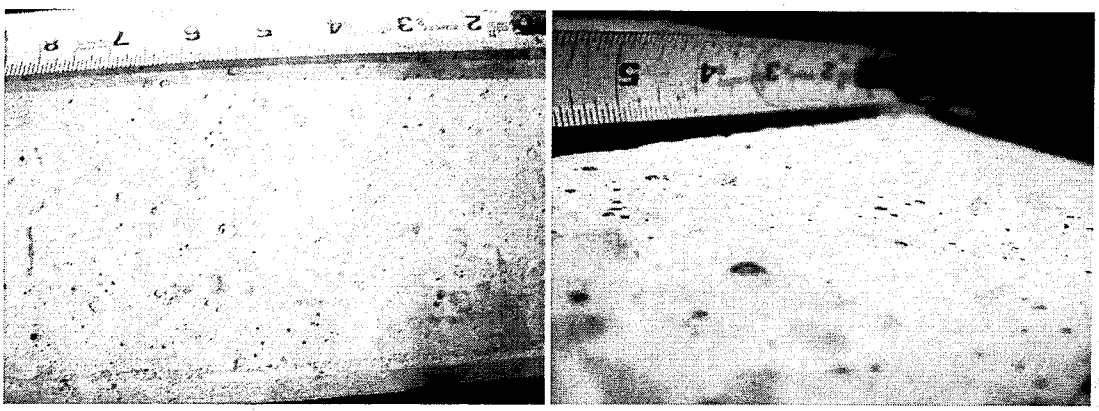

Figure 9-10: As-Placed Surface Finish – "Not So Rough" [Specimen 6A4]

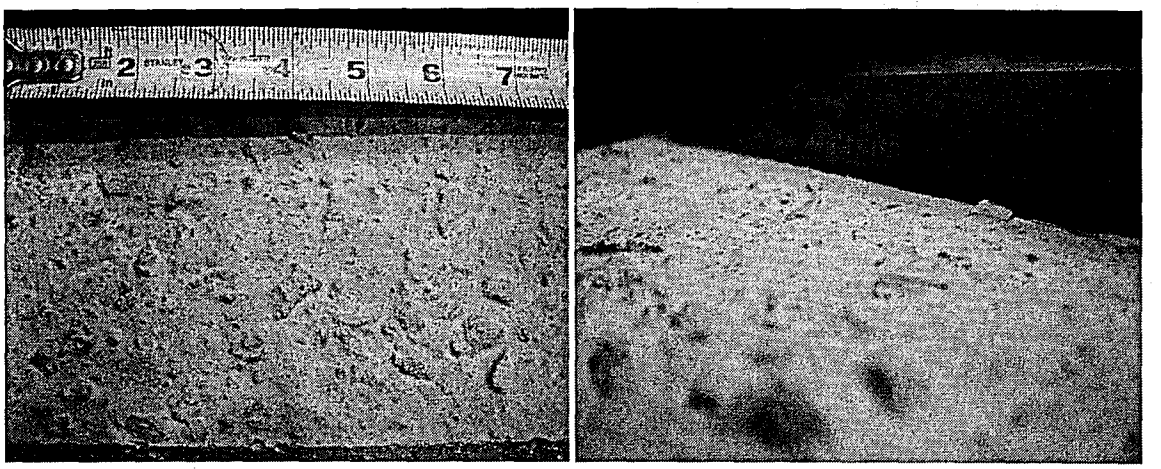

Figure 9-11: As-Placed Surface Finish – "Intermediate" [Specimen 6A5]

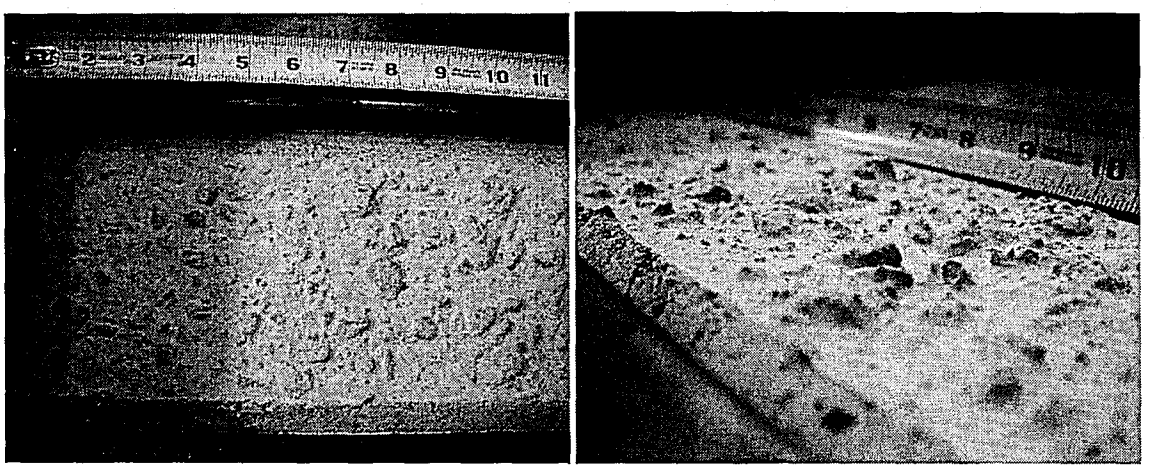

Figure 9-12: As-Placed Surface Finish – "Rough" [Specimen 6A7]

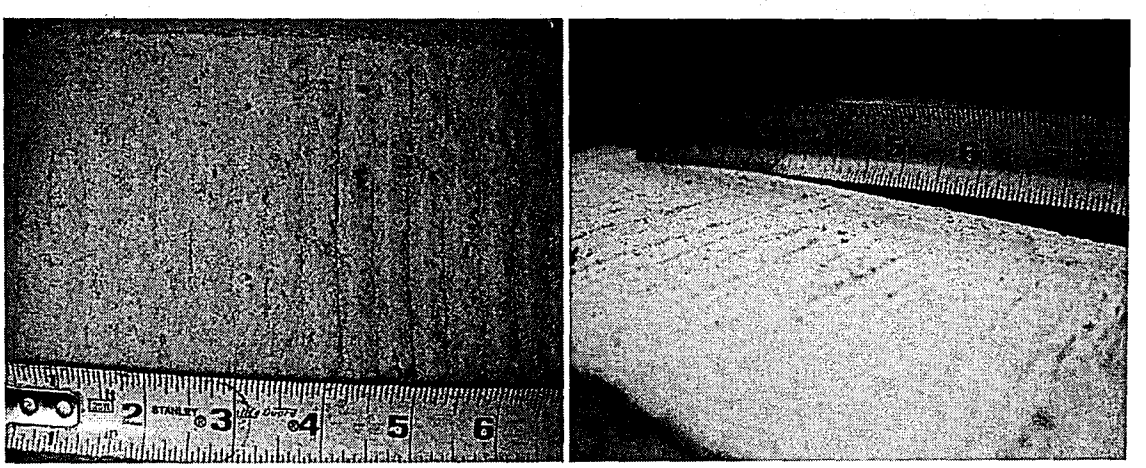

Figure 9-13: Rake Surface Finish – "Not So Rough" [Specimen 6R3]

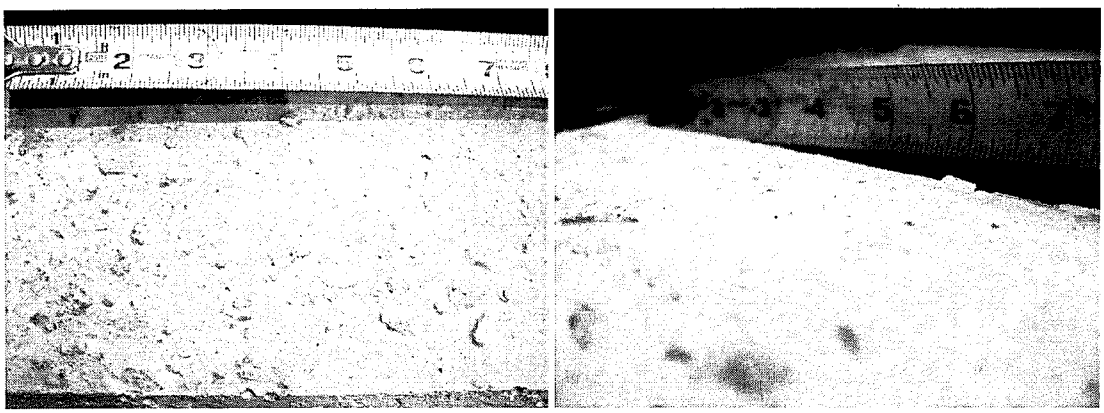

Figure 9-11: As-Placed Surface Finish – "Intermediate" [Specimen 6A5]

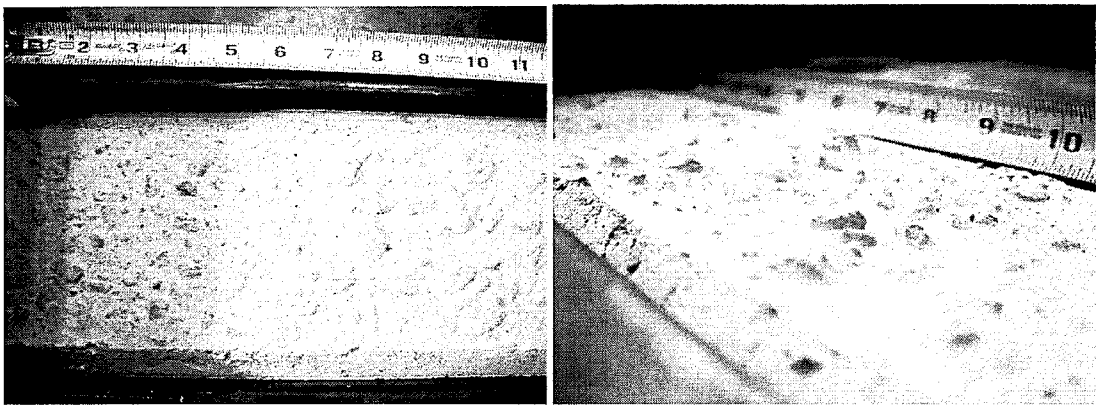

Figure 9-12: As-Placed Surface Finish – "Rough" [Specimen 6A7]

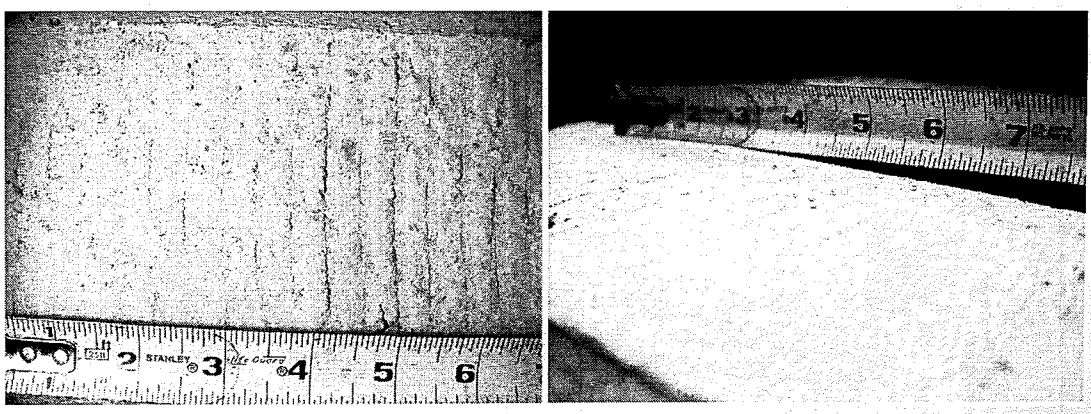

Figure 9-13: Rake Surface Finish – "Not So Rough" [Specimen 6R3]

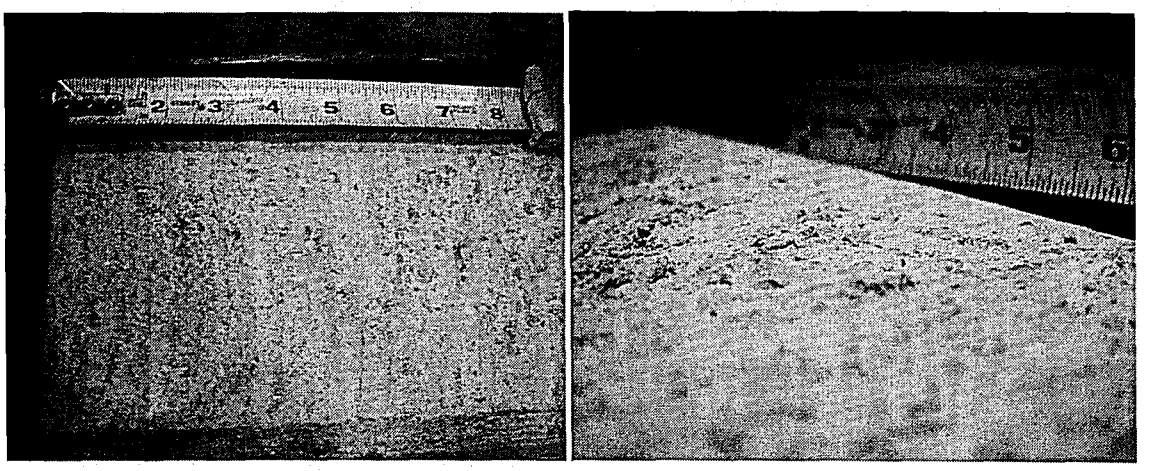

Figure 9-14: Rake Surface Finish – "Intermediate" [Specimen 6R6]

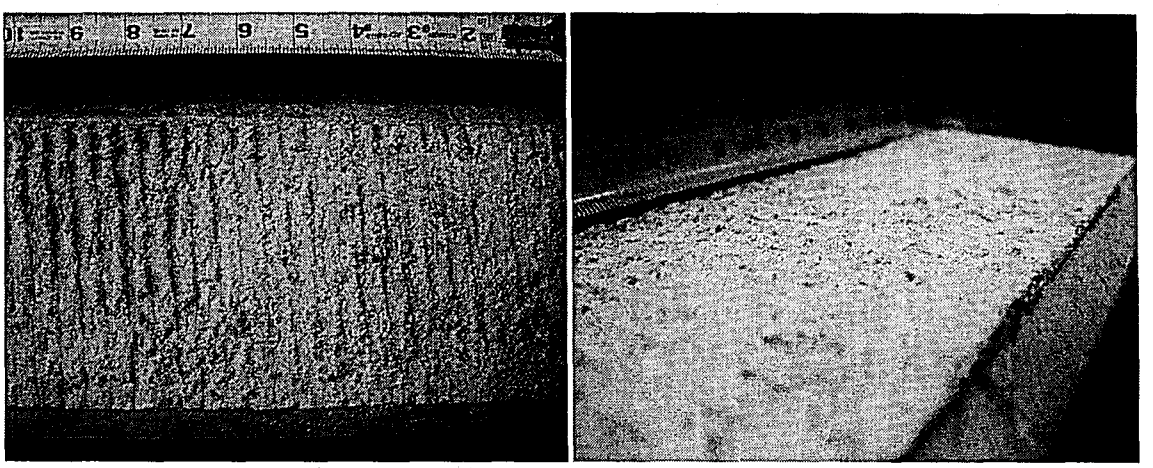

Figure 9-15: Rake Surface Finish – "Rough" [Specimen 6R7]

As seen in Figure 9-10 through Figure 9-12, the as-placed conditions varied from a roughness that is essentially smooth to one that is very rough. This variation is believed to be the result of the use of self consolidating concrete. Since the concrete mix is so fluid and no attempt is made to finish the surface, the resulting interface roughness will depend on how the aggregate settles once the concrete is placed. Some aggregate could protrude from the interface as was seen with the "rough" finishes or almost no aggregate could be present as was the case with the "not so rough" finishes. Patnaik (1999) experienced a similar problem when pouring his beams which were to have an as-placed surface finish. Because the mix he was using had a high slump, the proper finish with aggregate protruding could not be achieved. Thus, one should be cautious when

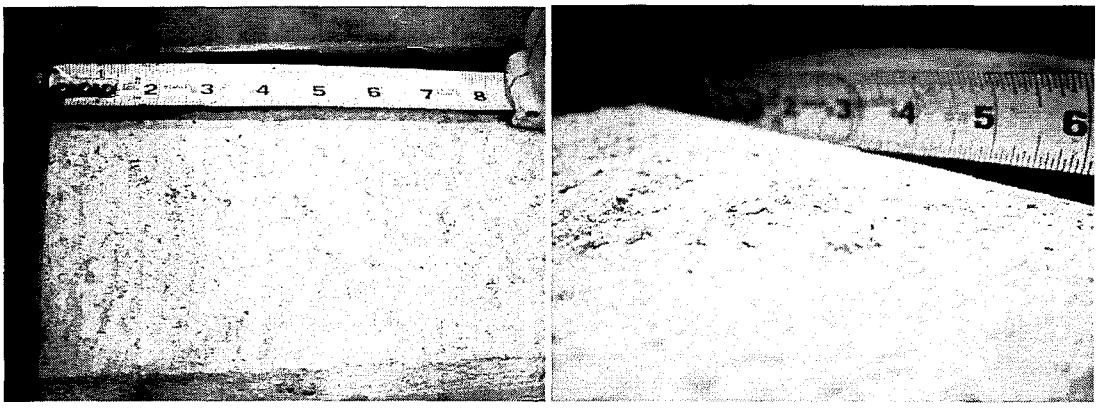

Figure 9-14: Rake Surface Finish – "Intermediate" [Specimen 6R6]

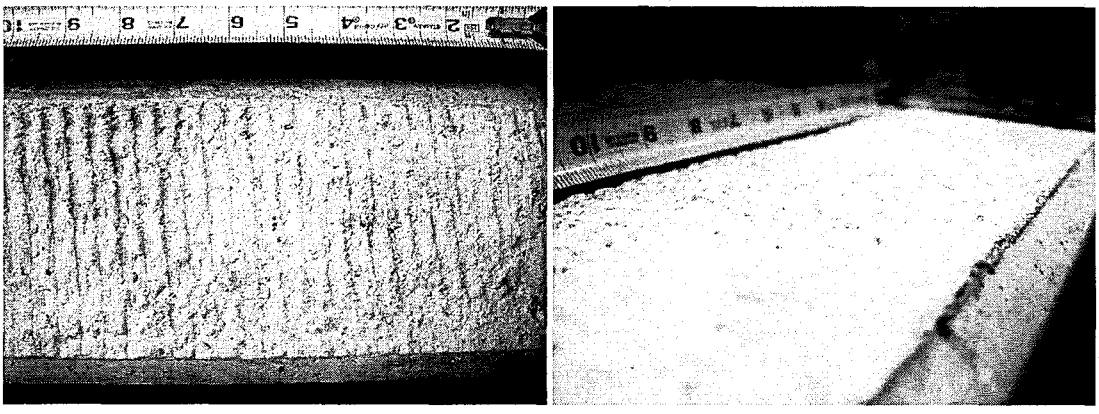

Figure 9-15: Rake Surface Finish – "Rough" [Specimen 6R7]

As seen in Figure 9-10 through Figure 9-12, the as-placed conditions varied from a roughness that is essentially smooth to one that is very rough. This variation is believed to be the result of the use of self consolidating concrete. Since the concrete mix is so fluid and no attempt is made to finish the surface, the resulting interface roughness will depend on how the aggregate settles once the concrete is placed. Some aggregate could protrude from the interface as was seen with the "rough" finishes or almost no aggregate could be present as was the case with the "not so rough" finishes. Patnaik (1999) experienced a similar problem when pouring his beams which were to have an as-placed surface finish. Because the mix he was using had a high slump, the proper finish with aggregate protruding could not be achieved. Thus, one should be cautious when

trying to obtain an as-placed surface finish when using SCC or a concrete mix with a high slump. The following guidelines were used in defining the surface categories for the as-placed surface finish:

- As-Placed "Rough" – Aggregate regularly protruding from the concrete surface an average height of 1/8 to 1/4 inch.
- As-Placed "Intermediate" – Aggregate protruding from about 75% of the concrete surface an average height of approximately 1/8 inch.
- As-Placed "Not So Rough" – Aggregate marginally protruding from about 50% or less of the concrete surface an average height of approximately 1/16 inch. The remaining surface where the aggregate is not protruding is essentially smooth.

The rake finishes did not achieve the typical ¼" amplitude rough finish which is required in the ACI (2008) and AASHTO (2007) specification. At most, the "rough" rake finishes were able to achieve a ⅛" amplitude. This failure to achieve the proper roughness most likely occurred because the finishers did not wait long enough for the concrete to set before applying the finish. This results in the roughness settling out which seems to have occurred with most of the web interfaces; some more drastically then others. It is difficult to quantify the roughness due to the inconsistency of the interface finish long the beam. Based on general observations and measurements, the following roughness amplitudes could be assigned to the different levels of the rake surface finish:

- Rake "Rough" – Indentations spaced at 1/4 inch running transverse to the span with an average height of 3/32 to 5/32 inch between peak and trough.
- Rake "Intermediate" – Indentations spaced at 1/4 inch running transverse to the span with an average height of 1/16 to 3/32 inch between peak and trough.

- Rake "Not So Rough" – Indentations spaced at 1/4 inch running transverse to the span with an average height of 1/32 to 1/16 inch between peak and trough.

For some of the as-placed and rake beams, the surface roughness varied between each end. This resulted in one end of the beam with a rough finish remaining composite while the other end with a not as rough finish failing at a lower load. This end to end variation of roughness was more prevalent with the as-placed specimens than the rake specimens. Table 9-1 presents all of the as-placed and rake specimens and their corresponding interface roughness on both sides of the beam.

Table 9-1: Interface Roughness of the As-Placed and Rake Specimens

Surface Finish	Specimen ID	Beam Side	Roughness
As-Placed	3A1	East	Intermediate
		West	Not So Rough
	3A2	East	Rough
		West	Rough
	6A3	East	Not So Rough
		West	Not So Rough
	6A4	East	Not So Rough
		West	Intermediate
	6A5	East	Intermediate
		West	Not So Rough
	6A6	East	Rough
		West	Not So Rough
	6A7	East	Intermediate
		West	Rough
	6A8	East	Intermediate
		West	Rough
Rake	3R1	East	Rough
		West	Not So Rough
	3R2	East	Not So Rough
		West	Intermediate
	6R3	East	Not So Rough
		West	Intermediate
	6R4	East	Rough
		West	Rough
	6R5	East	Not So Rough
		West	Not So Rough
	6R6	East	Intermediate
		West	Intermediate
	6R7	East	Rough
		West	Rough
	6R8	East	Intermediate
		West	Intermediate

9.5 Expanding the Quantity of Data

As previously discussed, the surface roughness varied from one end of the beam to the other. Since the specimens were designed to achieve a horizontal shear failure prior to a flexural failure, one end of the beam often failed before the other end while the section remained free of flexural cracking. The specimens were loaded until both ends exhibited an interface failure or until the beam reached its ultimate capacity. To thoroughly study the horizontal shear failure response, both ends of the beams were examined individually using the slip data, surface roughness, and horizontal shear stress. The data was not used if failure of one end of the beam contributed to the failure at the other end. An E or W is added to the specimen ID when referencing the east or west end of the beam, respectively (e.g. 3R1E and 3R1W).

The rationale behind dividing the test specimens into two sides was considered valid for a few reasons. The loading of the beam is symmetrical about the specimen's midspan meaning that both ends of the beam will experience the same forces, rotation, and deflection. Also, due to the extra clamping force at the loaded area, the middle interface of the composite specimen is able to remain intact for loads and horizontal shear stresses greater then the interface near at the ends of the beam. Therefore, one end of the specimen could fail in horizontal shear while the center and the other end still remain intact. Because the middle interface is still acting compositely, the stiffness of the composite end will not drastically change and will continue to take on load until it fails. Thus, the horizontal shear forces on either end of the specimen would be independent of each other. However, once the interface is lost through the load point on one end of the beam and the middle interface is no longer composite, the rest of the data on the other end of the beam cannot be used since the specimen is no longer symmetric. At this point, the stiffness and forces of the composite end of the beam will be significantly different then when the middle was composite.

9.6 Correcting the Load-Deflection Curves

As mentioned previously in Section 9.3, the load-deflection curves displayed a lack of stiffness (Figure 9-6). This behavior was suspicious since some of the beams should have been acting compositely based upon the slip and strain gauge data. Upon investigating the test setup, it was found that support pads were placed between the bottom web of the beam and the top clamping plate that the beam was bearing on as a support (Figure 9-16). These pads did exhibit some compressible properties and thus could affect the recorded stiffness of the composite beam.

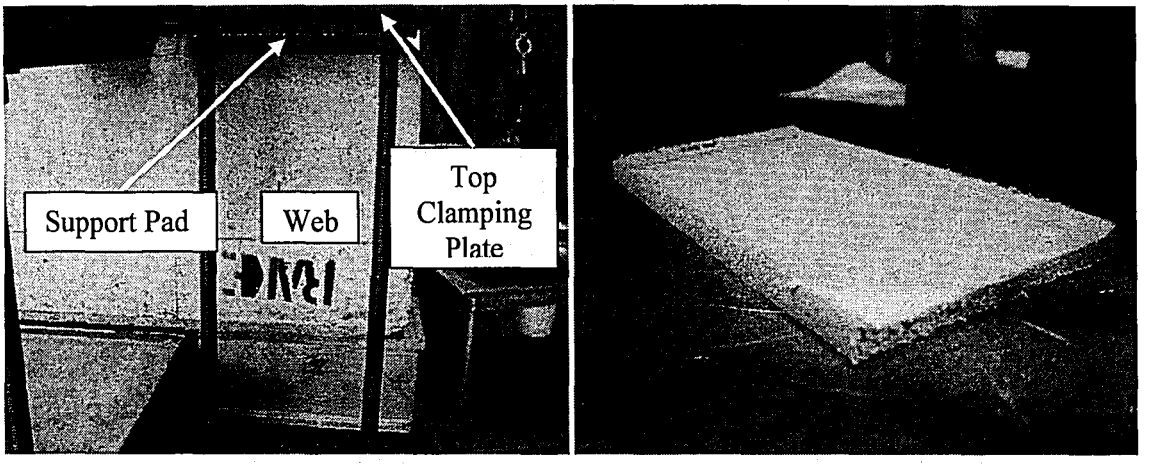

Figure 9-16: Support Pad

In order to determine the affect the support pads had on the deflection data, compression tests were run on the pads using the SATEC 600 kip universal testing machine. The compression tests were run on the actual pads that were used for the specimen tests. Two pieces of steel plate were cut to the proper dimensions to simulate the beam bearing down on the top clamping plate. The support pad was placed between the two pieces of steel and linearly loaded at a rate of 5 kips/min up to a load of 50 kips (Figure 9-17). This test was performed for both the east and west support pads.

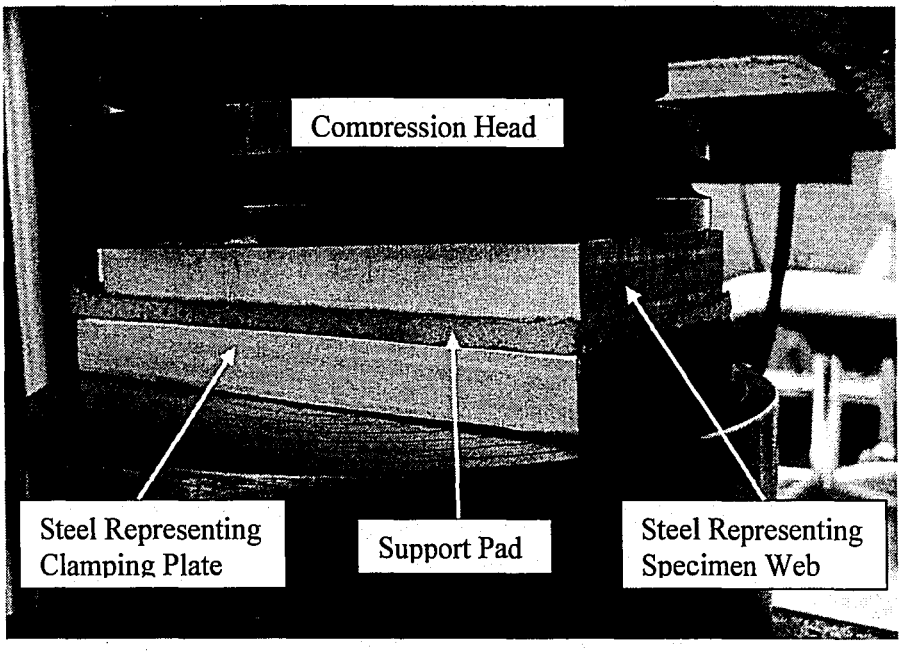

Figure 9-17: Support Pad Test Setup

The compression tests were run several times to obtain the average east and west pad load versus displacement curves. Figure 9-18 shows the results of the east and west compression tests. It can be observed that the pad exhibits an initial flexible response followed by a stiff behavior. This correlates with the expected behavior. At low loads, the pad fibers compress easily. Once they are adequately compressed, at a displacement of approximately 0.1 inch, the pad is solid and displays a stiff behavior. The load-deformation of the pad exhibits the same characteristics of the load-deflection for the composite concrete specimen tests shown in Figure 9-6. The average of the load-displacement slopes for the east and west support pad tests was determined in order to approximate the displacement of the pads. Since each support pad only takes half of the total load applied to the concrete beam, the load of the average load-displacement curve was doubled in order to determine the total contribution of the support pads to the recorded deflection of the beam.

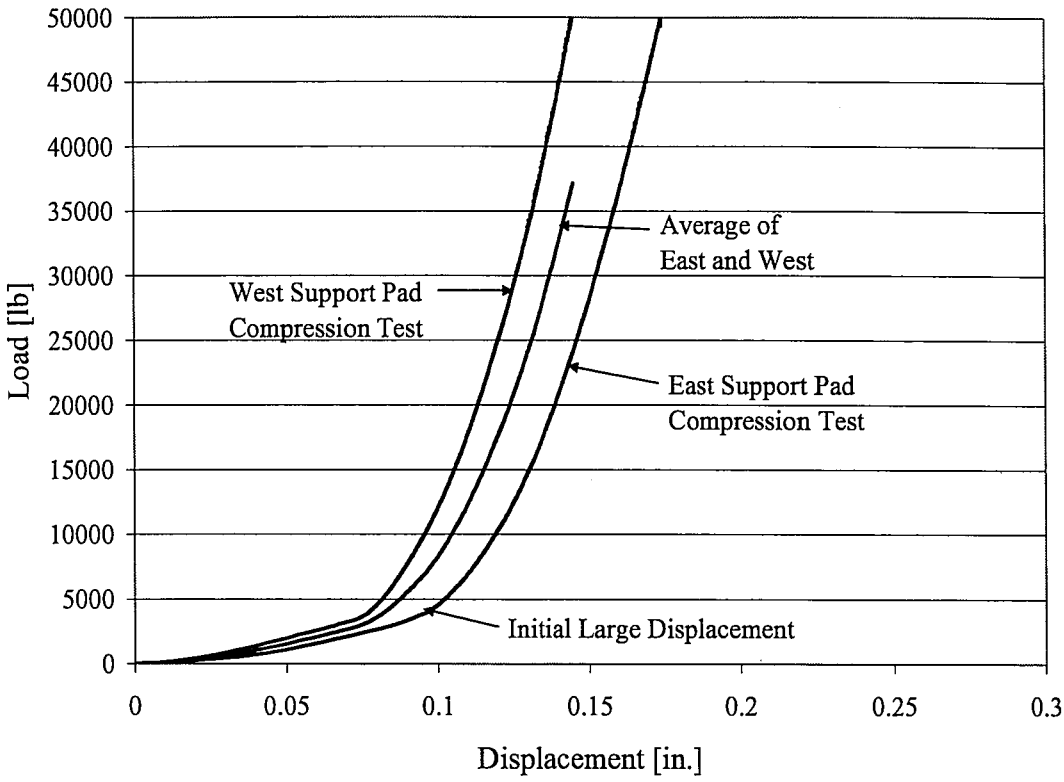

Figure 9-18: Support Pad Compression Test Results

The level of the initial large deflection varied for the tests of the concrete beams. This is most likely due to the amount the top clamping plate was initially tightened against the support pad and beam before the test. The tightening of the clamping plate would create some initial depression of the support pad thus creating a varying level of initial deflection when the test is finally started. After the initial large deflection, the behavior of the load-deflection curve was similar for all the composite beam tests. It was determined that the initial large deflection caused by the support pads could not be efficiently subtracted off the beam test data using the support pad compression test data. Therefore, the displacement of the average curve for the support pad tests was zeroed at 10 kips to eliminate the initial large displacement of these tests. The resulting support pad displacement was plotted versus the load in order to determine the equation relating the two variables (Figure 9-19).

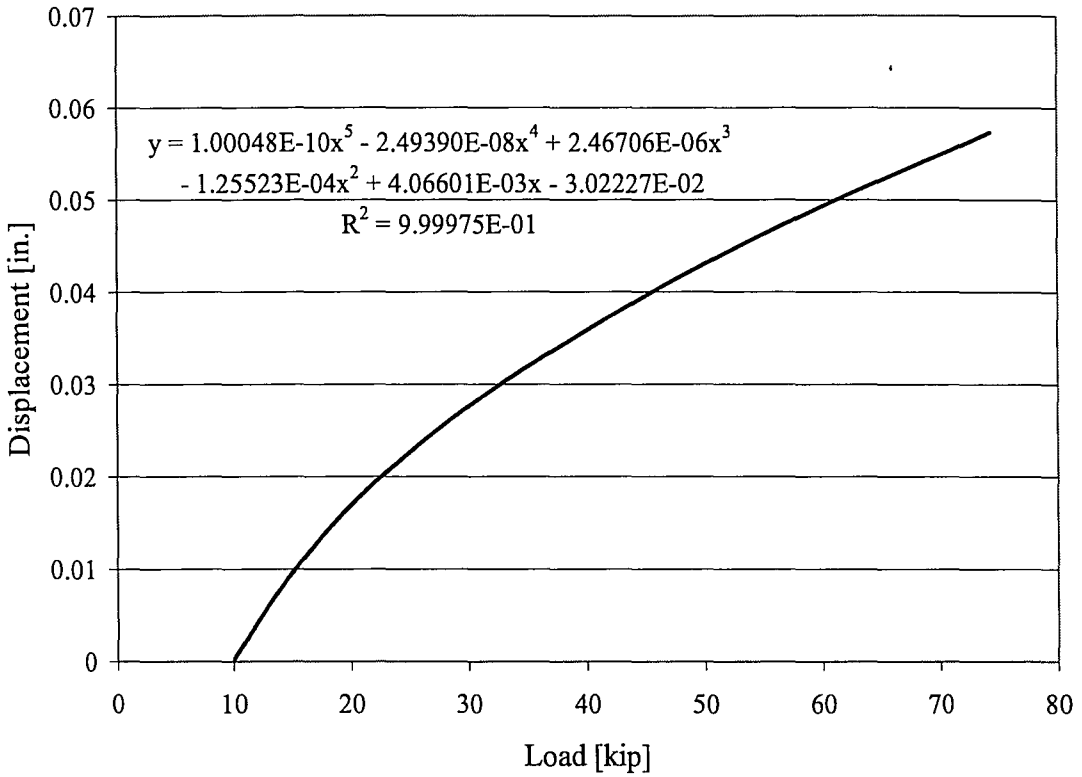

Figure 9-19: Displacement versus Load for the Average Compression Test Results

The equation of the displacement in terms of load was then used to subtract the effect of the support pad from the deflection of the beam above 10 kips. The slope of the revised load-deflection curve was determined and used to project the curve back from 10 kips to the x-axis. The resulting completed load-deflection curve was then shifted back to the origin of the x-axis. This process, shown in Figure 9-20, eliminated the initial large deflection and subtracted off the deflection contribution of the support pads. This correction was performed for each of the beam tests.

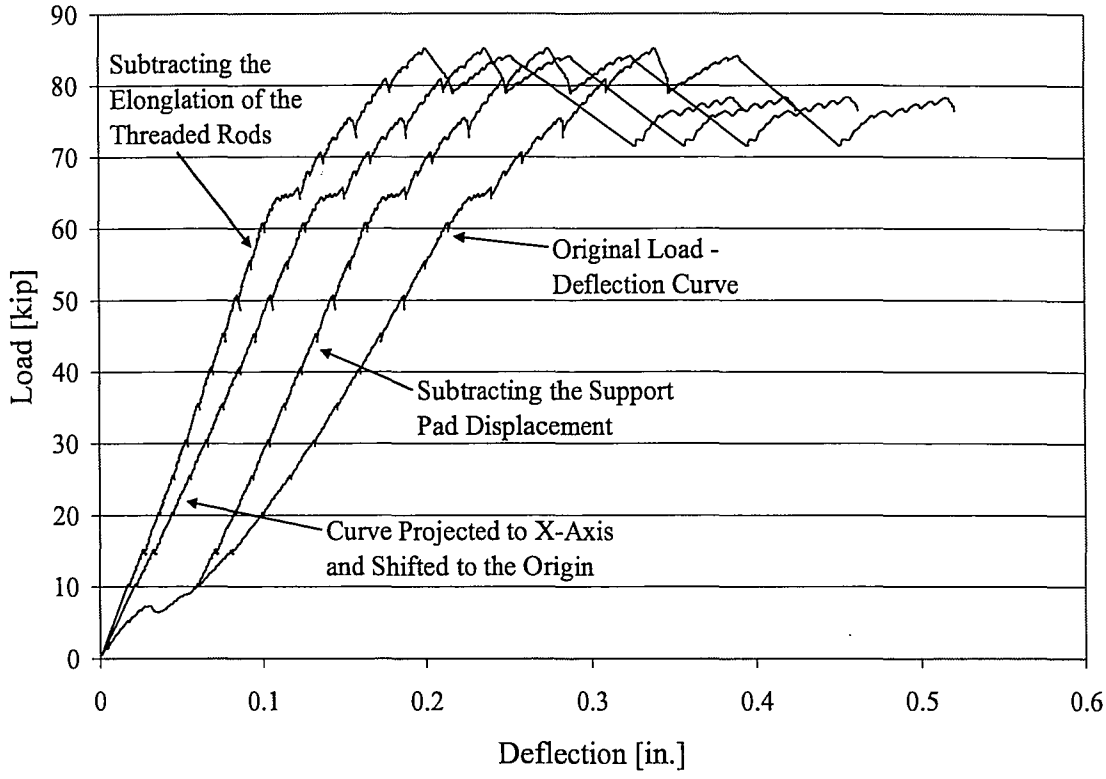

Figure 9-20: Process of Correcting the Load-Deflection Curve [Specimen 6R7]

Also taken into account was the elongation of the threaded rods that held the two clamping plates together. It was found that as the load increased the contribution from the elongation became relatively significant. The elongation was found using Equation 32 and resulting final load-deflection curve is shown in Figure 9-20.

$$\delta_{thr} = \frac{P_{thr} \cdot L_{thr}}{A_{thr} \cdot E_{thr}} \qquad \text{(Eq. 32)}$$

where,

δ_{thr} = change in length of the threaded rod [in.]

P_{thr} = load applied to one threaded rod [kip]

L_{thr} = original length of the threaded rod [in.]

A_{thr} = area of the threaded rod [in^2]

E_{thr} = modulus of elasticity of the threaded rod = 29,000 ksi

Figure 9-21 shows the final load-deflection curve plotted with the original curve and the bounds for the different levels of composite action of the interface. It can be seen that by subtracting off the effects of the support pads and threaded rods, the stiffness of the plot is very close to that of the fully composite beam. The remaining error may be attributed to other sources of deformation in the test setup.

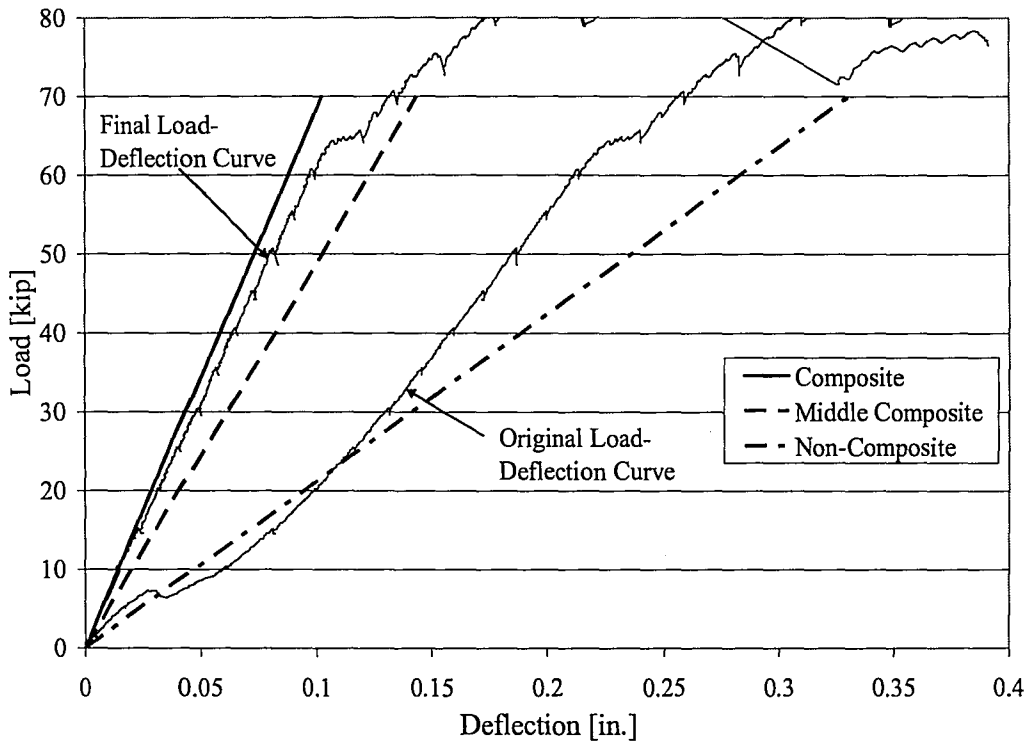

Figure 9-21: Final Corrected Load-Deflection Curve [Specimen 6R7]

Once all of the data was corrected, the final curves were plotted together for all of the test specimens. The trend in the stiffness of the plots seemed to correspond fairly well with the slip and strain data of the test specimens though none of the beams actually followed the full composite line show in Figure 9-21. Even the beams which were fully composite such as specimen 6R7 fell a bit short of the line. However, the difference in the deflections of the

calculated full composite line and the fully composite test specimens was only off by 0.005 inches or less at a load of 60 kips. This translates to a slope or stiffness of 682.7 kip/in. for the calculated composite beam compared to a stiffness of approximately 650 kip/in. for the composite test specimens. Also, there could be some other small effect from the test setup that was not realized that would create this discrepancy. Therefore, it was determined to average the stiffness of a few full composite test specimens and take this value as the stiffness of the full composite beam. The load-deflection curves of the other test specimens could then be compared to the experimentally derived composite curve to aid in quantifying their level of composite action. The slopes and corresponding calculated values of percent composite are tabulated in Table 9-2.

Table 9-2: Slope of Load-Deflection Line and Corresponding Percent Composite

Surface Finish	Specimen ID	Slope of Load-Deflection [kip/in]	Calculated Percent Composite	Average Percent Composite
Broom	3B1	482.7	53.5	67.0
	3B2	369.7	22.0	
	6B3	528.0	66.1	
	6B4	561.2	75.4	
	6B5	539.3	69.3	
	6B6	495.6	57.1	
As-Placed	3A1	460.6	47.3	75.1
	3A2	588.8	83.0	
	6A3	539.0	69.2	
	6A4	588.3	82.9	
	6A5	593.6	84.4	
	6A6	623.8	92.8	
	6A7	546.0	71.1	
	6A8	541.8	69.9	
Rake	3R1	642.1	97.9	88.7
	3R2	509.2	60.9	
	6R3	559.4	74.9	
	6R4	646.7	99.2	
	6R5	503.3	59.2	
	6R6	646.4	99.1	
	6R7	655.9	101.7	
	6R8	610.9	89.2	

For the values of the percent composite presented in Table 9-2, full composite is taken as 100% while composite in the middle and non-composite on the ends taken as 54.5%. The average percent composite for the broom specimens does not include beams 3B1 and 3B2 and the average percent composite for the rake specimens does not include beam 3R2. 3B1 and 3R2 were not included because the interface on one end of the beam was non-composite through the middle interface of the beam. 3B2 was excluded since the data used to determine the slope of the load-deflection curve is questionable for this beam.

It is clear from the stiffness results that there is an obvious trend between roughness and composite action. The specimens with a broom finish, which is the smoothest of the surface finishes, exhibited an average of 67% composite action. The as-placed finish, which represents a rougher condition but one less consistent than the rake, resulted in a 75% composite response. The rake finish, which is the roughest surface preparation, produced the highest average level of composite action at 89%. These results demonstrate that greater composite action is achieved with an increase in the roughness of the surface finish. Comparison of the load-deflection variation for the 3 ksi and 6 ksi topping slab specimens is inconclusive.

9.7 Behavior of Test Specimens

9.7.1 General

The testing procedure and observed events were very similar for all the specimens studied. However, the results indicated that the specimens were behaving differently from one another during the test. There was a wide range of behaviors for the test specimens, but for simplicity the more general behaviors will be summarized in the following sections. The specimen behavior is discussed relative to the level of composite behavior observed from the slip gauges.

9.7.2 Fully Composite Specimen Behavior

A few of the specimens experienced full composite action on both ends of the beam during the test procedure. Many other specimens displayed full composite behavior on only one end of the beam while the other end was partially composite. However, this different level of composite action on the other end of the beam did not influence the behavior of the composite side. The specimens that exhibited composite action had an as-placed or rake interface finish with a level of roughness ranging from "intermediate" to "rough". In the following paragraphs, the behavior of the composite specimens will be described in general; however, the data from specimen 6R7 will be used as a visual reference.

As the beam was loaded, the composite interface of the specimen experienced virtually zero slip. The small movement observed was within the resolution of the slip gauges. Once the load reached a certain point, the outer interface between the loading point and the end of the beam failed in horizontal shear. This resulted in the deflection of the specimen increasing and therefore the slope of the load deflection curve also increasing (Figure 9-22). At this point, the slip gauges located at the outer edges of the slab (SL1 on the west end and SL4 on the east end) recorded a jump in slip (Figure 9-23). The slip gauges located in the middle of the slab (SL2 on the middle-west and SL3 on the middle-east) did not experience any slip and therefore indicated the interface in the middle of the beam was still composite. The strain data on the outer part of the slab showed a rapid increase in strain which also indicated that the outer interface failed in horizontal shear (Figure 9-24). However, the strain data on the slab near the middle of the beam did not react in any way thus reinforcing the indication that the middle interface still remained intact (Figure 9-25).

As the loading continued, the slope of the load-deflection line and the slip of slip gauges on the outer edges of the slab continued to increase. Approximately 5 to 20 kips after the outer interface

failed, the bottom of the slab over the loaded area began to crack in flexure thus further signifying the non-composite behavior of the outer section of the specimen. Shortly following the slab cracking, flexural cracks were observed on the bottom of the web under the loaded area.

About 5 to 10 kips after the initiation of the web and slab flexural cracks, the middle interface between the loads suddenly failed through one of the loading areas. The whole slab shifted to the side in which the interface under the load failed. The interface under the load on the other side of the beam remained intact and the corresponding outer interface slip did not change. This behavior can be seen in Figure 9-23. The middle interface failed through the west loading area thus resulting in SL1, SL2, and SL3 experiencing a large jump in slip while SL4 remains unaffected. The shifting of the slab to the west can be seen by the jump in slip increasing as the gauge readings move further west (from SL3 to SL2 to SL1). Also observed at this point of the test was the strain data on the slab near the middle of the beam experienced a jump in strain thus signifying the failure of the section interface (Figure 9-25). The deflection of the beam also jumped when the middle interface failed because the two sections were now acting as separate members which will greatly reduce the stiffness of the beam (Figure 9-22).

This second failure of the composite interface occurs partly because the clamping force caused by the applied load is holding the interface together at that point and therefore is aiding in the horizontal shear capacity for the center interface. This contribution is seen in the AASHTO capacity equation (Eq. 9) as μP_c. Additionally, between the two point loads the horizontal shear value is theoretically zero. Thus, a much higher shear force is needed to fail the middle interface. Once the forces become too great due to the rotation of the web and slab, the weaker interface under the load will fail. Because the forces are relieved by this failure, the interface under the other loaded area will never experience a large jump in slip and neither will the corresponding outer interface.

If the load was continued after the failure of the middle interface, the bottom of the web along the beam length would start to experience significant flexural cracking. Once the load reached a high enough level, flexural-shear cracks would occur near the support. For specimen 6R7, the flexural-shear crack occurred before the middle interface failed as indicated in Figure 9-22 and Figure 9-23. However, this was the only composite specimen in which this took place. For the rest of the beams, the flexural-shear cracking occurred after the middle interface failed.

At this point in the test, the loading of the specimen ceased. If the specimen was loaded any further, the web would most likely fail violently from the opening of a flexural or flexural-shear crack. Figure 9-26 and Figure 9-27 show pictures of the failed outer interface and cracking of the web and slab at the end of the test, respectively.

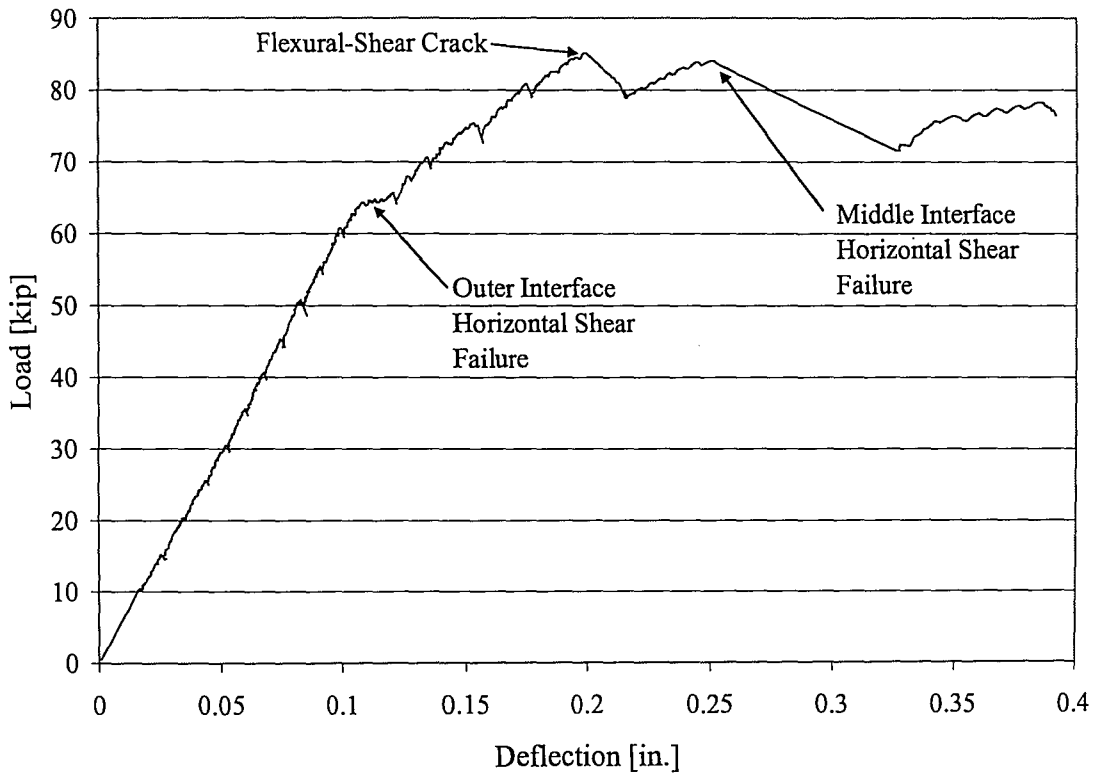

Figure 9-22: Load versus Deflection for a Composite Specimen [6R7]

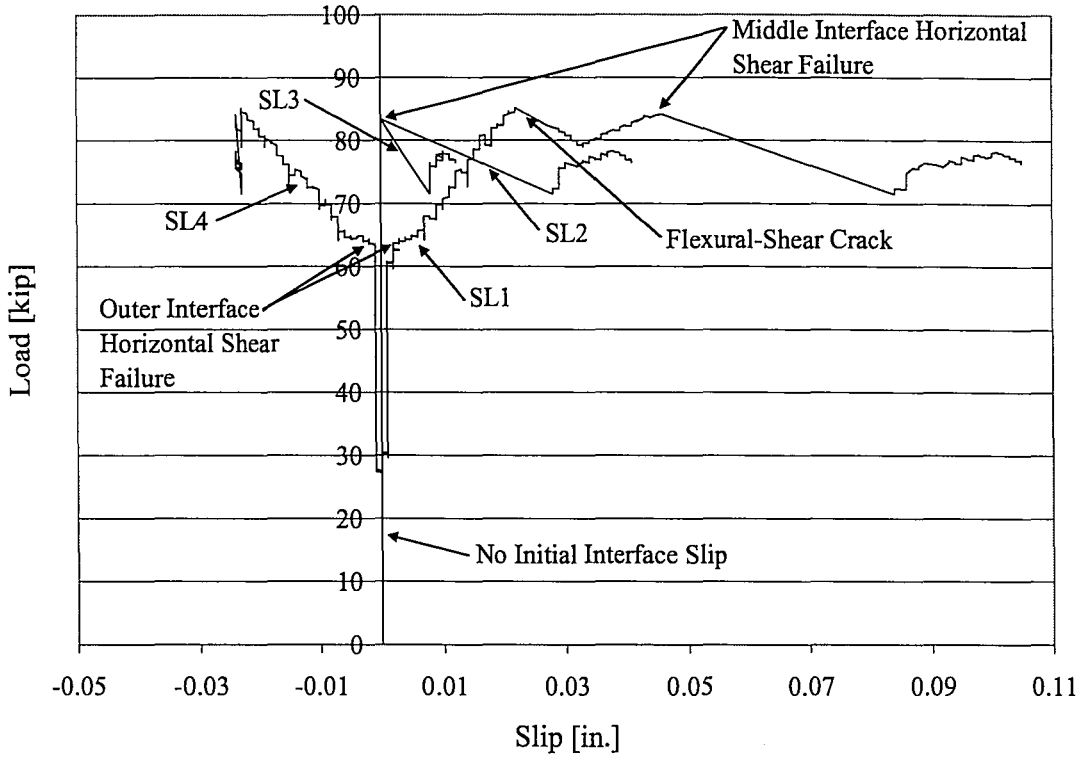

Figure 9-23: Load versus Slip for a Composite Specimen [6R7]

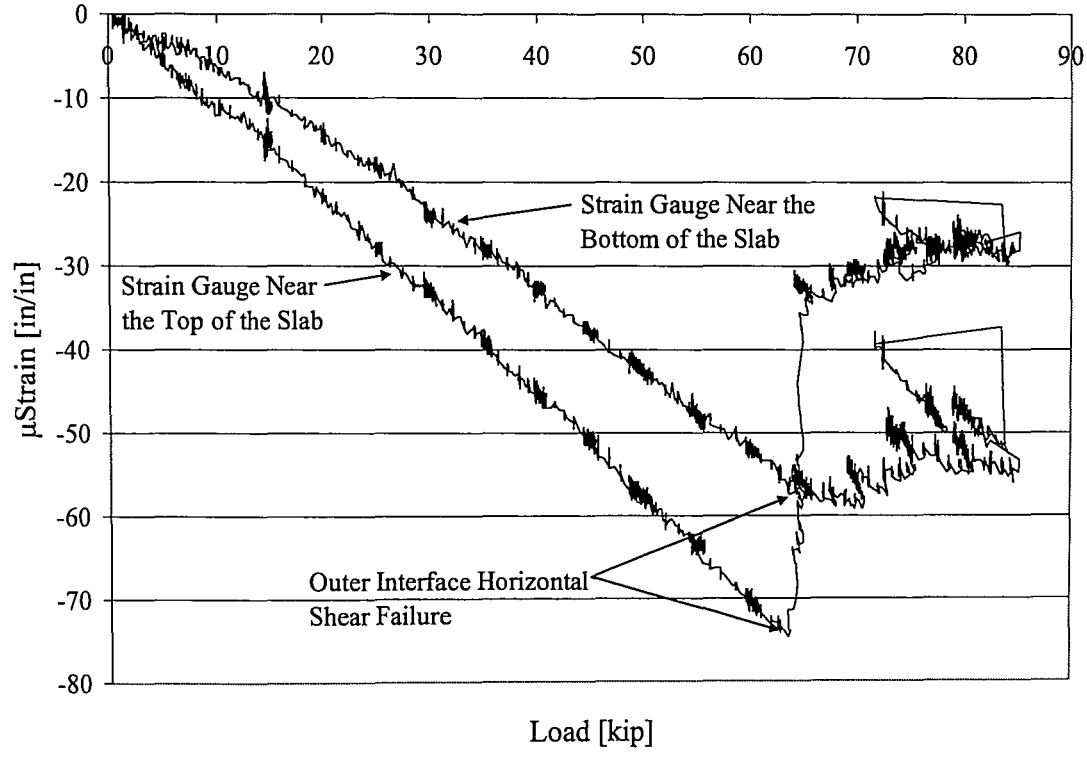

Figure 9-24: Strain Data for the Outer Slab Concrete of a Composite Specimen [6R7]

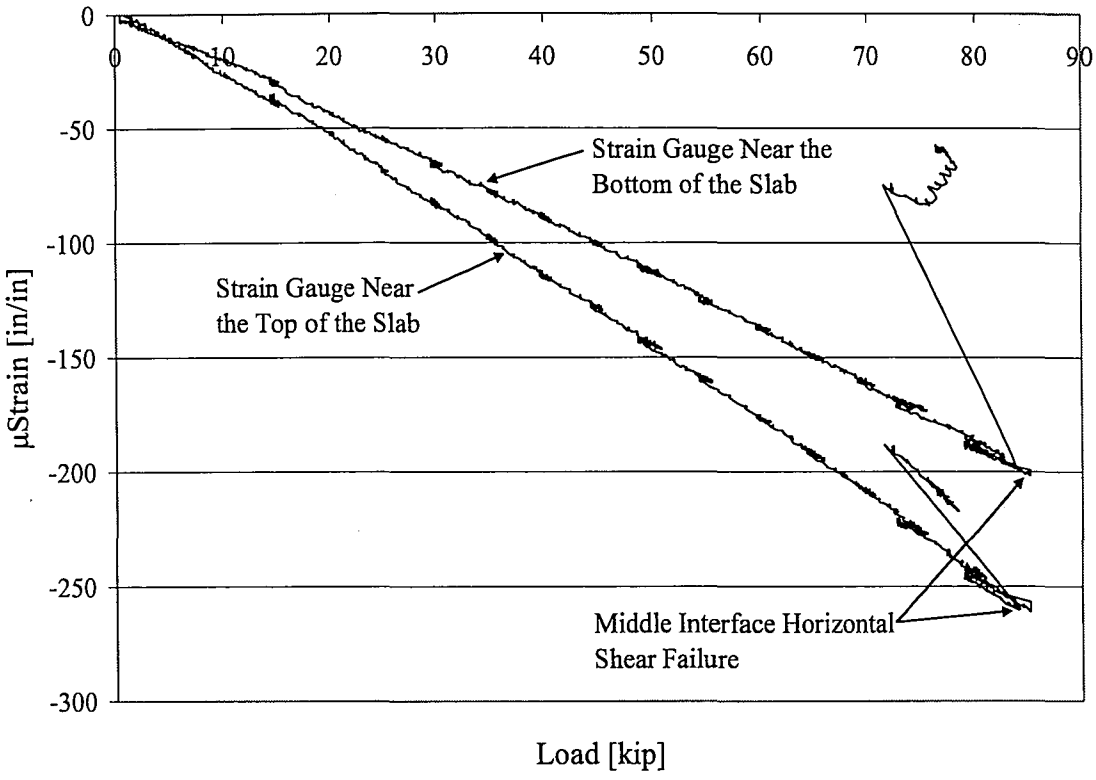

Figure 9-25: Strain Data for the Middle Slab Concrete of a Composite Specimen [6R7]

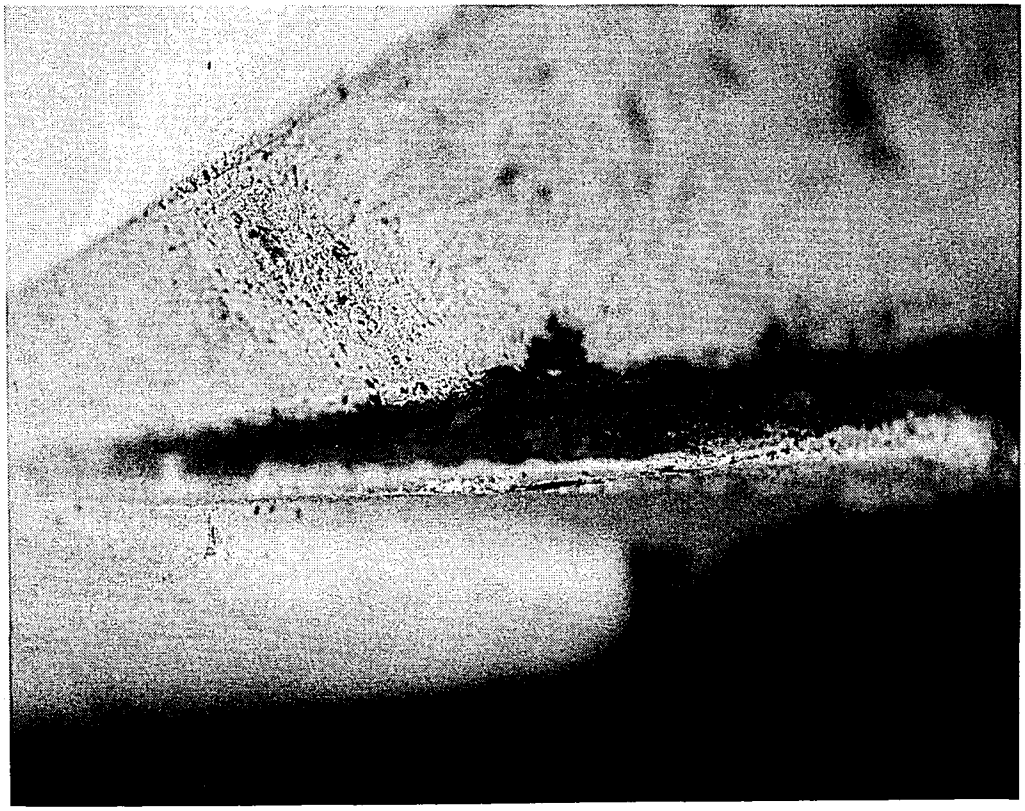

Figure 9-26: Failure of the Composite Interface

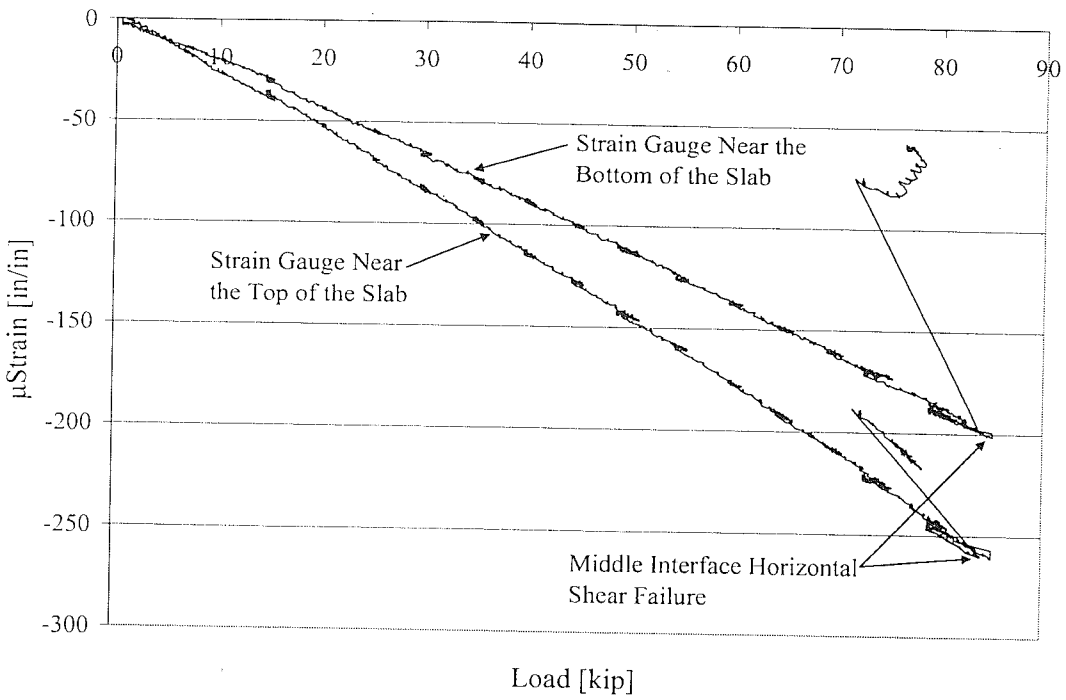

Figure 9-25: Strain Data for the Middle Slab Concrete of a Composite Specimen [6R7]

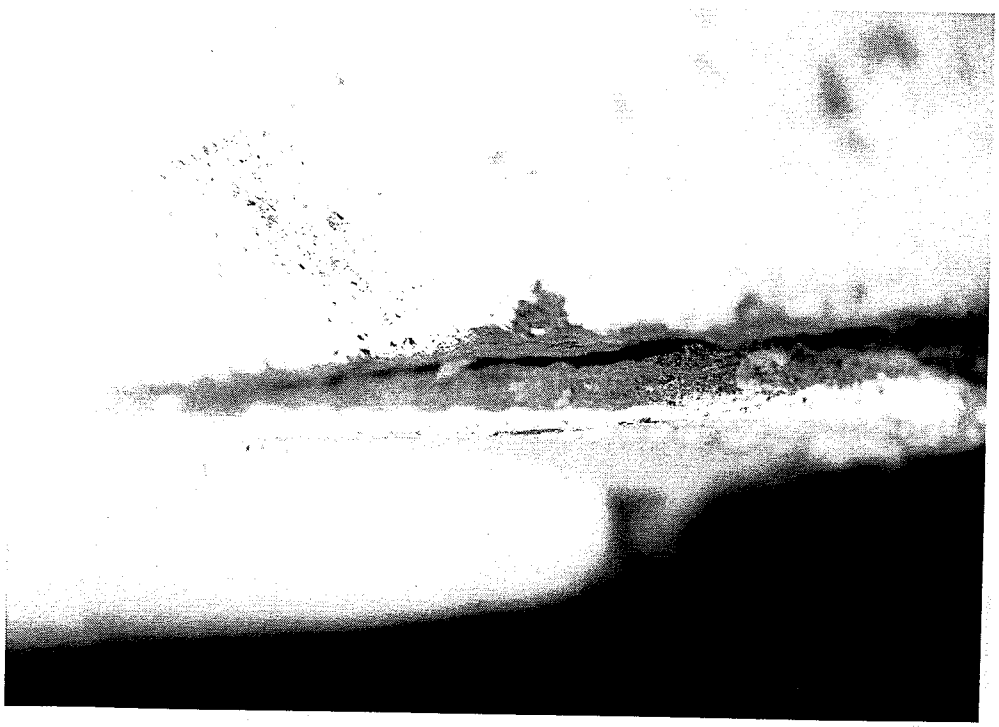

Figure 9-26: Failure of the Composite Interface

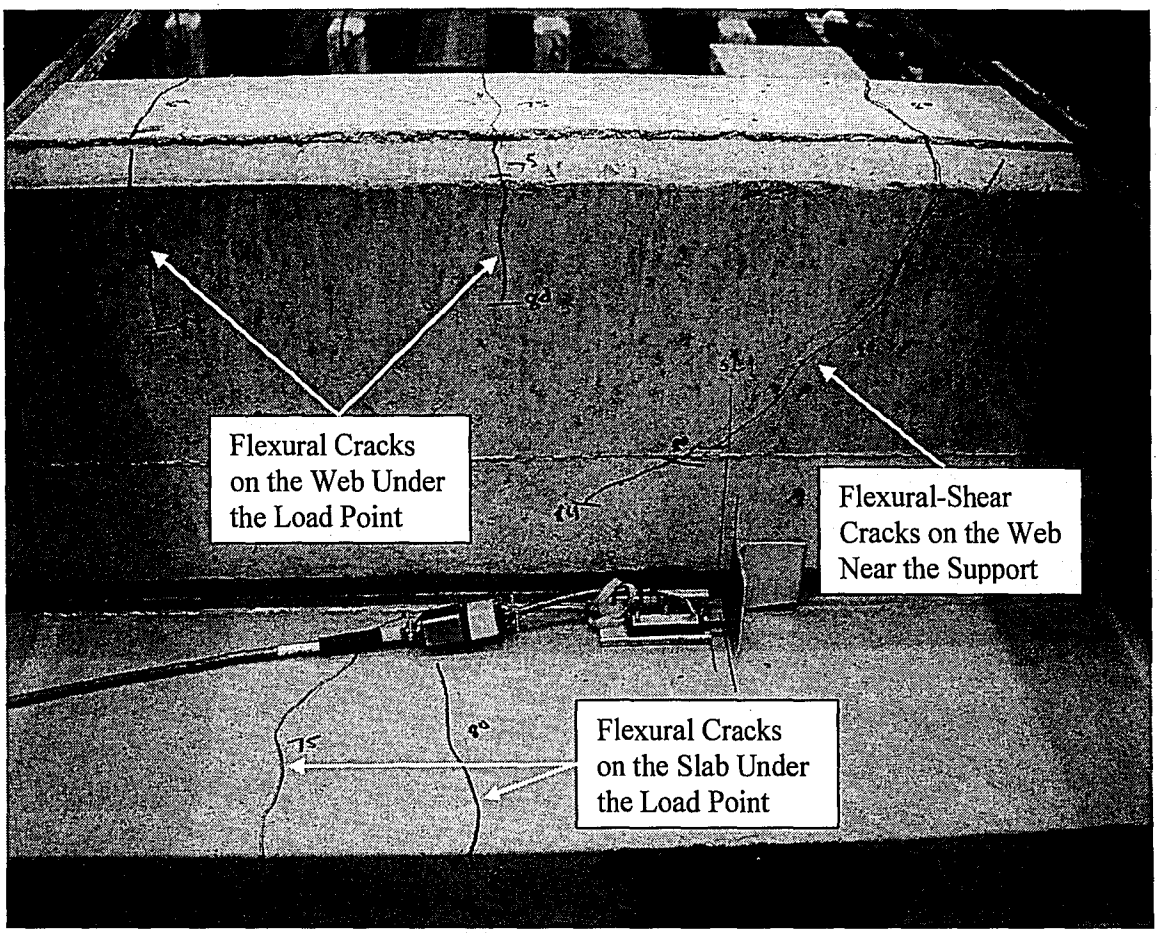

Figure 9-27: Cracks on West End of Specimen at Failure [Specimen 6R7]

9.7.3 Between Composite and Middle-Composite Specimen Behavior

The specimen in this category had a recorded load-slip response between that of the fully composite (essentially zero slip) and middle composite lines (Figure 9-2 and Figure 9-4). This type of behavior was generally exhibited by specimen which had an as-placed or rake interface finish with a level of roughness ranging from "intermediate" to "not so rough". The behavior of these specimens will be described in general using the data from specimen 6R8 as a visual reference. It should be noted that the east side of 6R8 has a slip between composite and middle composite while the west side is behaving compositely based on the slip and strain data. Thus, when mentioning the slip in Figure 9-29, the reference is to slip gauge SL4 which is on the east side of the beam. Also, the strain data in Figure 9-30 is for the east side of the slab.

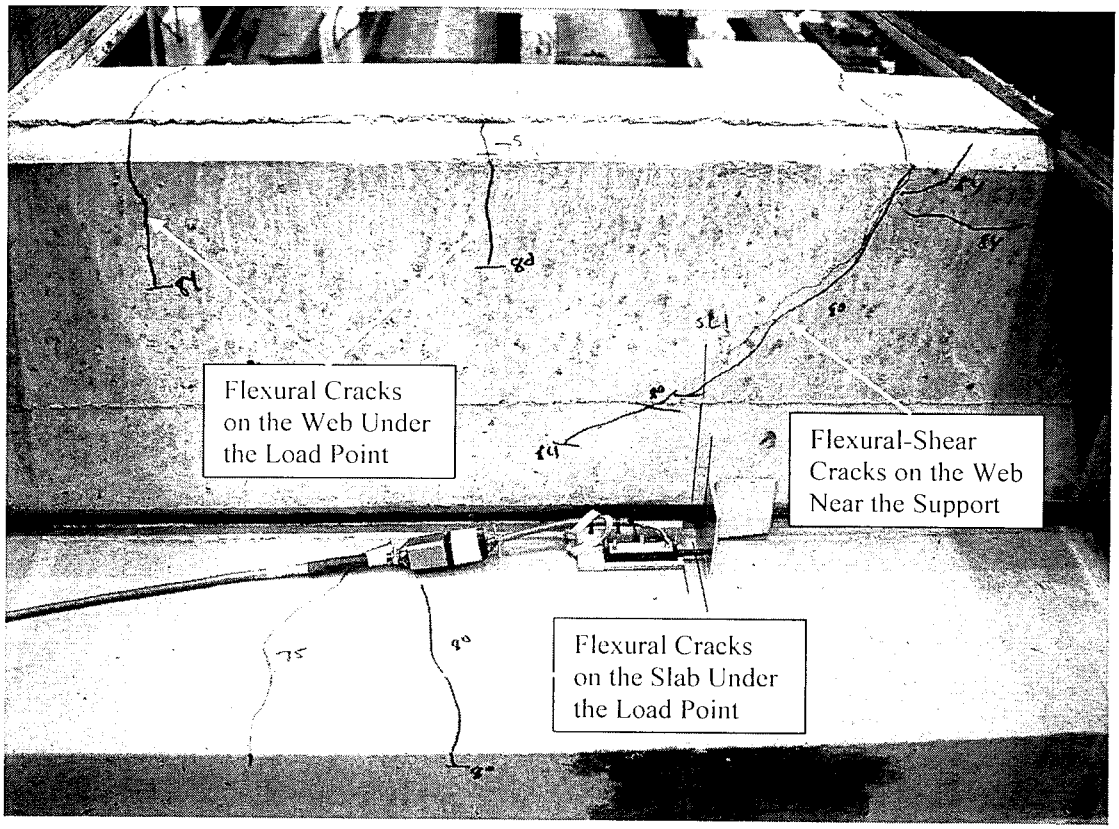

Figure 9-27: Cracks on West End of Specimen at Failure [Specimen 6R7]

9.7.3 Between Composite and Middle-Composite Specimen Behavior

The specimen in this category had a recorded load-slip response between that of the fully composite (essentially zero slip) and middle composite lines (Figure 9-2 and Figure 9-4). This type of behavior was generally exhibited by specimen which had an as-placed or rake interface finish with a level of roughness ranging from "intermediate" to "not so rough". The behavior of these specimens will be described in general using the data from specimen 6R8 as a visual reference. It should be noted that the east side of 6R8 has a slip between composite and middle composite while the west side is behaving compositely based on the slip and strain data. Thus, when mentioning the slip in Figure 9-29, the reference is to slip gauge SL4 which is on the east side of the beam. Also, the strain data in Figure 9-30 is for the east side of the slab.

As the load was applied to the specimen, the recorded slip gradually and linearly increased (Figure 9-29). The rate of the slip increase was not that significant and averaged about 0.001 inches for every ten kips. This small rate of slip could just be a rotational effect caused by the gauge position. Also, at the initial stages of loading, the strain gauge at the bottom of the slab near the end of the beam experienced some initial tensile strain (Figure 9-30). As the load continued, the strain began to transition into compression and eventually continued in compression in a linear manner. It should be noted that there was only a couple specimens that exhibited this behavior. Some of the beams had a linear strain rate similar to the fully composite specimens (Figure 9-24). Therefore, it is not certain which of the specimens without strain gauges experienced this initial tensile strain or why some of the specimen experienced this while others did not.

Once the load reached a certain point, the slip started to increase more rapidly and thus diverge from its original linear rate (Figure 9-29). At about the same time, the stiffness of the load-deflection curve began to decrease (Figure 9-28). Additionally, the strain gauge close to the bottom of the slab near the end of the beam experienced a jump in strain (Figure 9-30). The strain gauge close to the top of the slab started to deviate slightly from its linear path. All of this activity signifies that the outer interface is beginning to fail. The middle interface still remained intact as can be inferred by the strain data at the center of the beam (Figure 9-31).

As the load increased, the slip curve continued to follow its new slope. Approximately 10 to 20 kips after the slip began to deviate, a flexural crack appeared on the bottom of the slab concrete under the load. This crack signifies that the interface at this area is not acting compositely. Flexural cracks also started to appear on the bottom of the web.

Shortly after the flexural cracks started to form on the slab and web, the middle interface failed suddenly through the loaded area. This middle interface failure was very similar to the one

experienced by the composite specimens. The data confirms the failure by jumps in the deflection, the middle strain gauges, and the slip at the middle and corresponding outer interface (Figure 9-28; Figure 9-31; Figure 9-29). As the load is increased beyond this point, more flexural cracks occurred along the web and flexural-shear cracks began to form near the support. Eventually if the load is continued, the web will fail violently when one of the flexural or flexural-shear cracks opens up.

It should be noted in Figure 9-29 that the gradual slip, increase in slip, and eventual failure of the east end of the beam did not effect or influence the slip of the west end of the beam. This reinforces the notion that both ends of the beam behave independently and can be analyzed as separate members.

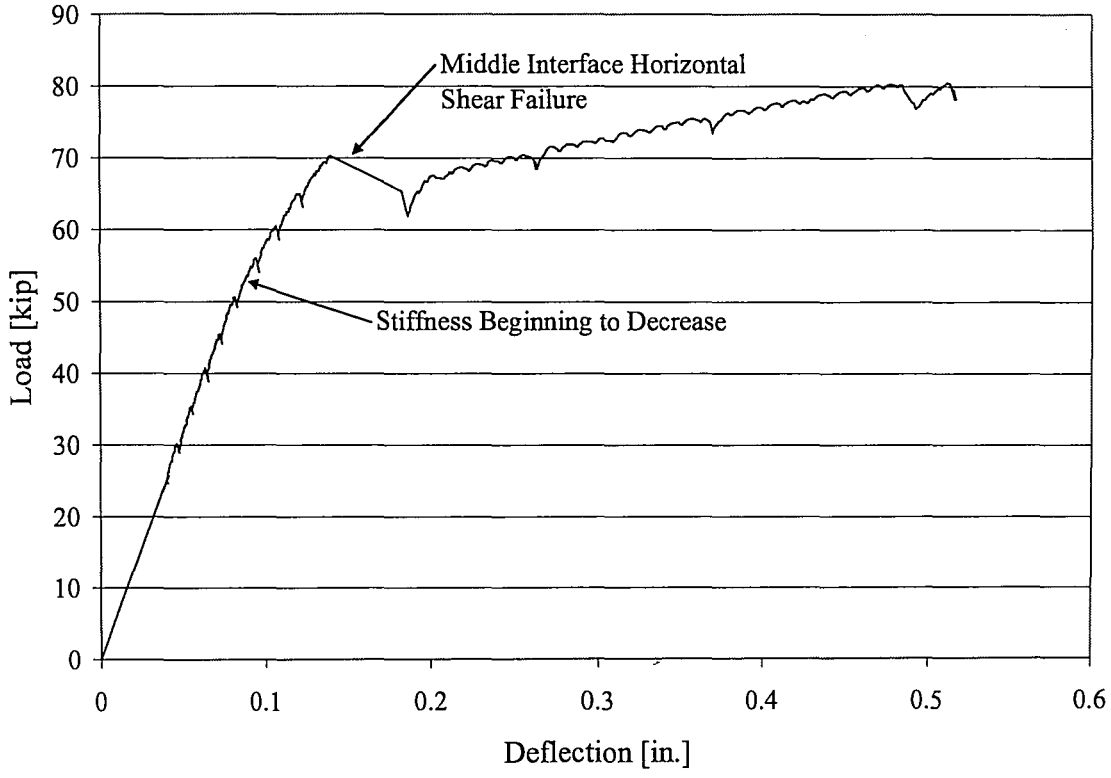

Figure 9-28: Load versus Deflection for a Specimen Between Composite and Middle-Composite [6R8]

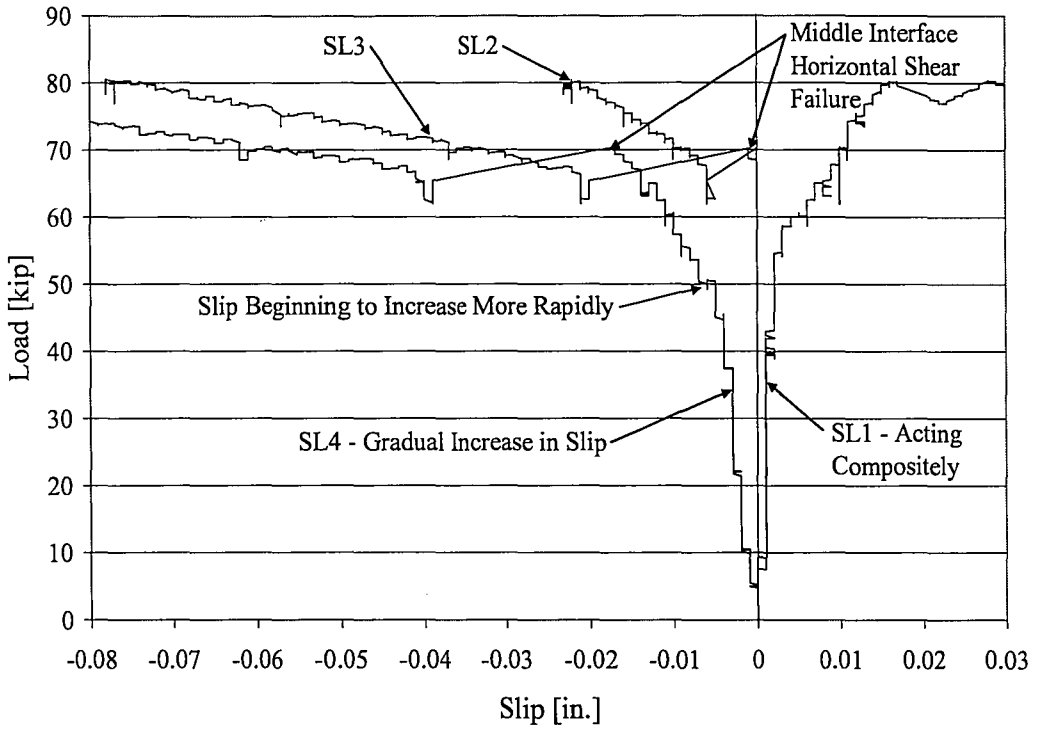

Figure 9-29: Load versus Slip for a Specimen Between Composite and Middle-Composite [6R8]

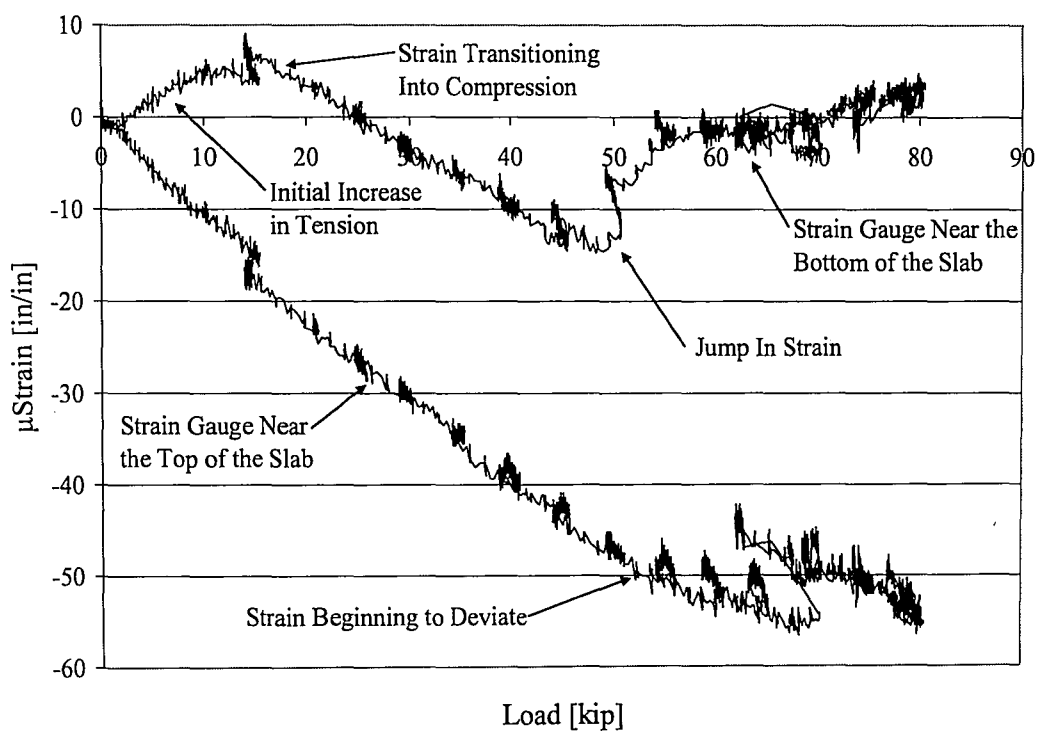

Figure 9-30: Strain Data for the Outer Slab Concrete of a Specimen Between Composite and Middle-Composite [6R8]

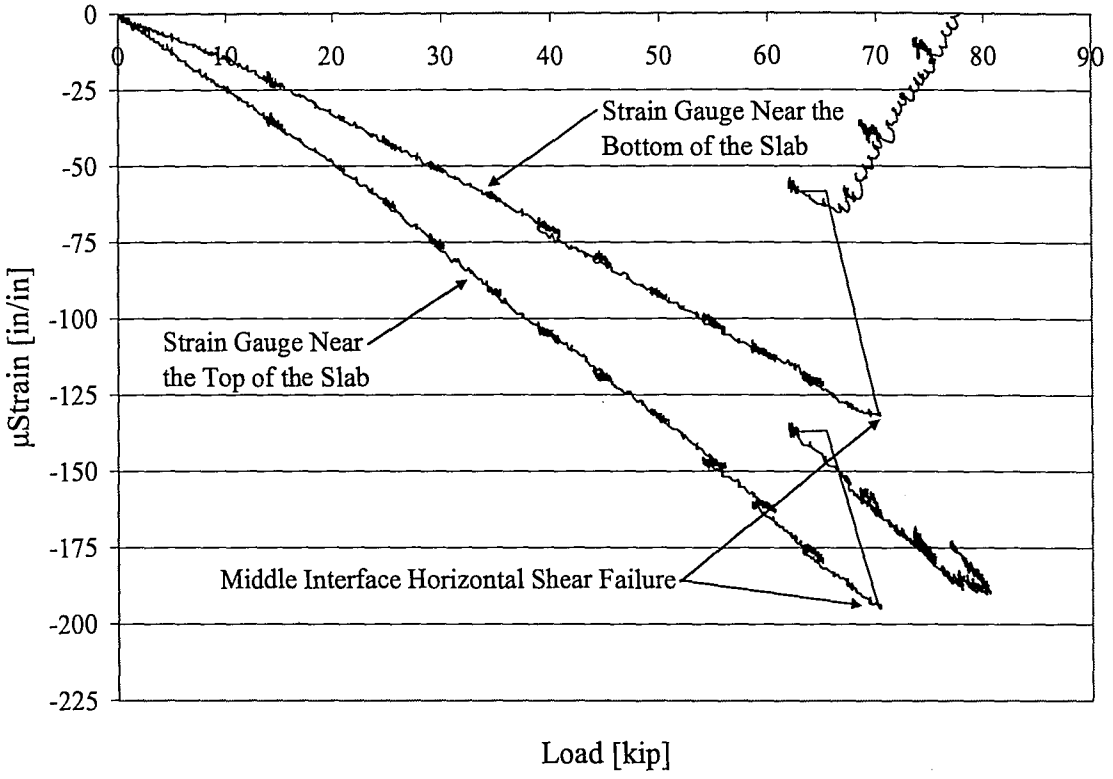

Figure 9-31: Strain Data for the Middle Slab Concrete of a Specimen Between Composite and Middle-Composite [6R8]

9.7.4 Between Middle-Composite and Non-Composite Specimen Behavior

The specimen in this category had a recorded slip curve which plotted between the calculated middle-composite and non-composite slip lines (Figure 9-2 and Figure 9-4). This behavior typically occurred for the specimen with a broom surface finish and a couple of the as-placed finishes with a roughness described as "not so rough." The general behavior of these specimens will be explained in the following paragraphs. The data from the test of specimen 6B5 will be used as a visual aid. However, this test did not have strain gauges on the outer portion of the slab concrete. Therefore, the strain data of specimen 3B2 was used as reference in this section. This was the only specimen in this category that had strain data on the outer portion of the slab.

The behavior of these specimens were fairly similar to the between composite and middle-composite specimen except that there was a large initial slip once the loading began (Figure 9-33). The initial large slip was accompanied by and initial increase in tensile strain at the bottom of the slab concrete near the end of the beam (Figure 9-34). It was believed that these specimens lost their composite action between the load point and the end of the slab very quickly. Initial cracks at the ends of the specimen were often seen prior to testing. These cracks are most likely a result of differential shrinkage which occurred during the curing of the slab as described in Section 7.4.3. Since the surface roughness was very low for these specimens, the interface bond at the cold joint may not have been able to resist the shrinkage strain. These initial cracks could have had a direct effect on the interface slipping so early in the loading process.

After about 10 to 15 kips of initial load, the large slip dissipated and the slip rate began to follow the rate of the between composite and middle-composite specimen (Figure 9-33). Also around this load, the strain at the bottom of the outer slab started to transition back into compression (Figure 9-34). This may indicate that the roughness of the interface could be interlocking the web and slab concrete thereby aiding in the restriction of the slip and ultimately creating this decrease in slip rate. The interlock transfers some of the forces and horizontal shear stresses between the two concrete members and thus is causing the section to act partially composite.

As the load increases beyond this point, the specimens behave very similar to the between composite and middle-composite specimen. The slip eventually begins to increase again which creates a change in the strain data at this location (Figure 9-33 and Figure 9-34). At this point, it is believed that the interlock of the roughness is failing and the specimen is beginning to act non-composite. Additionally, the load-deflection curve begins to deviate as the section loses stiffness (Figure 9-32). Flexural cracks appear on the bottom of the slab followed by cracks forming on the bottom of the web. Eventually, the center interface fails through one of the loading points

thus creating a jump in deflection, slip, and strain at the midspan (Figure 9-32, Figure 9-33, and Figure 9-35). If load is continued the specimen will begin cracking more severely along the web and eventually fail.

It should be noted that the increase in slip and failure of the center interface occurs at a lower load compared to specimens categorized as middle-composite to composite. This indicates that there is a trend between the roughness of the section and the strength and level of composite action of the specimen interface.

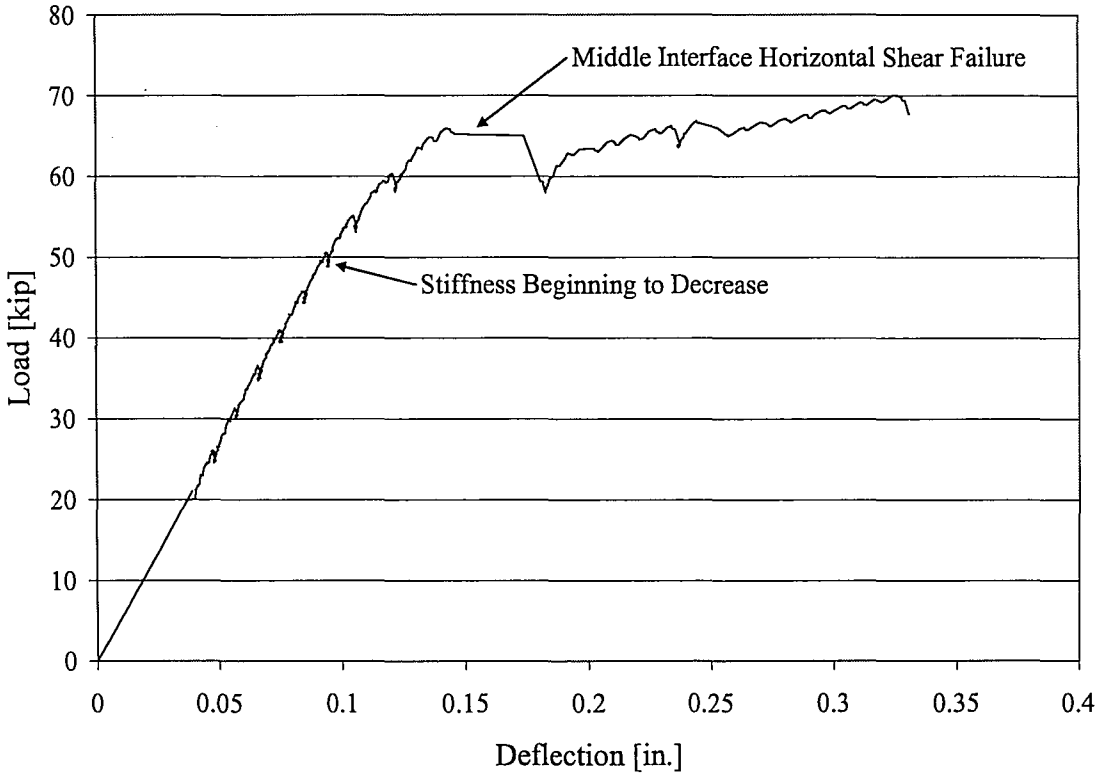

Figure 9-32: Load versus Deflection for a Specimen Between Middle-Composite and Non-Composite [6B5]

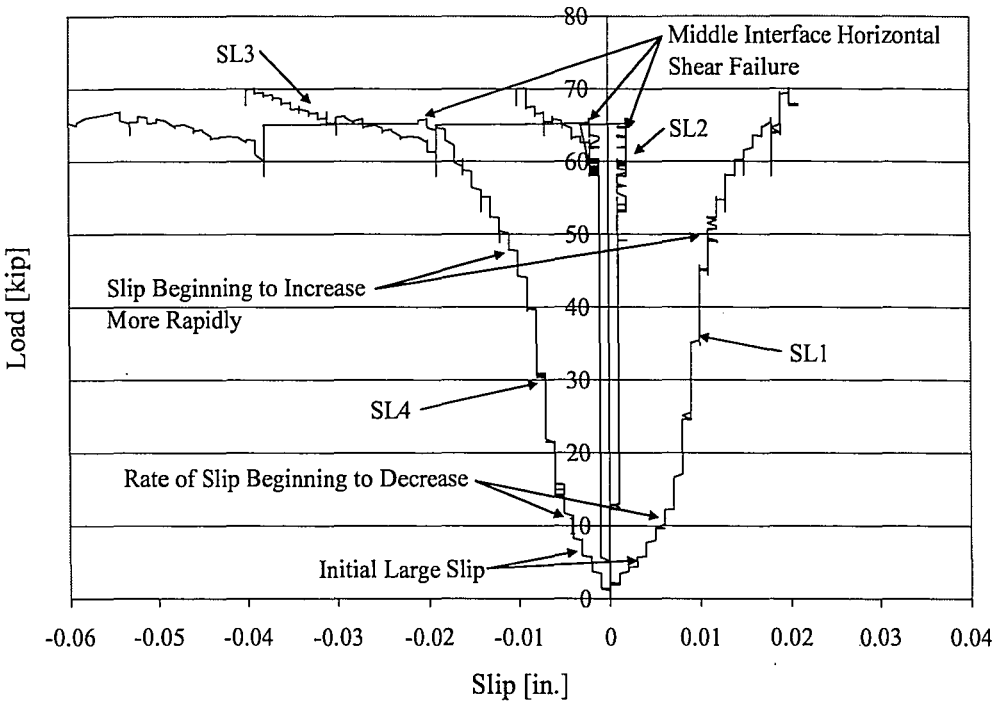

Figure 9-33: Load versus Slip for a Specimen Between Middle-Composite and Non-Composite [6B5]

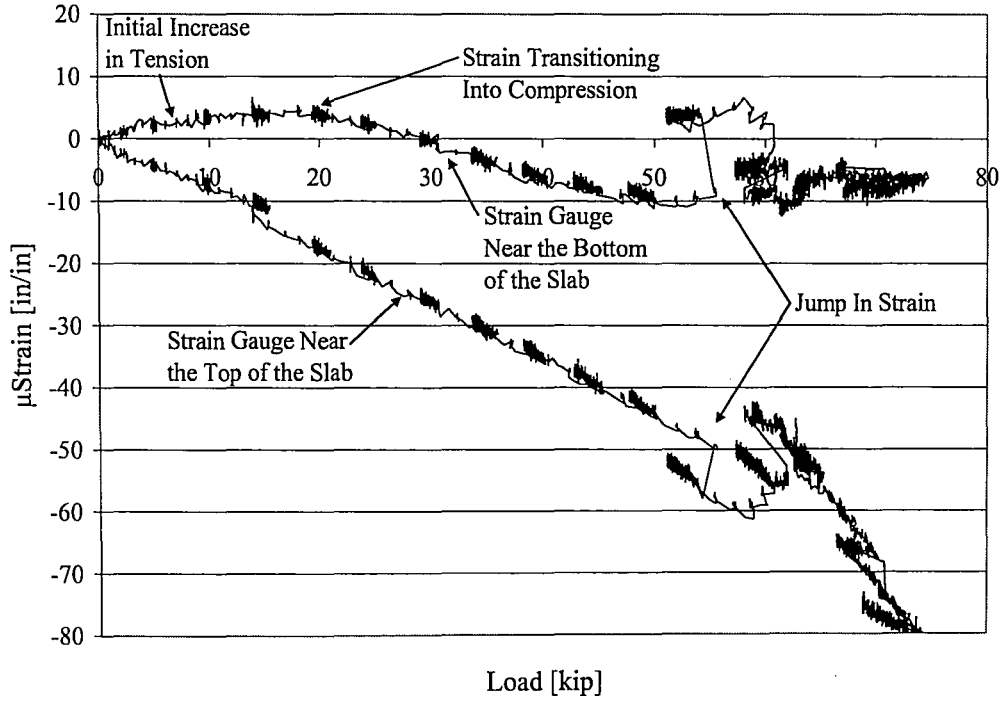

Figure 9-34: Strain Data for the Outer Slab Concrete of a Specimen Between Middle-Composite and Non-Composite [3B2]

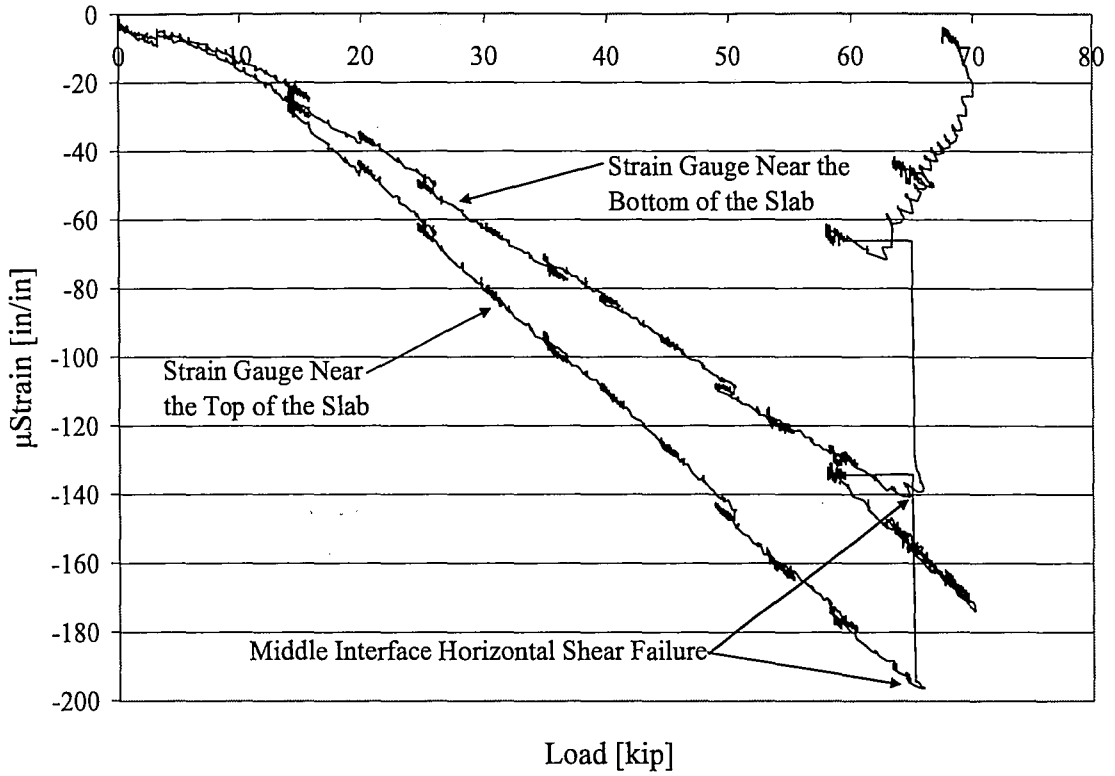

Figure 9-35: Strain Data for the Middle Slab Concrete of a Specimen Between Middle-Composite and Non-Composite [3B2]

9.7.5 Non-Composite Specimen Behavior

The last category is the specimens that behaved non-compositely. This only occurred for two beams; 3B1 and 3R2. For these specimens, one end was non-composite through the loading point while the other end behaved very close to composite. It should be noted that the interface of these two composite beams was already damaged before the tests were conducted. Thus, the lack of composite nature was not due to the loading of the beam or the roughness level but rather to unrelated circumstances. Specimen 3B1 was the beam which was initially placed into the test setup for several weeks and eventually the interface on one side of the beam became noticeably separated (see Section 7.4.3). Specimen 3R2 was picked up by its slab in order to assess the level of bond present between the slab and web concrete (see Section 7.4.3). During this process, one end of the beam remained intact and the other end separated up to the loading point. Even though

it was known that the results of these tests can not be used to determine the horizontal shear capacity, the tests were still run in order to use the data collected as a reference for other beams that may not act compositely.

The results of the test for specimen 3R2 are presented in Figure 9-36 and Figure 9-37. Beam 3B1 behaved very similarly to 3R2. Neither of the tests had strain gauges on the end of the beam that was non-composite. If strain gauges were present, the strain gauge near the bottom of the slab would probably be in tension throughout the test since the slab would be acting as a separate member and thus bending about its own centroid.

As soon as the test began, the non-composite end of the specimen experienced significant slip as seen by slip gauges SL3 and SL4 which were located between the load and the end of the slab (Figure 9-37). This slip continued to increase and follow the non-composite slip line calculated from beam theory (Figure 9-4). The slip gauge that was located between the loads (SL2) also slipped considerably during the test proving that the middle interface of the specimen was not intact. As the load continued, the rate of slip decreased slightly for a while before increasing again more significantly.

The slope of the load-deflection plot was lower then those for most of the other specimen behaviors. This plot did not follow the calculated non-composite slope because the other end of the beam was still acting compositely and thus increased the stiffness of the overall beam. The load-deflection plot started to deviate from its linear course once the non-composite interface began to slip more and the section started to crack.

At a load of approximately 60 to 70 kips, the bottom of the specimen web began to crack significantly on the side of the beam that was acting non-compositely and at midspan. The end of the beam that was acting compositely did not start to crack until much higher loads. The test was stopped after severe flexural and flexural shear cracking occurred on the web.

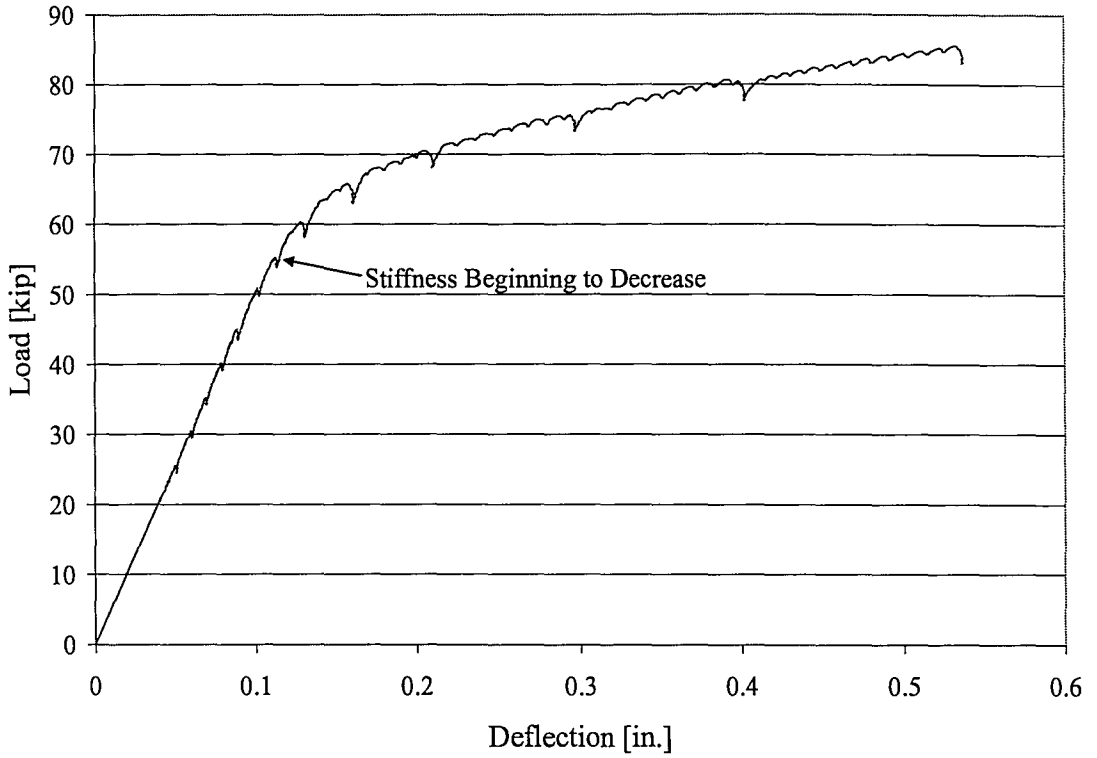

Figure 9-36: Load versus Deflection for a Half Non-Composite Specimen [3R2]

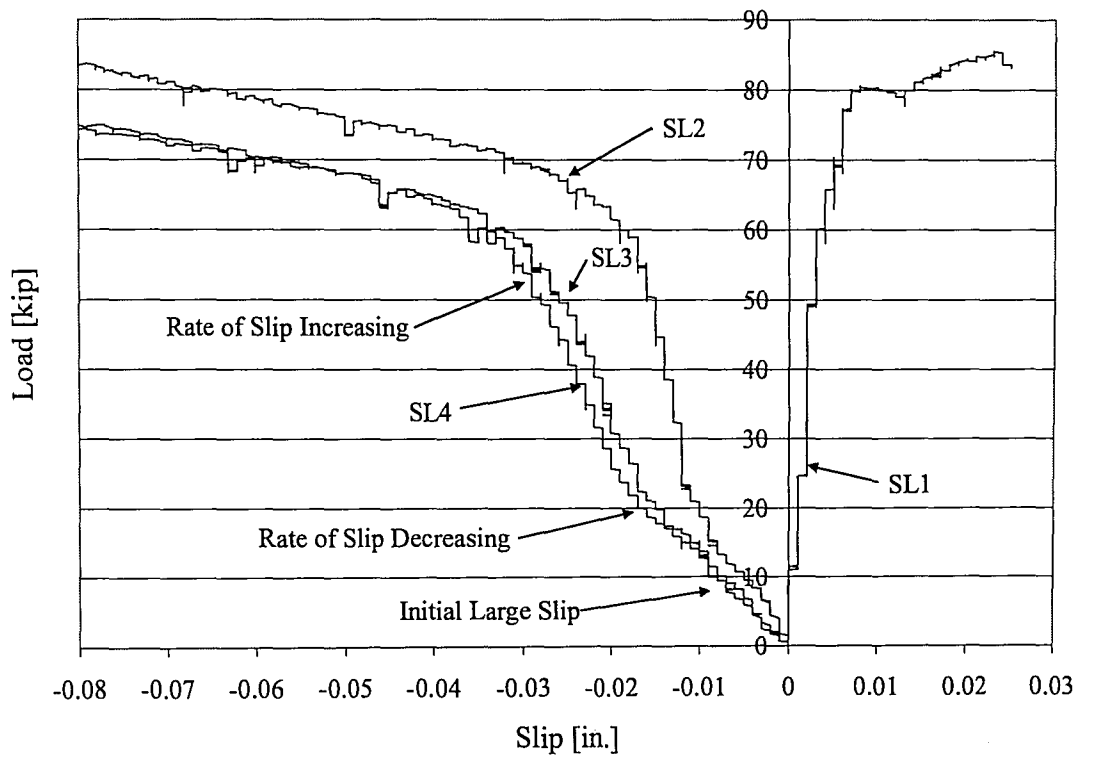

Figure 9-37: Load versus Slip for a Non-Composite Specimen [3R2]

9.7.6 Summary

There were four general behaviors that occurred for the specimen tests which where determined based on the level of composite action observed from the slip data. Some of the specimens had the same level of composite action on both sides of the beam while the behavior from one end to the other for the remaining specimens varied. The failure of the outer interface varied for the different specimen behaviors even though the failure of the center interface was very similar. Typically, the middle interface failed through the loaded area on the end of the beam that had a lower level of composite action and roughness. Additionally, it was observed that the behavior of the interface on end one of the beam did not effect the interface behavior on the other end unless one side was non-composite through the center of the beam. A summary of the behavior for each end of the test beams is presented in Table 9-3 through Table 9-5.

These three tables condense all the information needed to understand how each end of the specimens behaved during the test. The first three columns of the table present the specimen ID along with the roughness of the interface on each end of the beam. In the fourth column, the level of composite action experienced for each end of the beam is provided. These labels correspond to the four different categories of specimen behavior described in the previous sections. The next column describes the amount of initial slip that typically occurred for the between middle composite and non-composite specimen before the rate of slip started to decrease. Columns six and seven present the quantity of slip for the outer gauges and corresponding load when the rate of slip started to increase for each end of the test specimens. As mentioned before, this increase in slip indicates that the outer interface of the specimen has failed in horizontal shear. The instant when the rate of slip increased was found by fitting two linear lines to the different slopes of the load-slip data and determining where the two lines intersected. Columns eight and nine provide the end of the beam, slip value, and load value when the middle interface fails. Finally, column ten presents the loads when flexural cracks are observed on the bottom of the slab under the

loaded area. As mentioned previously, these flexural cracks indicate that the section is no longer acting compositely at this location. Studying all of this data will provide a better understanding on how each end of the specimens behaved during the test.

Table 9-3: Summary of the Broom Specimen Behavior

Specimen ID	Beam Side	Roughness	Level of Composite Action Based on Slip	Initial Large Slip Value and Load When It Dissipates [in.]	Slip Value at Outer Interface When Slip Rate Increases [in.]	Load at Outer Interface When Slip Rate Increases [kip]	Slip Value at Middle Interface Failure [in.]	Load at Middle Interface Failure [kip]	Load when the Slab Cracks [kip]
3B1	East	Not So Rough	C-MC		0.005	52.3			80
	West	Not So Rough	NC	0.018 @ 18kip	0.032	51.5			60
3B2	East	Not So Rough	MC-NC	0.006 @ 18kip	0.010	52.0			Not Recorded
	West	Not So Rough	MC-NC	0.006 @ 18kip	0.013	50.0			60
6B3	East	Not So Rough	MC-NC	0.005 @ 10kip	0.011	46.5	0.019	54.3	55
	West	Not So Rough	MC		0.007	47.5			60
6B4	East	Not So Rough	MC-NC	0.005 @ 12kip	0.010	49.0	0.015	60.0	60
	West	Not So Rough	MC-NC	0.004 @ 12kip	0.008	52.7			60
6B5	East	Not So Rough	MC-NC	0.004 @ 10kip	0.010	47.8	0.020	65.8	65
	West	Not So Rough	MC-NC	0.006 @ 10kip	0.011	52.3			65
6B6	East	Not So Rough	MC-NC	0.004 @ 16kip	0.008	49.8			65
	West	Not So Rough	MC-NC	0.006 @ 18kip	0.009	47.9	0.024	69.8	65

Legend for the Level of Composite Action

C = Composite

MC = Middle Composite

NC = Non-Composite

C-MC = Between Composite and Middle Composite

MC-NC = Between Middle Composite and Non-Composite

Table 9-4: Summary of the As-Placed Specimen Behavior

Specimen ID	Beam Side	Roughness	Level of Composite Action Based on Slip	Initial Large Slip Value and Load When It Dissipates [in.]	Slip Value at Outer Interface When Slip Rate Increases [in.]	Load at Outer Interface When Slip Rate Increases [kip]	Slip Value at Middle Interface Failure [in.]	Load at Middle Interface Failure [kip]	Load when the Slab Cracks [kip]
3A1	East	Intermediate	MC-NC	0.005 @ 11kip	0.013	52.0			Not Recorded
	West	Not So Rough	MC-NC	0.007 @ 19kip	0.010	36.8	0.028	65.0	65
3A2	East	Rough			No Slip Data	No Slip Data			90
	West	Rough	C-MC		0.007	55.0	0.033	80.0	75
6A3	East	Not So Rough	C-MC		0.005	45.0	0.010	54.3	54
	West	Not So Rough	MC	0.004 @ 15kip	0.007	49.0			65
6A4	East	Not So Rough	C-MC		0.006	51.0	0.018	65.5	65
	West	Intermediate	C		0.004	50.5			65
6A5	East	Intermediate	C		0.003	50.0			65
	West	Not So Rough	MC-NC	0.006 @ 15kip	0.010	40.0	0.012	48.5	55
6A6	East	Rough	C		0.002	65.0			80
	West	Not So Rough	MC-NC	0.005 @ 15kip	0.009	53.0	0.023	70.4	70
6A7	East	Intermediate	MC		0.008	53.0	0.028	67.5	65
	West	Rough	C		0.001	59.8			65
6A8	East	Intermediate	MC	0.003 @ 16kip	0.006	55.0	0.023	74.5	70
	West	Rough	C		0.003	65.0			75

Legend for the Level of Composite Action

C = Composite

MC = Middle Composite

NC = Non-Composite

C-MC = Between Composite and Middle Composite

MC-NC = Between Middle Composite and Non-Composite

Table 9-5: Summary of the Rake Specimen Behavior

Specimen ID	Beam Side	Roughness	Level of Composite Action Based on Slip	Initial Large Slip Value and Load When It Dissipates [in.]	Slip Value at Outer Interface When Slip Rate Increases [in.]	Load at Outer Interface When Slip Rate Increases [kip]	Slip Value at Middle Interface Failure [in.]	Load at Middle Interface Failure [kip]	Load when the Slab Cracks [kip]
3R1	East	Rough	C		0.002	70.0			80
	West	Not So Rough	MC		0.010	61.0	0.024	76.5	75
3R2	East	Not So Rough	NC	0.015 @ 21kip	0.028	55.0			65
	West	Intermediate	C		0.004	66.0			80
6R3	East	Not So Rough	C-MC		0.008	59.0			75
	West	Intermediate	MC-NC	0.006 @ 15kip	0.010	59.0	0.028	78.3	75
6R4	East	Rough	C		0.001	54.0			79
	West	Rough	C		0.001	70.0			79
6R5	East	Not So Rough	C-MC		0.005	51.0			70
	West	Not So Rough	C		0.003	53.5	0.018	75.0	70
6R6	East	Intermediate	C		0.001	80.2			85
	West	Intermediate	C		0.001	80.2	0.045	88.8	85
6R7	East	Rough	C		0.001	63.5	0.045	84.2	75
	West	Rough	C		0.002	63.7			75
6R8	East	Intermediate	C-MC		0.005	50.0	0.018	70.2	65
	West	Intermediate	C		0.003	57.5			75

Legend for the Level of Composite Action

C = Composite

MC = Middle Composite

NC = Non-Composite

C-MC = Between Composite and Middle Composite

MC-NC = Between Middle Composite and Non-Composite

9.8 ARAMIS System Test Results

The results of the ARAMIS 3D image correlation tests were compared to the data collected from the test specimens by the other instrumentation in order to verify the deflection of the beam and the strain distribution in the slab concrete. The deflection was validated by comparing the data recorded by the LVDT to the ARAMIS data. The resulting load versus deflection curves are presented in Figure 9-38. The deflection data recorded by the LVDT shown in this figure for specimen 6R8 is not corrected for the contribution of the support pad since the ARAMIS data would have also picked up this effect. It can be observed that the trends of both curves are very similar. The difference between the curves at the drop in load and jump in deflection occurred because a data point was not taken by the ARAMIS system at the instant that the center interface of the specimen failed. Overall, the ARAMIS system was able to accurately capture the deflection behavior of the test specimen.

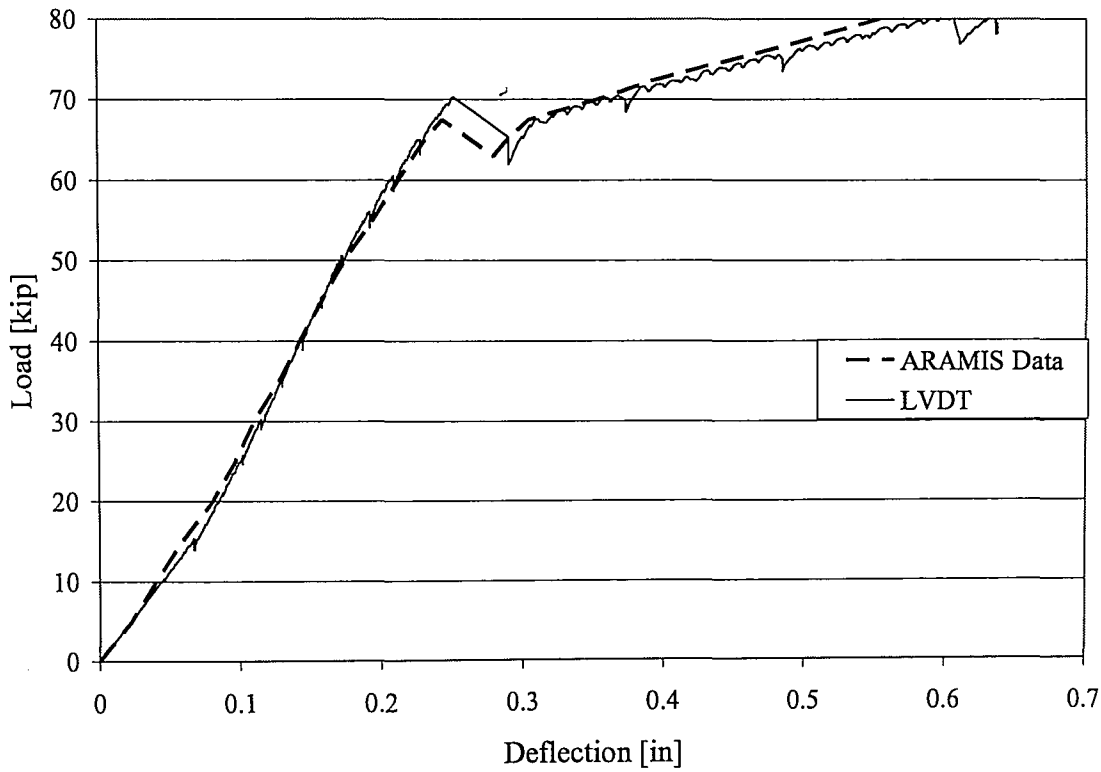

Figure 9-38: Load versus Deflection from the ARAMIS System and the LVDT [Specimen 6R8]

For these experiments, the main purpose of running the ARAMIS tests was to determine the strain distribution on the specimen slab between the loading points to discover whether or not there were uniform levels of axial strain as predicted by the finite element model (Figure 8-24). Figure 9-39 shows on overlay of the typical strain distributions on the slab concrete recorded by the ARAMIS system for two consecutive load levels; 62.5 kips and 65 kips. These strain distributions were recorded on the slab from the midspan of the beam to a location just short of the loading point as seen previously in Figure 8-30. Even though the strains recorded do fall within the upper and lower predicted strain levels of the finite element model for the slab concrete, the distributions of the strain are more erratic and less uniform for the ARAMIS data. The differences in the strain distributions may be due to the level of composite action or the stiffness of the specimen at certain locations along the beam. Even with this irregular strain distribution, the expected trend still exists of a higher compression level at the top of the slab which gradually decreases as you move toward the bottom of the slab. When the middle interface failed over the location of the slab where the ARAMIS system was recording, the strain at the bottom of the slab started to transition into tension indicating that the web and slab are behaving as two separate members. This correlates with the observations made from the specimen behavior.

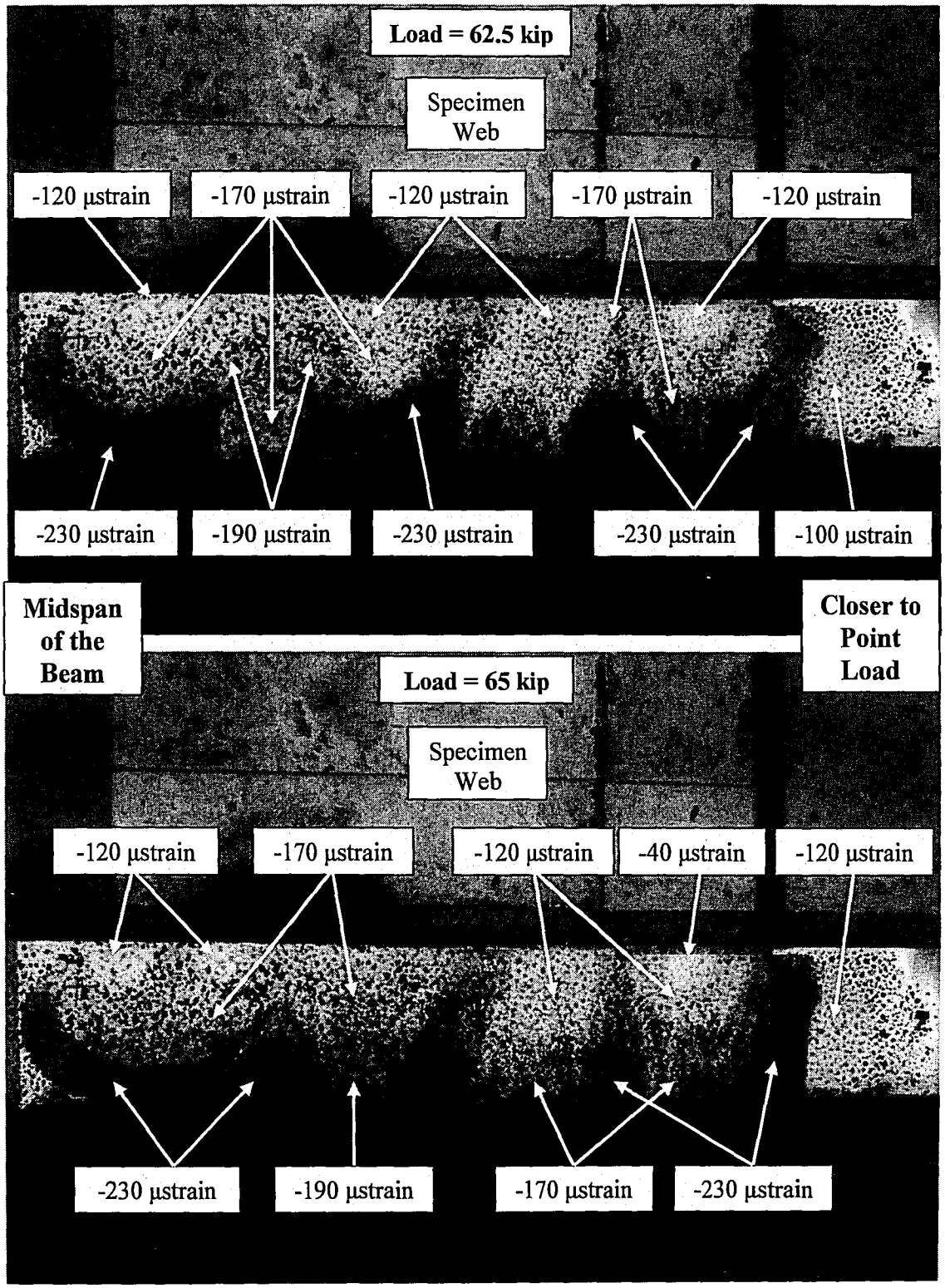

Figure 9-39: Strain Distributions Recorded by the ARAMIS System at Two Load Levels

[Specimen 6R8]

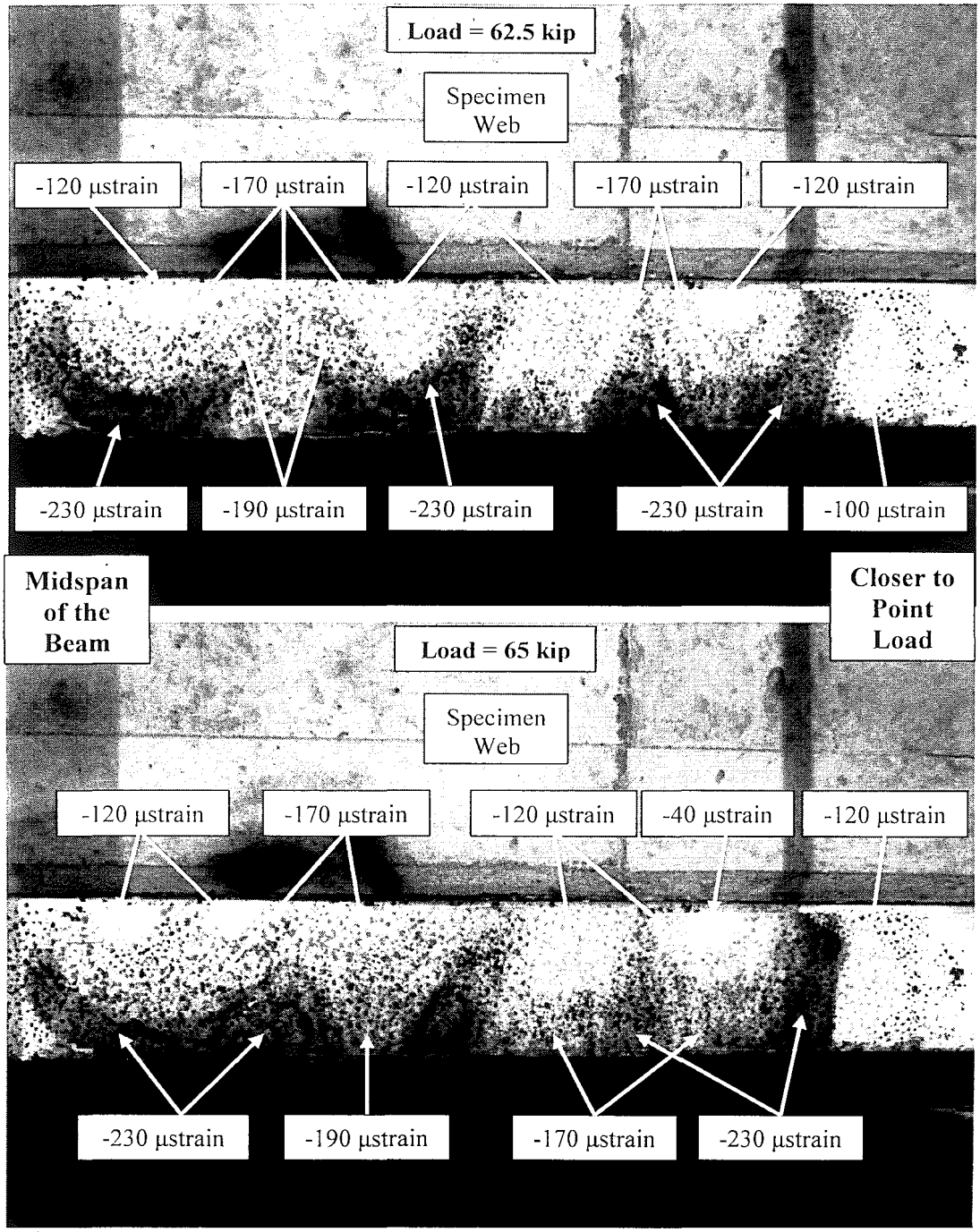

Figure 9-39: Strain Distributions Recorded by the ARAMIS System at Two Load Levels

[Specimen 6R8]

Strain data from the ARAMIS tests were collected at the locations of the strain gauges in order to compare the two data sets. Figure 9-40 and Figure 9-41 present plots of the data collected from the strain gauges compared to the strain data collected by the ARAMIS system. The general trend of the ARAMIS strain data is fairly close to the data from the strain gauges. The strain data recorded near the top of the slab by the ARAMIS system was always at a higher level of compression than the data recorded at the bottom of the slab. The jumps in the ARAMIS data are most likely the result of the device recording at a resolution of 50 μstrain which cannot accurately pick up the minute changes in strain during the test.

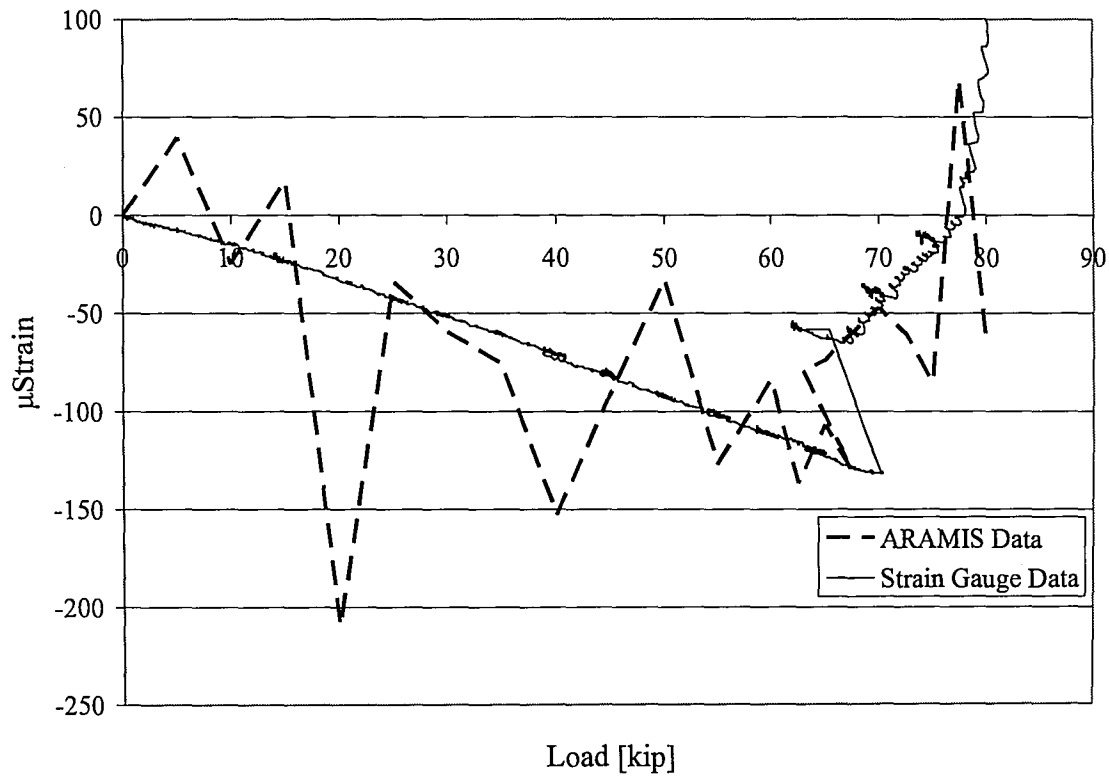

Figure 9-40: Strain Data near the Bottom of the Slab from the ARAMIS Data and the Strain Gauge [Specimen 6R8]

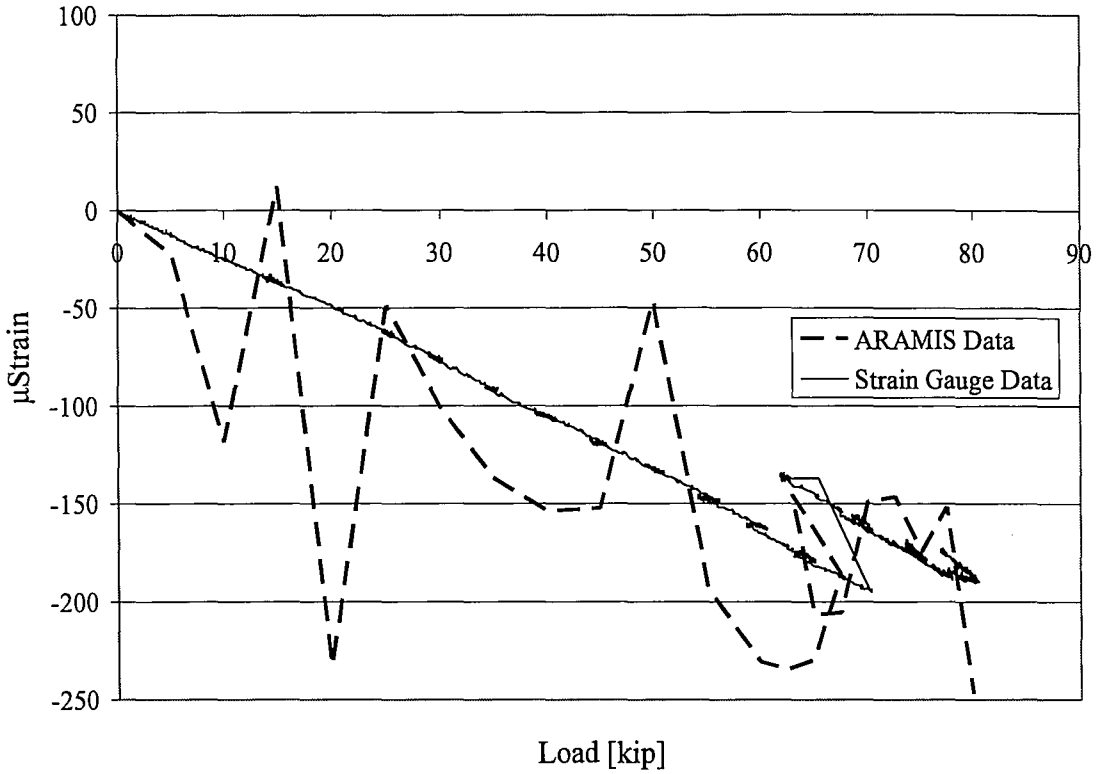

Figure 9-41: Strain Data near the Top of the Slab from the ARAMIS System and the Strain Gauge [Specimen 6R8]

Overall, the ARAMIS system was able to capture the deflection of the test specimen to an accurate level. The strain values measured correlated with the strain gauges used on the specimen. While the values were not exact, the ARAMIS system adequately tracked with the strain gauge data. The ARAMIS data revealed that the distributions of axial strain in the specimen flange is not as ideal as that predicted by the finite element model. The axial strain trends the same as the finite element results but regions of high and low strain occur along the section. This illustrates that the transfer of horizontal shear stress cannot be taken as a simple response. Furthermore, the variation in the strain distribution from point to point indicates that the use of discrete strain gauge data may be unreliable for determining the horizontal shear stress values. The strain gauge method was used in earlier studies; however, based on the ARAMIS results, it is not repeated here.

9.9 Horizontal Shear Stress Results

The test specimens were designed so the outer interface between the load point and the end of the slab would reach high levels of horizontal shear stress before cracking of the section occurred. Therefore, the main interest in this research program was to determine when the outer interface failed. As mentioned above, the interface typically failed a second time under the loaded area. This secondary failure is a result of a slightly increased clamping force and the theoretically low values of horizontal shear stress between the point loads. Thus, a much larger horizontal shear stress is needed to fail the middle interface. It was determined that the clamping force does not have an effect on the failure of the outside interface since there is essentially no clamping force near the end of the slab-beam interface where the slip failure initiates and because the outer interface failed at loads well below the interface under the loaded area. This negligible effect was also observed from the horizontal shear results of the finite element model. It is important to see the effect and contribution the clamping force has on the interface directly under the load as it will aid in creating a higher horizontal shear capacity at that point. However, the ultimate focus of this research project is on the outer interface which will be discussed in the following paragraphs.

As discussed in the previous section, the failure of the outer interface for the specimen with a fully composite behavior was well defined with an obvious jump in slip. For the beams that behaved either between composite and middle composite or between middle composite and non-composite, the failure is assumed to occur when the slip rate begins to increase prior to the failure of the interface under the loaded area (Figure 9-29 and Figure 9-33). This assumption is based on the fact that the stiffness seen from the load deflection curve starts to decrease at this point (Figure 9-28 and Figure 9-32) and there is a jump in the strain data (Figure 9-30 and Figure 9-34). The initial large slip and tensile strain of the between middle composite and non-composite

specimens could indicate that the interface was lost at an early stage of the test. However, the strain does return to compression and there is a decrease in the rate of slip indicating that there is some interlock of the slab and web concrete and therefore they are acting partially composite. The interlock does contribute to the horizontal shear stress just as the cohesion or bond does. Since the bond may have been lost, the horizontal shear stresses for these specimens will only be the result of the interlock and thus be taken as a lower bound for the horizontal shear capacity.

The horizontal shear data for three of the test specimens was not included in this analysis. Specimens 3B1 and 3R2 were both excluded because the interface was initially non-composite through the center of the beam. Specimen 3B2 was omitted because the data used to determine the slope of the load-deflection curve was questionable and thus resulted in a very low stiffness for the specimen.

A summary of the horizontal shear stresses are presented in Table 9-6 through Table 9-8. These tables provide the average interface width on each end of the beam that was measured and recorded prior to the pour of the slab concrete. For every specimen test, the outer interface failed before cracking of the section occurred. Therefore, the use of the classical elastic method (Eq. 6) for determining the horizontal shear stress is valid for all of the tests. It should be noted that the values of I_{tr} and Q_{tr} used in calculating the horizontal shear stress by the elastic method include the contribution of the prestressed and slab steel. The horizontal shear stress was also calculated using the ACI and AASHTO simplified elastic beam behavior equations (Eq. 3 and 4, respectively) for means of comparison. It can be seen in these tables that the horizontal shear stresses achieved from the tests were approximately six to ten times greater than the recommended values presented by the ACI code for composite sections without interface reinforcement.

The horizontal shear stress was calculated using the strain gauge data near the midspan of the beam as described in the previous chapter. It was found that this method provides an estimate of the horizontals shear capacity that is generally conservative by approximately 150 to 200 psi compared to the horizontal shear stress found using the elastic method (Eq. 6). This difference may be the result of the distribution of axial strains in the slab not being as uniform between the load points as previously predicted in the finite element model (Figure 8-24) but rather more erratic and dispersed as recorded by the ARAMIS system (Figure 9-39) mentioned earlier. Since the strain gauges are located on discrete points of the specimen, the recorded values may not be an accurate representation of the strains at other locations between on the slab such as near the load points. The previous research of Deschenes and Naito (2006) also resulted in horizontal shear values from the strain data that were not very consistent from test to test (Table 5-6). Therefore, the horizontal shear stress found by the classical elastic method will be used as a means of comparison in later sections and chapters since the results from this equation are more consistent for all the tests and also because this method is typically used in the previous research and structural engineering design practices.

Table 9-6: Summary of the Horizontal Shear Stress for the Broom Specimens

Specimen ID	Beam Side	Roughness	f'c [ksi]	Load at Outer Interface Failure [kip]	Interface Width b_v [in.]	From Strain $v = C/Lb_v$ [psi]	Elastic $v = VQ/Ib_v$ [psi]	ACI $v = V/b_v d$ [psi]	AASHTO $v = V/b_v d_v$ [psi]
6B3	East	Not So Rough	5.08	46.5	4.25	294	476	456	534
	West	Not So Rough		47.5	4.3125	297	479	459	537
6B4	East	Not So Rough	5.24	49.0	4.375	326	488	467	546
	West	Not So Rough		52.7	4.25	364	541	517	605
6B5	East	Not So Rough	5.30	47.8	4.25	363	490	468	548
	West	Not So Rough		52.3	4.3125	405	529	505	592
6B6	East	Not So Rough	5.40	49.8	4.3125	329	505	481	563
	West	Not So Rough		47.9	4.375	311	478	456	534

Table 9-7: Summary of the Horizontal Shear Stress for the As-Placed Specimens

Specimen ID	Beam Side	Roughness	f'c [ksi]	Load at Outer Interface Failure [kip]	Interface Width b_v [in.]	From Strain $v = C/Lb_v$ [psi]	Elastic $v = VQ/Ib_v$ [psi]	ACI $v = V/b_vd$ [psi]	AASHTO $v = V/b_vd_v$ [psi]
3A1	East	Intermediate	4.53	52.0	3.0	No Strain Data	750	722	846
	West	Not So Rough		36.8	3.0	No Strain Data	530	511	598
3A2	East	Rough	4.53	No Data					
	West	Rough		55.0	3.0	589	793	764	894
6A3	East	Not So Rough	5.46	45.0	3.0	502	654	625	732
	West	Not So Rough		49.0	3.0	549	712	681	797
6A4	East	Not So Rough	6.26	51.0	3.125	558	718	680	796
	West	Intermediate		50.5	3.125	550	711	673	788
6A5	East	Intermediate	6.26	50.0	3.0	476	734	694	813
	West	Not So Rough		40.0	3.0	375	587	556	650
6A6	East	Rough	6.52	65.0	4.0	555	726	677	793
	West	Not So Rough		53.0	4.0	449	592	552	646
6A7	East	Intermediate	5.03	53.0	4.00	409	576	552	646
	West	Rough		59.8	4.0625	457	640	613	718
6A8	East	Intermediate	5.03	55.0	4.0625	514	589	564	660
	West	Rough		65.0	4.125	592	685	657	769

Table 9-8: Summary of the Horizontal Shear Stress for the Rake Specimens

Specimen ID	Beam Side	Roughness	f'c [ksi]	Load at Outer Interface Failure [kip]	Interface Width b_v [in.]	From Strain $v = C/Lb_v$ [psi]	Elastic $v = VQ/Ib_v$ [psi]	ACI $v = V/b_vd$ [psi]	AASHTO $v = V/b_vd_v$ [psi]
3R1	East	Rough	4.53	70.0	3.0	782	1006	972	1138
	West	Not So Rough		61.0	3.0	668	877	847	992
6R3	East	Not So Rough	5.19	59.0	3.5	560	731	702	822
	West	Intermediate		59.0	3.25	603	787	756	886
6R4	East	Rough	5.19	54.0	3.125	579	749	720	843
	West	Rough		70.0	3.25	742	934	897	1051
6R5	East	Not So Rough	5.46	51.0	3.125	487	710	680	796
	West	Not So Rough		53.5	3.375	476	690	660	773
6R6	East	Intermediate	5.46	80.2	4.0	664	873	835	978
	West	Intermediate		80.2	4.0	664	873	835	978
6R7	East	Rough	5.08	63.5	3.25	652	850	814	953
	West	Rough		63.7	3.1875	665	869	833	975
6R8	East	Intermediate	5.24	50.0	3.0625	478	712	680	796
	West	Intermediate		57.5	3.0	567	835	799	935

9.10 Trends in the Experimental Data

In order to understand the influence the different experimental variables in this research program had on the behavior of the specimens, the trends of the data are studied; specifically the deflection, interface slip, and horizontal shear stress. Conclusions can be independently drawn from each set of data in order to evaluate the effect of the surface finish and roughness on the composite interface.

It was found that in general the slope of the load-deflection lines increased as the surface finish increases from broom to as-placed to rake. The slope of these lines is related to the stiffness of the overall section. As the sections stiffness decreases due to the partial or non-composite nature of the interface, the slope of the load-deflection line will also decrease. In this way, the approximate percent composite action of the section can be estimated. Because the percent composite is related to the slope, the general trend of an increase in the percent of composite action with a rougher surface finish is to be expected. The slopes and corresponding percent composite for each test specimen was tabulated earlier in Table 9-2. Based on this data, a summary of the average slope and percent composite along with the standard deviation for each surface finish is presented in Table 9-9. The data was fairly consistent for the broom specimens which exhibited a low variation in slope due to the uniformity of the surface roughness. The as-placed and rake specimens exhibited higher variations in the data due to greater variation in the surface roughness. A plot of the approximate average load-deflection lines for each surface finish is presented in Figure 9-42. From this data, it can be inferred that the roughness of the surface finish will influence the level of composite action and thus the stiffness of the beam section.

Table 9-9: Average and Standard Deviation of the Slope of the Load-Deflection Line and Percent Composite for Each Surface Finish

Surface Finish	Average Slope of Load-Deflection [kip/in]	Standard Deviation of the Slope of Load-Deflection [kip/in]	Average Percent Composite [%]	Standard Deviation of the Percent Composite [%]
Broom	531.0	27.3	67.0	7.6
As-Placed	560.2	50.2	75.1	14.0
Rake	609.2	57.4	88.7	16.0

Note: Average and Standard Deviation Calculations do not include Specimens 3B1, 3B2, and 3R2

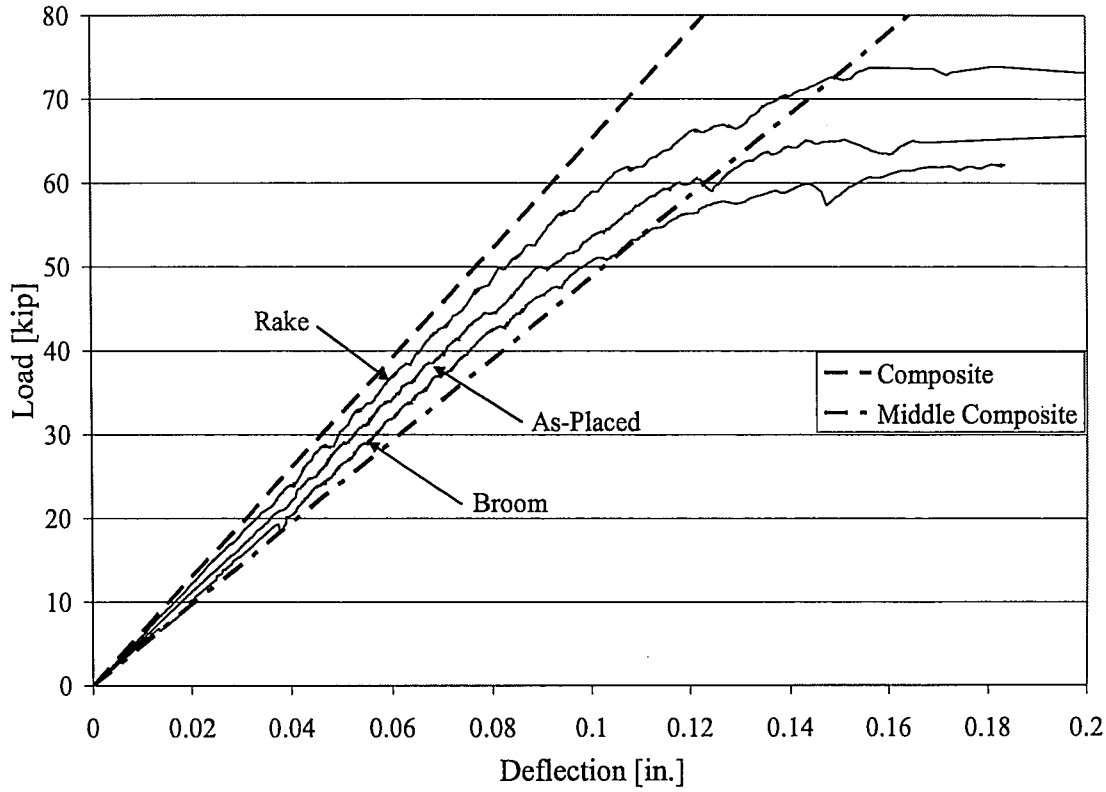

Figure 9-42: Average Load versus Deflection Plot for Each Surface Finish

The degree of interface slip experienced by the composite section also seemed to be influenced by the surface finish and corresponding level of roughness. Additionally, the magnitude of slip appears to relate to the degree of composite action experienced by the interface. In order to quantify the level of slip for the different surface finishes, the slope of the horizontal shear stress-outer interface slip response for each end of the specimen was calculated using least squares up to

a load of 40 kips which corresponds to a horizontals shear stress of approximately 450 psi. The results of these calculations for each surface finish are presented in Table 9-10 through Table 9-12.

Table 9-10: Slope of the Outer Interface Slip for the Broom Specimens

Specimen ID	Beam Side	Roughness	Level of Composite Action Based on Slip	Outer Interface Slip Slope [kip/in^3]
3B1	East	Not So Rough	C-MC	98.5
	West	Not So Rough	NC	25.2
3B2	East	Not So Rough	MC-NC	60.2
	West	Not So Rough	MC-NC	49.6
6B3	East	Not So Rough	MC-NC	42.8
	West	Not So Rough	MC	72.5
6B4	East	Not So Rough	MC-NC	43.6
	West	Not So Rough	MC-NC	62.7
6B5	East	Not So Rough	MC-NC	40.4
	West	Not So Rough	MC-NC	32.7
6B6	East	Not So Rough	MC-NC	58.4
	West	Not So Rough	MC-NC	45.7

Table 9-11: Slope of the Outer Interface Slip for the As-Placed Specimens

Specimen ID	Beam Side	Roughness	Level of Composite Action Based on Slip	Outer Interface Slip Slope [kip/in^3]
3A1	East	Intermediate	MC-NC	47.8
	West	Not So Rough	MC-NC	49.8
3A2	East	Rough		No Slip Data
	West	Rough	C-MC	98.3
6A3	East	Not So Rough	C-MC	149.5
	West	Not So Rough	MC	90.3
6A4	East	Not So Rough	C-MC	127.8
	West	Intermediate	C	156.2
6A5	East	Intermediate	C	244.9
	West	Not So Rough	MC-NC	51.9
6A6	East	Rough	C	178.4
	West	Not So Rough	MC-NC	57.9
6A7	East	Intermediate	MC	73.5
	West	Rough	C	154.0
6A8	East	Intermediate	MC	74.2
	West	Rough	C	249.4

Table 9-12: Slope of the Outer Interface Slip for the Rake Specimens

Specimen ID	Beam Side	Roughness	Level of Composite Action Based on Slip	Outer Interface Slip Slope [kip/in^3]
3R1	East	Rough	C	209.3
	West	Not So Rough	MC	76.4
3R2	East	Not So Rough	NC	22.3
	West	Intermediate	C	226.3
6R3	East	Not So Rough	C-MC	97.5
	West	Intermediate	MC-NC	53.3
6R4	East	Rough	C	208.6
	West	Rough	C	265.4
6R5	East	Not So Rough	C-MC	147.7
	West	Not So Rough	C	201.9
6R6	East	Intermediate	C	205.3
	West	Intermediate	C	201.7
6R7	East	Rough	C	314.5
	West	Rough	C	319.8
6R8	East	Intermediate	C-MC	135.3
	West	Intermediate	C	276.0

Using the data from the previous three tables, the average and standard deviation of the slope for the outer interface slip lines were determined for each surface finish. Additionally, the average and standard deviation of the slope for the roughness variation within the as-placed and rake surface finishes were calculated. These results are presented in Table 9-13. It is clear from the results that the slip of the interface decreases as the surface finish roughness increases from broom to as-placed to rake. Additionally for the as-placed and rake specimens, the slope of the slip decreases as the degree of roughness increases from "not so rough" to "intermediate" to "rough."

Table 9-13: Average and Standard Deviation of the Slope of the Outer Interface Slip for Each Surface Finish and Roughness

Surface Finish	All Specimen		"Not So Rough" Specimen		"Intermediate" Specimen		"Rough" Specimen	
	Average [kip/in^3]	Standard Deviation [kip/in^3]	Average [kip/in^3]	Standard Deviation [kip/in^3]	Average [kip/in^3]	Standard Deviation [kip/in^3]	Average [kip/in^3]	Standard Deviation [kip/in^3]
Broom	50	13	50	13	N/A	N/A	N/A	N/A
As-Placed	120	67	88	43	119	81	170	63
Rake	194	84	131	56	174	84	262	54

Note: Average and Standard Deviation Calculations do not include Specimens 3B1, 3B2, and 3R2

The horizontal shear stress was calculated for each end of the composite concrete specimens. The results were presented earlier in Table 9-6 through Table 9-8. Using this data, the average and standard deviation of the horizontal shear stress for each surface finish and the roughness within the as-placed and rake finishes were determined and tabulated in Table 9-14. These values are based upon the classical elastic method (Eq. 6) since this equation is dependant on the section properties of a beam and will result in a more accurate representation of the horizontal shear stress. As seen in the table, the horizontal shear stress increases by roughly 25% as the surface finish increases from broom to as-placed to rake. Also for the as-placed and rake specimens, as the roughness of the interface surface increased, the horizontal shear strength increased by approximately 6% and 8%, respectively. The standard deviation for the broom specimens is lower than those for the as-placed and rake specimens because the roughness of the broom surface finish was more consistent than the as-placed and rake surface finishes.

Using the experimentally derived data, design recommendations are developed. The design horizontal shear strength for each surface finish is computed based on a 99% probability of exceedance. Using a normal distribution, this corresponds to a strength of 2.33 standard deviations less than the mean. The values for the design horizontal shear strength are presented in Table 9-15. The correlation between strength and roughness still exists; however, due to the large variability in the as-placed surface roughness, the design strength trends toward that of the broom finish. In comparison to the ACI 318 recommendation of 80 psi, the broom, as-placed, and rake finishes provided 5.4, 5.8, and 7.1 times the ACI recommendations, respectively.

Table 9-14: Average and Standard Deviation of the Horizontal Shear Stress for Each Surface Finish and Roughness

Surface Finish	All Specimen		"Not So Rough" Specimen		"Intermediate" Specimen		"Rough" Specimen	
	Average [psi]	Standard Deviation [psi]	Average [psi]	Standard Deviation [psi]	Average [psi]	Standard Deviation [psi]	Average [psi]	Standard Deviation [psi]
Broom	498	27	498	27	N/A	N/A	N/A	N/A
As-Placed	667	87	632	75	672	83	711	65
Rake	821	107	752	99	816	68	882	96

Note: Average and Standard Deviation Calculations do not include Specimens 3B1, 3B2, and 3R2

Table 9-15: Design Horizontal Shear Stresses

Surface Finish	Design Horizontal Shear Stress [psi]
Broom	435
As-Placed	466
Rake	571

The horizontal shear capacity of the whole beam was also investigated. This means that once one end of the specimen failed, the entire beam is considered to have failed, and the information on the other end of the specimen is discarded. By doing this, the data is reduced by half and the averages for the rougher surfaces do not include as many specimens since the beam typically fails on the end with the lower roughness. The average horizontal shear stresses resulting from considering the beam as a whole are presented in Table 9-16. There is still a definite positive trend between the horizontal shear stress and the surface finishes of the specimens. Additionally, the difference in the horizontal shear stress within the as-placed and rake specimen still trend positively with increased roughness.

Table 9-16: Average and Standard Deviation for the Horizontal Shear Stress Considering the Beam as a Whole

Surface Finish	All Specimen		"Not So Rough" Specimen		"Intermediate" Specimen		"Rough" Specimen	
	Average [psi]	Standard Deviation [psi]	Average [psi]	Standard Deviation [psi]	Average [psi]	Standard Deviation [psi]	Average [psi]	Standard Deviation [psi]
Broom	483	7	483	7	N/A	N/A	N/A	N/A
As-Placed	630	86	591	50	626	75	793	N/A
Rake	803	72	773	91	811	78	823	64

Note: Average and Standard Deviation Calculations do not include Specimens 3B1, 3B2, and 3R2

The influence of the slab concrete compressive strength on the horizontal shear stress was found to be inconclusive. For all of the test specimens, the slab compressive strengths did not vary that greatly; thus the differences in the horizontal shear stresses were not significant. The degree of roughness and composite action of the interface seemed to have more influence on the resulting horizontal shear stresses for the specimens.

9.11 Conclusions

Overall, the specimen behavior was broken down into four categories; specifically, composite, between composite and middle composite, between middle composite and non-composite, and non-composite. By dividing each specimen into two individual ends, the trend of the surface finish and corresponding roughness could be analyzed. Based on the results and discussion presented for the second phase of this experimental program, the following conclusions can be made for composite beams without interface reinforcement:

1. The horizontal shear strength achieved from the tests were approximately six to ten times greater than the recommended value of 80 psi using in ACI 318-08 for composite sections without interface reinforcement.

2. The horizontal shear capacity of a specimen increases with increasing surface roughness. This positive trend is corroborated with the increase in the stiffness of the load-deflection responses and horizontal shear stress-interface slip data.

3. An average shear strength of 498 psi was achieved and a design horizontal shear strength of 435 psi is recommended for precast members with a broom surface finish.

4. An average shear strength of 667 psi was achieved and a design horizontal shear strength of 466 psi is recommended for precast members with an as-placed surface finish.

5. An average shear strength of 821 psi was achieved and a design horizontal shear strength of 571 psi is recommended for precast members with an rake surface finish.

6. The effect of the slab compressive strength on the horizontal shear capacity was found to be inconclusive.

7. As revealed by the ARAMIS 3D image correlation system tests, the strain distribution of concrete members may not be as uniform as predicted by finite element modeling. Therefore, difficulties arise when trying to accurately predict the horizontal shear stress from strain data.

10 Discussion, Conclusions, and Recommendations

A series of structural tests were conducted on composite prestressed beams without interface ties. The test specimens were designed to achieve high levels of horizontal shear stress before cracking of the section occurs. The contribution to the horizontal shear capacity provided by the roughness of the interface surface finish and the compressive strength of the slab concrete were investigated. Several specimen of each combination of the research variables were fabricated and tested in order to determine the horizontal shear capacity which can be achieved. The following sections provide the conclusions and recommendations found by this research project.

10.1 Comparing Results to Previous Research

The results from the second phase of the experimental program demonstrated that the level of horizontal shear stress was directly related to the roughness of the surface finish applied to the precast member of the composite section. This general positive trend was also seen in the experimental results from the first phase conducted by Deschenes and Naito (2006). However, in the first phase, the level of horizontal shear stress achieved was much higher than that for the second phase. This increased capacity may be the result of the slab concrete being placed only a day after the web was cast. This relatively short time period between placements could allow the topping to achieve a greater bond since the base concrete is still hydrating. Also, the topping and base members would cure at the same rate thus negating the effects experienced from differential shrinkage. Therefore, the results of the first phase experiments should be taken as an upper bound for the horizontal shear capacity of a composite concrete section.

Other previous research studies resulted in horizontal shear strengths less than those achieved for this experimental program. This reduction in the other research programs can be attributed to the goal and scope of those studies. The results from the CTA (1976) test series were low due to deliberate improper fabrication techniques that were performed as part of the research. The

remaining previous research tests results could be lower due to early flexure cracks that often times propagated to the interface thus causing the section to slip earlier than it should. Additionally, the horizontal shear stresses for these tests were often calculated using cracked section properties with the elastic equation which does not provide a proper representation of the stresses acting on the interface. Furthermore, it is important to recall that many of these studies only contained one or two specimens with no interface reinforcement. The reliability of the data may be in question. Regardless of the lower strengths reported, all of the previous research results exhibited horizontal shear strengths in excess of the recommended values presented in ACI 318.

Contrary to the previous research, an interface bond was not able to be obtained for a specimen with a smooth surface finish for this research project. It was found that bonding to a web with a smooth surface finish is difficult due to the presence of a cold joint and the lack of roughness on which the slab concrete can grip. In the previous research, specimens with a smooth surface finish were reported to reach relatively high levels of horizontal shear stress (Reverz, 1953; CTA, 1974). However, the specimens were tested relatively soon after the slab concrete was cast which would eliminate the effect of differential shrinkage and the resulting strains on the concrete bond. Additionally, the interface widths for these specimens were fairly large thus providing a better chance of the two concretes to bond.

The effect of the compressive strength on the horizontal shear capacity was found to be inconclusive for this research project. However, the slab compressive strengths did not vary that greatly between the test specimens. This does not provide a reliable spread in data from which comparisons can be made. Contrary to this, it was found in previous research by Patnaik (1999) and Deschenes and Naito (2006) that the horizontal shear capacity will increase as the compressive strength of the slab concrete increases. The variation in the slab concrete

compressive strength was much greater for the test specimens from these research projects thus providing a better opportunity for comparison. In order to verify this tend, future work should be conducted to better understand the effects of the slab concrete compressive strength on the horizontal shear stress of a composite beam.

10.2 Conclusions

Overall, the horizontal shear strength achieved from this series of experiments were approximately six to ten times greater than the recommended values presented by the ACI 318 code for composite sections without interface reinforcement. It was concluded from these experiments that the interface roughness had a pronounced effect on the level of composite action and thus the horizontal shear stress that could be attained. For these tests, the desired roughness was not always achieved for the specimen interface. Thus, the results from this experimental program could be considered a lower bound to the horizontal shear capacity that could be obtained from specimen with a proper level of roughness.

Since it was found that the roughness of the interface has a significant effect on the resulting horizontal shear stress, it is important to achieve the proper level of roughness for each surface finish applied. Care should be taken to apply the surface finish at the proper time during the initial cure of the concrete so that the finish does not eventually settle out leaving a lower roughness than what is desired. This is especially important when high slump or self consolidating concrete is used for the precast member. Additionally, the uniformity of the surface finish is important. Marginal variations are acceptable; however, the overall finish should be consistent in order to avoid the possibility of a lower interface strength on one end of the composite beam.

It was also found that when a relatively large time period occurred between the placement of the concrete slab and the precast web, differential shrinkage will occur which can create premature

cracking and delamination of the composite interface. These effects should be taken into account when designing a composite section.

10.3 Recommendations

Based on the results and conclusions obtained from this experimental program, the following recommendations can be made for composite beams without interface reinforcement:

1. Composite beams with a broom surface finish can achieve a design horizontal shear capacity of 435 psi. The finish should be applied with a coarse bristle broom to create a rough texture on the surface.

2. Composite beams with an as-placed surface finish can achieve a design horizontal shear capacity of 465 psi. For this finish, coarse aggregate should be protruding approximately 1/8 to 1/4 inch from the interface to provide roughness. Additional roughness can potentially be achieved by spreading coarse aggregate on the freshly cast surface.

3. Composite beams with a rough surface finish can achieve a design horizontal shear capacity of 570 psi. This finish should be applied with a 1/4 inch rake to create a very rough texture on the surface with amplitudes of approximately 1/8 to 1/4 inch. Proper attention should be placed toward ensuring that the roughness is applied uniformly when the surface has achieved and adequate set.

4. It is advised not to use a smooth surface finish for composite beams. The uncertainly of the bonding capabilities to a smooth surface could result in the composite interface failing prematurely. The time and labor required to obtain a smooth surface finish should instead be used in applying a rougher finish to help ensure the integrity of the surface finish.

For these recommendations, shear ties are not required across the composite interface of the beam. However, it should be noted that these recommendations only pertain to sections where the stresses that occur are the result of a loading which produces a positive moment in the beam. In negative moment regions where there would be uplift on the section, some horizontal shear reinforcement should be placed across the interface to avoid separation of the section. The contributions of these ties to the horizontal shear stress do not need to be considered since the design of the section capacity should be based on the contribution of the concrete alone. In addition, for cases where the composite member may be subjected to uplift forces or dynamic motions, a minimum amount of interface reinforcement should be used to ensure that the integrity of the interface is maintained.

References

ACI-ASCE Committee 333 (1960). Tentative Recommendations for Design of Composite Beams and Girders, for Buildings. *ACI Journal, 57*(6), 609 – 628.

ACI Committee 209 (1992). Prediction of Creep, Shrinkage, and Temperature Effects in Concrete Structures. *ACI Committee Report, ACI 209R-92.*

American Association of State Highway and Transportation Officials (2005). *AASHTO LRFD Bridge Design Specifications*. Washington DC.

American Association of State Highway and Transportation Officials (2007). *AASHTO LRFD Bridge Design Specifications*. Washington DC.

American Concrete Institute (1963). *Building Code Requirements for Structural Concrete and Commentary*. ACI 318-63.

American Concrete Institute (1971). *Building Code Requirements for Structural Concrete and Commentary*. ACI 318-71.

American Concrete Institute (2005). *Building Code Requirements for Structural Concrete and Commentary*. ACI 318-05.

American Concrete Institute (2008). *Building Code Requirements for Structural Concrete and Commentary*. ACI 318-08.

ASTM Standard C 31/C 31M (2006), *Standard Practice for Making and Curing Concrete Test Cylinders in the Field*. ASTM International, West Conshohocken, PA.

ASTM Standard C 39/C 39M (2001), *Standard Test Method for Compressive Strength of Cylindrical Concrete Specimens*. ASTM International, West Conshohocken, PA.

ASTM Standard C 469 (1994), *Standard Test Method for Static Modulus of Elasticity and Poisson's Ratio of Concrete in Compression.* ASTM International, West Conshohocken, PA.

Bryson, J.O., Skoda, L.F., & Watstein, D. (1965). Flexural Behavior of Prestressed Split-Beam Composite Concrete Sections. *PCI Journal, 10*(3), 77-91.

Bryson, J. O., & Carpenter, E. F. (1970). Flexural Behavior of Prestressed Concrete Composite Tee-Beams. *National Bureau of Standards, Building Science Series 31.*

Concrete Technology Associates (1974). Composite Systems without Roughness. *Technical Bulletin 74-B6.*

Concrete Technology Associates (1976). Composite Systems without Ties. *Technical Bulletin 76-B4.*

Deschenes, D., & Naito, C. (2006). Horizontal Shear Capacity of Composite Concrete Beams Without Ties. *2006 PCI National Bridge Conference.*

Evans, R. H., & Chung, H. W. (1969). Horizontal Shear Failure of Prestressed Composite T-Beams with Cast-in-Situ Lightweight Concrete Deck. *Concrete*, 124 – 126.

Gohnert, M. (2003). Horizontal Shear Transfer Across A Roughened Surface. *Cement and Concrete Composite, 25*, 379-385.

GOM mbH, (2008). GOM - Measuring Systems - ARAMIS. Retrieved May 4, 2008, from GOM - Optical Measuring Techniques Web site: www.gom.com

Hanson, N. W. (1960). Precast-Prestressed Concrete Bridges; 2. Horizontal Shear Connections. *Journal of the Research and Development Laboratories*, Portland Cement Association, *2*(2), 38 – 58.

Kaar, P. H., Kriz, L. B., & Hognestad, E. (1960). Precast-Prestressed Concrete Bridges; 1. Pilot Tests of Continuous Girders. *Journal of the Research and Development Laboratories*, *2*(2), 21-37.

Kosmatka, S.H., Kerkhoff, B., & Panarese, W.C. (2005). *Design and Control of Concrete Mixtures*. Skokie, Illinois: Portland Cement Association.

Loov, R. E., & Patnaik, A. K. (1994). Horizontal Shear Strength of Composite Concrete Beams With a Rough Interface. *PCI Journal*, *39*(1), 48 - 69.

Mattock, A. H., & Kaar, P. H. (1961). Precast-Prestressed Concrete Bridges, 4 – Shear Tests of Continuous Girders. *Journal of the Research and Development Laboratories*, Portland Cement Association, *3*(1), 47 – 56.

Nilson, A. H. (1987). *Design of Prestressed Concrete*. New York: John Wiley & Sons.

Nosseir, S. B., & Murtha, R. N. (1971). Ultimate Horizontal Shear Strength of Prestressed Split Beams. *Naval Civil Engineering Laboratory Technical Report NCEL TR 707*.

Ozell, A. M., & Cochran, J. W. (1956). Behavior of Composite Lintel Beams in Bending. *PCI Journal*, *1*(1), 38 – 48.

Patnaik, A.K. (1999). Longitudinal Shear Strength of Composite Concrete Beams with a Rough Interface and no Ties. *Australian Journal of Structural Engineering*, *SE1*(3), 157-166.

Precast/Prestressed Concrete Institute, (2004). *PCI Design Handbook: Precast and Prestressed Concrete*. Chicago, Illinois: Precast/Prestressed Concrete Institute.

Revesz, S. (1953). Behavior of Composite T-Beams with Prestressed and Unprestressed Reinforcement. *ACI Journal*, *24*(6), 585 – 592.

Saemann, J. C., & Washa, G. W. (1964). Horizontal Shear Connections Between Precast Beams and Cast-in-Place Slabs. *ACI Journal*, *61*(11), 1383 – 1409.

Schmidt, T., Tyson, J., & Galanulis, K. (2003). Full-Field Dynamic Displacement and Strain Measurement Using Advanced 3D Correlation Photogrammetry. *Experimental Techniques*. Part I: *27*(3), 47-50; Part II: *27*(4), 44-47.

Schmidt, T., Tyson, J., Revilock Jr., D.M., Padula II, S., Pereira, J.M., Melis, M, & Lyle K. (2005). Performance Verification of 3D Image Correlation Using Digital High-Speed Cameras. Proceedings of 2005 SEM Conference. Portland, OR.

Seible, F., & Latham, C.T. (1990). Horizontal Load Transfer in Structural Concrete Bridge Deck Overlays. *Journal of Structural Engineering ASCE, 116*(10), 2691-2709.

Trilion Quality Systems LLC, (2008). ARAMIS. Retrieved May 4, 2008, from Trilion Quality Systems Web site: www.trilion.com

Vita

Jonathan D. Kovach was born of September 20, 1983 in Cleveland, Ohio. He is the son of Robert and Margret Kovach. Jonathan earned his Bachelor of Science degree in Civil Engineering at Ohio University in June 2006. In the fall of 2006, he attended Lehigh University to pursue his Master of Science degree in Structural Engineering. Jonathan will receive his degree in September of 2008. After graduation, Jonathan will work as a structural engineer for Wiss, Janney, Elstner Associates, Inc. in Cleveland, Ohio.

END OF TITLE